DIRECT DIGITAL CONTROL OF D.C. MACHINES

BY
AUBREY PAUL VON ZWIKLITZ
B.Sc(Eng.) (RAND)

Thesis submitted in fulfilment of the requirements for the degree of M.Sc (Eng.) at the University of Cape Town

September 1972

ACKNOWLEDGEMENTS.

Sincere thanks are due, in the first place, to my supervisor, Mr. S.G. Mclaren, for help, encouragement and assistance at all times. I should also like to thank Mr. H.F. Weehuizen, upon whose work a great deal of this thesis was based, for his help.

A word of appreciation to Mr. J.A.C. Chapman, not only for his thyristor firing circuits, but also for a number of useful ideas, and to Professor N.C. Enslin, for his encouragement.

Finally, thanks are due to the Council of Scientific and Industrial Research for their very generous financial support.

SUMMARY.

This thesis set out to improve on previous methods of digital control of a three phase fully controlled thyristor bridge, using phase control of the thyristors, and to use this bridge for the purpose of controlling the speed of a separately excited D.C. machine, under the supervision of a small digital computer. Interfacing equipment for this purpose was designed and built.

Various methods of speed detection were considered, and a simple digital tachometer designed and built. This tachometer was able to feed a digital number, related to the speed of the machine, to the computer, and was accurate to better than 1%.

A direct digital control system was then implemented. The behaviour of the system was first studied under open loop conditions in order to determine the parameters of the system, and to discover any shortcomings in it.

The behaviour of the closed loop system was then studied, using z-transform analysis, at sampling rates of from twice to eight times the natural frequency of the machine. Initially, the computer was used as an integral controller. The behaviour of the mathematical model was compared to that of the actual system, and the correlation found to be very good.

The control system was then compensated, using compensation routines based on the z-transform analysis, and the behaviour of various compensated systems studied at sampling rates varying from 0,4 to 1 second. Again, the actual system response was found to correspond closely to the designed behaviour.

Finally, a dual-machine control system, on a time sharing basis, was implemented, and a degree of interrelation between the speeds of the two machines introduced.

The control algorithms developed were able to provide speed control to better than 1% accuracy, with a 5% or less overshoot in the step response, a delay of one sampling period but no overshoot in the ramp response, and satisfactory behaviour under load transient conditions. The time, and memory, utilization was such that such algorithms could be extended to the control of several machines, using the single computer, if sufficient input and output facilities were available.

CONTENTS.

CHAPTER 1.
INTRODUCTION.

1.1. INTRODUCTION TO DIRECT DIGITAL CONTROL.

The development of the digital computer has led, inevitably, to its playing an increasingly important role in the field of control. Computers have been used in several varying ways in controlling industrial processes, the three most common being:[1]

(i) Control of set points, the actual process concerned being controlled by conventional analogue feedback methods.

(ii) Direct digital control, where the computer acts as an integral part of the feedback system.

(iii) Modelling techniques, where the behaviour of the system under consideration is compared to that of a mathematical model, and appropriate action is taken by the controller.

The process, or "mini" computer, is probably best suited to the second category, and it is this type of control which was the subject of this thesis.

Direct digital control has been used fairly extensively in the Chemical Engineering industry for some time [2,3], and in applications where slow time constants facilitated relatively slow sampling times (of the order of 1 second or more.[3]) Obviously, to be economical, the computer used in process control must be able to control several loops or processes, so that the time to execute a control algorithm and the time between samples become important considerations.

In 1963, Klock and Schoeffler [3] put forward the following advantages of direct digital control: " ... lower capital investment by replacing many analogue controllers and recorders with one time-shared D.D.C. computer; better control, because

/..each..

each controller parameter can be changed over a wider range than can the corresponding parameter of an analogue controller, and in addition the control parameters are non-interacting ... and can be varied in a much smoother manner; straightforward data logging because the desired data is present in a single location, in digital form, and may easily be printed out .... (here the time between samples would once again be important) ... ; ease of communication with a general purpose digital computer which need not be tied up 100% of the time on the process, but used only as needed by the operator; ease of automatic start-up and shut-down by a general purpose computer communicating with the D.D.C. computer; and potentially improved control algorithms, such as non-interacting control, non-linear control, and the like."

All of these advantages are clearly equally valid for electrical systems having faster time constants, and therefore faster sampling rates, provided that a sufficiently large number of machines or systems can be controlled simultaneously. The work done for this thesis considered the time-shared control of two machines (see chapter 8), and this can, in theory, be considerably extended using the algorithms developed.

1.2. D.D.C. APPLIED TO THYRISTOR DRIVEN MACHINES.

In 1969, Fallside and Jackson [4] first proposed a system for the direct digital control of a three phase thyristor bridge providing a source of D.C. power (fig. 1.1).

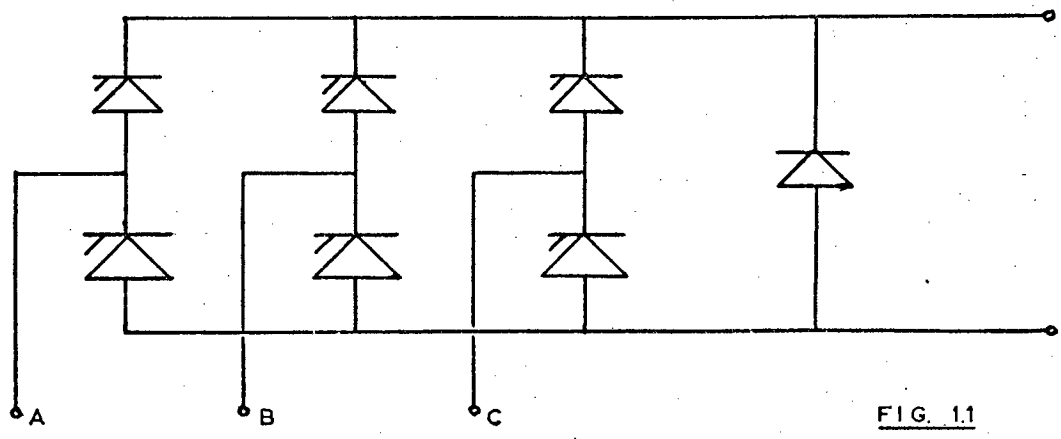

FIG. 1.1
THREE PHASE THYRISTOR BRIDGE.

The thyristor is a device ideally suited to digital control, particularly when used in phase control applications. It will conduct current provided that the cathode-anode voltage is positive, and provided that a signal is present at the gate [5]. It will then continue to conduct until the current through it drops to zero. For single phase applications, phase control is achieved by delaying the gate signal by a delay angle θ after the cathode-anode voltage has passed through zero, going positive (fig. 1.2).

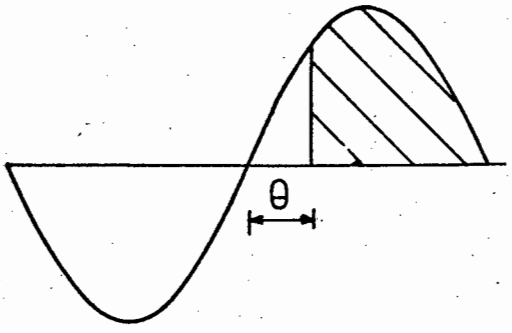

FIG. 1.2

SINGLE PHASE WAVE.

THYRISTOR CONDUCTS OVER CROSS-HATCHED PORTION.

This principle can be extended to three phase applications, provided that no attempt is made to switch on a thyristor until the voltage across it exceeds the previous phase voltage, as it will not conduct until this occurs (fig. 1.3).

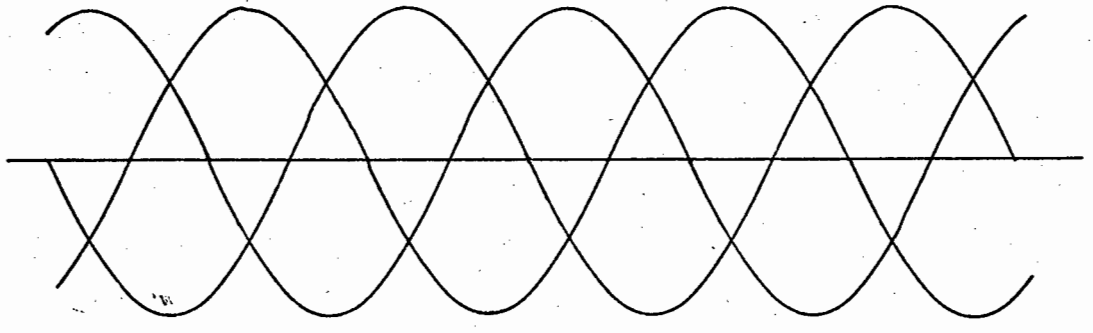

FIG. 1.3

THREE PHASE WAVE.

Details of the switching arrangements for the thyristors are given in chapter 2.

As the control system was initially envisaged and implemented, [4,6,7], the computer itself carried out the waveform cross-over detection, countdown firing angle delay, selection of the appropriate thyristor and provision of a firing pulse to the gate trigger circuit. This was clearly extremely time consuming, and problems were introduced when a delay of more than 60° was required (if this was so, an additional cross-over would occur during a countdown routine) [7].

It was therefore decided to construct an external local memory to store the firing angle delay set by the computer, and to perform the crossover detection, countdown detection and production of a firing pulse to the requisite thyristor. The interface designed was an improvement on a previous model [7], and is fully discussed in chapter 2.

Previous models made use a analogue feedback models [7]. This thesis introduced the use of a digital tachometer for the provision of a speed feedback signal. The problems and advantages which this introduced are discussed in chapter 3.

It is of interest to note that most D.D.C. systems in practice appear to make use of a standard three term algorithm, containing terms for proportional, derivative and integral control [1,2,3]. The use of the z-transform and z-transform analysis (see chapter 5), suggested various other algorithms. these were implemented and their effect on the control system studied.

CHAPTER 2.

DEVELOPMENT OF THE THYRISTOR FIRING INTERFACE.

2.1. INTRODUCTION.

The interface was required to store a binary number corresponding to the required firing angle delay, as given out by the computer. The countdown was to be initiated after a crossover point had been detected, and on conclusion of the count a firing pulse was to be given out to the correct thyristor.

It was decided for simplicity to use a different binary counter for each phase, as opposed to the previous system [7], where only two counters were used, but where addressing and delay problems were encountered.

A block diagram of the interface for each phase is shown in fig. 2.1.

FIG. 2.1
BLOCK DIAGRAM OF FIRING INTERFACE.

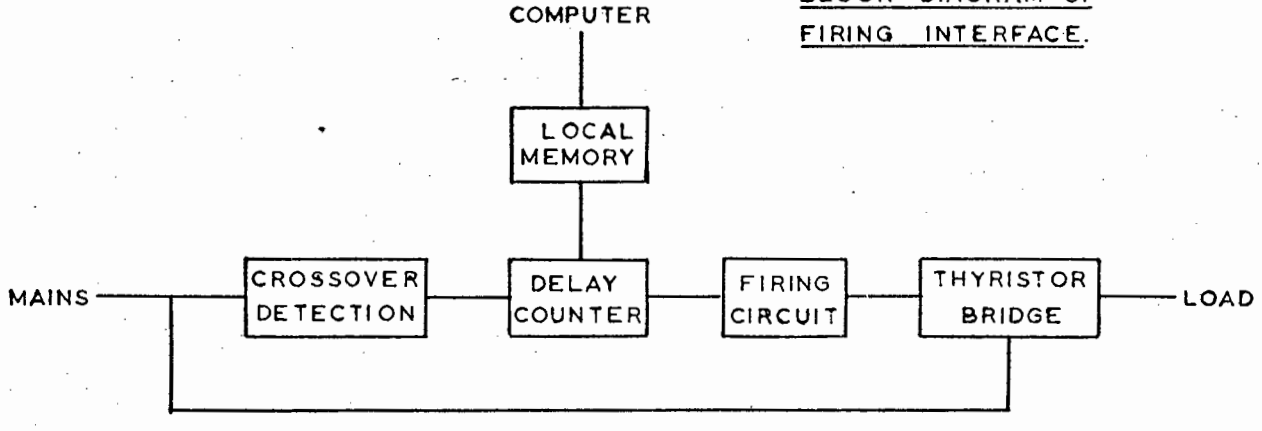

2.2. CROSSOVER DETECTION.

It was seen from fig. 1.2. that no thyristor should be switched on before the voltage across it exceeded that of the previous phase, i.e. the voltage of the particular phase had to have a

/..phase..

phase displacement of 30° before being switched on, and could be controlled until its phase angle reached 150°, when its voltage would in turn be exceeded by the voltage of the next phase. Thus control of the firing angle would be possible from 30° to 150°, a range of 120°. (It should be remembered that the thyristor will conduct until the current through it drops to zero, i.e. at least until the angle reaches 180°, but that once the phase angle passes 150°, no more control is possible.)

It was therefore necessary for the crossover detection system to introduce a delay of 30° after the phase voltage concerned had passed through zero before any countdown firing routine could begin. This was possible in three ways:

(i) By software means, i.e. detect the phase voltage zero crossing, and include a count of 30° in every firing angle set. Such a system would result in a loss of accuracy, since now 150° would have to be quantised, 30° of which, or 1/5, could never be subdivided. In addition, noise might be a problem here, as the mains waveform, containing the transients caused by the switching of the other thyristors, would be sampled for crossover detection, and spurious zeroes might well be detected.

(ii) By detection of the actual crossovers, i.e. use of comparators between every two sets of voltages. This system would require six comparatively expensive comparators, and again switching transients would create serious problems.

(iii) By introducing a phase shift of 30° in the waveform and detecting a zero crossing in the phase shifted waveform. This would suggest the use of a phase shifting transformer, the use of which would also introduce the advantage of isolation for the detection circuit.

The final system selected utilized a delta-star transformer to feed the thyristors, and a delta-delta transformer to feed the logic circuits [8] (fig. 2.2). Fig. 2.4a shows the phase shift of 30°, so that a zero crossing of the phase shifted waveform corresponds to a crossover point on the waveform feeding the thyristors.

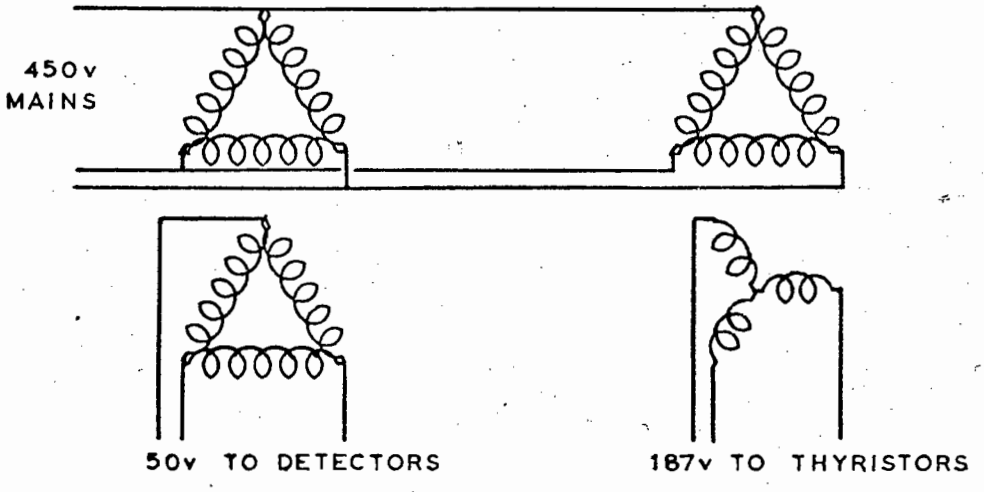

FIG. 2.2. TRANSFORMER CONNECTIONS

The signal was amplitude limited by putting it across a back-to-back diode pair, squared by a Schmitt trigger circuit and then inverted (fig. 2.3). The waveforms thus obtained are shown in fig. 2.4b.

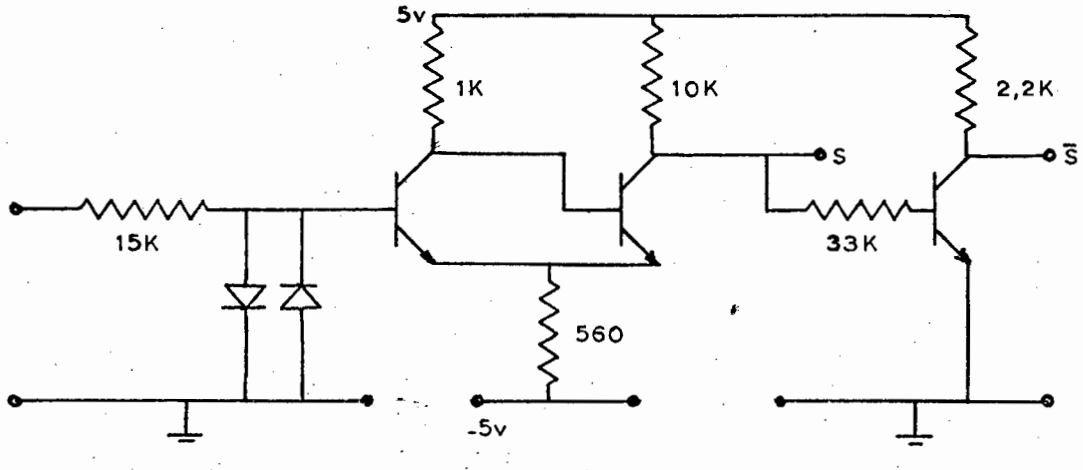

FIG. 2.3.
LIMITING AND SQUARING CIRCUIT.

S - SCHMITT OUTPUT
S̄ - INVERSE OF SCHMITT.

Fig. 2.4 (opposite)

Fig. 2.4a.

Three phase waveform (above) with displaced phase voltage below. Note that a zero of the displaced voltage corresponds to a crossover point of the mains voltage.

Fig. 2.4b.

Squaring process of interface.

Waveforms are: (i) Transformer output voltage (15v r.m.s.)
(ii) Limited voltage (1,4v peak to peak)
(iii) Schmitt Trigger output (5v)

Fig. 2.4c.

Firing Interface waveforms.

Waveforms are: (i) Schmitt Trigger output.
(ii) Gating flip-flop output.
(iii) Counter flip-flop output.
(iv) Firing Circuit enable pulses.

All voltages are of 5v amplitude.

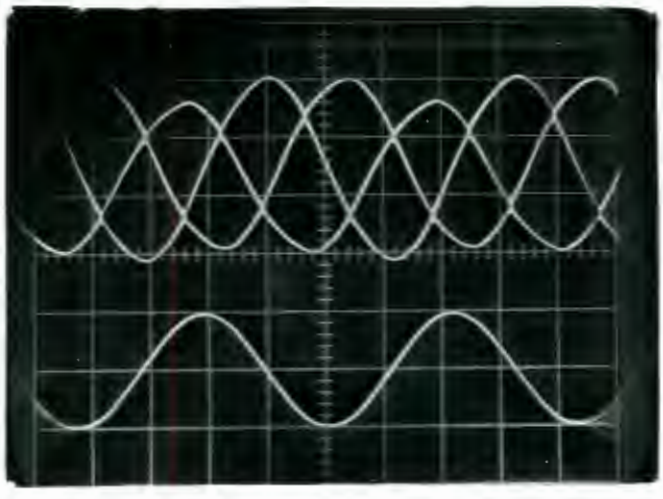

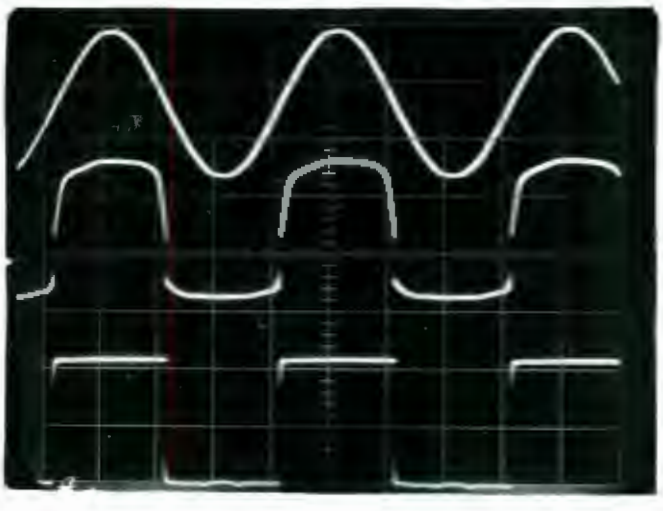

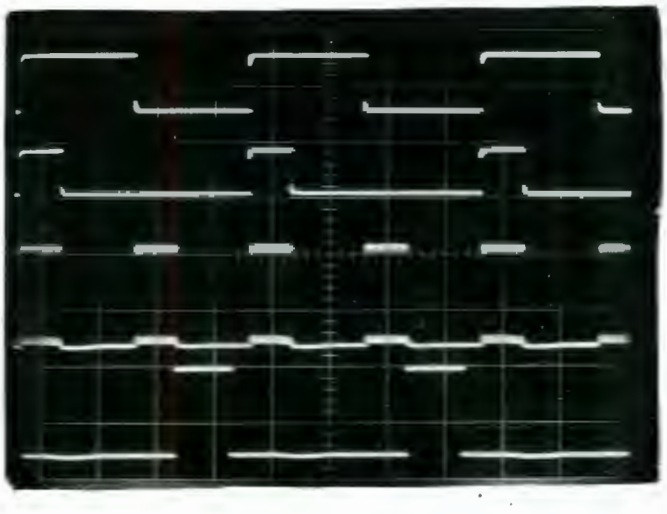

2.3. THE DELAY COUNTER.

The delay counters consisted of a number of D-type flip-flops connected to give a down-counting ring counter [9].

The Schmitt trigger output, and its inverse for each phase, were fed into an integrating circuit, consisting of a resistor and capacitor in series tied to the 5^{V} rail, in order to produce a negative going voltage spike every time the voltage in question went to zero. A diode in each network prevented positive spikes. These spikes triggered the preset terminal of a D flip-flop, setting its Q output high. This output was gated with the output of a free running multivibrator (fig. 2.5), whose frequency was adjusted so that 256 pulses could be counted in 120° of a mains cycle (i.e. to allow for an 8 bit setting of the firing angle, since $2^{8}=256$)

The period of the A.M.V. was thus (1/3 x 20) ÷ 256 ≈26 μsecs.

The A.M.V. was designed using conventional methods [10].

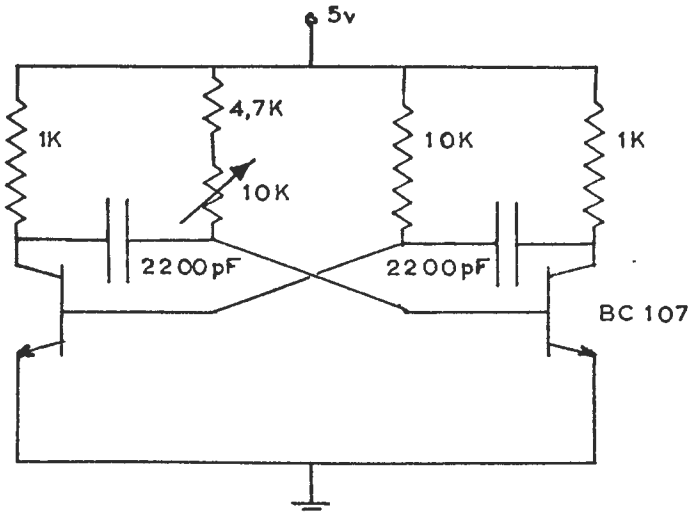

FIG. 2.5. ASTABLE MULTIVIBRATOR.

Each counter had two such gates, depending on which zero crossing (i.e. positive-going or negative-going) was taking place. The prescence of either series of pulses would set the counter going.

The counter had each $\bar{Q}$ output of its flip-flops connected to an 8 input NAND gate, the output of which went low when the counter reached zero. The low pulse was connected to the clear terminals of the gating flip-flops, so as to shut the gates when the count reached zero, by pulling the Q outputs of these flip-flops low. At the same time, this signal was also sent to a buffer inverter gate, which was connected to the gates from the local memory (see section 2.4), which gates fed the preset and clear inputs of the counter flip-flops, so that on the count reaching zero, it was automatically reset to the count set up in the local memory, and would begin to count again when one of the input gates was reopened.

It was found necessary to set all the flip-flops simultaneously to either high or low states on resetting, as the ring counter, by its nature, would tend to propagate a high signal, if its components were not being absolutely held either high or low, as the conditions required.

The inverse of the 8 input NAND gate signal was also gated with either the Schmitt trigger signal or its inverse, to give a negative pulse to one of six M.M.V.'s required to pulse the firing circuits. (See section 2.5).

The waveforms of the delay counter are shown in fig. 2.4c, while fig. 2.6 shows the delay counter and its associated logic.

FIG. 2.6. SCHEMATIC OF DELAY COUNTER AND LOGIC.

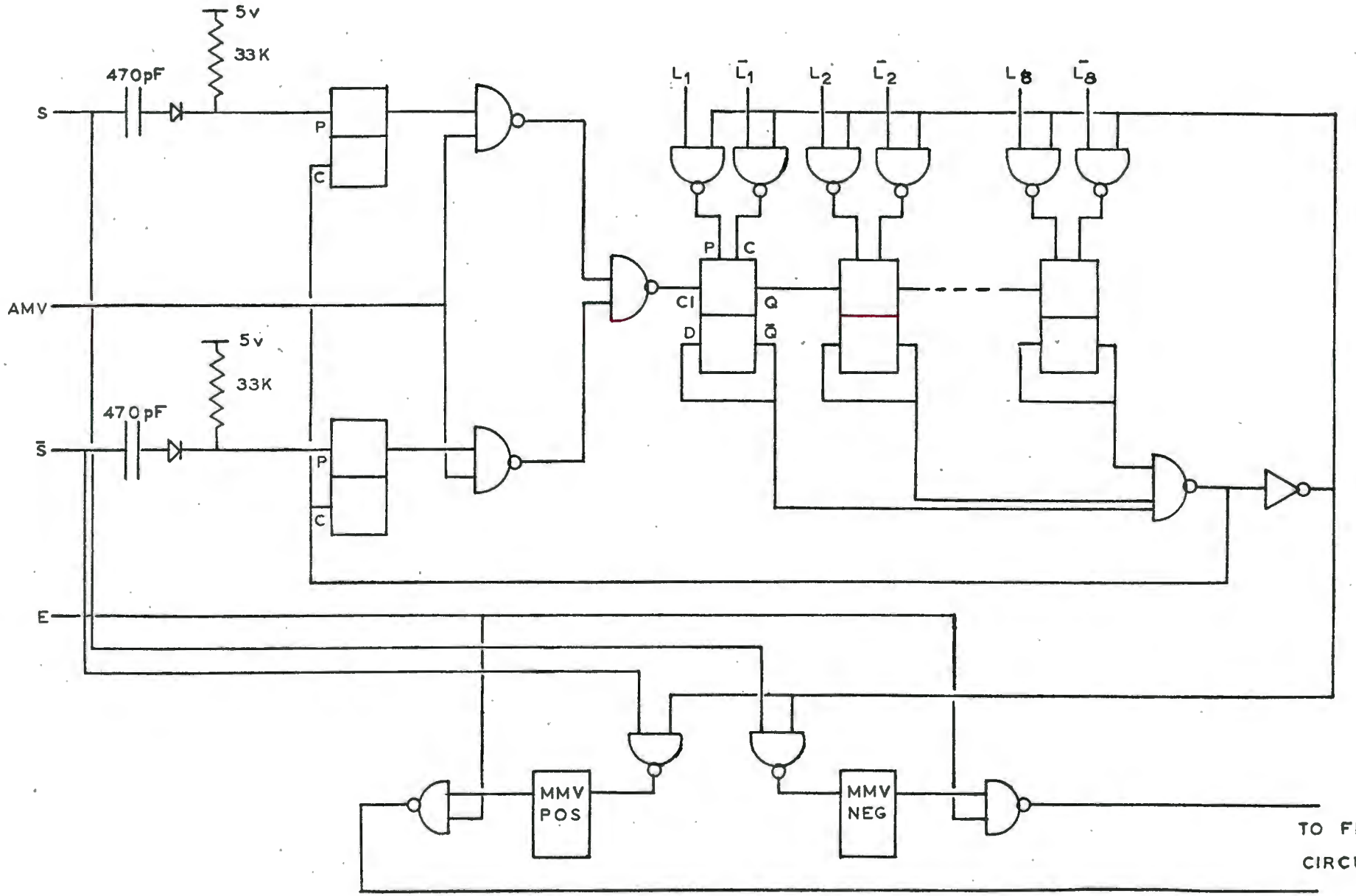

2.4. THE LOCAL MEMORY.

This consisted of two Quad Latches. These have the characteristic that the output of each latch will follow its input, if the clock input of the chip (hereafter referred to as the strobe), is high. If the strobe input is low, the output of the latch holds the value which the input had when the strobe went low [9].

Thus eight bits, or lines, of data, as well as a strobe line were required to be fed by the computer to the interface. Each of these lines had to be able to held either high or low (see section 4.1). The outputs of the latches, and their inverses, were gated into the preset and clear inputs respectively of the eight flip-flops constituting each counter. (L_1 - L_8 and $\bar{L}_1$ - $\bar{L}_8$ of figure 2.6)

In order to reduce the noise susceptibility of the interface, it was found necessary to invert the input line signal to the strobe. It was observed that, despite the fact that the ground of the interface was solidly earthed, the strobe when held low tended to go slightly high, causing the setting to alter spuriously. If the line was normally high, and only pulsed low, this tendency was reduced. The only extra requirement was as additional inverter, as clearly the latch itself functioned as described above, although the logic of the line from the computer might be altered.

2.5. THE FIRING CIRCUITS.

The actual firing circuits used were on a standard module developed by Mr. J. Chapman of the Electrical Engineering Department, U.C.T. The provided effectively D.C. triggering to the thyristors, thus enabling them to be fired into highly inductive loads (see section 4.2).

The inputs to the firing circuits were the outputs of the six M.M.V.'s, gated with an additional enable signal, which, if

/..pulled..

pulled low, would cut off the firing pulses and thus switch the machine off immediately, should this be required. (Line E in fig. 2.6)

The M.M.V. pulse lengths had to be sufficient to fire the thyristors until commutation had taken place and, as this would occur at most after 60° or 3,3 msecs, it was found that a pulse length of 5 msecs was ample. The M.M.V.'s used were integrated circuit types, and this pulse width was obtained using external timing resistors of 22KΩ and capacitors of 0,33μF. (11)

2.6. COMMENT.

The interface thus constructed was found to give complete control to the firing circuits over the full range of 256 bits, or 6,7msecs, i.e. a delay variation, over the full possible range of 120°, of 26μsecs.

Because of the fact that the logic for each phase was independent, no additional logic was necessary to select the thyristor corresponding to a particular phase.

Fig. 2.7 shows the completed interface.

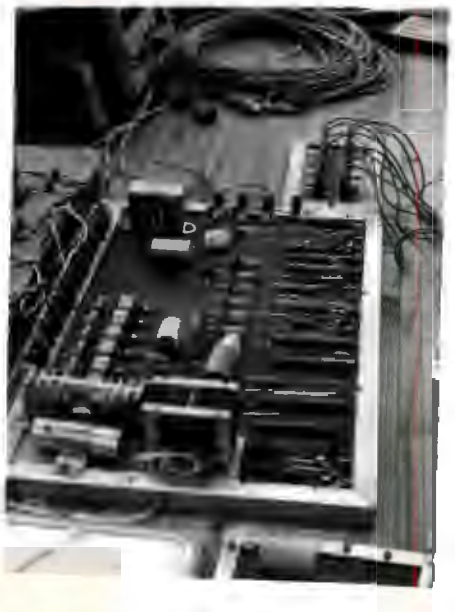

FIG. 2.7

PHOTOGRAPH OF THYRISTOR FIRING INTERFACE.

CHAPTER 3.

DEVELOPMENT OF THE DIGITAL TACHOMETER.

3.1. INTRODUCTION.

A number of fairly complex types of digital tachometer were considered [12,13,14]. However, since measurement of acceleration was not required, and since at that stage extreme accuracy was not required, it was decided to design a simpler system. The tachometer finally developed had a small time delay inherent in its design, a theoretical accuracy of 0,1% and an actual accuracy of greater than 1%.

3.2. THE TACHOMETER.

Two possible methods of measuring speed digitally were considered. Both were based on the principle of a hole or slot in a disc producing a pulse when light was applied to a photosensitive device through the slot or disc. These were:

(i) To count a number of pulses produced by slots or holes in the disc in a fixed time period. This would require a disc with a large number of slots in order that the sampling time at all realistic. This would have led to problems of accuracy in the machining of the disc.

(ii) To count the number of pulses at a fixed (high) frequency produced in between a small number of slots in a disc, i.e. a variable time, fixed displacement system. This was the system adopted.

Clearly, the minimum count that could be accumulated would occur at maximum speed, which was to be in the range 1200 - 1500 r.p.m. To give a 0,1% accuracy, this count should be at least 1000. Since $1024 = 2^{10}$, at least a ten bit binary counter would be required.

At the lower end of the speed range to be measured, the count would clearly be larger, tending to infinity at low speeds.

Thus the first obvious drawback of the proposed system presents itself - there has to be a lower limit to the speed which can be measured, and overflow logic must be provided to detect when the speed is less than this minimum.

The minimum speed specified for control purposes in this instance was 300 r.p.m. Clearly, additional bits would be required to measure speeds below the maximum. If an additional two bits were added, this would give a range of speeds up to 4 times the minimum, at the prescribed accuracy. As it was not anticipated that tests would be run much above even 1000 r.p.m., the range 300 - 1200 r.p.m. was selected. Obviously, higher speeds could be measured, albeit with reduced accuracy, but lower speeds could not.

The high frequency pulses were produced by a 100KHz crystal oscillator, the circuit of which is shown in fig. 3.1. .

FIG. 3.1. 100KHz CRYSTAL OSCILLATOR.

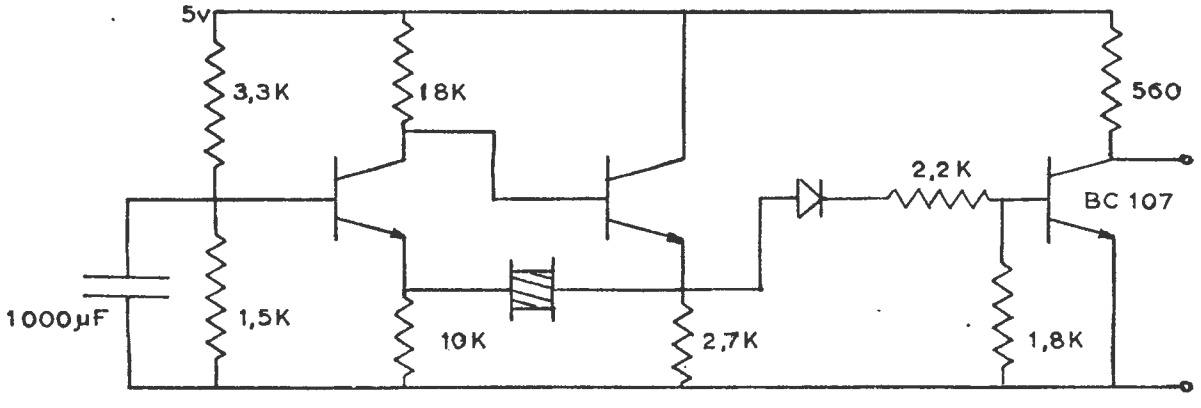

The frequency of this oscillator was measured as 99,955KHz.

Thus, at 1200 r.p.m., 1000 pulses would be counted, each pulse having a period of 10 µsecs, i.e. time for 1000 pulses would be 10 msecs.

Now, a disc at 1200 r.p.m. would rotate once in 50 msecs, i.e. in 10 msecs, it would rotate 1/5 of a revolution. Thus five slots would be required.

Then at the lowest speed read, i.e. 300 r.p.m., a count would be accumulated in 40 msecs, or reset every 80 msecs, using the system proposed. This time lag was small enough in comparison with the time constants of the machine (appendix 3) or even the sampling times used for the closed loop system (section 6.1), and therefore deemed acceptable.

The disc used is shown in fig. 3.2.

FIG. 3.2.

PHOTOGRAPH OF TACHO. DISC.

The pulses of light were produced by a phototransistor [15] designed to saturate when light was shone on it through a slot in the disc. The phototransistor pulses were then squared in a Shmitt trigger circuit, as shown in fig. 3.3.

The squared phototransistor pulses were used to switch a D flip-flop alternately on and off. The output of this flip-flop was gated with the oscillator pulses into a 12 bit D flip-flop ripple counter [9] with overflow logic.

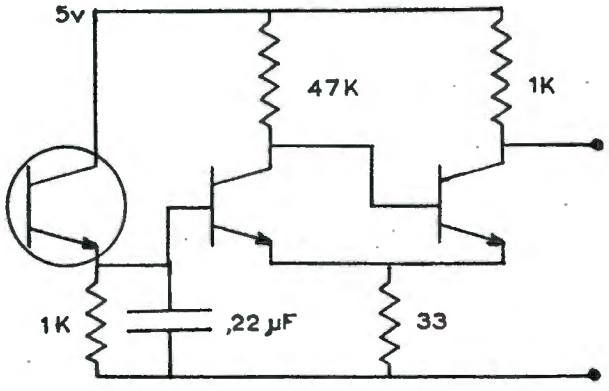

FIG. 3.3.
PHOTOTRANSISTOR AND
SCHMITT TRIGGER CIRCUIT.

The action of the gate flip-flop being switched off triggered a monostable multivibrator for 70 μsecs [11], during which time the strobes of the latches used were held low, setting the latches to the current count, while the final count was held in the counter (since the input gate to the counter was closed). The strobe line was gated with a line from the computer, so that the count could be restrained from resetting the latches if these were being sensed by the computer.

A further M.M.V. was triggered for 7 μsecs by the first one resetting. The inverse of this short pulse was used to reset the counter to zero, and could be used to indicate to the computer that the count had been completed, if the speed was to be sampled asynchronously.

The counter and storage circuits are shown schematically in fig. 3.4.

Thus a twelve bit count, plus an overflow indicator, could be interrogated by the computer, which, through simple arithmetic manipulation, could transform the count to apeed reading (see appendix 2). The waveforms obtained from the logic circuit are shown in fig. 3.5, while fig. 3.6 shows the actual interface.

FIG. 3.4. SCHEMATIC OF DIGITAL TACHOMETER INTERFACE.

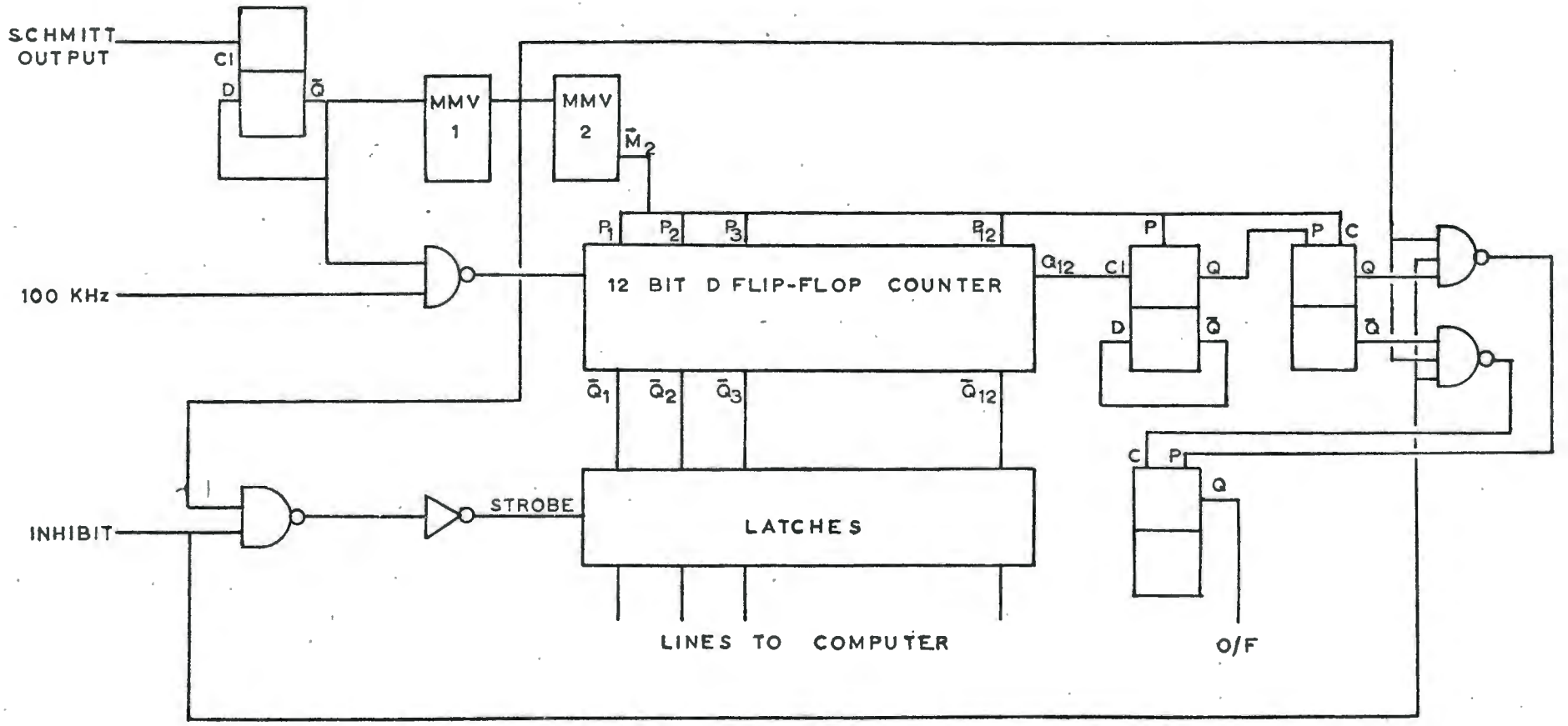

Fig. 3.5 (opposite)

Fig. 3.5a.

Digital tachometer counting waveforms.

Waveforms are:
(i) Phototransistor pulses.
(ii) Squared pulses.
(iii) Counter gating flip-flop output.
(iv) Counter flip-flop output. Note that this voltage is held on for a short time after the gate goes low.

Fig. 3.5b.

Digital tachometer reset logic waveforms.

Waveforms are:
(i) Counter gating flip-flop output.
(ii) Monostable 1 output. While this is high, the count is held and transferred to the latches.
(iii) Counter flip-flop output, showing the holding effect of monostable 1.

Fig. 3.6 (opposite)

Photograph of digital tachometer interface.

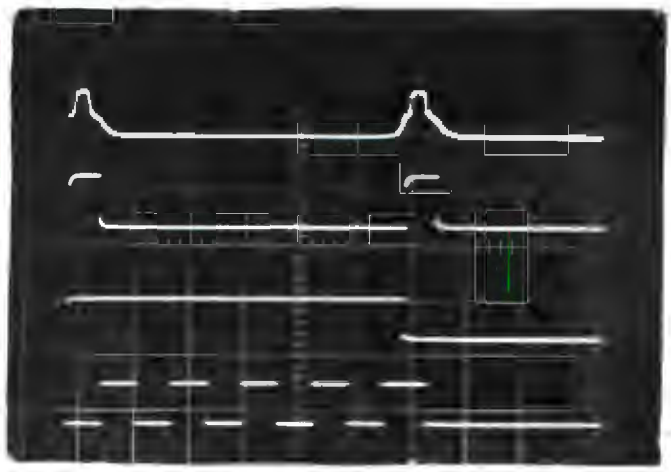

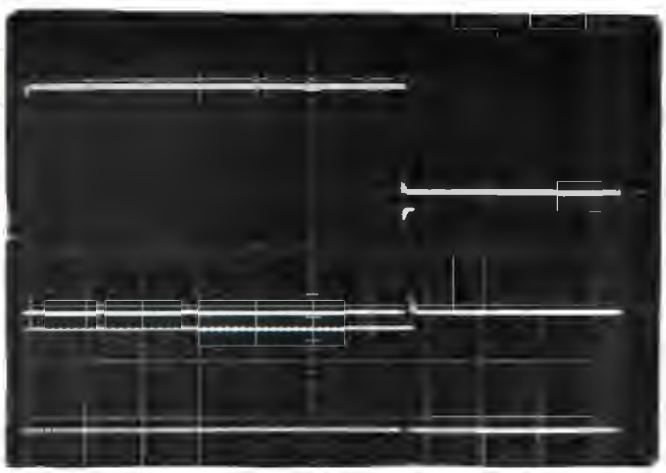

The inherent inaccuracies in the tachometer were mainly centred on the disc; the accuracy of the machining of the slots, and the eccentricity of the mounting would both contribute to the production of "tacho ripple", similar to that experienced from normal A.C. and D.C. tachogenerators (7). However, noise was not a problem at all, despite the fact that no special screening was provided for the leads from the transistor to the interface itself.

Table 3.1. shows the results when successive counts were logged by the computer at approximately 1500, 1000 and 500 r.p.m. The test was carried out under open loop conditions, i.e. an angle was set and the speed logged. For this reason, the speeds in column 1 of the table are approximate. The counts shown are octal numbers.

It can clearly be seen that the numbers come in groups of 5, corresponding to the five possible gaps between slots on the disc.

TABLE 3.1

SPEED (R.P.M.)	COUNT	% ACCURACY
1500	1421 1414 1415 1422 1416 1420 1414 1415 1421 1417	,38
1000	2240 2241 2234 2235 2242 2237 2242 2234 2235 2244	,51

3.3. COMMENT.

From table 3.1, it can be seen that an accuracy of better than 1% could be expected, from a comparatively simple tachometer. This also serves to indicate that precautions would be necessary, under closed loop conditions, to allow for variations in speed readings due to tachometer errors.

CHAPTER 4.

OPEN LOOP COMPONENTS AND THEIR BEHAVIOUR.

4.1. THE COMPUTER.

The computer used for this thesis was a Varian 620/i 18 bit, 8K word machine [16]. The machine had as input/output devices a teletype, high speed paper tape punch and reader, and in addition 24 output and 24 sense lines. The output, or EXC lines could be individually set to a logical high or low state by instructions in the computer program, while the sense lines could be individually interrogated, under program control, and subsequent action determined by the logical state of these lines.

A facility for parallel input and output of a complete word (i.e. 18 bits) of information, asynchronously or under program control, known as the direct memory access facility, was also available, but was not used for this thesis.

An additional 8 interrupt lines were available. Detection of a low logic state on one of these lines causes the program under execution to be interrupted, and the program jumps to a specified location to carry out a particular sub-routine associated with the interrupt line concerned. The eight lines have a system of priorities, eg. line 1 takes priority over line 2, etc. This facility was used to control the sampling rate of the machine under closed loop conditions (see chapters 6 and 7) as well as to effect the time shared control of two machines (see chapter 8).

4.2. THE THYRISTOR BRIDGE AND MOTOR.

The thyristors used were BTX47 1200R [17], rated at 16a, 800v, with an RCA flywheel diode, rated at 18a, 600v. The flywheel diode was found to be necessary (see section 4.4), although it is generally not considered essential for fully controlled

/..thyristor..

thyristor bridge applications.

It has been suggested [19] that a motor driven by a 3 phase thyristor bridge would display small variations in speed, due largely to the discontinuous nature of the current supplied. For applications such as those considered for this thesis, this would clearly not be a satisfactory situation. Bingley [20] gives curves for the determination of a "critical inductance" in order to ensure that the current remains continuous. In this case, an empirical method was used to determine the size of the inductance required, based on the components available. It was found, by viewing the current waveform on an oscilloscope trace while the inductances available were connected in turn in the circuit, that an inductance of 0,2H would be adequate.

In order to suppress voltage spikes, R-C snubber networks, consisting of a resistor of 10Ω and a capacitor of ,22μF, were connected in parallel with each thyristor. As shown in section 4.4, these tended to have a "ringing" effect with the inductance, leading to the build-up of considerable voltages across the choke, and were therefore removed. It was felt that the thyristors were sufficiently overrated for voltage spikes not to be a serious danger.

Overload protection for each thyristor was provided by a 13a fuse.

The motor driven was rated at 220v, 58a. This was coupled to a load machine rated at 220v, 17a. However, the real current limitation was that imposed by the thyristors, and the maximum (continutous) current was limited in all tests to 16a.

The determination of the machine constants is discussed in detail in appendix 3, as is the determination of the gain of the bridge.

The block diagram of the moter is shown in fig. 4.1a, while fig. 4.1b shows the reduced block diagram and the actual values determined in appendix 3.

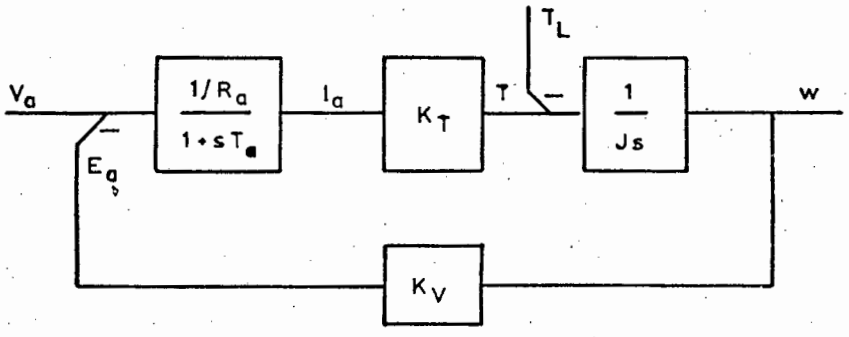

FIG. 4.1a.
BLOCK DIAGRAM OF SEPARATELY EXCITED MOTOR.

$K_T = K_V = (K_m)$

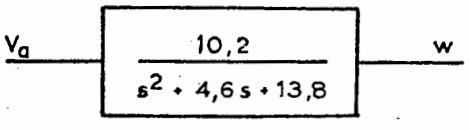

FIG. 4.1b.
REDUCED BLOCK DIAGRAM, SHOWING NUMERICAL VALUES.

4.3. INSTRUMENTATION.

Figure 4.2 shows the motor circuit, with the recording, monitoring and measuring instruments attached.

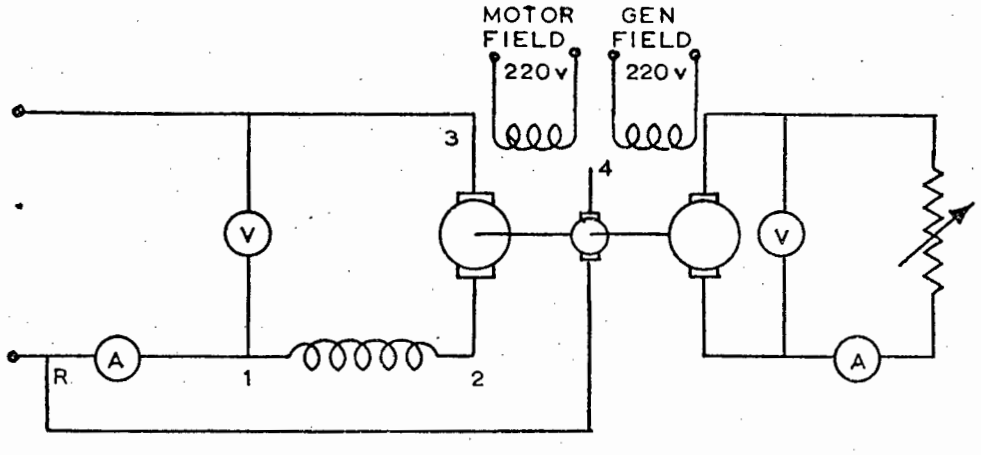

FIG. 4.2.
MOTOR AND GENERATOR CIRCUIT.

The voltages of points 1,2,3, and 4, with reference to point R, were taken to operational amplifiers feeding an ultra-violet recorder, to enable the waveforms of current, choke voltage, bridge output voltage and tachogenerator voltage to be recorded. (Voltage 1 was measured across a 30a shunt).

The amplifier for the tachogenerator voltage also fed a Hewlett Packard 7005B X-Y recorder with external time base.

In addition, a C.R.O. was connected to monitor the current and voltage waveforms of the motor.

4.4. OPEN LOOP CHARACTERISTICS.

The purposes of the tests on open loop were:

(i) To measure the constants of the machine (see appendix 3).

(ii) To investigate the effects of the prescence or absence of the flywheel diode and R-C snubber networks on the thyristor bridge.

(iii) To test the accuracy of the digital tachometer (see section 3.2 and table 3.1).

It was found that the behaviour of the system under steady state or positive step conditions did not depend on the prescence or absence of either the flywheel diode or the snubber networks. It was also noted that under these conditions current was flowing at all times. However, under negative step conditions, the current was no longer conditions, and the effects of the diode and snubber networks had to be considered.

Before considering the details of this behaviour, it is of interest to consider the steady state behaviour of the system. Fig. 4.3 shows the waveforms, under steady state conditions of (from top) (i) bridge output voltage; (ii) current; (iii) speed (or tachogenerator voltage); and (iv) choke voltage. The flywheel diode and the snubber networks were connected. The bridge voltage at the time was measured at 134v D.C., while the choke voltage was measured at 66v A.C. and 5v D.C.

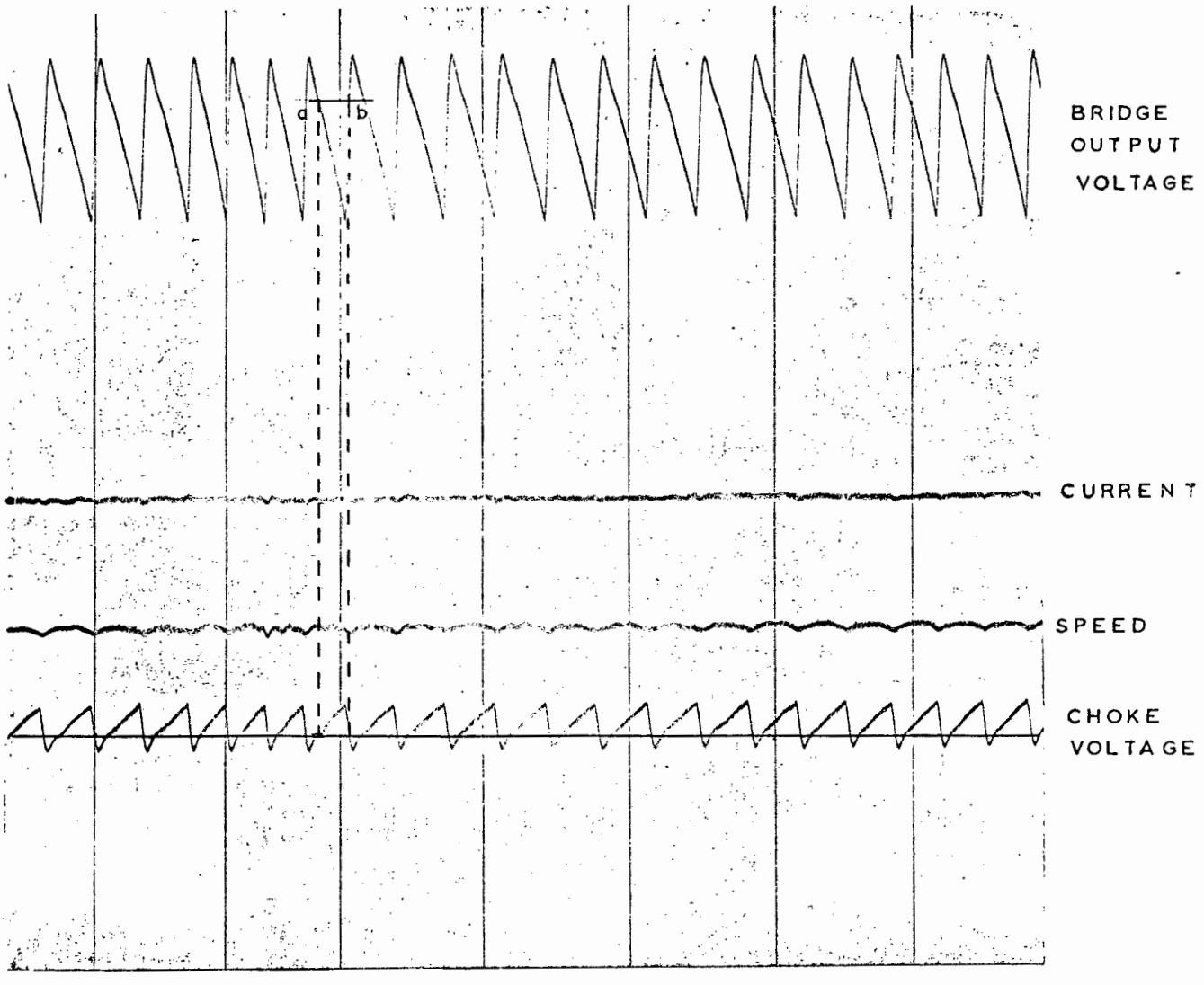

FIG. 4.3.

STEADY STATE WAVEFORMS

It can clearly be seen that as the instantaneous output voltage of the bridge drops below the back e.m.f. of the machine (a), the voltage across the choke reverses and adds to the input voltage, to try to maintain a balanced condition. When V_{in} once again exceeds the back e.m.f. (b), the choke voltage once again reverses, and opposes this voltage.

The size of the voltage swing on the choke would depend on the magnitude and degree of discontinuity of the bridge output voltage, i.e. at low voltages corresponding to large firing angles and hence a discontinuous voltage, the choke voltage

/..can..

can be expected to be far higher than at high speeds, where the output voltage is continuous and far smoother.

Figs. 4.4a and 4.4b show the effect of a negative step on the system. In fig. 4.4a, the current falls fairly rapidly to zero (the current on this trace has been amplified for clarity), as the voltage drops to its new setting, while the choke voltage rises to oppose this (part a on the trace). The current remains at zero until, at point b on fig. 4.4b, the average output voltage of the bridge exceeds the back e.m.f. of the motor (which has been superimposed over the bridge output voltage waveform), whereupon the current starts to flow again. (Note that figs. 4.4a and b are not contiguous - as the speed trace shows, the entire trace is not shown).

The long period of zero current would seem to indicate that, for an extended period, the machine is incapable of control, while the excess inertial energy is dissipated. This was in fact found to be the case under closed loop conditions.

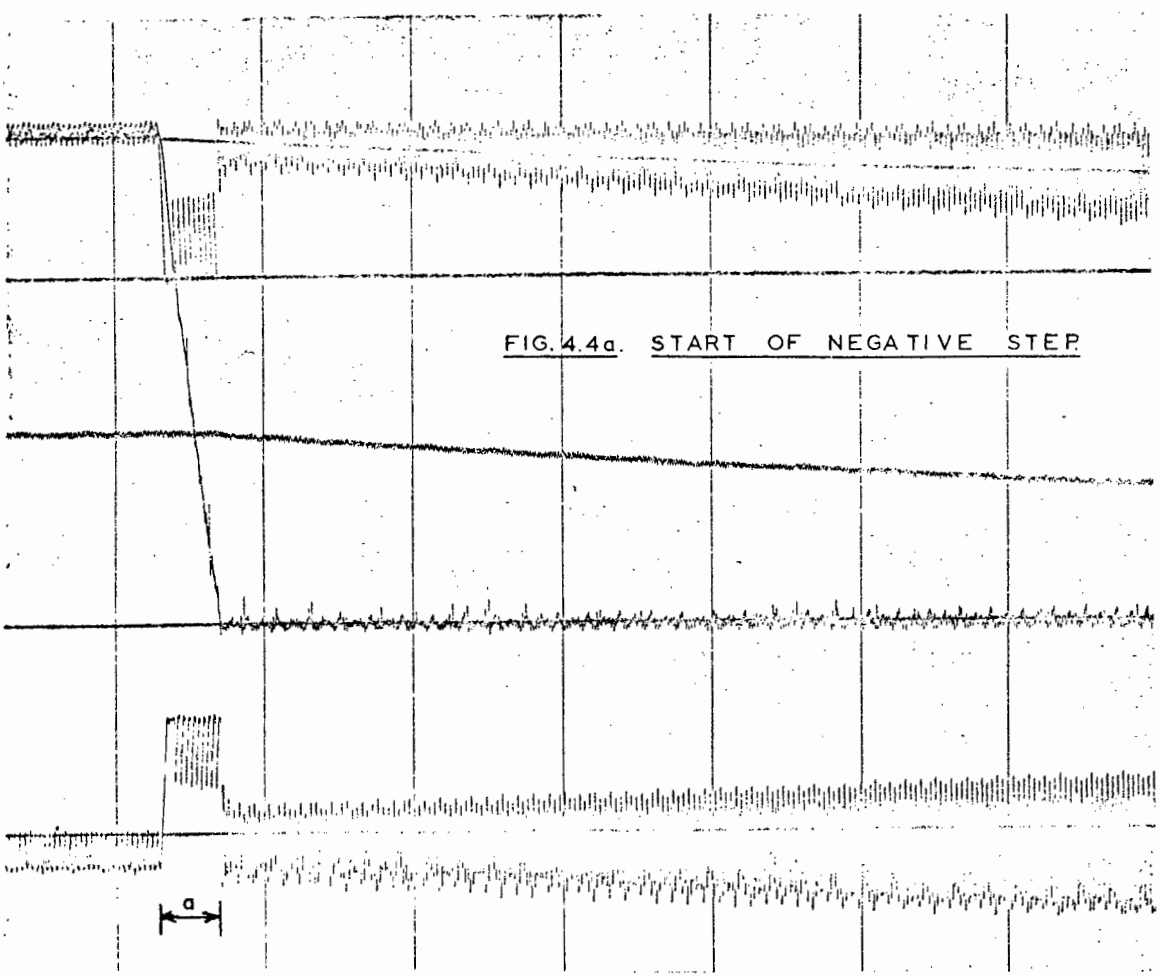

FIG. 4.4a. START OF NEGATIVE STEP

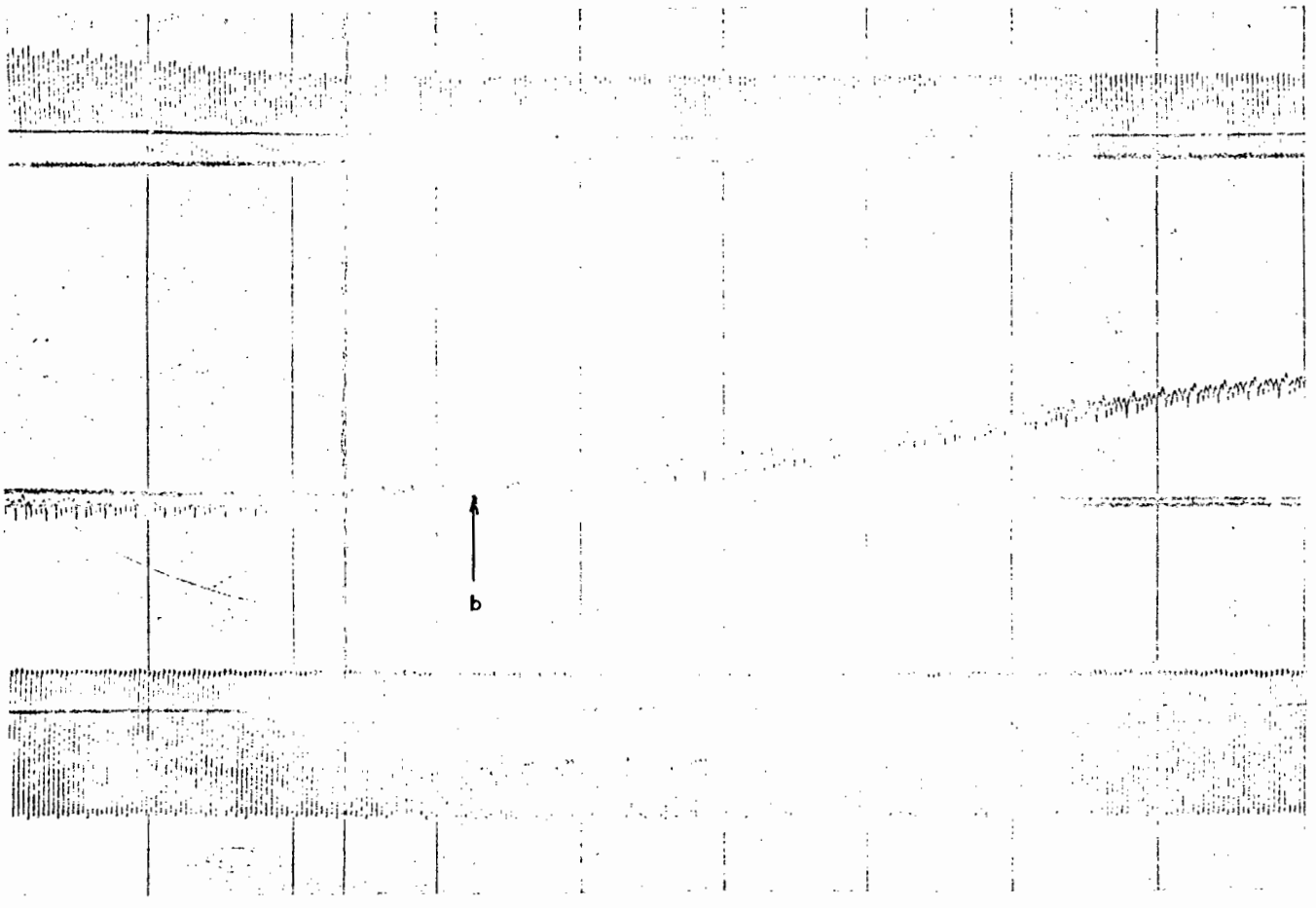

FIG. 4.4b. CURRENT RECOVERY AFTER APPLICATION OF A NEGATIVE STEP.

The waveform displaying anomalous behaviour and giving some cause for concern in fig. 4.4 is the choke voltage, shown expanded in amplitude but on a smaller time scale in fig. 4.5. The large amplitude of this voltage while the average current is zero (see fig. 4.6) indicates a large di/dt for small currents, which could only be attributed to the snubber networks having a "ringing" effect with the choke.

This is borne out by the traces shown in figs. 4.7 and 4.8, which show the traces for a negative step, without the snubbers, with and without the flywheel diode. These traces illustrate the fact that the choke voltage became far smaller while the current was not flowing, and serve to highlight the effects of the flywheel diode.

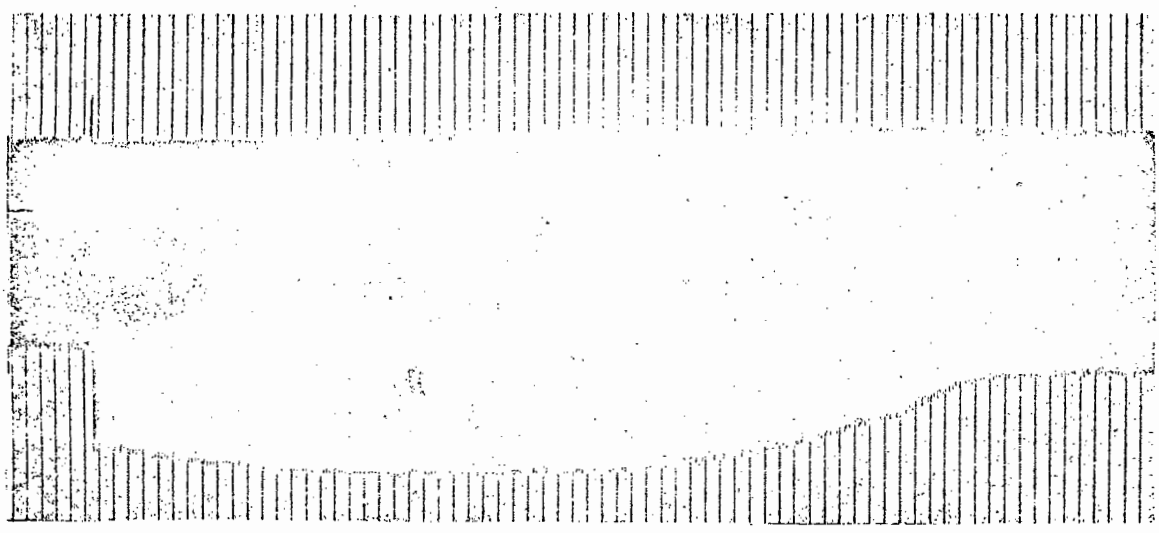

FIG. 4.5. CHOKE VOLTAGE FOR NEGATIVE STEP WITH SNUBBER NETWORKS CONNECTED.

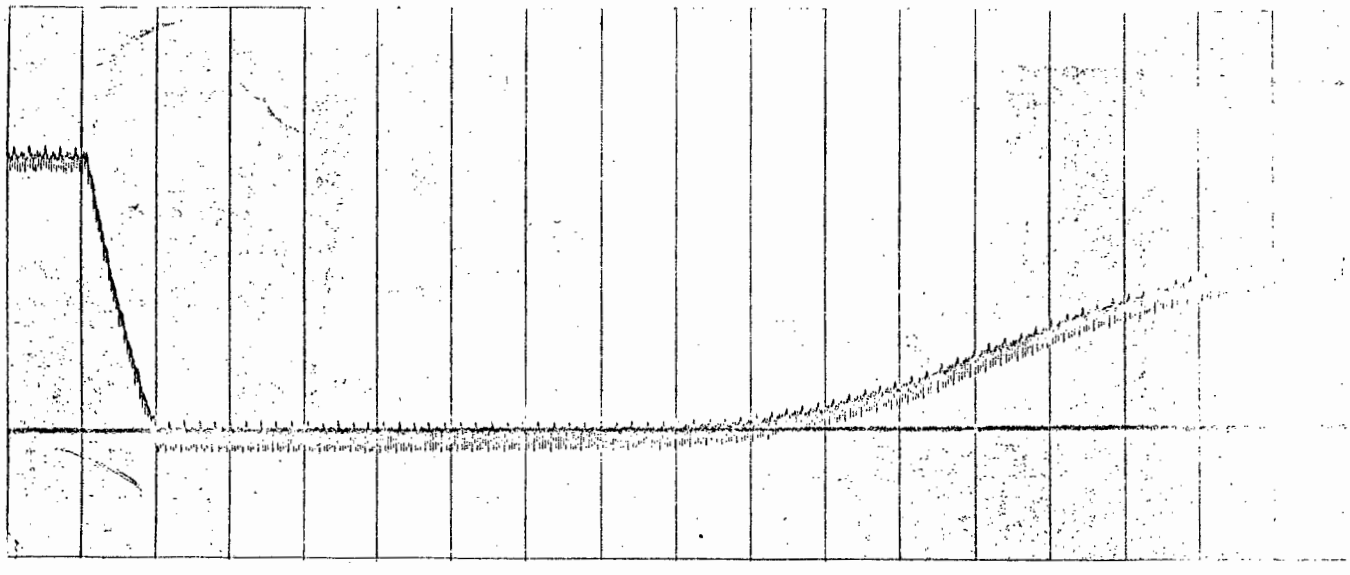

FIG. 4.6. CURRENT FOR NEGATIVE STEP WITH SNUBBER NETWORKS CONNECTED.

NOTE SPIKES WITH HIGH di/dt

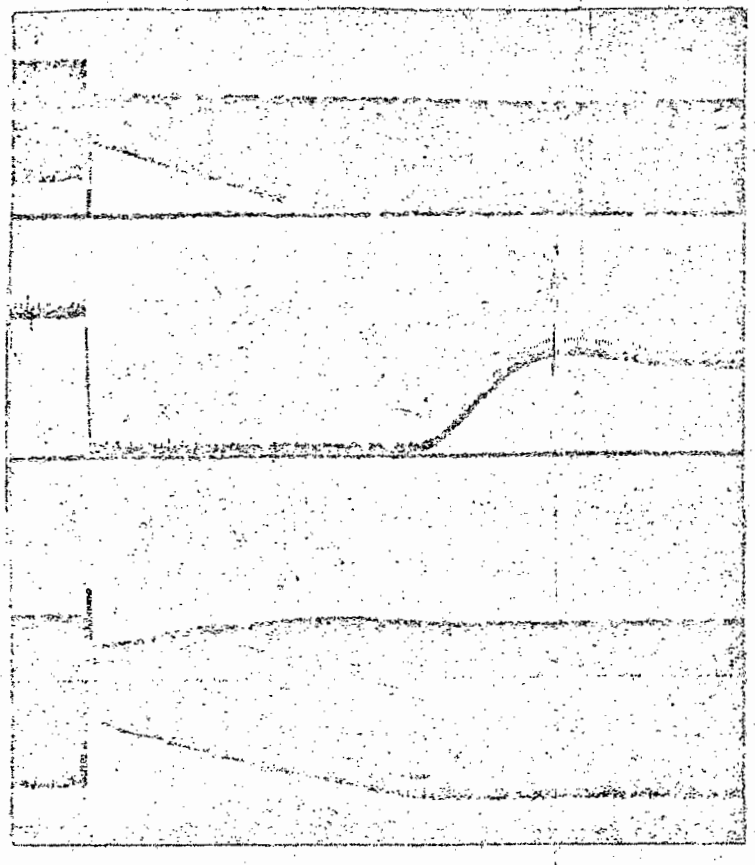

FIG. 4.7.

TRACES OF BRIDGE VOLTAGE, CURRENT AND CHOKE VOLTAGE, WITH FLYWHEEL DIODE CONNECTED AND NO SNUBBER NETWORKS, FOR A NEGATIVE STEP.

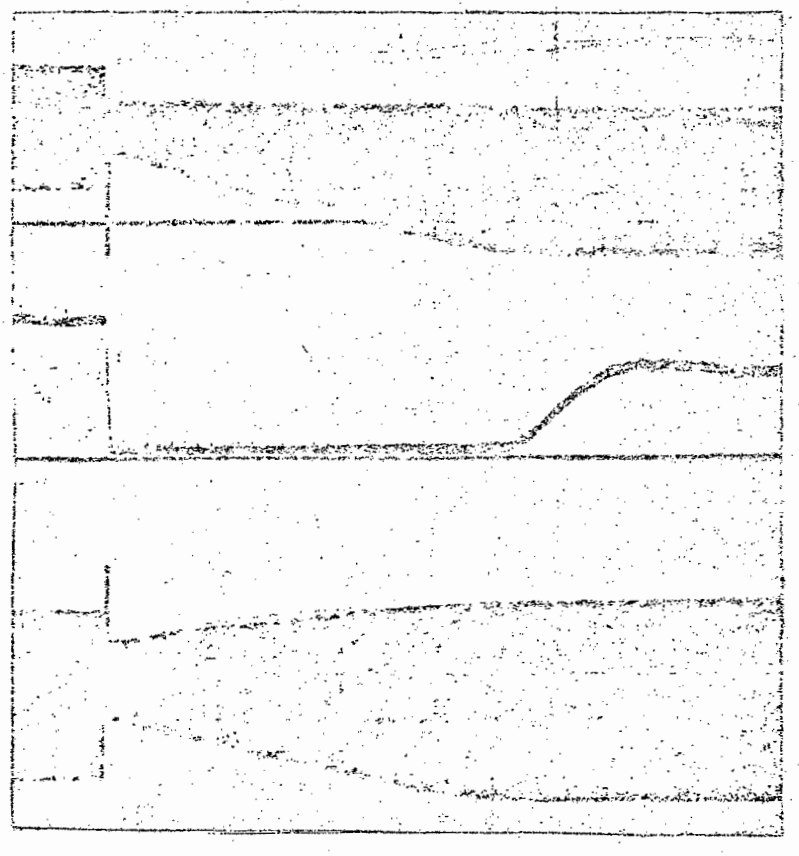

FIG. 4.8.

TRACES AS IN FIG. 4.7, BUT WITH FLYWHEEL DIODE DISCONNECTED.

NOTE THAT CURRENT IS OFF FOR LONGER.

The function of the flywheel diode is to prevent the voltage across the bridge from going negative. This it does by going into a conducting state whenever the instantaneous voltage falls below zero. It therefore, (i) restricts the size of the spike produced across the choke when the current switches off; and (ii) has the effect of causing the current to be turned on again sooner, since the average output voltage must be higher, for the same firing angle setting, if the instantaneous voltage cannot drop below zero.

If it is accepted that, while the current is equal to zero, there cannot be any control, then clearly the prescence of the flywheel diode must improve the controllability of the machine. This aspect is discussed further in section 6.4.

The speed trace for a positive and negative step on no load is shown in fig. 4.9, while fig. 4.10 shows the same trace taken on load. Here it can be clearly seen that the negative step response closely approximates the positive response when the excess energy can be dissipated (in this case in the load), so that the current is only zero for a short time.

4.5. COMMENT.

From the tests mentioned above, the machine constants could be obtained (see appendix 3), so that a mathematical model of the closed loop system could be constructed.

The tests also served to point out the difficulties which might be expected in trying to control this particular system. It could be concluded that, from a control point of view, the most satisfactory system would be one with a flywheel diode and without any snubber networks (although in industrial applications presumably some other sort of surge suppression would be necessary), and preferably running on load.

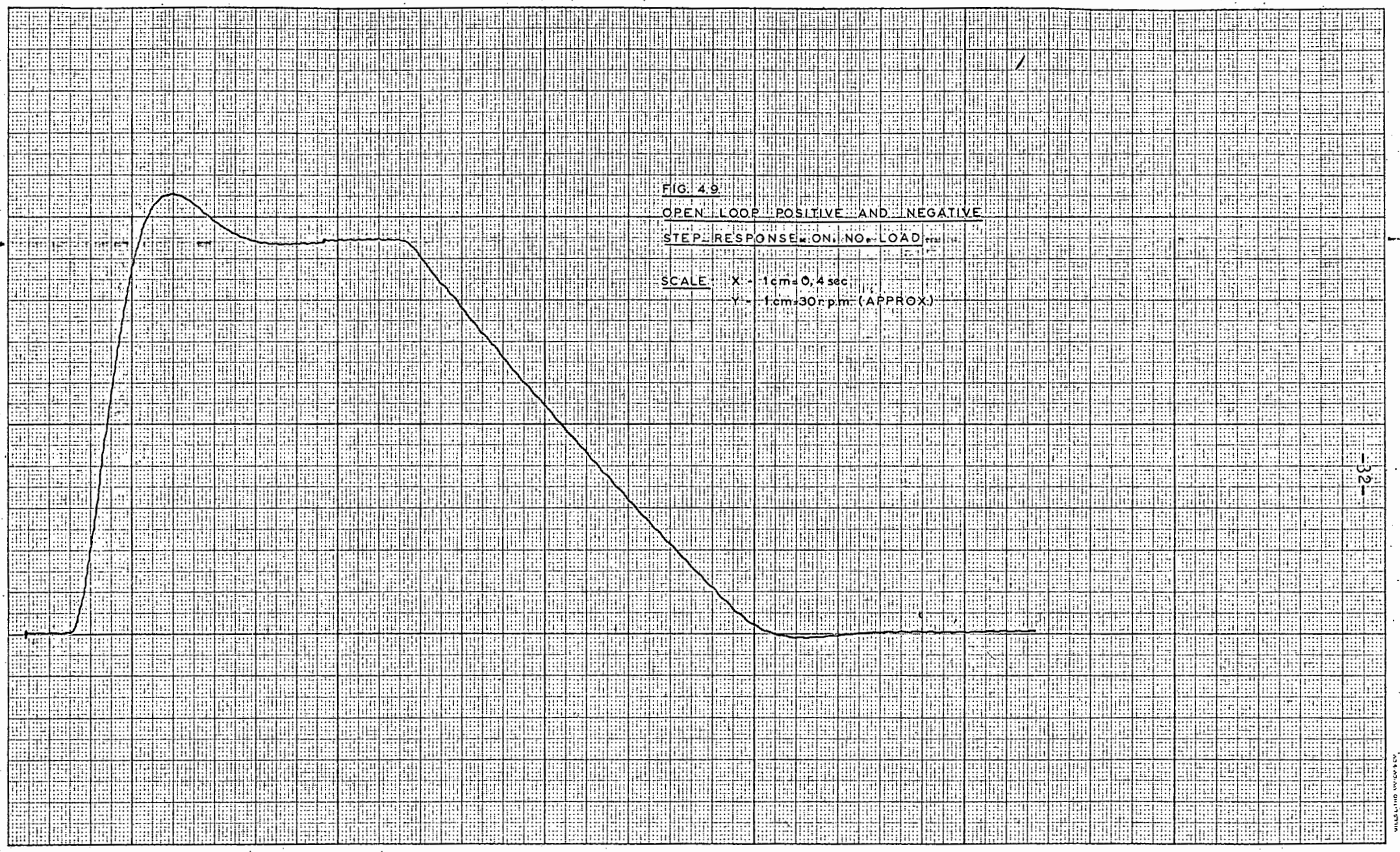

FIG. 4.9

OPEN LOOP POSITIVE AND NEGATIVE STEP RESPONSE ON NO LOAD

SCALE: X - 1 cm = 0,4 sec

Y - 1 cm = 30 r.p.m. (APPROX.)

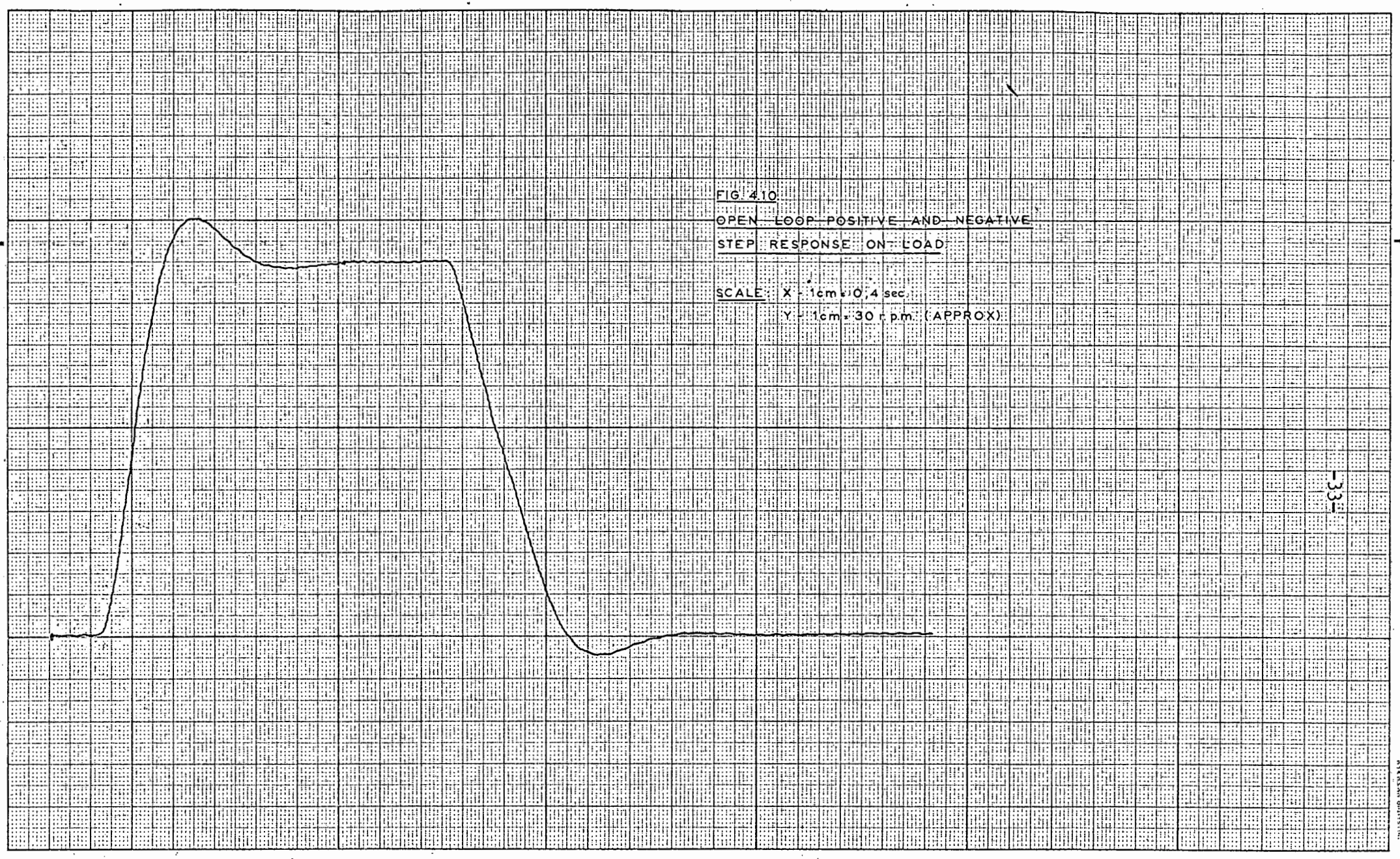

FIG 4.10

OPEN LOOP POSITIVE AND NEGATIVE STEP RESPONSE ON LOAD

SCALE: X - 1cm = 0,4 sec.

Y - 1cm = 30 r.p.m. (APPROX)

CHAPTER 5.

INTRODUCTION TO THE Z-TRANSFORM.

5.1. INTRODUCTION.

One of the significant differences between direct digital and conventional analogue control systems is the fact that in a direct digital control system, such as a computer control system, there is no continuous flow of data. The operation of the computer, by its very nature, involves sampling of an input (in this case speed), and the production of an output (the thyristor firing angles), at discrete sampling intervals. Because of the extremely fast process time of the computer (cycle time for the machine used was 1,8 μsecs), it can be assumed that, for sampling rates of the order of hundreds of milliseconds, the input and output processes occur simultaneously.

The significance of sampled data systems was summed up by Linvill [21] in 1951 as follows:

"If the sampling frequency in a system being supplied intermittent data is high compared with the signal frequency and to the critical frequencies of the system, then the fact that the data are not supplied continuously has no important implications and the whole system behaves essentially as a continuous system. When the sampling frequency cannot be made high enough for this to be true, quite clearly the system will not behave as a continuous system."

The natural frequency of the machine used for this thesis (see appendix 3) was approximately 0,5 Hz. Weehuizen [7], by using sampling frequencies of 8 Hz or more was able to analyse and simulate his system as a continuous system. This thesis set out to investigate the control at lower sampling frequencies (1 - 3 Hz), and here the behaviour could no longer be looked upon as continuous, although the sampling theorem was still being complied with. A study of sampled-data

/..system..

system analysis was therefore necessary in order to be able to model the behaviour of the system, and to analyse its behaviour.

5.2. DEVELOPMENT OF THE Z-TRANSFORM.

The early methods of sampled-data system analysis [21 - 23] compared the sampling process with the process of amplitude modulation of the input signal, and performed the system analysis in the frequency domain.

The conventional Laplace transform approach to the analysis of control systems was extended to that of sampled-data control systems by the development of the z-transform [24 -27].

The z-transform may be defined as follows [28]:

The output of an ideal sampler when subjected to an input e(t) in defined as:

$$e^*(t) = \sum_{n=0}^{\infty} e(nT)\delta(t-nT) \qquad \text{.....(5.1)}$$

where $\delta(t)$ is the Dirac delta function.

This output can thus be looked upon as a train of impulses whose respective impulse strengths are equal to the magnitude of e(t) at the corresponding sampling instants t = nT (fig.5.1)

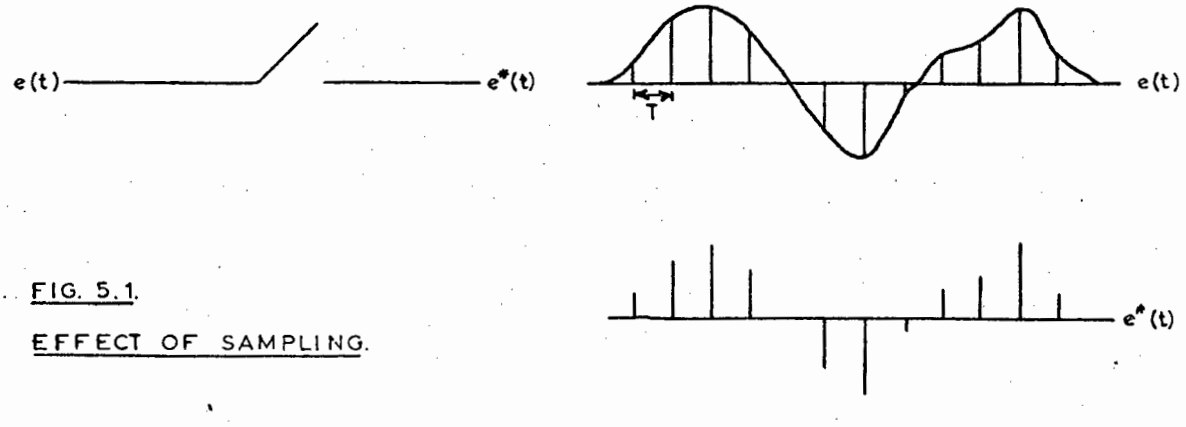

FIG. 5.1.
EFFECT OF SAMPLING.

It should be remembered that, according to the sampling theorem, the frequency of sampling must be at least twice the maximum frequency contained in the signal being sampled in order that no information be lost.

The Laplace transform of $e^*(t)$ may be obtained as follows:

$$E(s) = \sum_{n=0}^{\infty} e(nT)e^{-nTs} \quad \ldots\ldots\ldots\ldots\ldots\ldots (5.2)$$

$$\text{Let } z = e^{Ts} \quad \ldots\ldots\ldots\ldots\ldots\ldots\ldots\ldots (5.3)$$

$$\text{Then } E(s) = E(z) = \sum_{n=0}^{\infty} e(nT)z^{-n} \quad \ldots\ldots\ldots\ldots (5.4)$$

i.e. $E(z)$ is the Laplace transform of $e^*(t)$ with $s = (1/T)\ln(z)$

In general, any continuous function that has a Laplace transform will also have a z transform. Thus a transfer function of s will have a z transform, and the output $C(z)$ when an input signal $R(z)$ is applied to such a transfer function $G(z)$ can be obtained by:

$$C(z) = G(z)R(z) \quad \ldots\ldots\ldots\ldots\ldots\ldots\ldots (5.5)$$

provided that it is the input signal $r(t)$ that is being sampled.

The time sequence corresponding to such a function $C(z)$ can be derived by expanding $C(z)$ as a power series in z^{-1}. Each term will then correspond to the time function at a particular sampling instant. This fact, while providing a comparatively simple method of deriving the time sequence, also serves to highlight one of the major drawbacks of the z-transform method of analysis as originally developed, namely that it only served to describe the behaviour of the system under consideration at the instants of sampling.

5.3. THE MODIFIED Z-TRANSFORM.

The development of the modified z-transform [25,31,32] helped to eliminate the difficulty mentioned above and contributed to the more widespread use of the z-transform method of sampled-data system analysis.

To quote Jury [32]: "..with the advent of the modified z-transform method, the limitations of the z-transform method are completely removed and.... it is now possible to design any sampled-data control system to obtain all of the design information to complete analogy with continuous systems."

The modified z-transform method [29] may be described by the delay of a continuous function by a time dt, where d is non-integral. An integer n is chosen, such that it is the next highest integer after d.

Then m is defined as:

$$n = d+m \quad \ldots\ldots\ldots\ldots\ldots\ldots \quad (5.6)$$

where m is a positive number less than unity.

If F(s) is the Laplace transform of f(t), then the Laplace transform F(s,d) of the delayed function is:

$$L(f(t-dT)) = F(s,d) = F(s)e^{-dTs} \quad \ldots\ldots\ldots\ldots \quad (5.7)$$

$$= e^{-nTs}F(s)e^{mTs} \quad \ldots\ldots\ldots\ldots\ldots \quad (5.8)$$

$$\text{Then } F(z,d) = z^{-n}F(z,m) \quad \ldots\ldots\ldots\ldots\ldots\ldots \quad (5.9)$$

where F(z,m) is defined as the z transform of $F(s)e^{mTs}$.

Tables of z transforms and modified z transforms are readily available [29,30].

5.4. BLOCK DIAGRAMS AND TRANSFER FUNCTIONS.

The block diagram algebra of sampled-data control systems is affected to a large extent by the position of the samplers in the systems [30]. Fig. 5.2 shows, in block diagram form, the

/..system..

system used for this thesis.

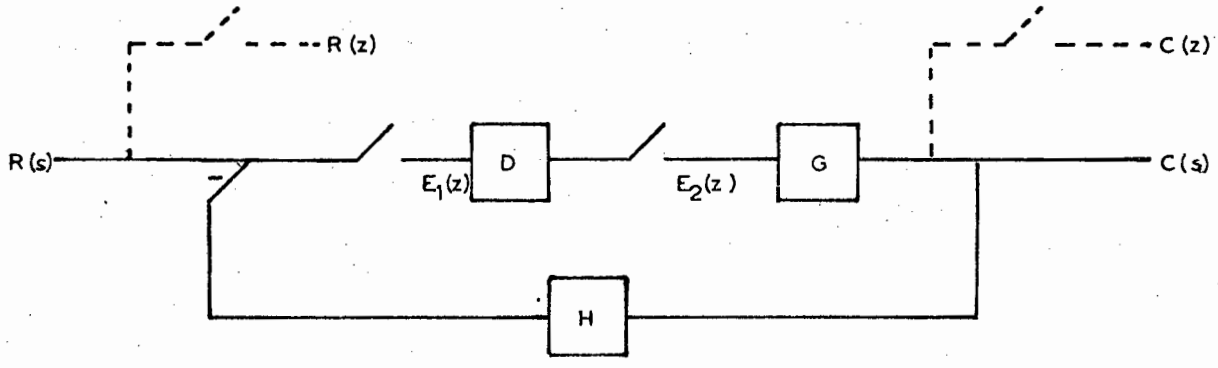

FIG. 5.2.

BLOCK DIAGRAM OF FEEDBACK CONTROL SYSTEM.

D represents the digital computer, while G represents the thyristor bridge and motor. H is the feedback transfer function. The ficticious samplers on the input and output serve to indicate that the functions R(z) and C(z) represent the input and output respectively only at sampling instants.

This system may be shown to have a transfer function [30]:

$$C(z) = \frac{D(z)G(z)}{1 + D(z)GH(z)} \; R(z) \quad \ldots\ldots\ldots\ldots \quad (5.11)$$

or, using the modified z-transform:

$$C(z,m) = \frac{D(z)G(z,m)}{1 + D(z)GH(z)} \; R(z) \quad \ldots\ldots\ldots\ldots (5.12)$$

Clearly, D(z) will not have a modified z-transform, since the computer only acts at sampling instants.

5.5 STABILITY.

Because of the fact that the left half plane in the s plane is mapped on to the unit circle in the z plane [26], it is a condition for the stability of a closed loop sampled-data control system that the closed loop poles lie within the unit circle in the z plane.

5.6. COMMENT.

The z-transform method of analysis was used to analyse the behaviour of the system used in this thesis, and as a design tool in the provision of compensation (see chapter 7). Once the parameters of the system had been fairly accurately measured, it was not particularly difficult to find the z-transform of the entire system (see appendix 4).

In particular, the use of a power series expansion proved an extremely useful method of prediction of speed waveforms, particularly when the modified z-transform was used.

CHAPTER 6.

INTEGRAL CONTROL.

6.1. INTRODUCTION.

The first type of control procedure to be adopted made use of the computer as a simple integrator having a variable gain. This had the advantage of being fairly straightforward to simulate. In particular, as the computer had such a simple transfer function, the model of the machine itself could be tested and hence the degree of error introduced estimated.

It was felt that this was necessary before any type of compensation could be introduced since, according to Zinober [33], any small variation in the parameters, when implementing a digital compensation program, might lead to instability. This aspect is discussed further in section 7.5.

6.2. THE MACHINE TRANSFER FUNCTION.

In section 4.2 and appendix 3, the machine transfer function is shown to be:

$$G_1(s) = \frac{K_T/JL}{s^2 + s(R/L) + (K_V K_T)/(JL)} \quad \ldots\ldots(6.1)$$

The thyristor bridge had a gain K', which, as shown in fig. A3.3, can be assumed to be constant over the working range of voltages. The bridge can be looked upon as a perfect zero order hold [30], in that it holds a steady output proportional to the input, at least over the working range, and that it changes its value virtually instantaneously as the input changes. This fact was made use of during the open loop tests, when a step could be applied in either direction merely by changing the firing angle.

Such a device has a transfer function of the form:

$$G_2(s) = \frac{K'(1-e^{-Ts})}{s} \quad \ldots\ldots\ldots\ldots\ldots\ldots (6.2)$$

Thus the total open loop transfer function of the bridge and motor is given by:

$$G(s) = G_1(s)G_2(s) \quad \ldots\ldots\ldots\ldots\ldots\ldots (6.3)$$

The z-transform of this function is given by:

$$G(z) = \frac{K_1}{a^2 + b^2} \left\{ \frac{z(1 - e^{-aT}(\cos bT + a/b \sin bT))}{z^2 - 2ze^{-at}\cos bT + e^{-2aT}} - \frac{e^{-aT}(\cos bT - a/b \sin bT - e^{-aT})}{z^2 - 2ze^{-aT}\cos bT + e^{-2aT}} \right\} \quad (6.4)$$

where $K_1 = \frac{K'K_V}{JL}$

$a = \frac{R}{2L}$

$b = \sqrt{\frac{K_V K_T}{JL} - \frac{R^2}{4L^2}}$

T = sampling time.

The full derivation of this transfer function is shown in appendix 4.

It can be seen from equation (6.4) that the poles and zero of G(z) vary with the sampling rate. Therefore it was considered necessary to compute the position of these in the z plane for varying values of T. As mentioned in section 5.5, closed loop poles lying within the unit circle would be an indication of stability, and thus the position of the open loop poles would be of interest.

Table 6.1 shows the variation in gain and the positions of the zero and poles as the sampling time is changed. The poles are always imaginary, but, as fig. 6.1 shows, remain within the unit circle.

TABLE 6.1

J= .64 KV= 1.37171

TIME	GAIN	ZERO	REAL P	IMAG P
.3	1.01681	.625543	.303794	.403843
.4	1.49791	.526838	.132841	.379972
.5	1.92607	.437394	8.88242E-03	.320496
.599999	2.27068	.356094	-7.07994E-02	.24537
.699999	2.5221	.282371	-.113093	.1698
.799999	2.68504	.216097	-.126732	.100951
.899999	2.77285	.157471	-.1206	4.59493E-02
.999999	2.80274	.106882	-.102639	5.68762E-03

The open loop response of the system could be predicted by multiplying G(z) by a unit step input function and taking a power series expansion of the resulting C(z). (See equation 5.5)

The result of such a power series expansion of C(z) for R(z) given by z/(z-1), the z transform of the unit step 1/s, is shown in fig. 6.2. Clearly, the sampling rate would not affect the shape of this curve, which follows the actual open loop response curve, fig. 6.3, almost exactly. The actual overshoot is about 1% greater than calculated, and the time to reach this maximum is almost identical (it is not possible to tell exactly where the step was applied on the trace of figure 6.3).

Appendix 5 shows the mathematical derivation of the output function and the time sequence represented by this, as shown in fig. 6.2.

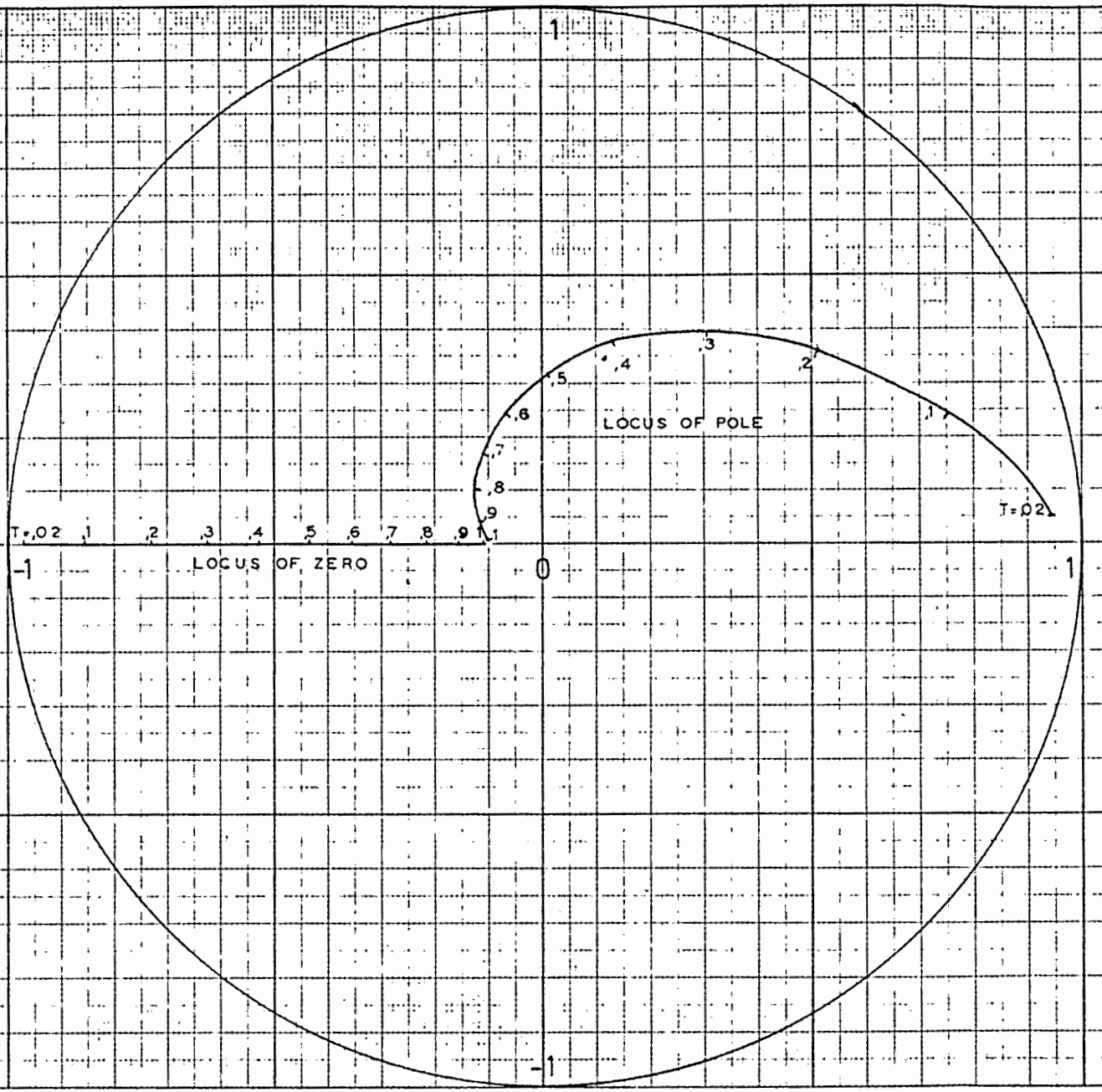

FIG. 61.
LOCUS OF POLES AND ZERO OF G(z), THE MOTOR-BRIDGE TRANSFER FUNCTION, IN THE Z-PLANE, FOR VARYING SAMPLING RATE

LOCUS FOR POLE SHOWN HAS A MIRROR IMAGE FOR NEGATIVE IMAGINARY VALUES.

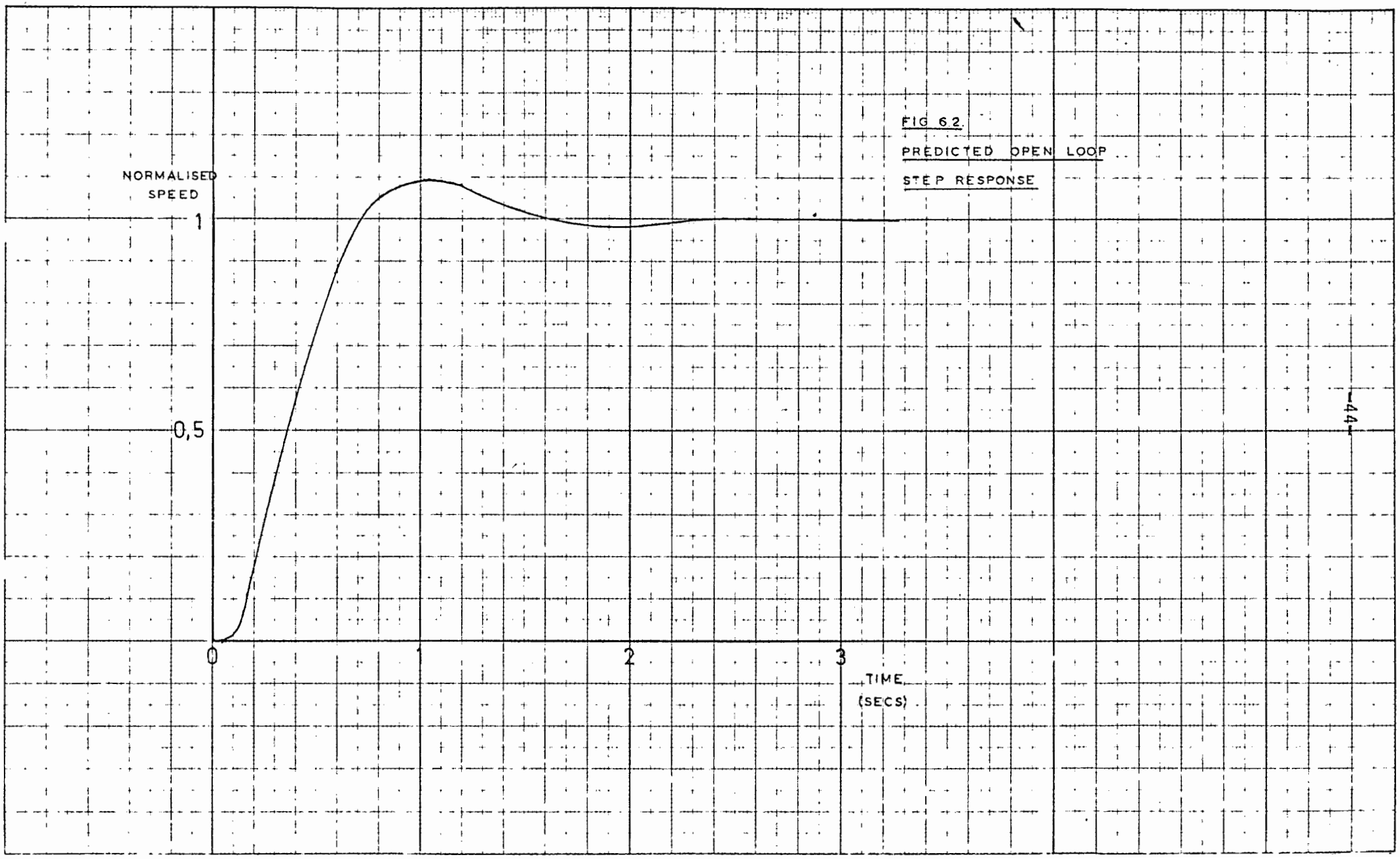

FIG 6.2.
PREDICTED OPEN LOOP STEP RESPONSE

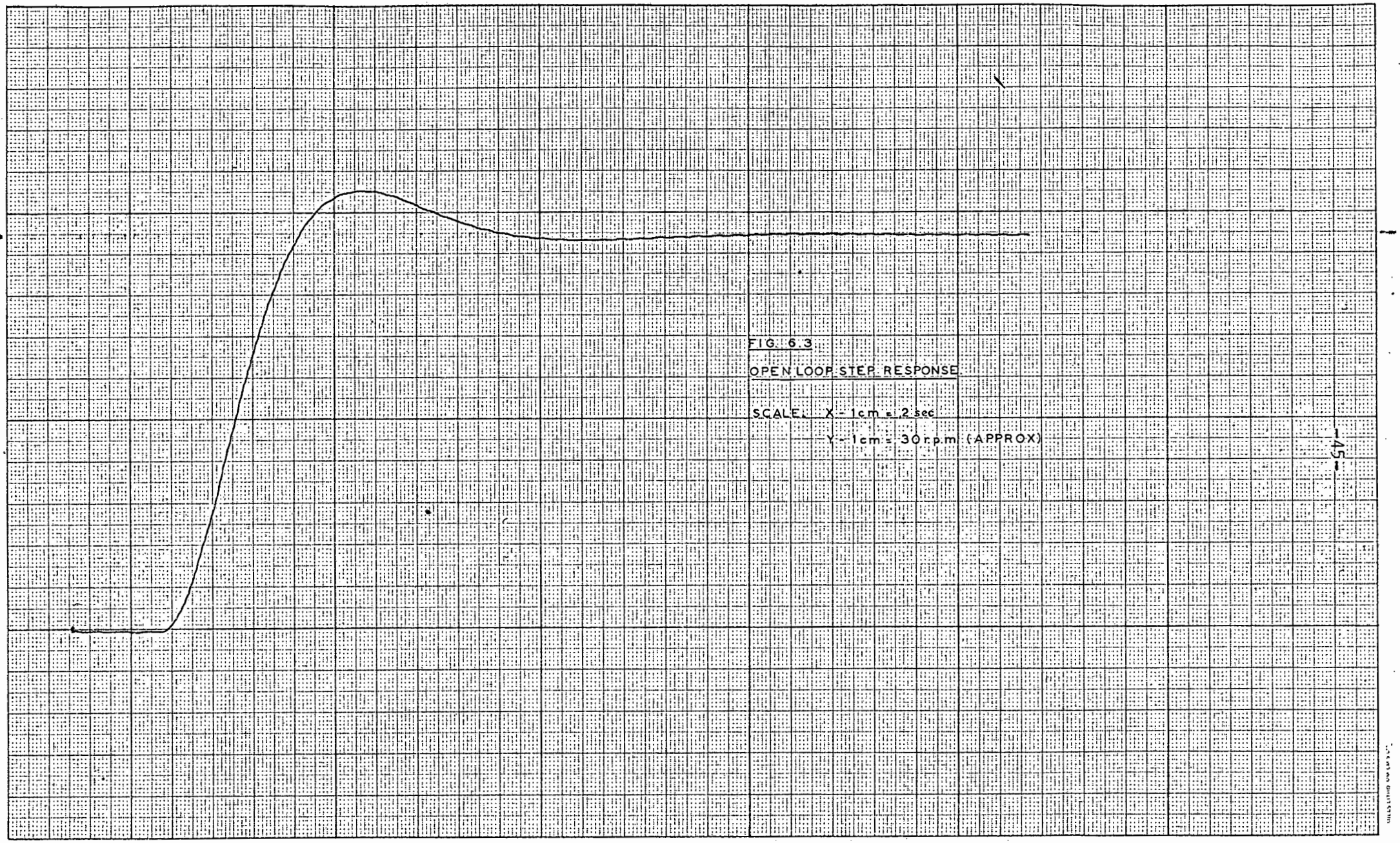

FIG. 6.3

OPEN LOOP STEP RESPONSE

SCALE. X - 1 cm = .2 sec

Y - 1 cm = 30 r.p.m. (APPROX)

6.3. DIGITAL SIMULATION OF THE CLOSED LOOP SYSTEM.

It was required to simulate the behaviour of the system, with the computer acting as an integrator, for various sampling rates and at various gains. This was to be done using the z-transform method; by establishing the closed loop transfer function, multiplying this by an input function (in this case a unit step) and deriving the time sequence of the output by means of a power series expansion of the output C(z) in z^{-1}.

Initially, the z-transform was used, but this can only give expected values at sampling instants (see section 5.2). The mathematical calculations for this were sufficiently simple for these to be carried out on the Varian computer, using a BASIC compiler. The results thus obtained helped to confirm whether the method used was correct or not, but gave insufficient results, as the performance between sampling instants, particularly at lower sampling rates, was required.

More complete results were obtained using the modified z-transform (see appendix 4), but this method was too complex for the limited storage capacity of the BASIC compiler. The system was therefore simulated on the Univac 1106 computer in the computer centre at the University of Cape Town, using FORTRAN.

In all simulations, and in the actual implementation of integral control, a gain figure K was specified. This value referred to the speed error required to cause a change of 1 in the firing angle setting, eg. if the error at any time was 16 r.p.m., then a gain figure K of 8 would cause the setting to be altered by 2, while if K was 16, the angle was altered by 1. Clearly, in the simulation, the actual gain of the integrator had to be modified to take into account conversion from radians per second (the output speed dimension given by the transfer function) to r.p.m. (the speed read by the computer from the digital tachometer), and to convert the firing

/..angle..

angle setting to degrees (since the bridge gain derived in appendix 3 was in volts per degree).

The mathematical derivations of the transfer function output as a function of z, and the power series expansion, are shown in appendix 6.

In all cases, m was varied from 0,1 to 1,0 in steps of 0,1, to give 10 values of the output between each sampling instant. K was varied from 8 to 24 in steps of 4. By the nature of the program and the definition of K, values of K of more than 20 would introduce a large amount of quantization error (an error of at least 11 r.p.m. would be required to make any change in the output for K = 20). In addition, the predicted curves showed these responses to be sluggish. For these reasons, only values of K between 8 and 16 were used in practice.

The results of these simulations, for sampling times ranging from 0,3 to 1 second, are shown in figures 6.4 to 6.12, interspersed with the actual curves obtained. The scale in all these curves is 1cm = 0,2 seconds on the x axis, and 1cm approximately = 30 r.p.m. on the y axis. In all cases, the degree of overshoot depends on K, i.e. the curve with the greatest overshoot is for K = 8, and the most damped curve is that predicted for K = 16. The upper sampling limit of 1 sec. was imposed by the sampling theorem, since the natural frequency of the machine (see appendix 3) is 3,19 rads per sec, or approximately 0,5 Hz.

From the results obtained, it can be seen that the stability and amount of overshoot expected were functions of both the gain and the sampling rate. It is interesting to note that the amount of overshoot predicted at the highest gain figure used, i.e. K = 8, showed a distinct minimum at a sampling rate of the order of 0,6 seconds, although for lower gains the amount of overshoot anticipated decreased, until extremely overdamped responses could be expected at low gains and low sampling rates.

6.4. IMPLEMENTATION OF DIGITAL CONTROL.

In order to be able to vary the sampling rate, the program was written to operate in the interrupt mode. This interrupt signal was supplied by a pulse generator, and the frequency of sampling could thus be varied at will. The effect of integration was obtained by varying the output by an amount proprtional to the difference between the reference and actual speeds, until this error was zero, or small enough to be neglected.

Appendix 7 shows the flow diagram for the integral control program. It should be noted that initially a limit was placed on the size of any one variation in the firing angle setting, in order to limit the rate of change of current across the thyristors. In the final program, this was set at $\pm$ 40, which in practice was bigger than any step required, except at very high gains. No step of more than 400 r.p.m. was applied for the same reason, and the tests whose results are shown were all run between 500 and 800 r.p.m. This range also ensured that the machine was operating over the linear range of the thyristor bridge transfer function. However, it should be noted that if the behaviour was not restricted to the linear region, the gain of the bridge would be decreased, with consequent increase in stability.

It should also be noted that the tachometer ripple effect described in chapter 3 had to be taken account of and compensated by the allowance of a dead band. In practice, this dead band was found to be of the order of $\pm$12 r.p.m., i.e. any error smaller than 12 r.p.m. would be regarded as zero.

Despite this, however, the speed generally settled down much closer to the desired value than within 12 r.p.m., as table 6.2 shows. This table lists a sequence when an input step of 300 r.p.m. was applied, at a sampling rate of 0,6 secs with K = 12 and shows the speed read and the action taken (i.e. the firing angle set). The first value shown is that present before the step was applied.

TABLE 6.2

SPEED	SETTING
497	130
502	105
772	103
825	105
793	104
788	104
799	104
802	104
802	104
801	104
799	104
801	104

The results obtained on load for various sampling times with gains of 8, 12 and 16 are shown on figs. 6.4 to 6.19, along with the predicted curves. It must be noted that it was again impossible to control the exact point on the traces where the step originated. This was in part attributable to the method of applying the step, which was:

(i) The interrupt was disabled.

(ii) The new speed was typed in and stored as the reference.

(iii) The interrupt was re-enabled.

The time before the next interrupt pulse occurred was thus variable.

Comparison with the predicted results shows excellent correlation from a time point of view, and that generally the overshoot obtained was snaller than had been anticipated - a factor probably largely caused by the damping effect of the load. This also led to the conclusion that the component values inserted into the mathematical model were trustworthy, and that the model used gave a good enough approximation to reality for it to be used in the implementation of the compensation programs.

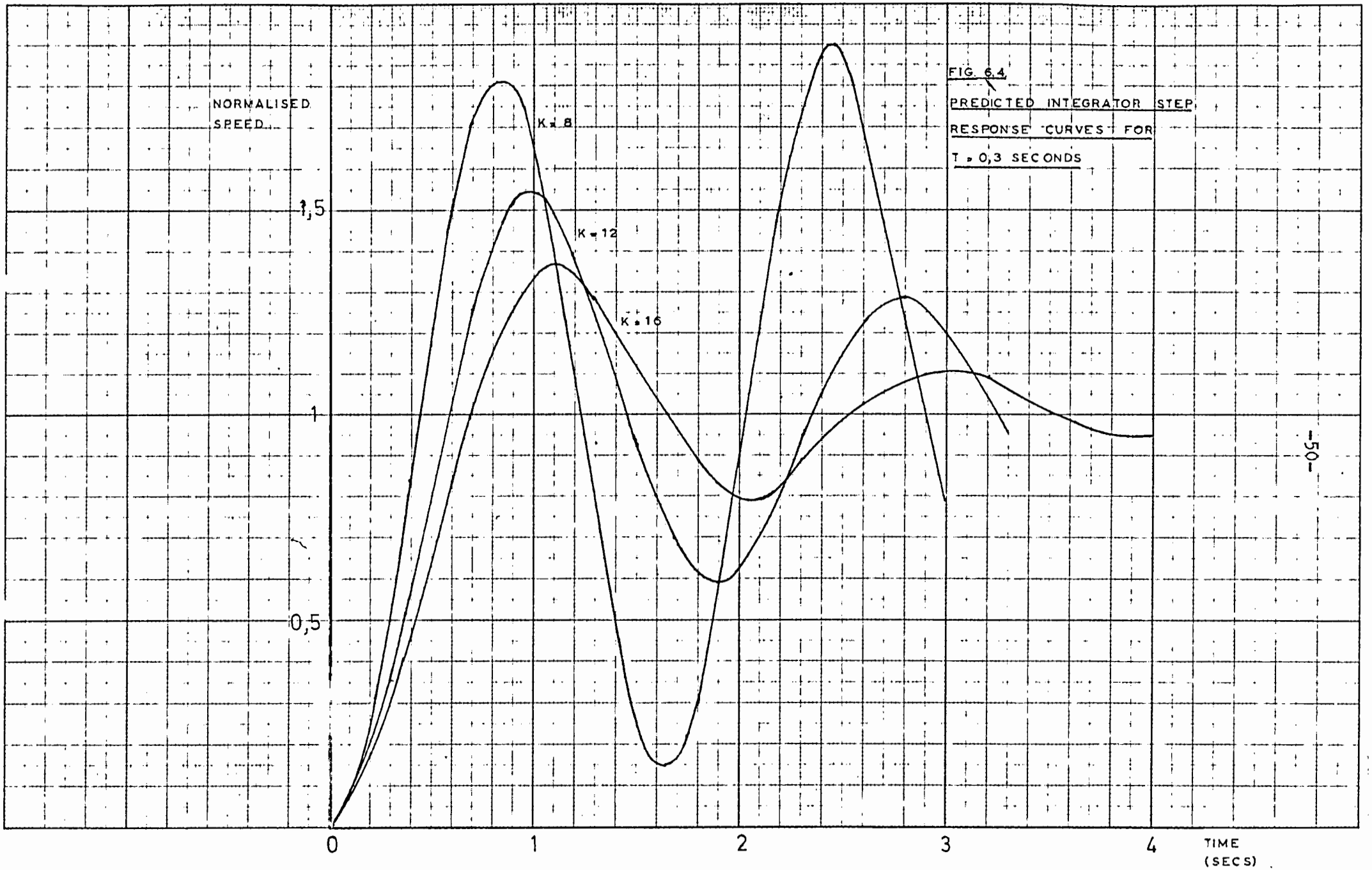

FIG. 6.4
PREDICTED INTEGRATOR STEP RESPONSE CURVES FOR T = 0,3 SECONDS

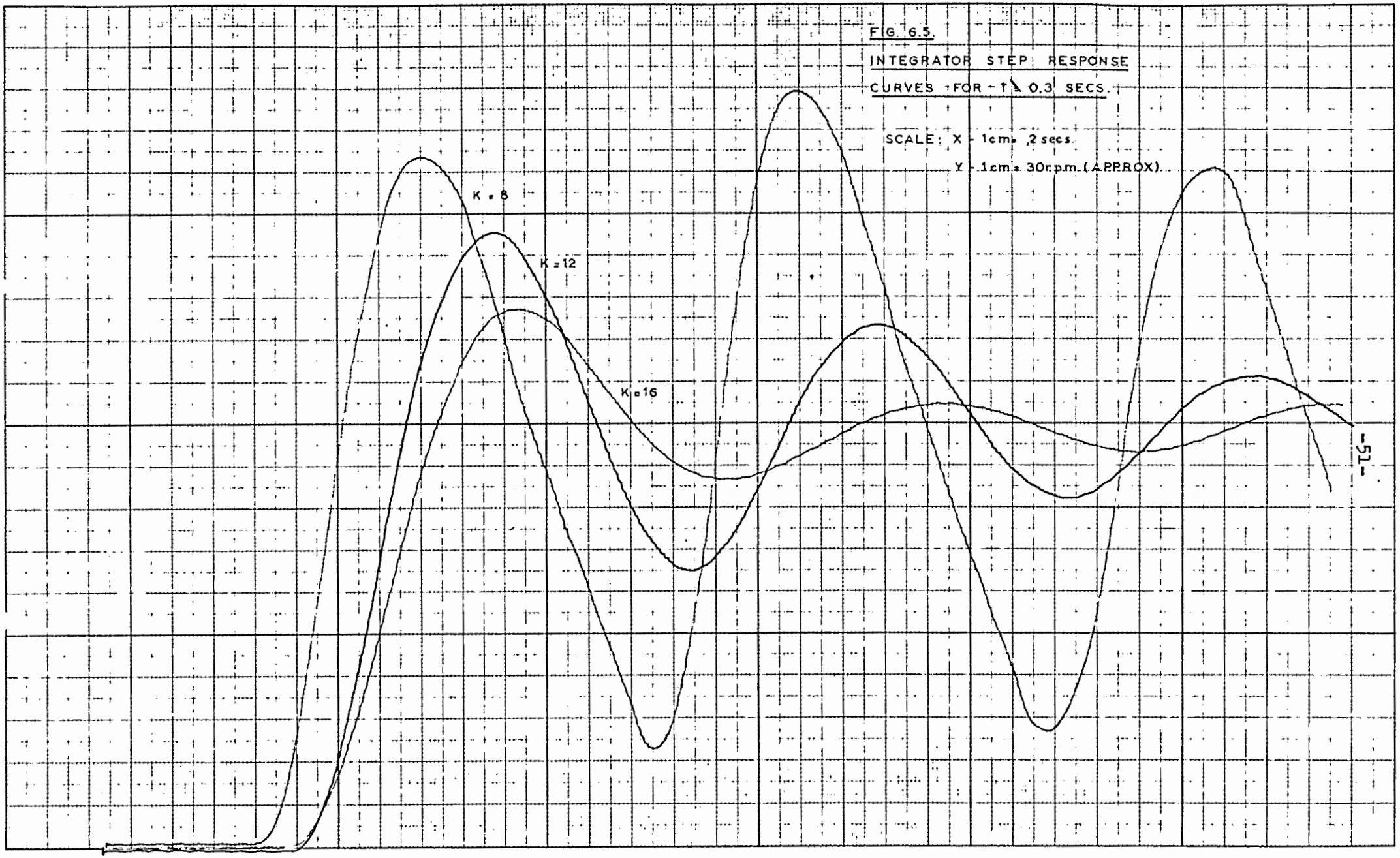
FIG. 6.5.
INTEGRATOR STEP RESPONSE
CURVES FOR T = 0.3 SECS.
SCALE: X - 1cm = .2 secs.
Y - 1cm = 30r.p.m. (APPROX).
K = 8
K = 12
K = 16

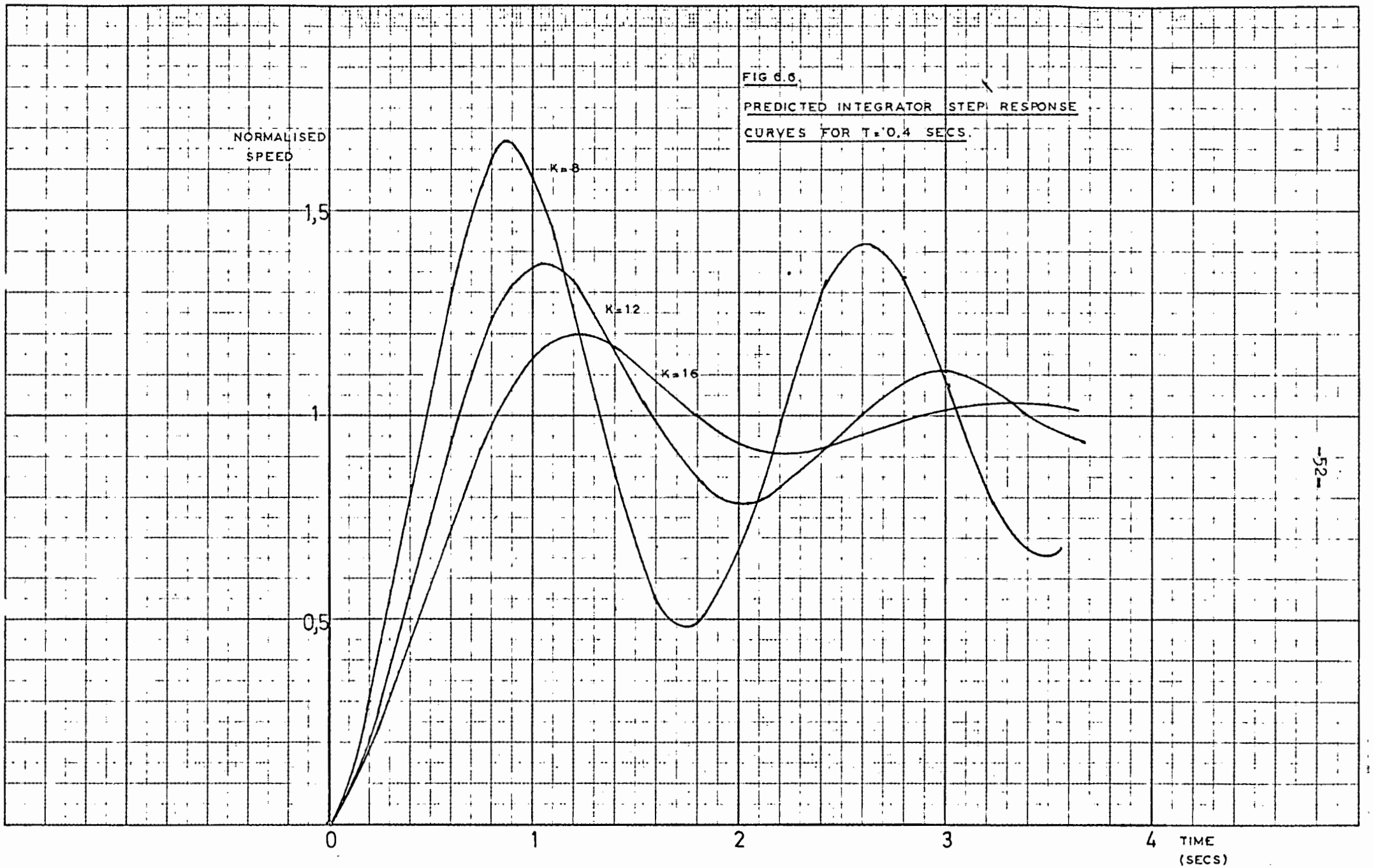

FIG 6.6.
PREDICTED INTEGRATOR STEP RESPONSE CURVES FOR T=0,4 SECS.

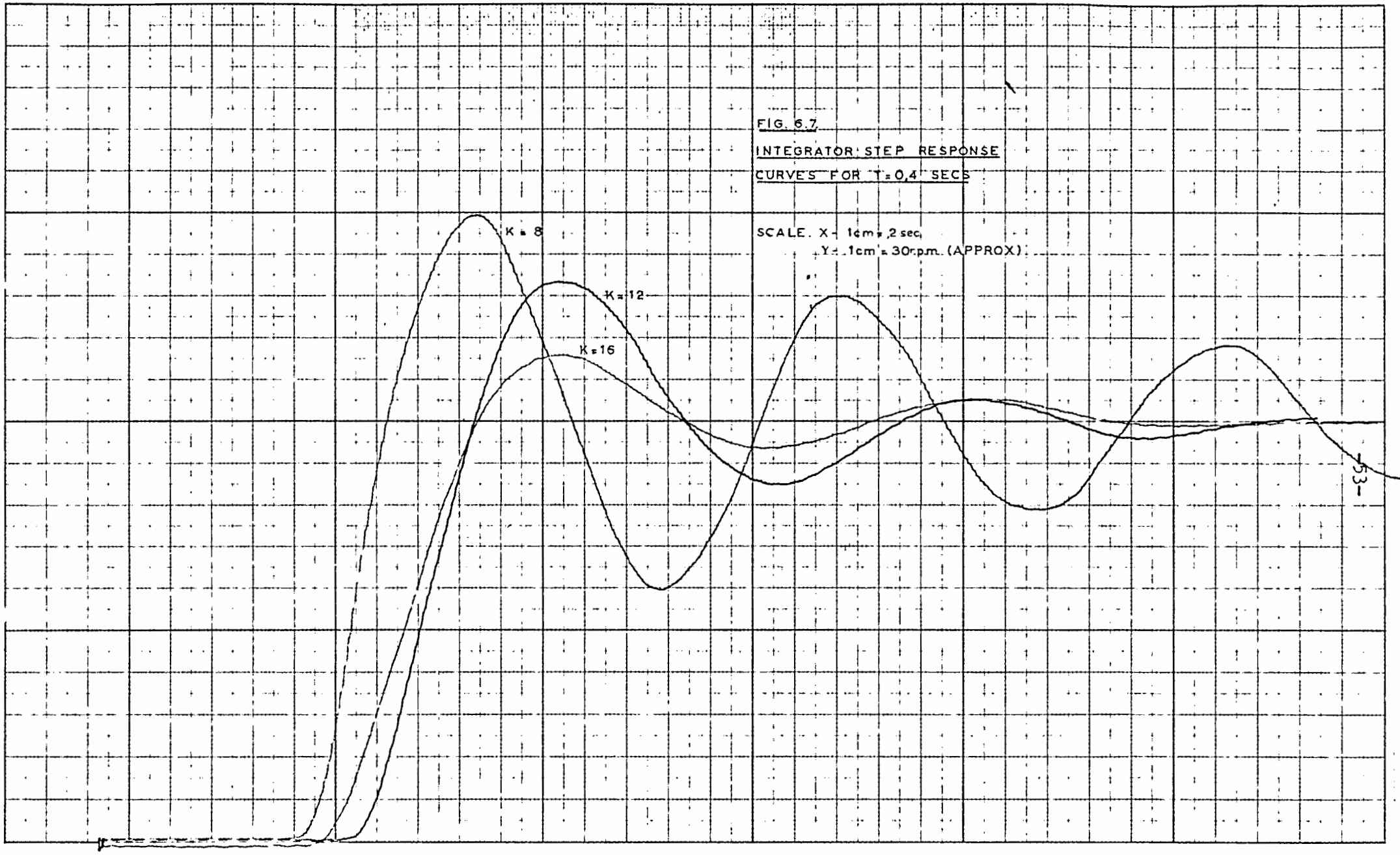

FIG. 6.7

INTEGRATOR STEP RESPONSE CURVES FOR T = 0,4 SECS

SCALE. X - 1cm = ,2 sec
Y - 1cm = 30r.p.m. (APPROX).

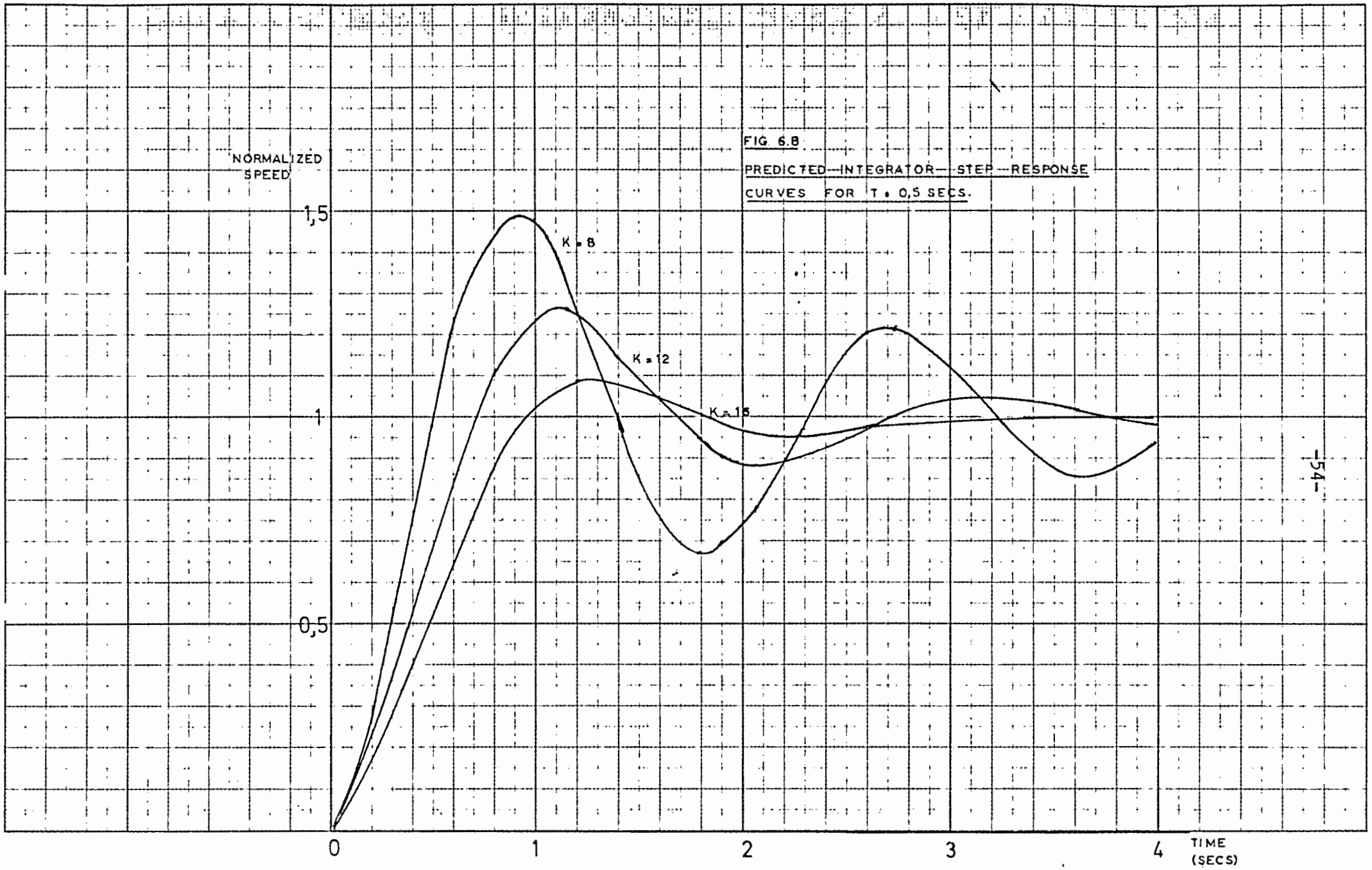

FIG. 6.8
PREDICTED INTEGRATOR STEP RESPONSE CURVES FOR T = 0,5 SECS.

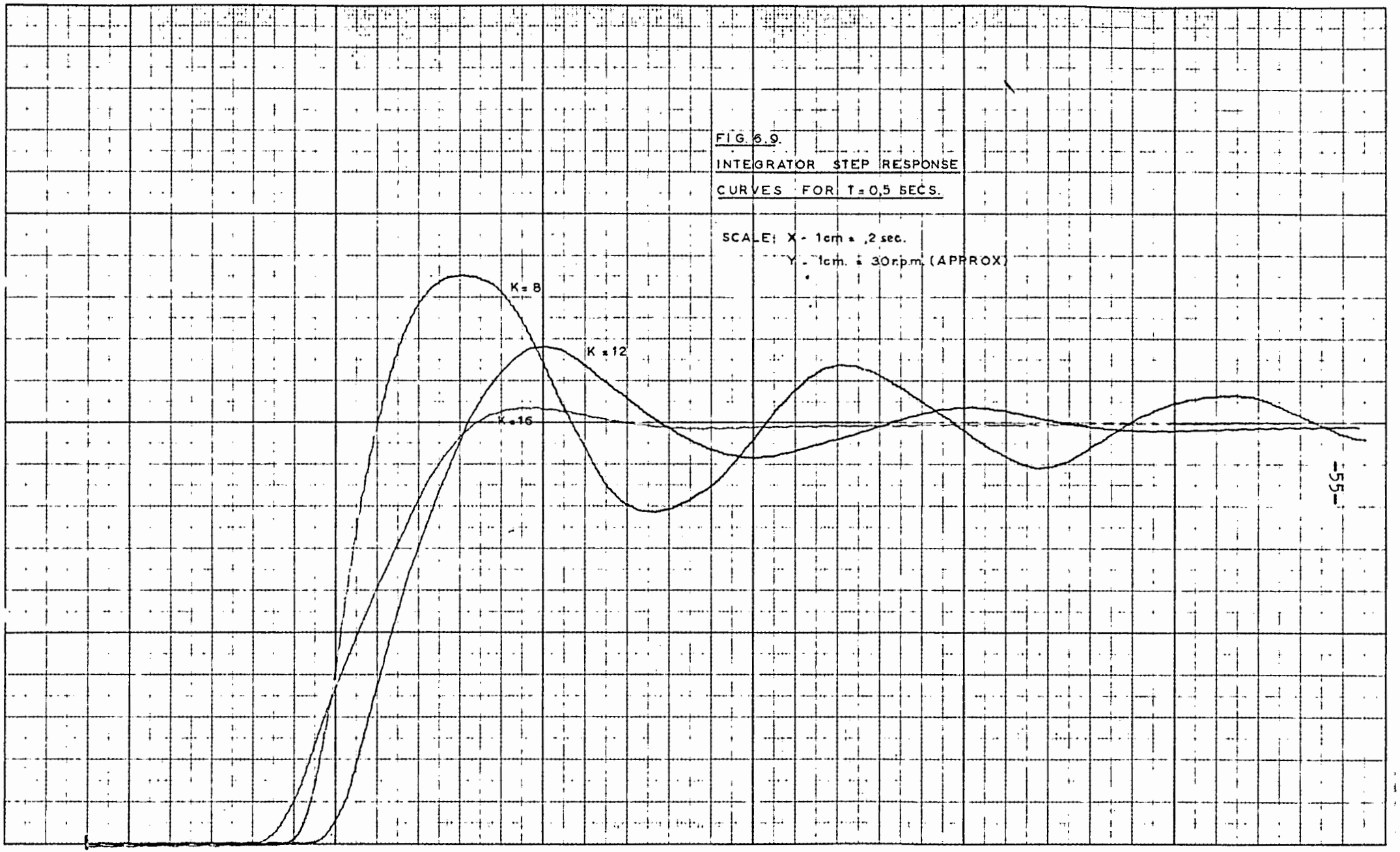
FIG 6.9.
INTEGRATOR STEP RESPONSE
CURVES FOR T = 0,5 SECS.
SCALE: X - 1cm = ,2 sec.
Y - 1cm. = 30r.p.m. (APPROX)
K = 8
K = 12
K = 16

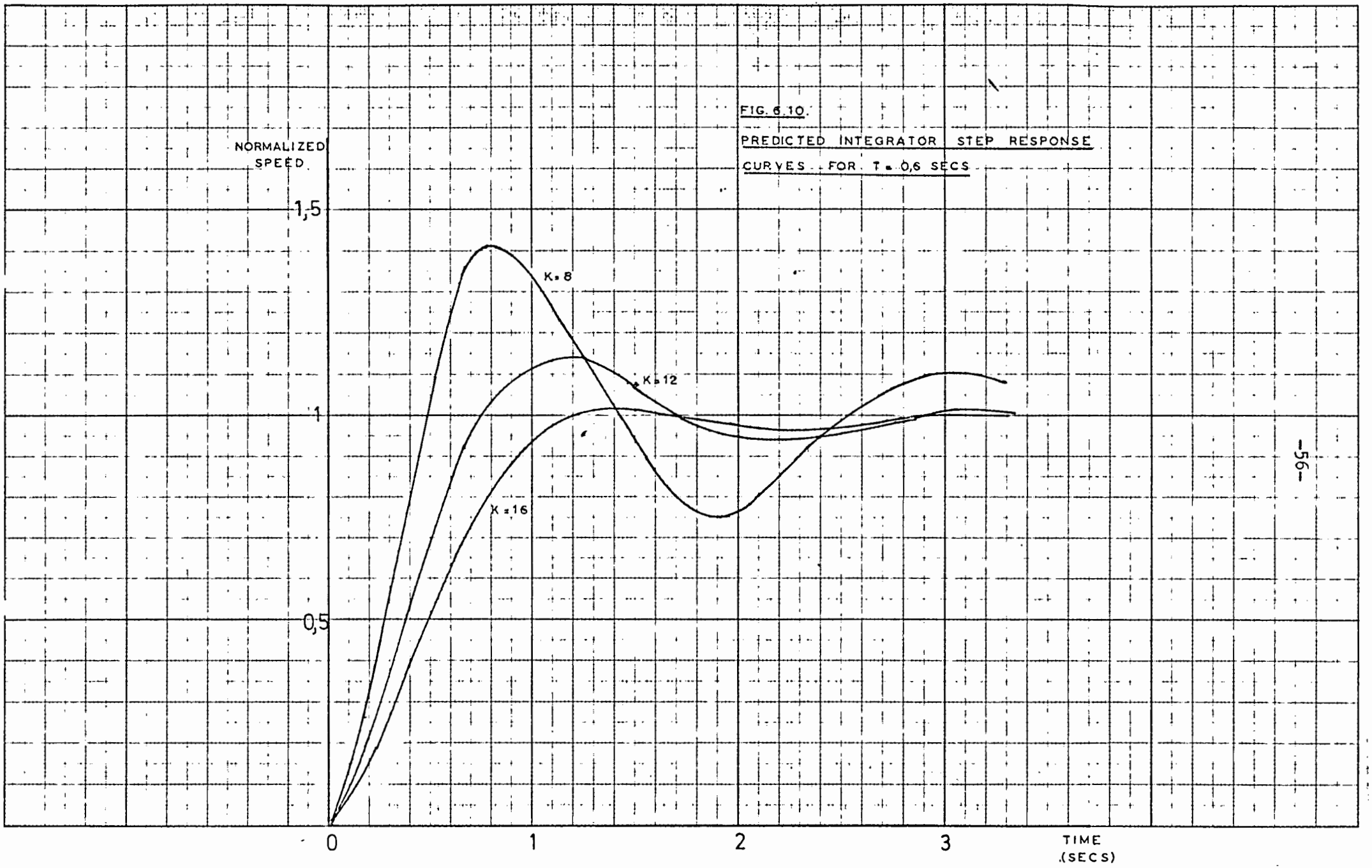

FIG. 6.10.
PREDICTED INTEGRATOR STEP RESPONSE CURVES FOR T = 0,6 SECS

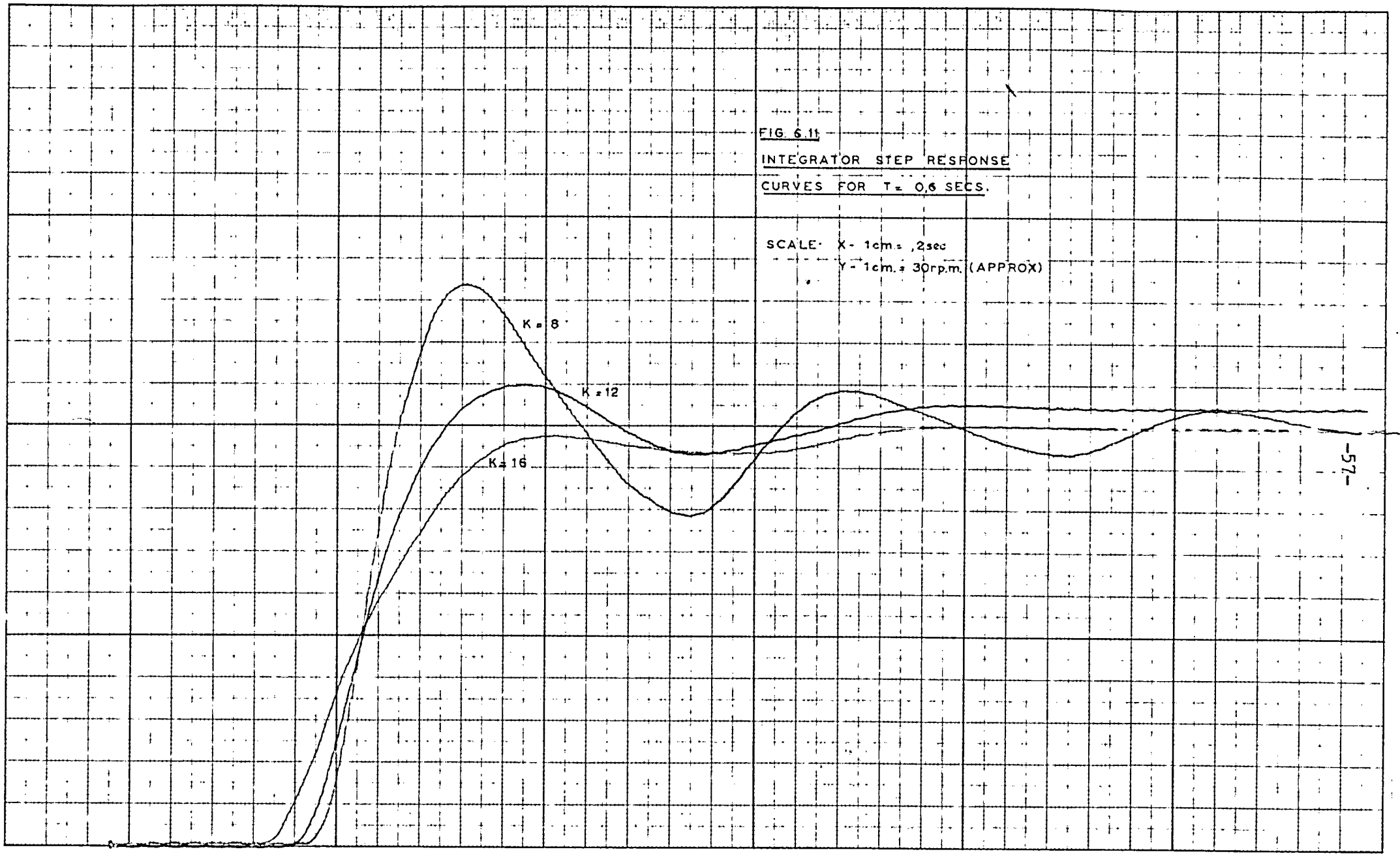
FIG 6.11
INTEGRATOR STEP RESPONSE
CURVES FOR T = 0,6 SECS.
SCALE: X - 1cm. = ,2sec
Y - 1cm. = 30rp.m. (APPROX)
K = 8
K = 12
K = 16

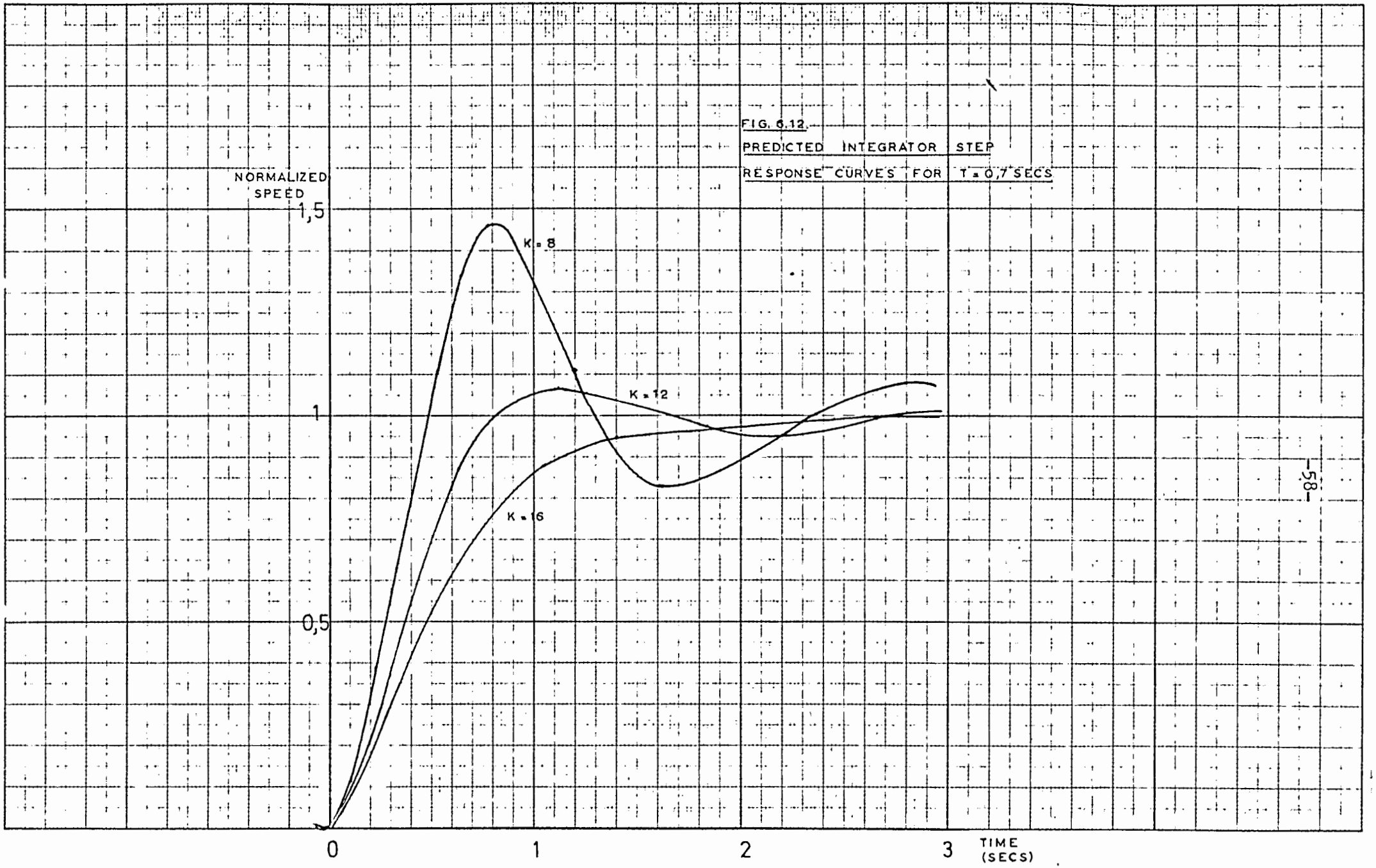

FIG. 6.12.
PREDICTED INTEGRATOR STEP RESPONSE CURVES FOR T = 0,7 SECS

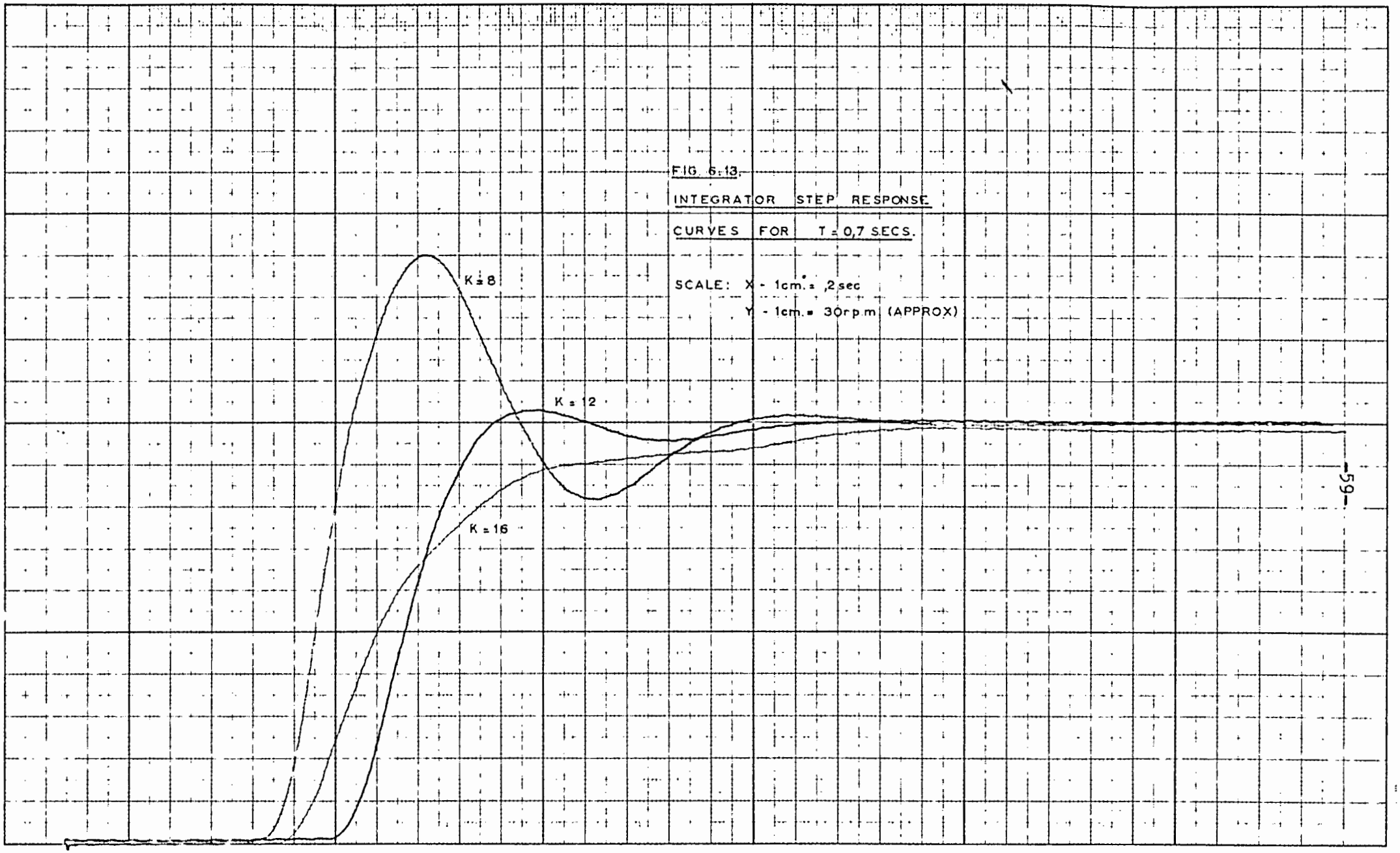
FIG. 6.13.
INTEGRATOR STEP RESPONSE
CURVES FOR T = 0,7 SECS.
SCALE: X - 1cm. = ,2 sec
Y - 1cm. = 30r.p.m. (APPROX)
K = 8
K = 12
K = 16

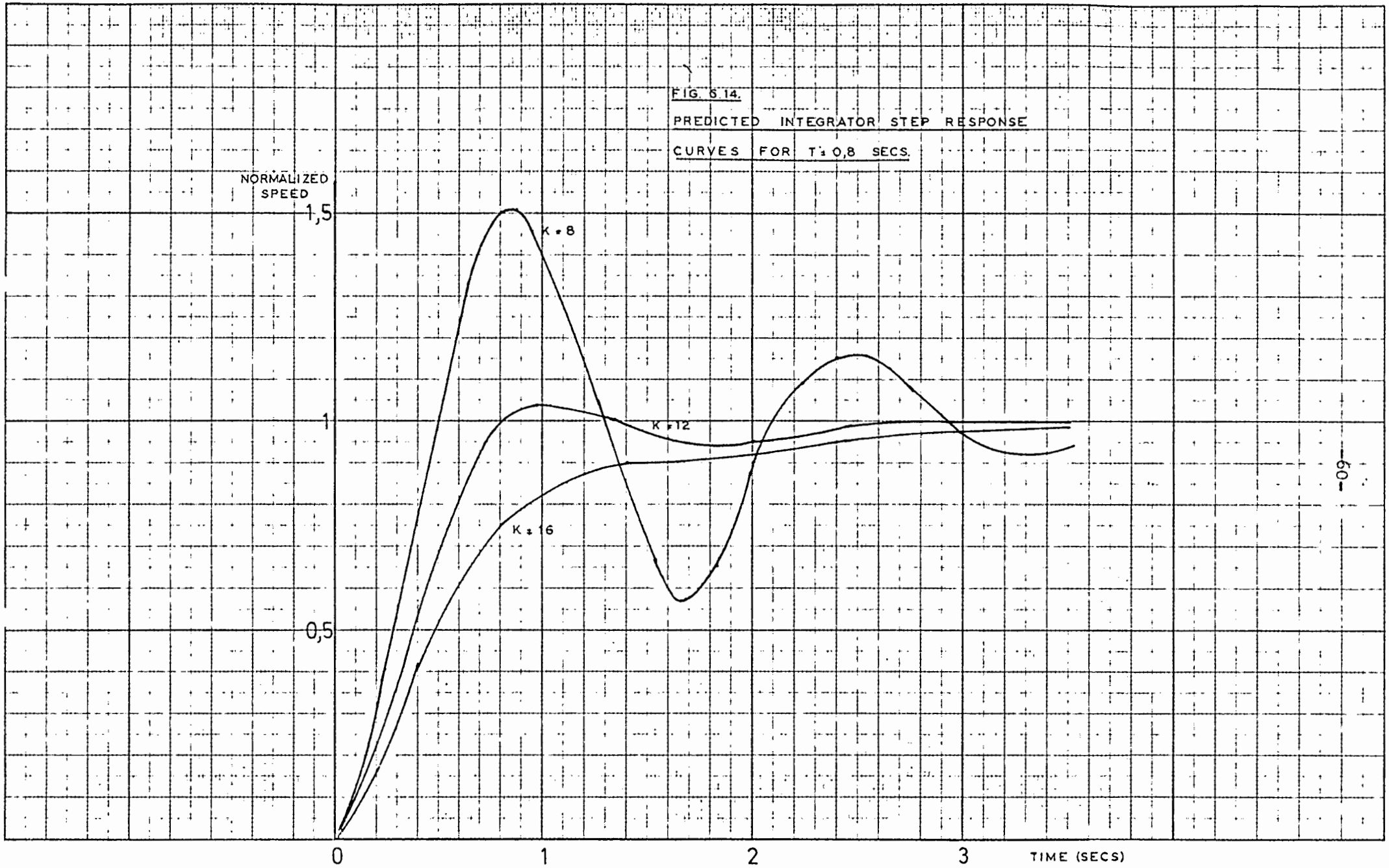

FIG. 6.14.
PREDICTED INTEGRATOR STEP RESPONSE CURVES FOR T = 0,8 SECS.

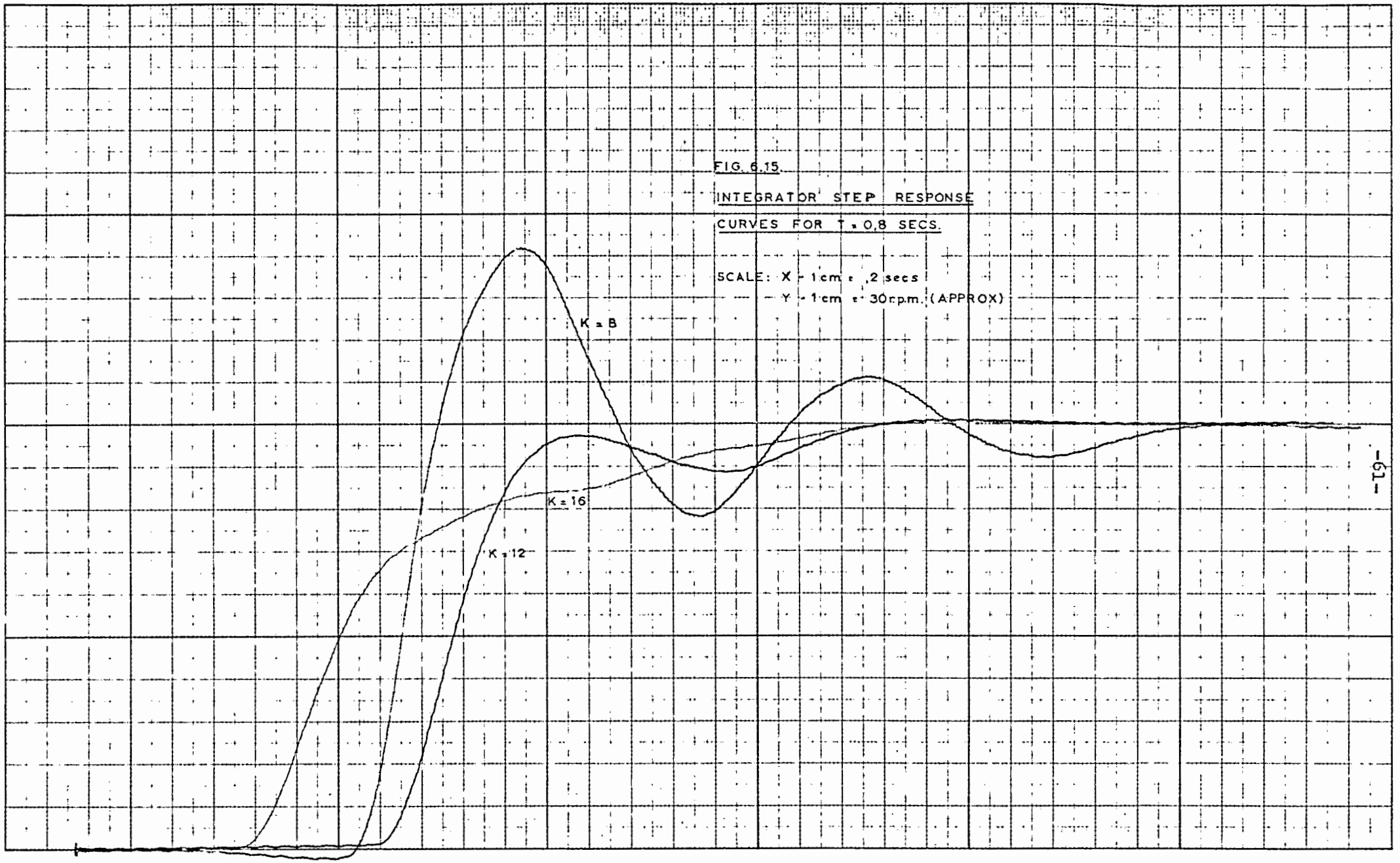

FIG. 6.15.

INTEGRATOR STEP RESPONSE CURVES FOR T = 0,8 SECS.

SCALE: X - 1 cm = ,2 secs
Y - 1 cm = 30 r.p.m. (APPROX)

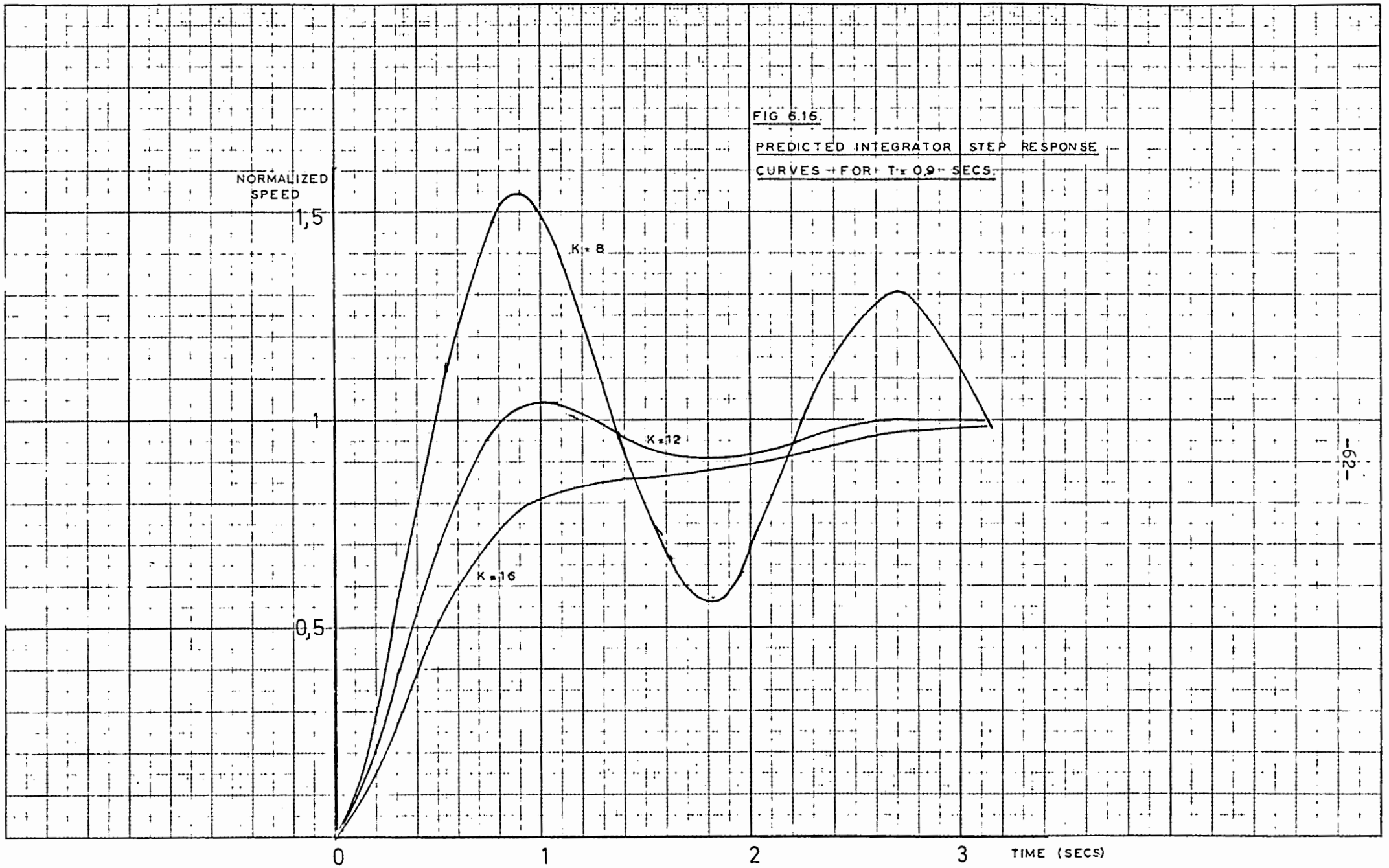

FIG 6.16.

PREDICTED INTEGRATOR STEP RESPONSE CURVES FOR T = 0,9 SECS.

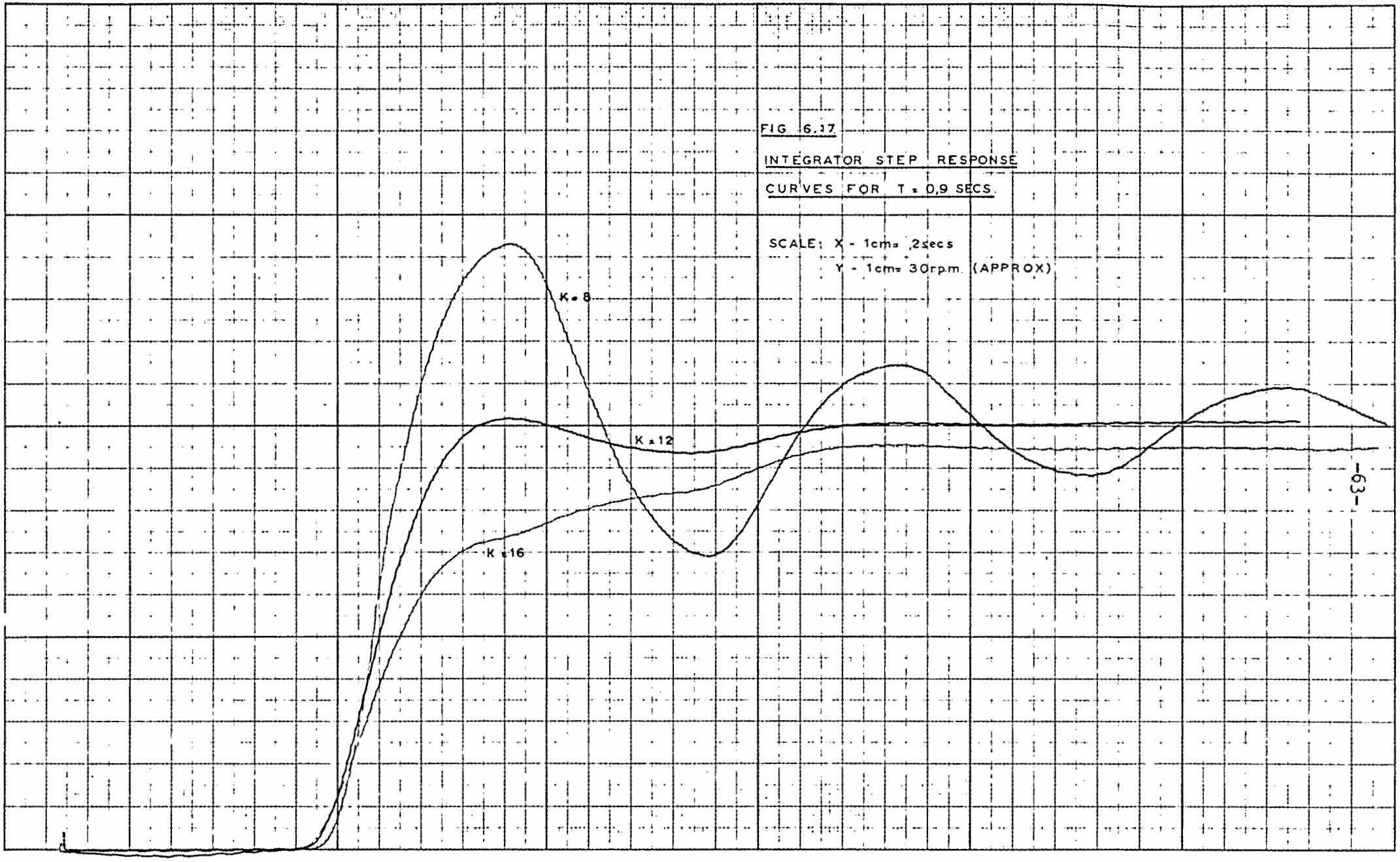
FIG 6.17
INTEGRATOR STEP RESPONSE
CURVES FOR T = 0,9 SECS.
SCALE: X - 1cm = ,2secs
Y - 1cm = 30rpm. (APPROX)
K = 8
K = 12
K = 16

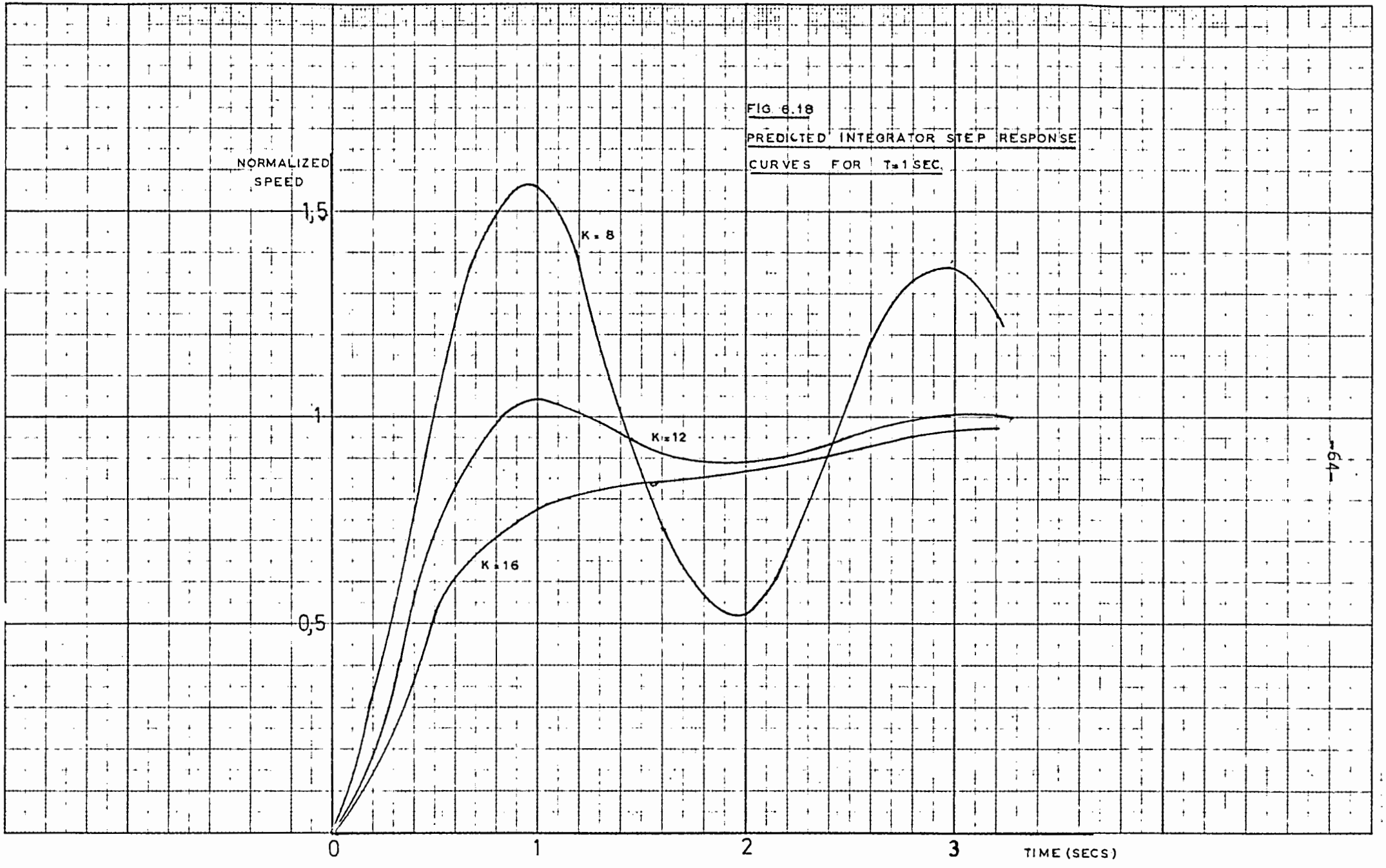

FIG 6.18
PREDICTED INTEGRATOR STEP RESPONSE CURVES FOR T=1 SEC.

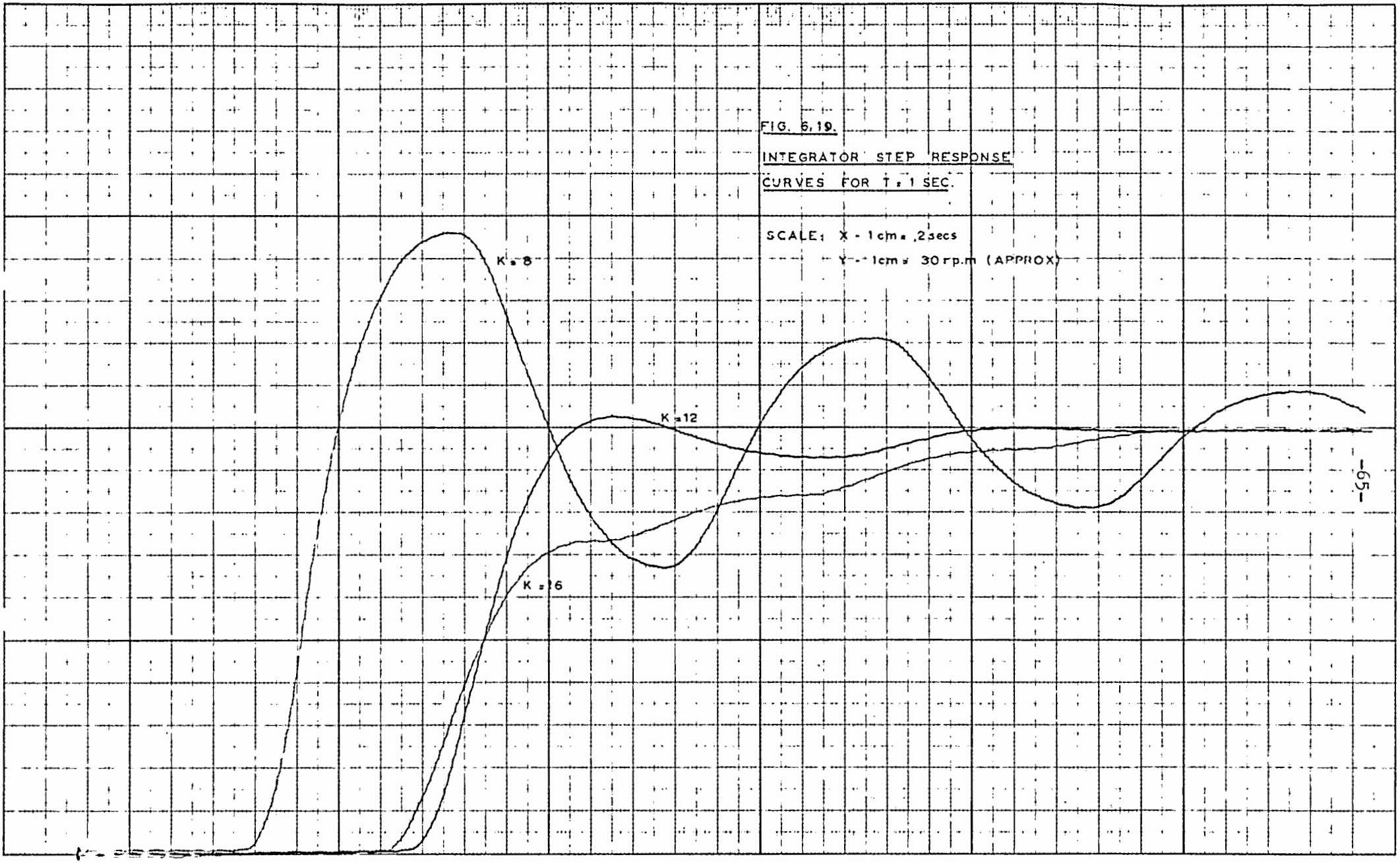
FIG. 6.19.
INTEGRATOR STEP RESPONSE
CURVES FOR T = 1 SEC.
SCALE: X - 1cm = .2secs
Y - 1cm = 30 r.p.m (APPROX)
K = 8
K = 12
K = 16

Steps applied under no load conditions did not produce such satisfactory results, as figures 6.20 to 6.22 show. This was particularly true at high gains, when some degree of damped oscillation had been expected.

The causes of this problem were allied to the problems created by the application of negative steps, shown in figs. 6.23 to 6.25 (on load) and 6.26 to 6.28 (no load), and lie in the behaviour of the machine when the current drops to zero.

As discussed in section 4.4, regeneration is not possible using the three phase fully controlled bridge, since current cannot flow out of the machine. Thus the energy of the machine, once no current is being fed into it, can either be expended in the load, if one is present, or in friction. The machine thus gradually slows down, until its e.m.f. drops below the average D.C. voltage of the bridge.

Figure 6.29 shows the voltage, speed, current and choke voltage waveforms at a sampling rate of 0,6 secs with K = 12 when positive and negative steps are applied on load, while figure 6.30 shows the no load traces. Here one can clearly see that the voltage continues to to build up for some time after the speed has dropped below the reference, before it exceeds the machine back e.m.f., whereupon the current comes on again and the machine once more behaves as if a positive step has been applied to it, as the speed traces clearly show.

Similar behaviour can be expected on no load for a positive step if an overshoot of any large magnitude should occur, since at the next sampling instant one would expect the voltage to be reduced, and if this is to a value below the machine e.m.f., the current will drop to zero.

That the absence of a flywheel diode will add to the seriousness of this effect is clearly shown in fig. 6.31, which shows the effect of positive and negative steps on no load without a flywheel diode, at a sampling rate of 0,6 secs

/..with...

with K = 12. Here, because the instantaneous voltage can go negative, the average bridge voltage takes longer to exceed the machine back e.m.f.; consequently the speed drops further than would be the case with the diode connected, and when, after a longer period, the current does turn on again, the effect is far more severe.

6.5. EFFECT OF LOAD CHANGES.

Figures 6.32 to 6. 34 show the effect of switching off a load and then re-applying it when the machine is running at 500 r.p.m., with gains of K = 8 (fig. 6.32), 12 (fig. 6.33) and 16 (fig. 6.34). In each case, sampling rates of 0,4, 0,6 and ß second are shown. The load used in all cases was a resistance of 18,5Ω, which drew a current of 3,5 amps from the generator at the speed at which these readings were taken.

The vertical scale of these traces is approximately 20 r.p.m. per cm. It is of interest to note that the speed did not consistently return to the value before the step was applied. The small error introduced can be attributed to the ±12 r.p.m. deadband introduced, which was necessary because of the imperfections in the tachometer used.

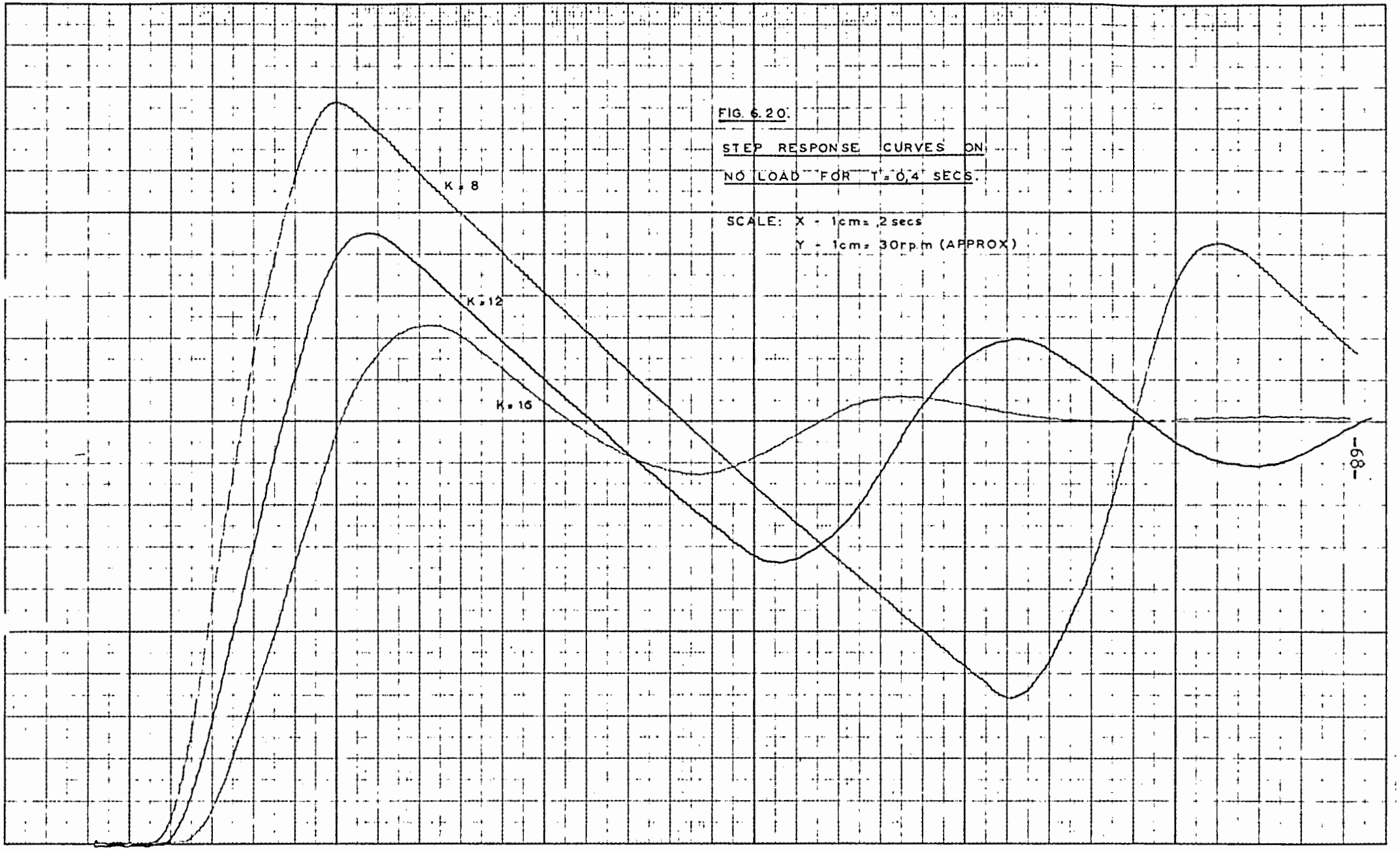

FIG. 6.20.

STEP RESPONSE CURVES ON NO LOAD FOR T = 0,4 SECS.

SCALE: X - 1cm = ,2 secs
Y - 1cm = 30rp.m (APPROX)

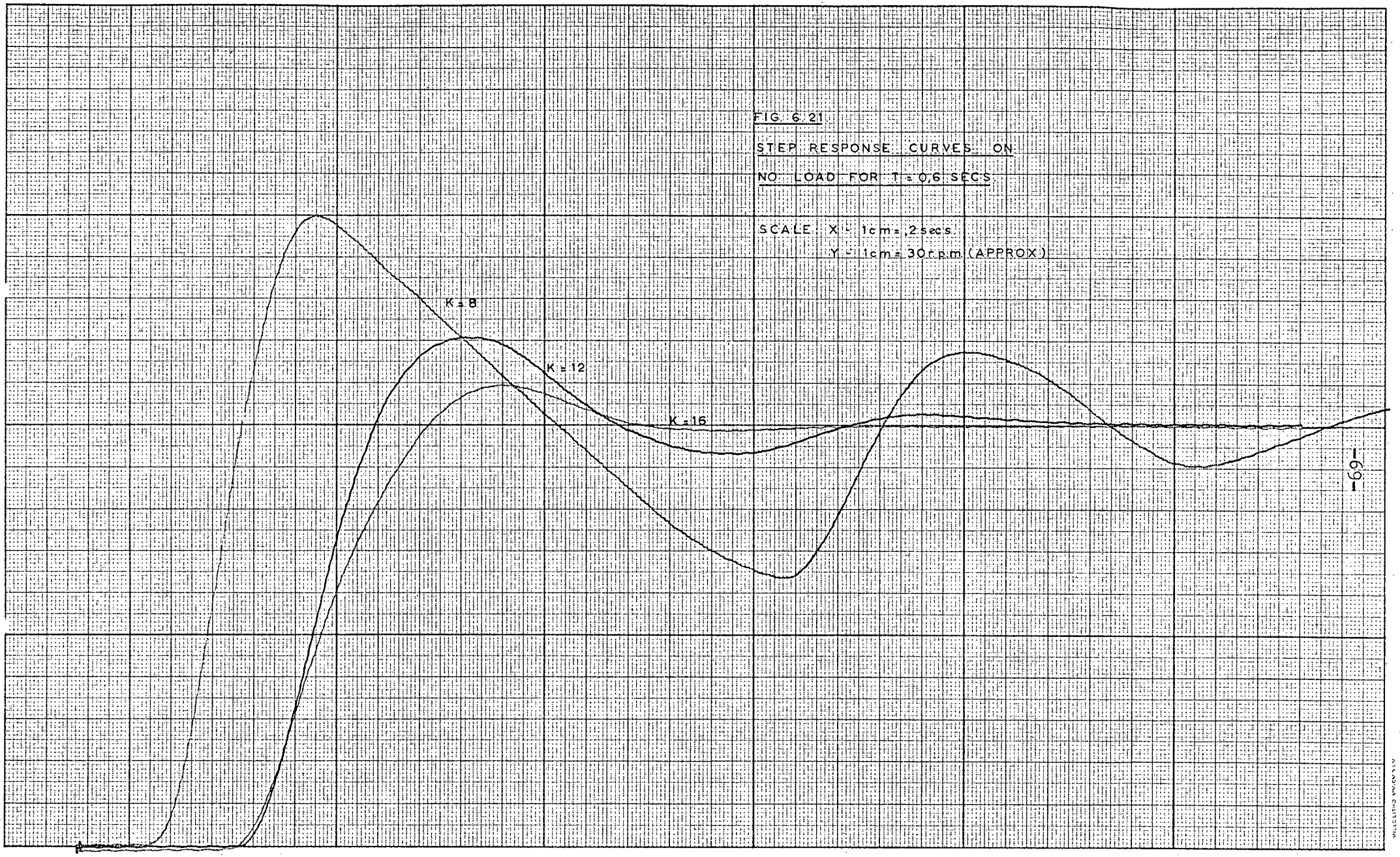

FIG. 6.21

STEP RESPONSE CURVES ON NO LOAD FOR T = 0,6 SECS

SCALE X - 1cm = ,2 secs
Y - 1cm = 30 r.p.m (APPROX)

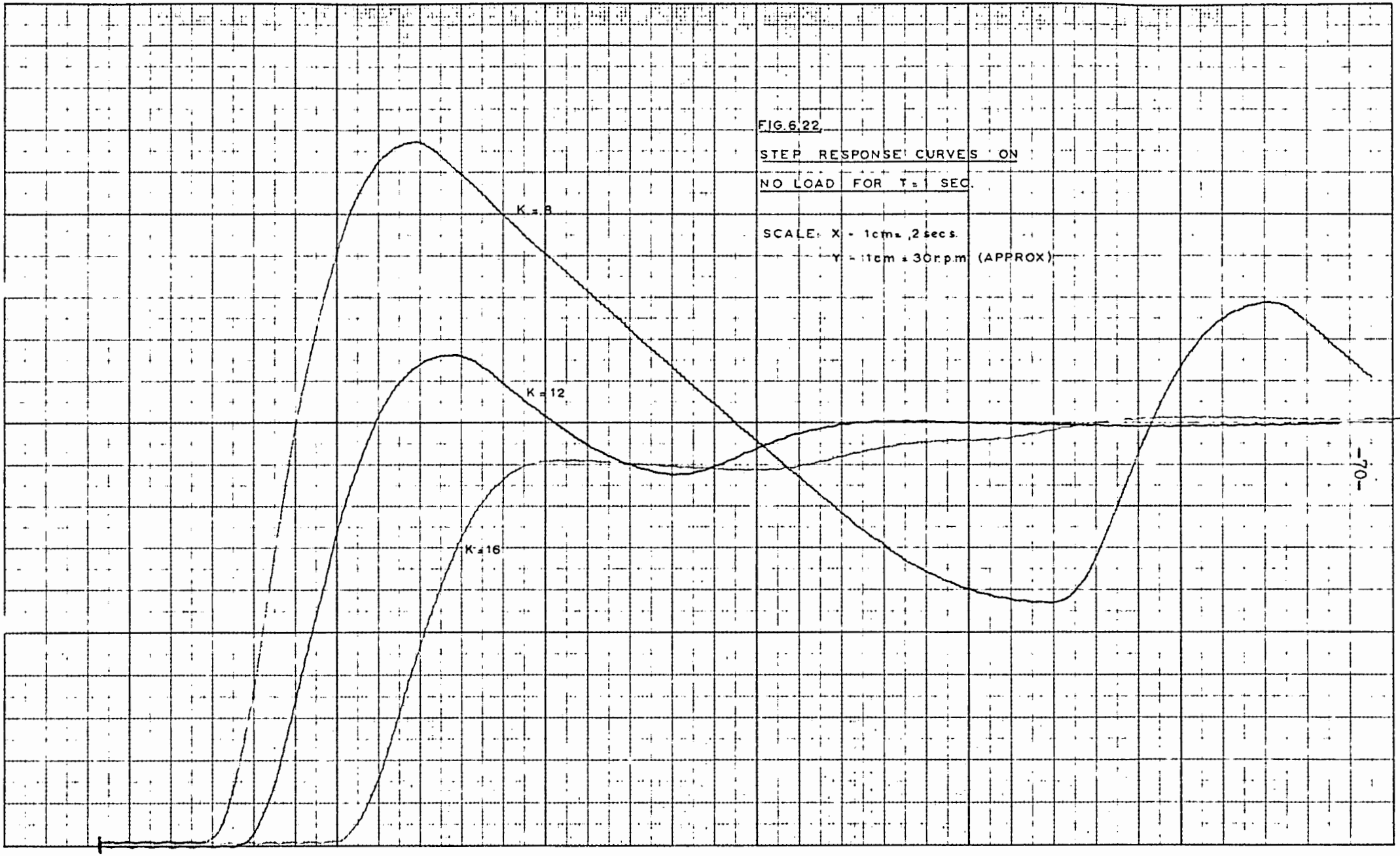

FIG.6.22.

STEP RESPONSE CURVES ON NO LOAD FOR T = 1 SEC.

SCALE: X - 1cm = .2 secs.

Y - 1cm = 30 r.p.m (APPROX)

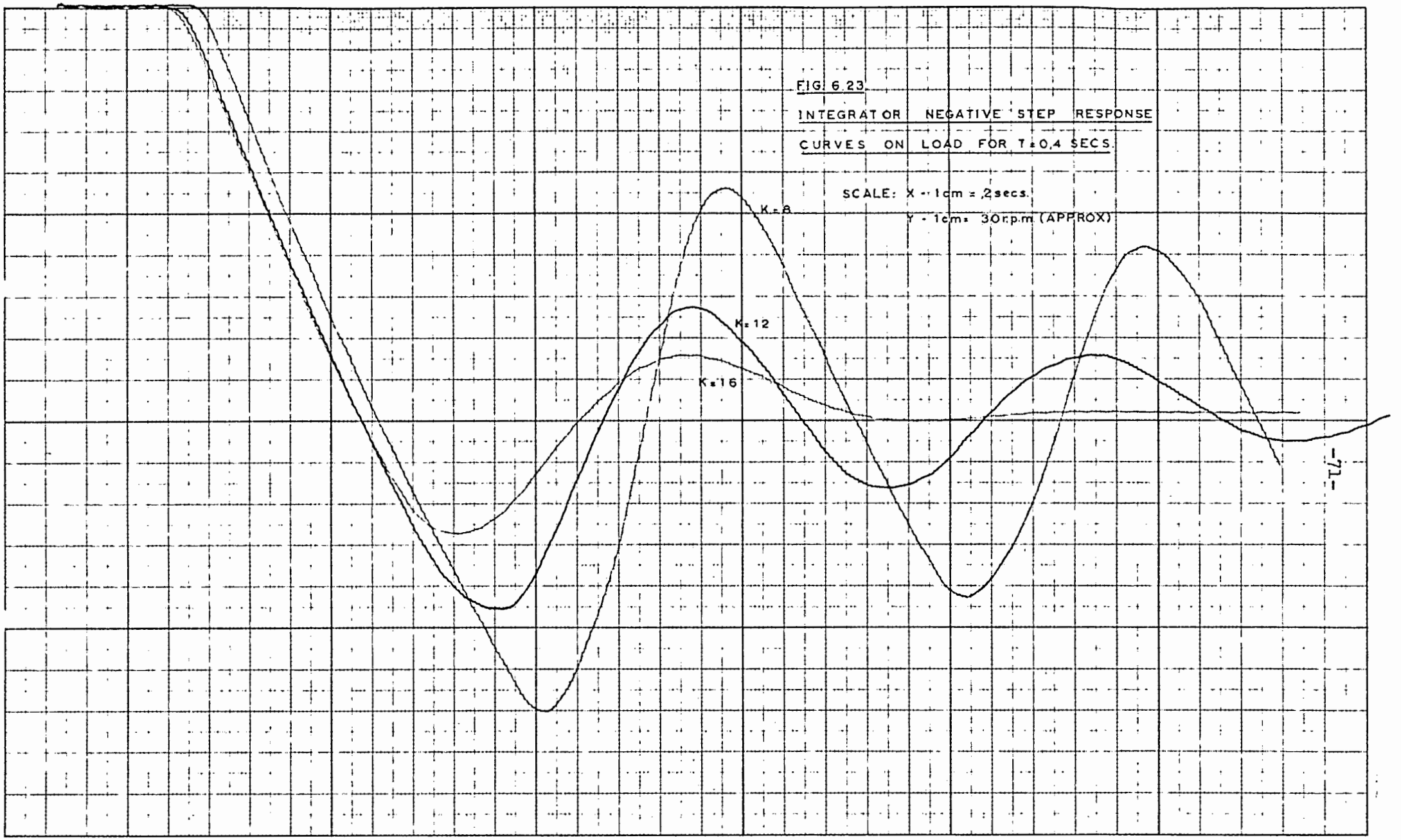
FIG 6.23
INTEGRATOR NEGATIVE STEP RESPONSE
CURVES ON LOAD FOR T=0.4 SECS.
SCALE: X - 1cm = .2secs.
Y - 1cm = 30r.p.m (APPROX)
K=8
K=12
K=16

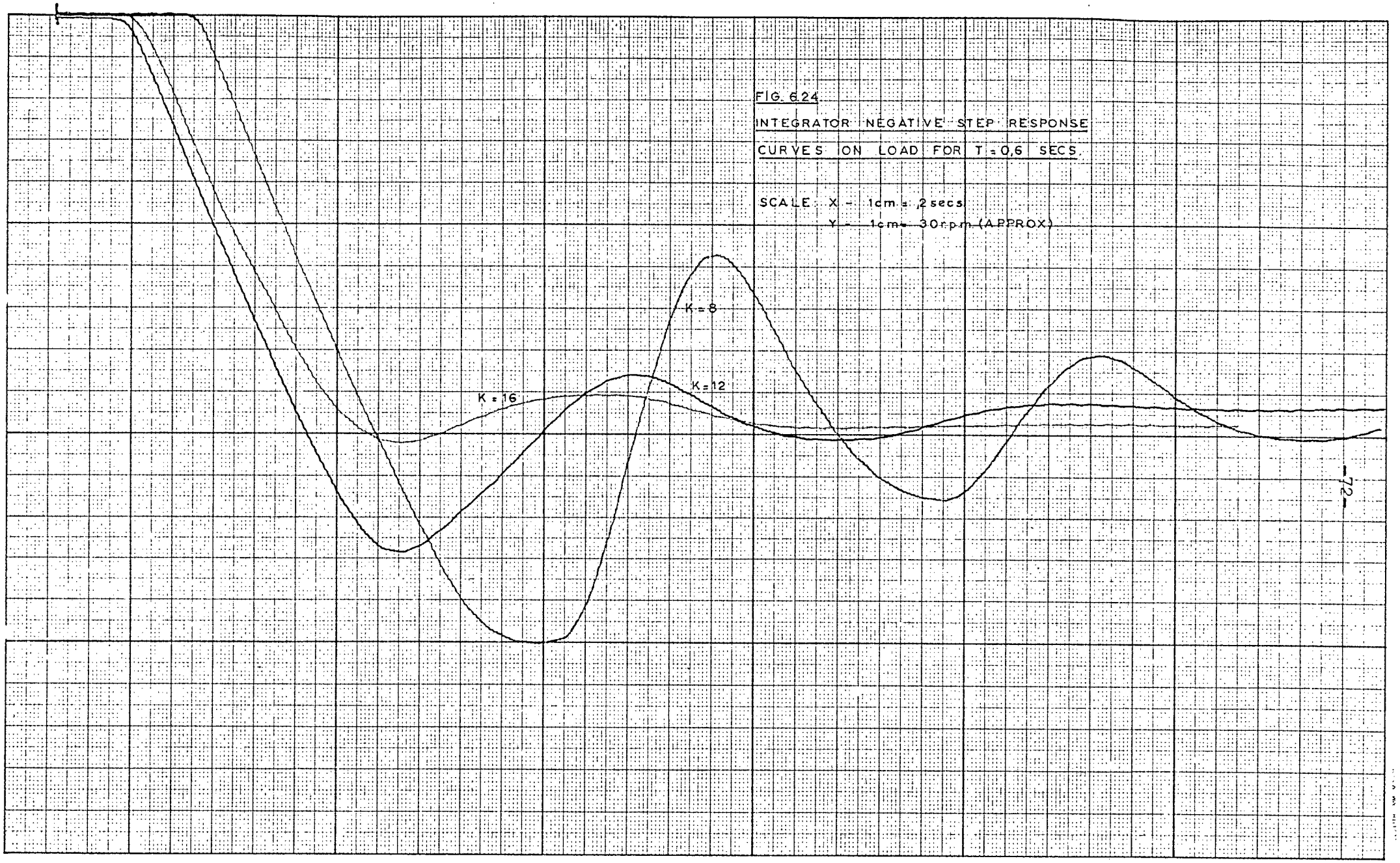
FIG. 6.24
INTEGRATOR NEGATIVE STEP RESPONSE
CURVES ON LOAD FOR T = 0,6 SECS.
SCALE: X - 1cm = ,2 secs
Y - 1cm = 30 r.p.m. (APPROX)
K = 8
K = 12
K = 16

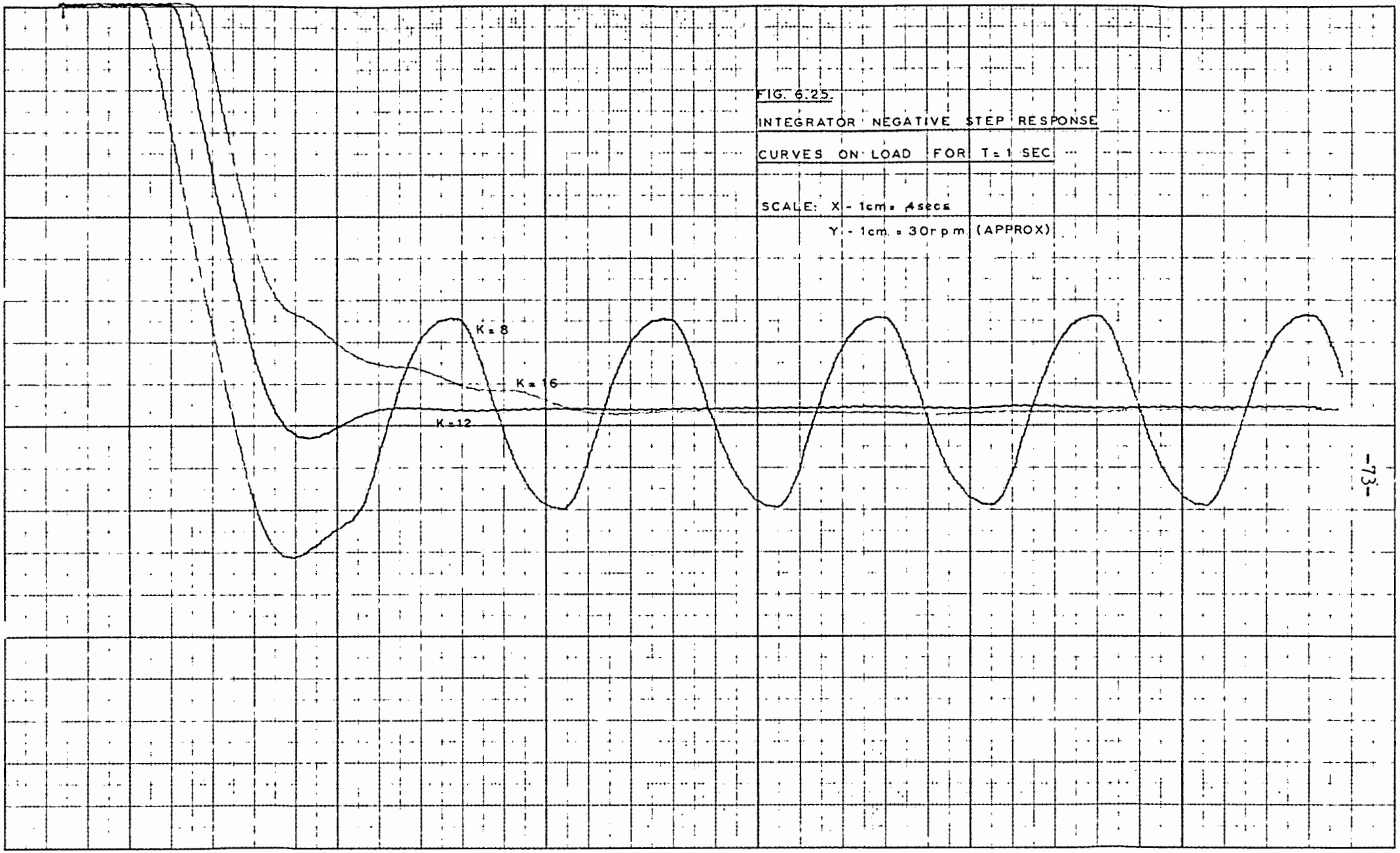

FIG. 6.25.
INTEGRATOR NEGATIVE STEP RESPONSE
CURVES ON LOAD FOR T = 1 SEC

SCALE: X - 1cm = 4secs
Y - 1cm = 30rpm (APPROX)

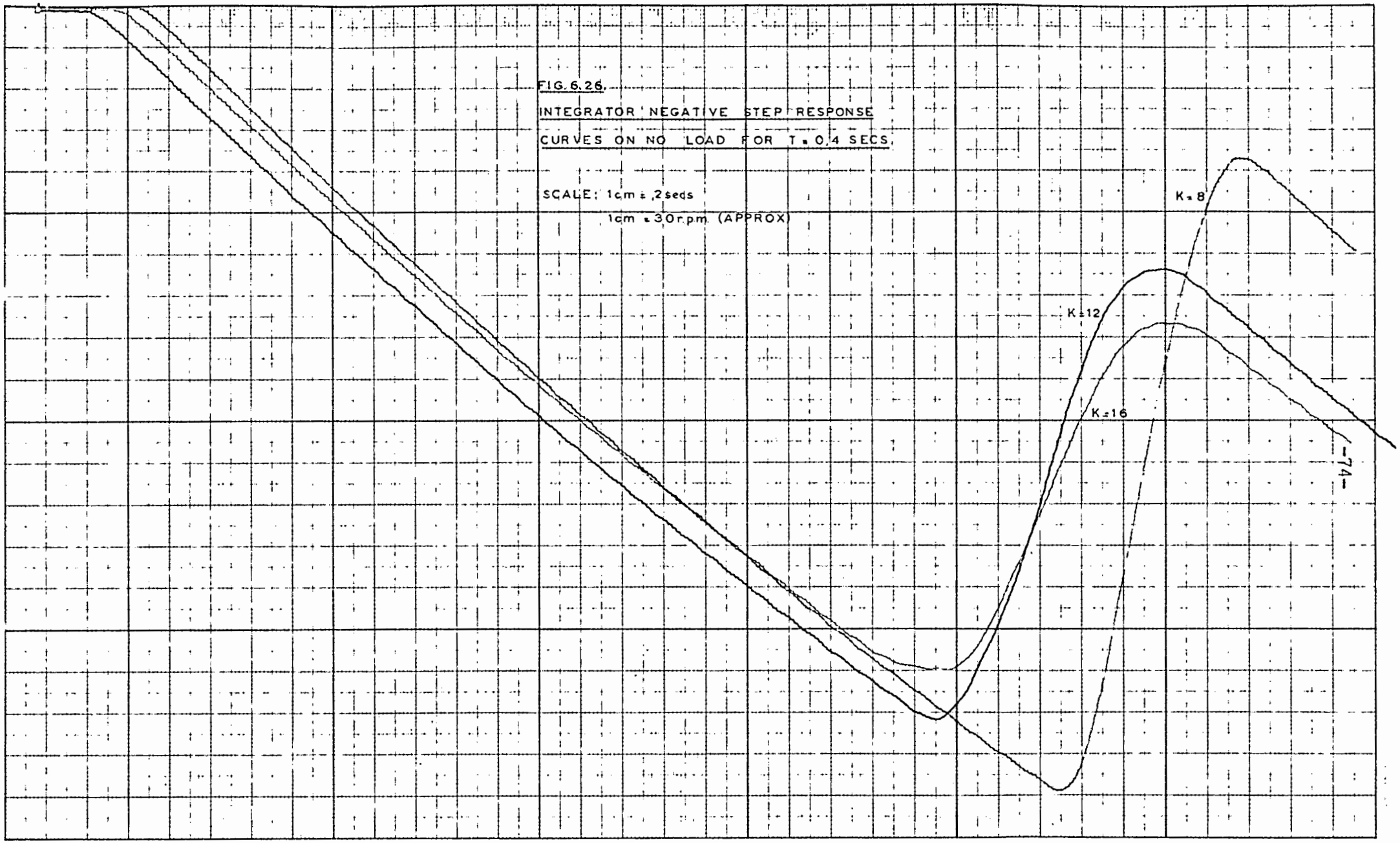
FIG. 6.26.
INTEGRATOR NEGATIVE STEP RESPONSE
CURVES ON NO LOAD FOR T = 0.4 SECS.
SCALE: 1cm = .2 secs
1cm = 30 r.p.m. (APPROX)
K = 8
K = 12
K = 16

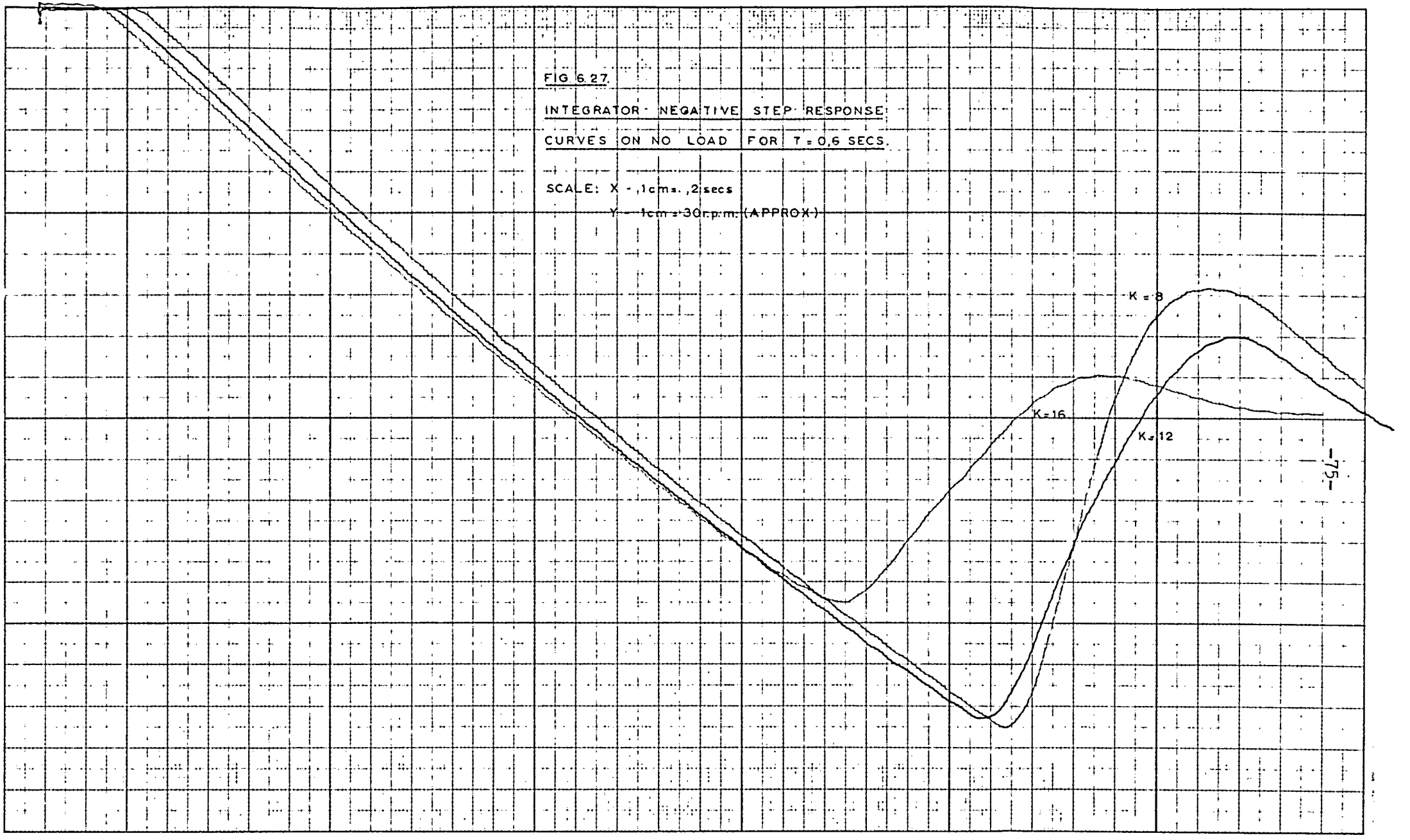

FIG 6.27.

INTEGRATOR NEGATIVE STEP RESPONSE CURVES ON NO LOAD FOR T = 0,6 SECS.

SCALE: X - 1cm = 2 secs

Y - 1cm = 30 r.p.m. (APPROX)

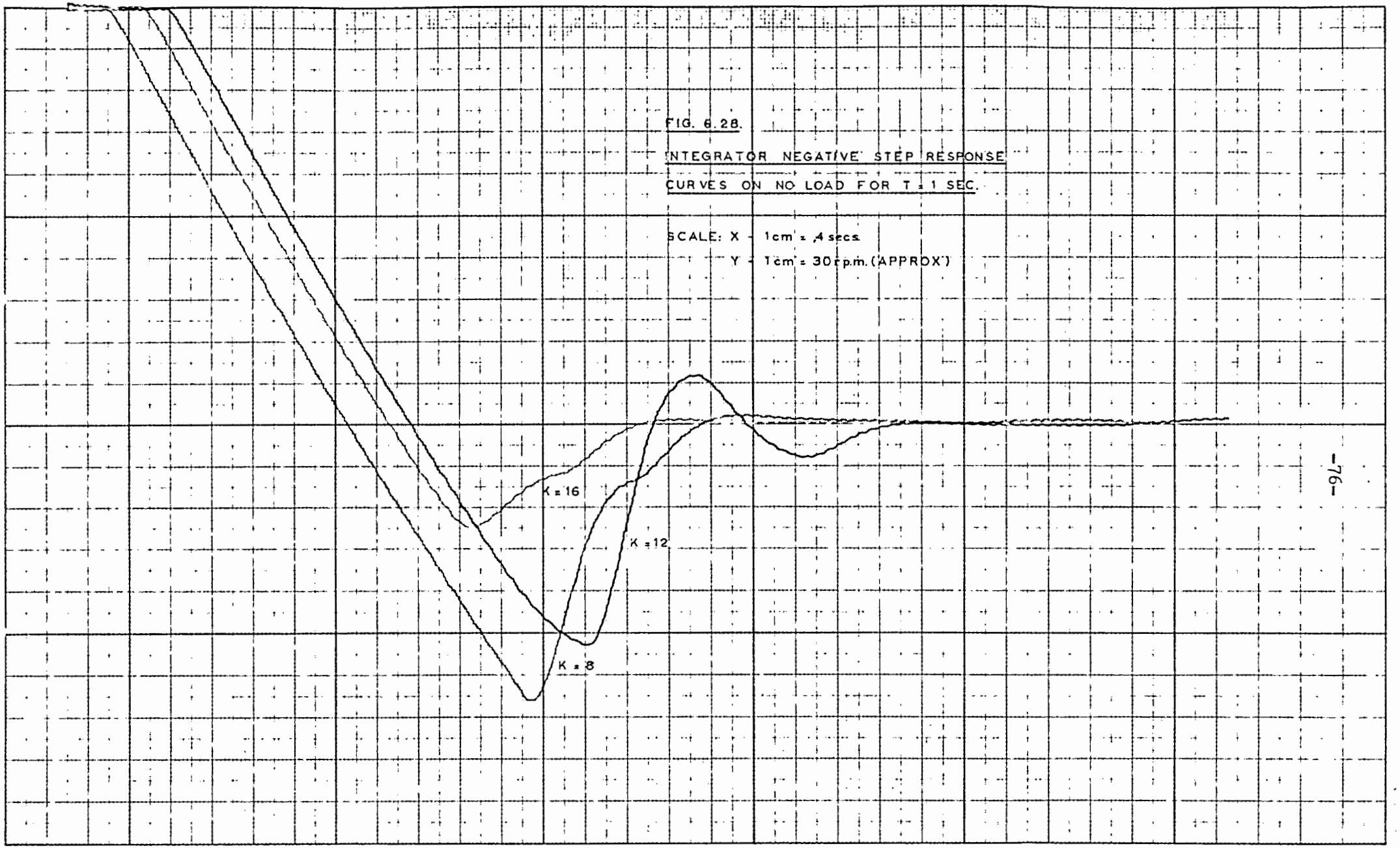

FIG. 6.28.

INTEGRATOR NEGATIVE STEP RESPONSE CURVES ON NO LOAD FOR T = 1 SEC.

SCALE: X - 1cm = .4 secs.
Y - 1cm = 30 r.p.m. (APPROX.)

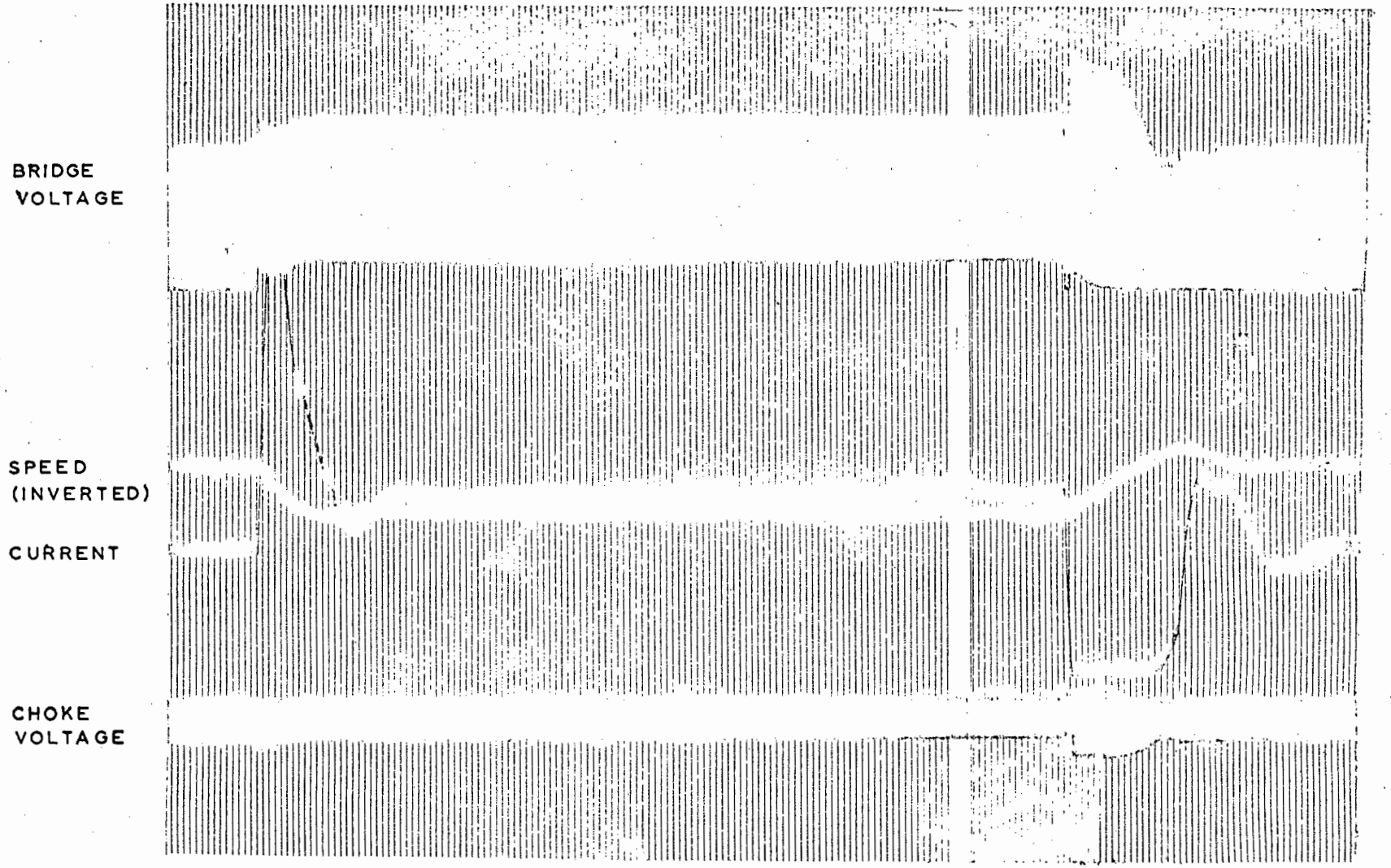

FIG. 6.29.

WAVEFORMS FOR POSITIVE AND NEGATIVE STEPS ON LOAD.

T = 0,6 SECS, K = 12.

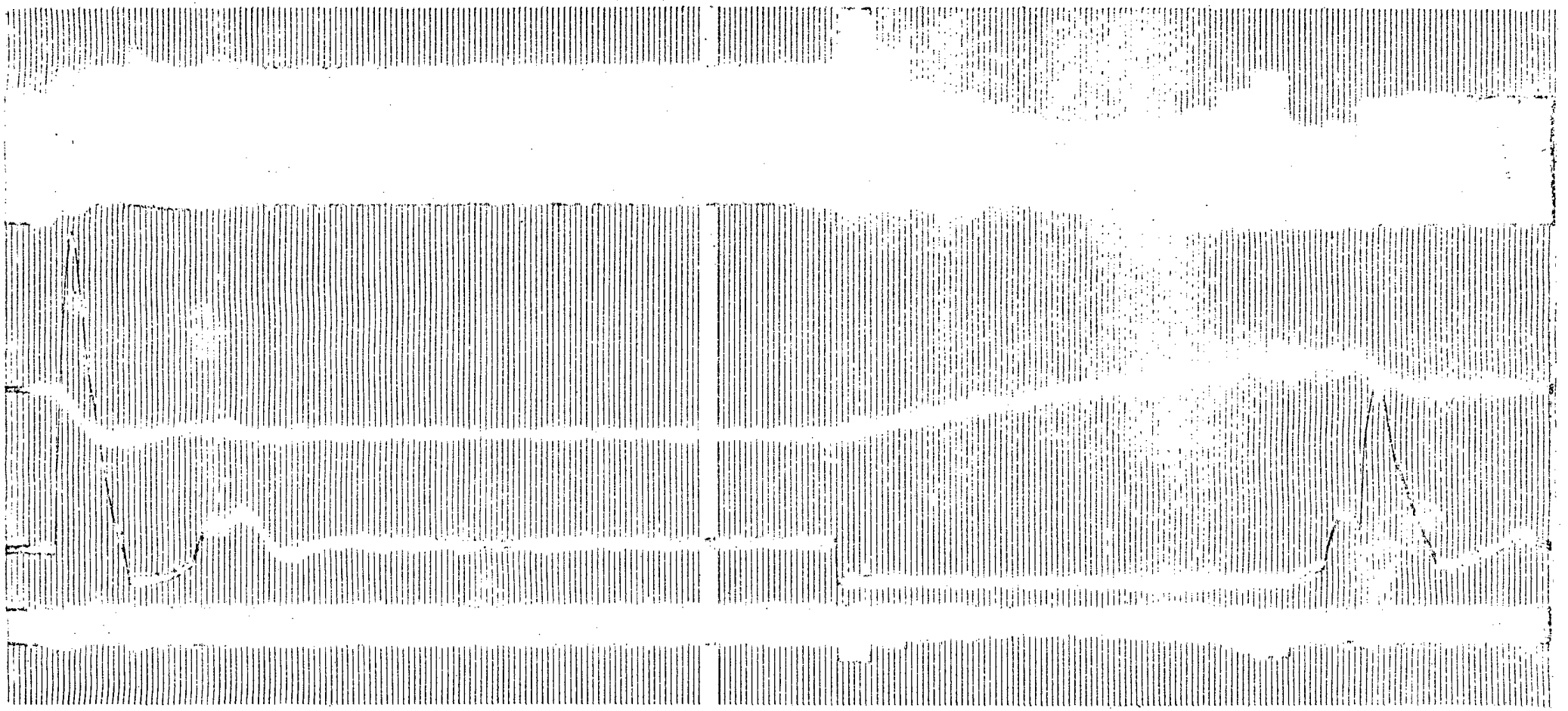

FIG. 6.30.
WAVEFORMS FOR POSITIVE AND NEGATIVE STEPS ON NO LOAD.
T = 0,6 SECS, K = 12.

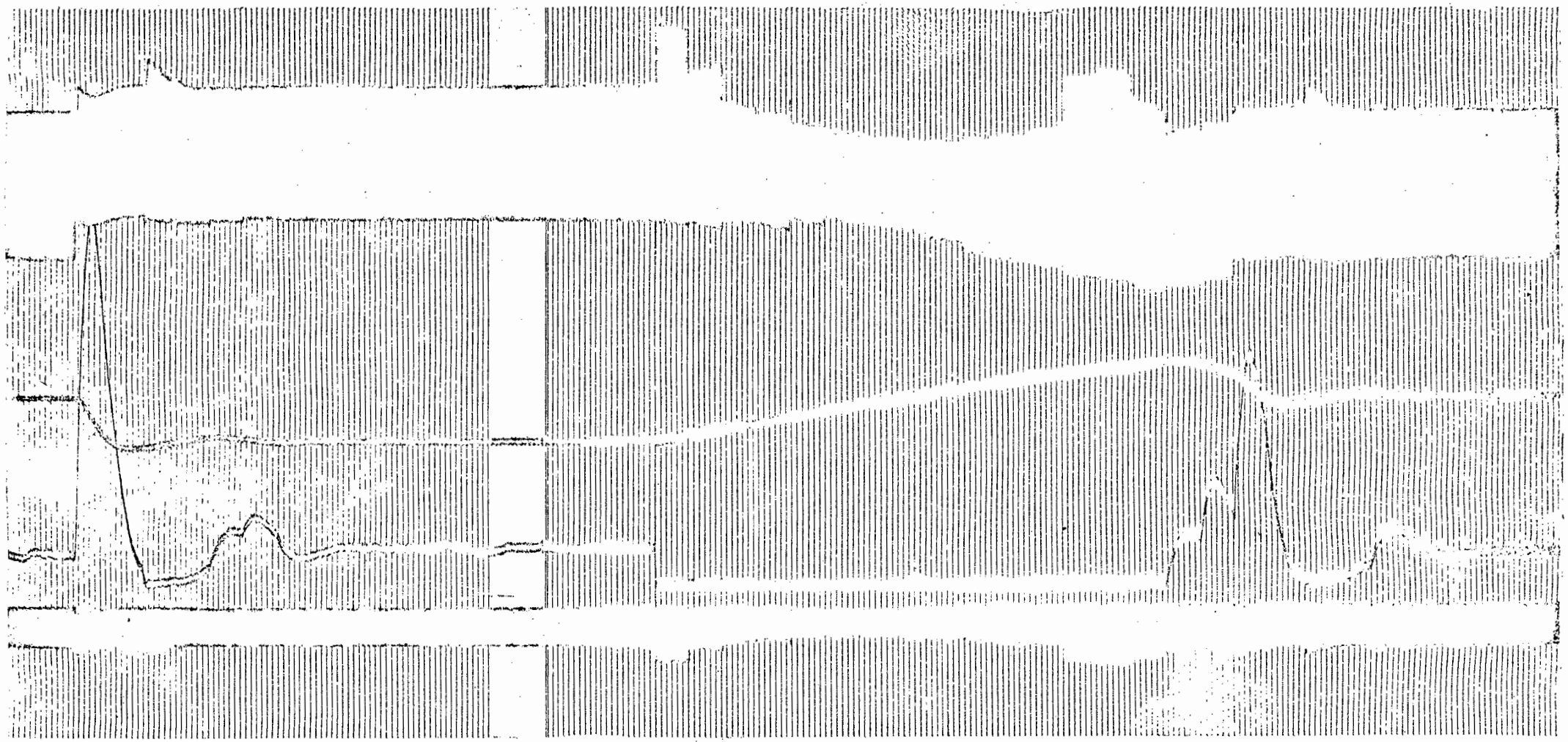

FIG. 6.31.

WAVEFORMS FOR POSITIVE AND NEGATIVE STEPS ON NO LOAD WITH FLYWHEEL DIODE DISCONNECTED. T = 0,6 SECS, K = 12.

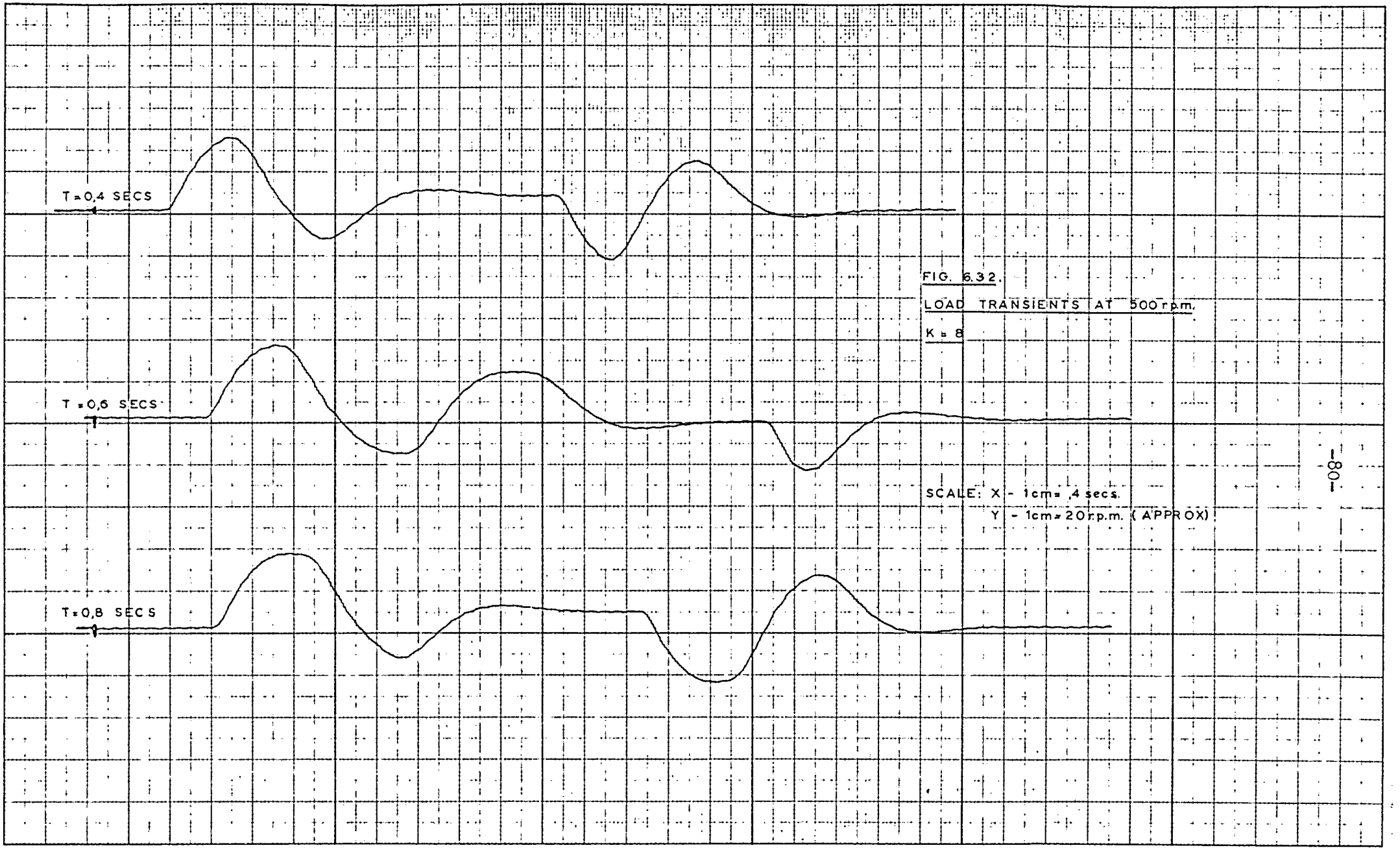

FIG. 6.32.

LOAD TRANSIENTS AT 500 r.p.m.

K = 8

SCALE: X - 1cm = ,4 secs.

Y - 1cm = 20 r.p.m. (APPROX)

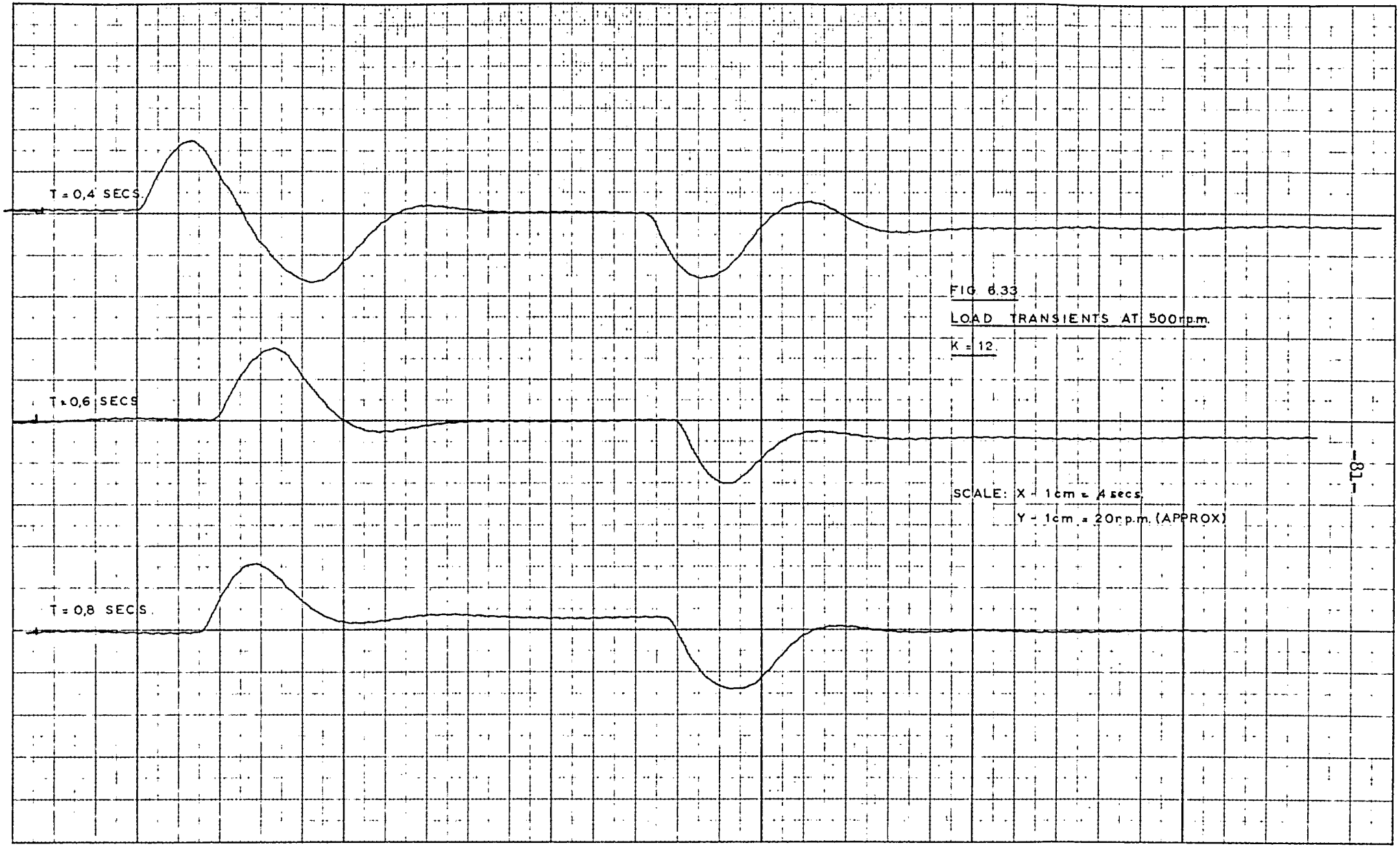

FIG 6.33

LOAD TRANSIENTS AT 500r.p.m.

K = 12

SCALE: X - 1cm = 4 secs.

Y - 1cm = 20r.p.m. (APPROX)

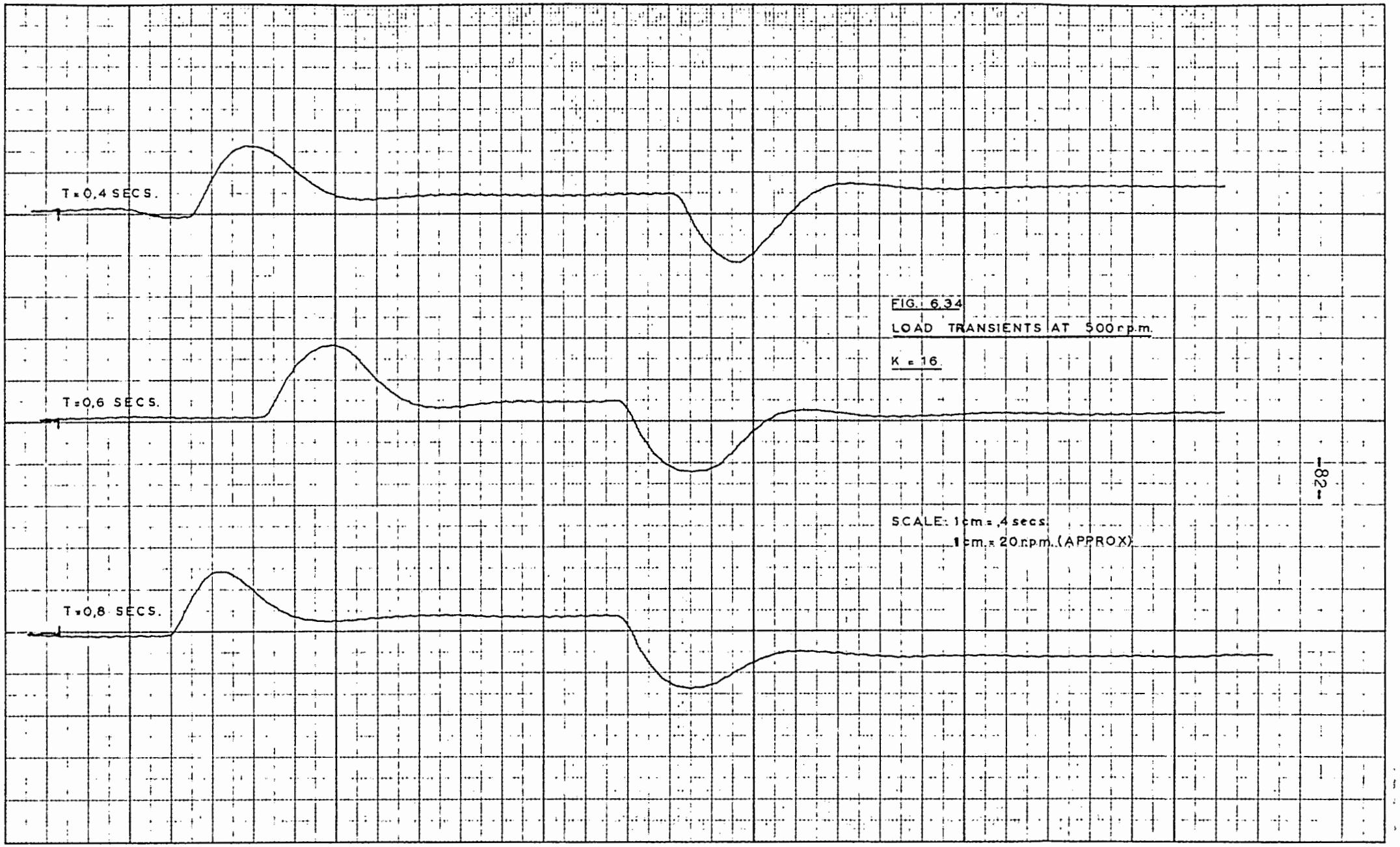
T=0,4 SECS.
T=0,6 SECS.
T=0,8 SECS.
FIG. 6.34
LOAD TRANSIENTS AT 500 r.p.m.
K = 16
SCALE: 1 cm = ,4 secs.
1 cm. = 20 r.p.m. (APPROX)

6.6. RAMP RESPONSE.

The system was also tested to determine the response to a ramp input. This ramp was generated digitally by the computer, which merely added a certain amount to the reference speed until the final desired speed was obtained, the increment depending on the rate of change of speed required.

A gain of K = 12 was used.

Figs. 6.35 to 6.37 show the positive ramp response of the system for a rate of change of speed of 60 r.p.m. per second at sampling rates of 0,4, 0,6 and 0,8 secs. The table shown on the graph in each case is the print-out generated by the computer fast punch on line, giving the reference and actual speeds, and the interface angle setting, at each sampling instant.

The final step in each case is seen to be smaller than the previous steps, but this was not felt to have materially affected the pattern of behaviour, which showed that the machine would follow a ramp with a finite error, decreasing this error to zero when the steady state speed was reached. Naturally, the faster the sampling time, the smoother the response obtained.

The negative ramp response curves served to verify the point made in section 6.4 that complete control is only possible while continuous current is supplied.

Figs. 6.38 to 6.40 show the negative ramp responses for K = 12 at sampling rates of 0,4, 0,6 and 0,8 secs respectively, for a rate of change of speed of 60 r.p.m. per second. Fig. 6.41 shows the waveforms for T = 0,6, and it can clearly be seen that the current remains on, and hence the response is the same, except reversed in direction, as for the positive ramp response.

Figures 6.42 qnd 6.43 show the effect of doubling the rate of change of speed, with K = 12 at 0,6 sec. sampling rate. The current still remained continuous, and hence the ramp was followed with little or no undershoot.

However, if the rate of change of speed was once again doubled to 240 r.p.m. per second, the reference speed fell faster than the excess energy of the machine could be expended, and hence the reference could not be followed, as figures 6.44 and 6.45 show. The final speed was correct, but the machine dropped to that speed in its own time, and a fairly large undershoot was experienced.

Clearly, the maximum possible rate of decrease of speed would depend upon the load applied to the machine, and, the greater the load, the faster the speed can be decreased without a temporary loss of control and accompanying undershoot.

6.7. COMMENT.

It was found that a sampling rate of 0,6 seconds, with K =12, gave a generally satisfying performance, which for the step response gave an overshoot of approximately 10%, with a settling time of the order of 2,5 seconds. It was found that this sampling rate was satisfactory for a ramp input or when load transients were applied. However, it was felt that a compensation program should be able to improve on this performance.

The implementation of the integral control program served to confirm the accuracy of the mathematical model used, while helping to highlight the main difficulties implicit in the system used, i.e. the lack of control introduced when the current falls to zero, and the problems associated with this condition.

FIG. 6.35

INTEGRATOR RAMP RESPONSE WITH

T = 0,4 SECS. K = 12.

SCALE: X - 1cm = ,4secs

Y - 1cm = 20 r.p.m (APPROX)

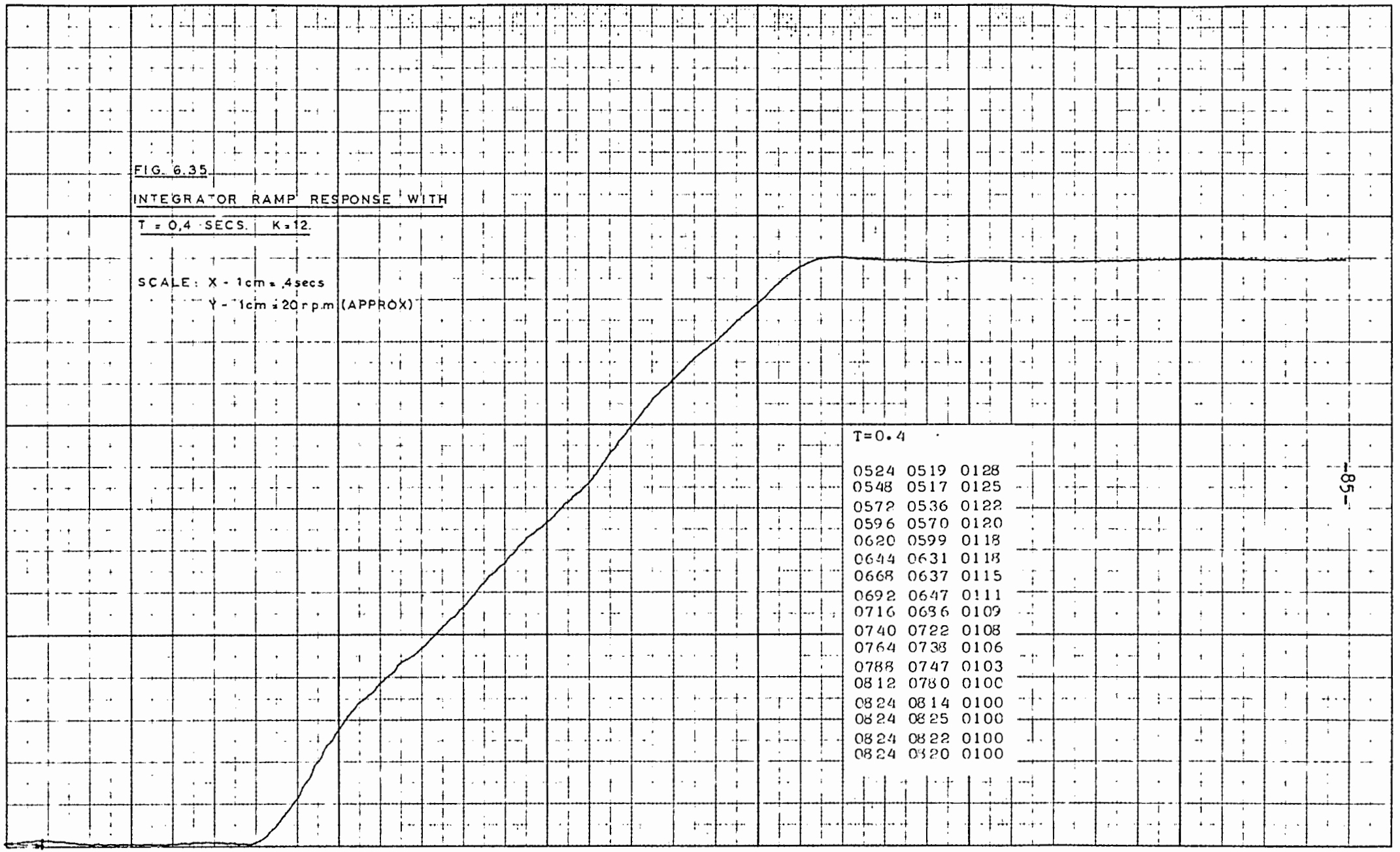

T=0.4

0524	0519	0128
0548	0517	0125
0572	0536	0122
0596	0570	0120
0620	0599	0118
0644	0631	0118
0668	0637	0115
0692	0647	0111
0716	0636	0109
0740	0722	0108
0764	0738	0106
0788	0747	0103
0812	0780	0100
0824	0814	0100
0824	0825	0100
0824	0822	0100
0824	0820	0100

FIG.6.36

INTEGRATOR RAMP RESPONSE FOR

T = 0.6 SECS K = 12.

SCALE: X = 1cm = 4secs.

Y = 1cm = 20rp.m (APPROX)

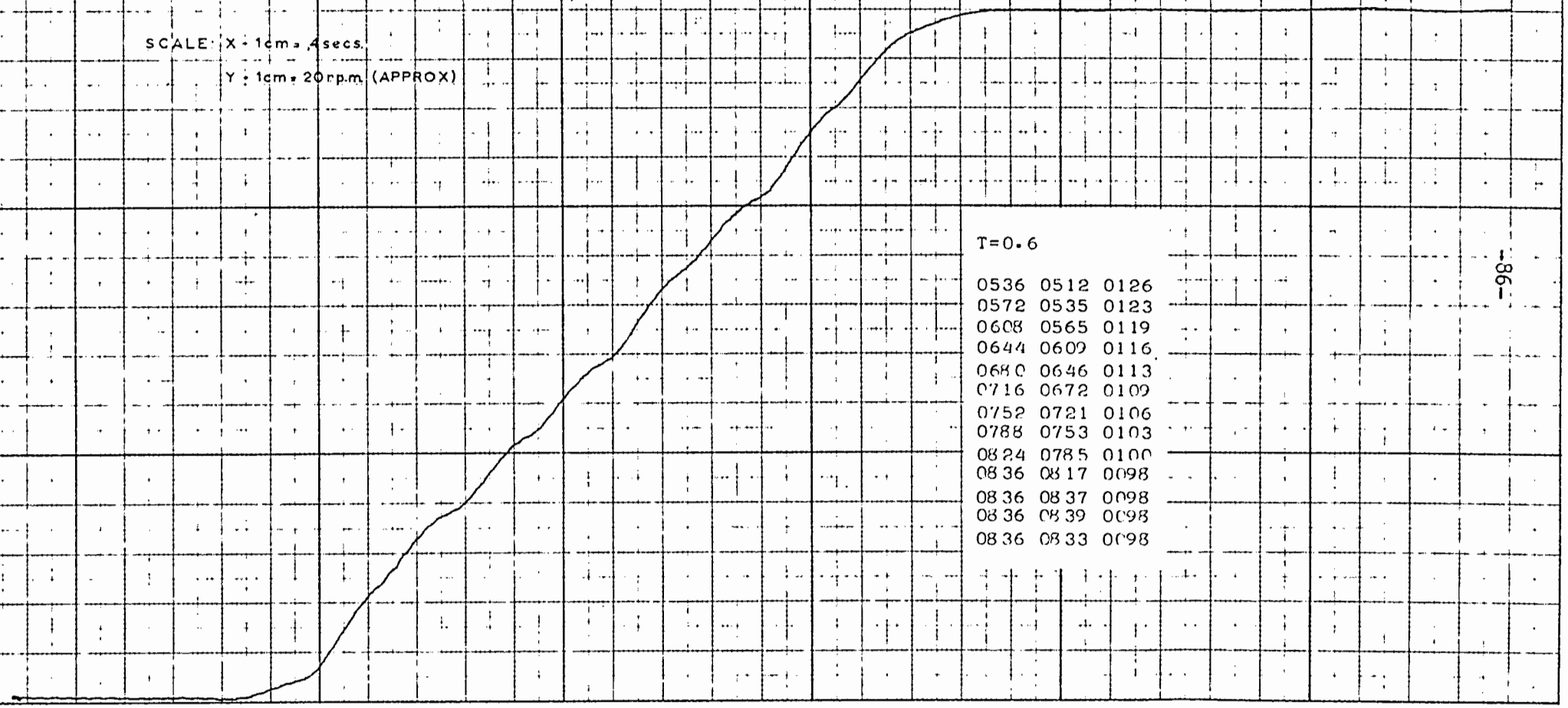

T=0.6

0536 0512 0126
0572 0535 0123
0608 0565 0119
0644 0609 0116
0680 0646 0113
0716 0672 0109
0752 0721 0106
0788 0753 0103
0824 0785 0100
0836 0817 0098
0836 0837 0098
0836 0839 0098
0836 0833 0098

FIG. 6.37

INTEGRATOR RAMP RESPONSE FOR

T = 0.8 SECS K = 12

SCALE: X - 1cm = .4secs.

Y - 1cm = 20r.p.m. (APPROX)

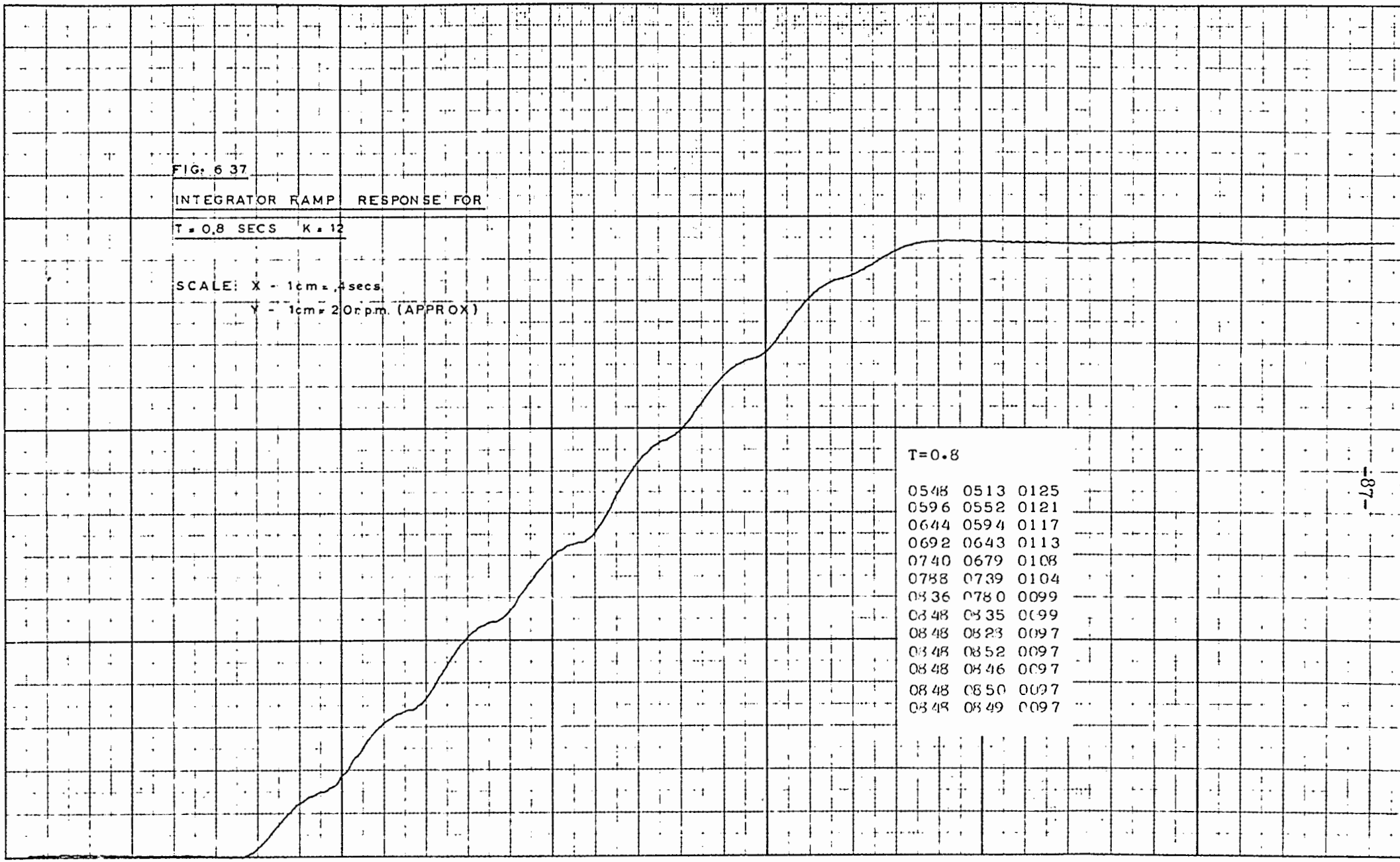

T=0.8

0548	0513	0125
0596	0552	0121
0644	0594	0117
0692	0643	0113
0740	0679	0108
0788	0739	0104
0836	0780	0099
0848	0835	0099
0848	0823	0097
0848	0852	0097
0848	0846	0097
0848	0850	0097
0848	0849	0097

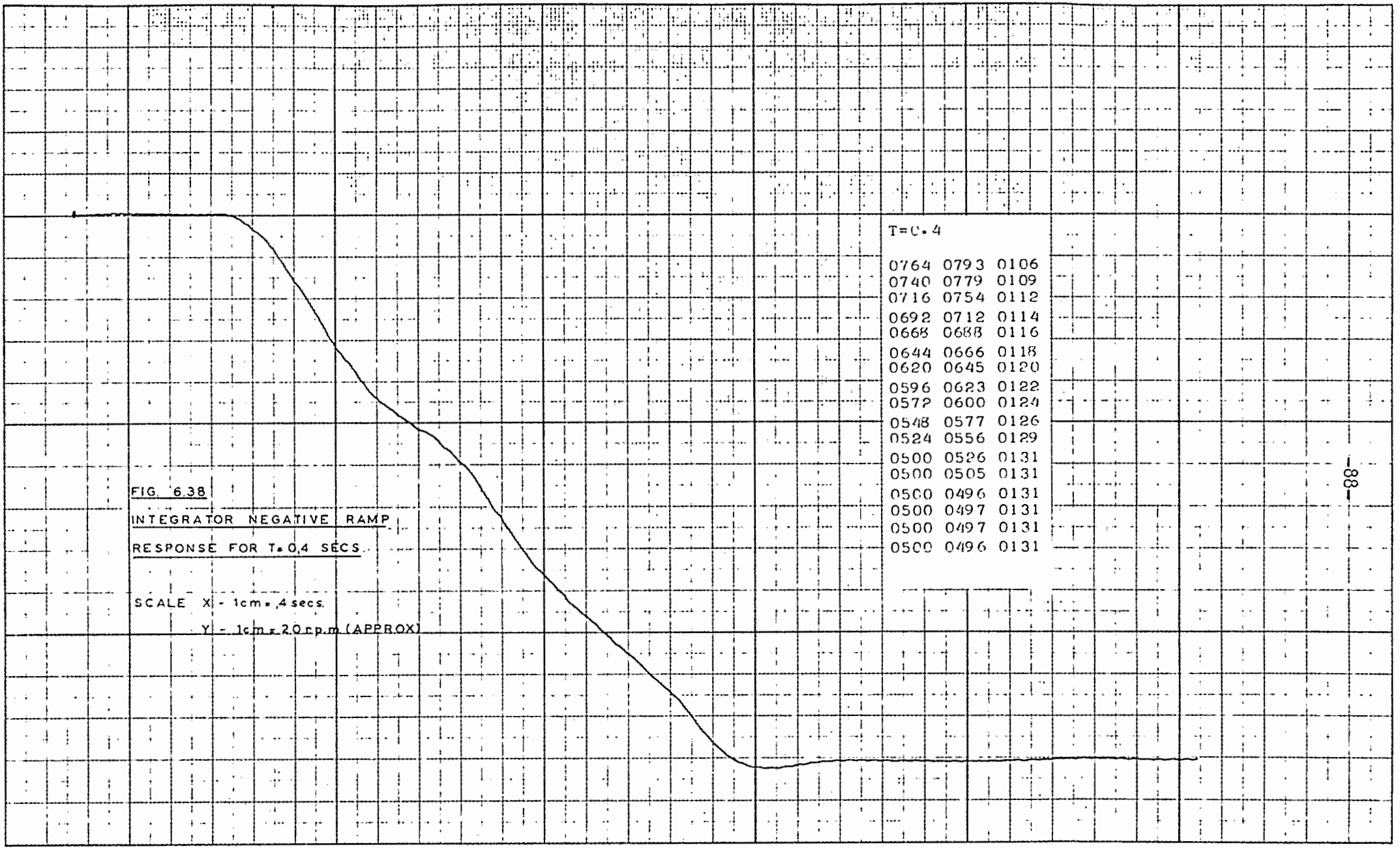

FIG. 6.38

INTEGRATOR NEGATIVE RAMP

RESPONSE FOR T=0,4 SECS

SCALE X - 1cm = ,4 secs.

Y - 1cm = 2.0 r.p.m. (APPROX)

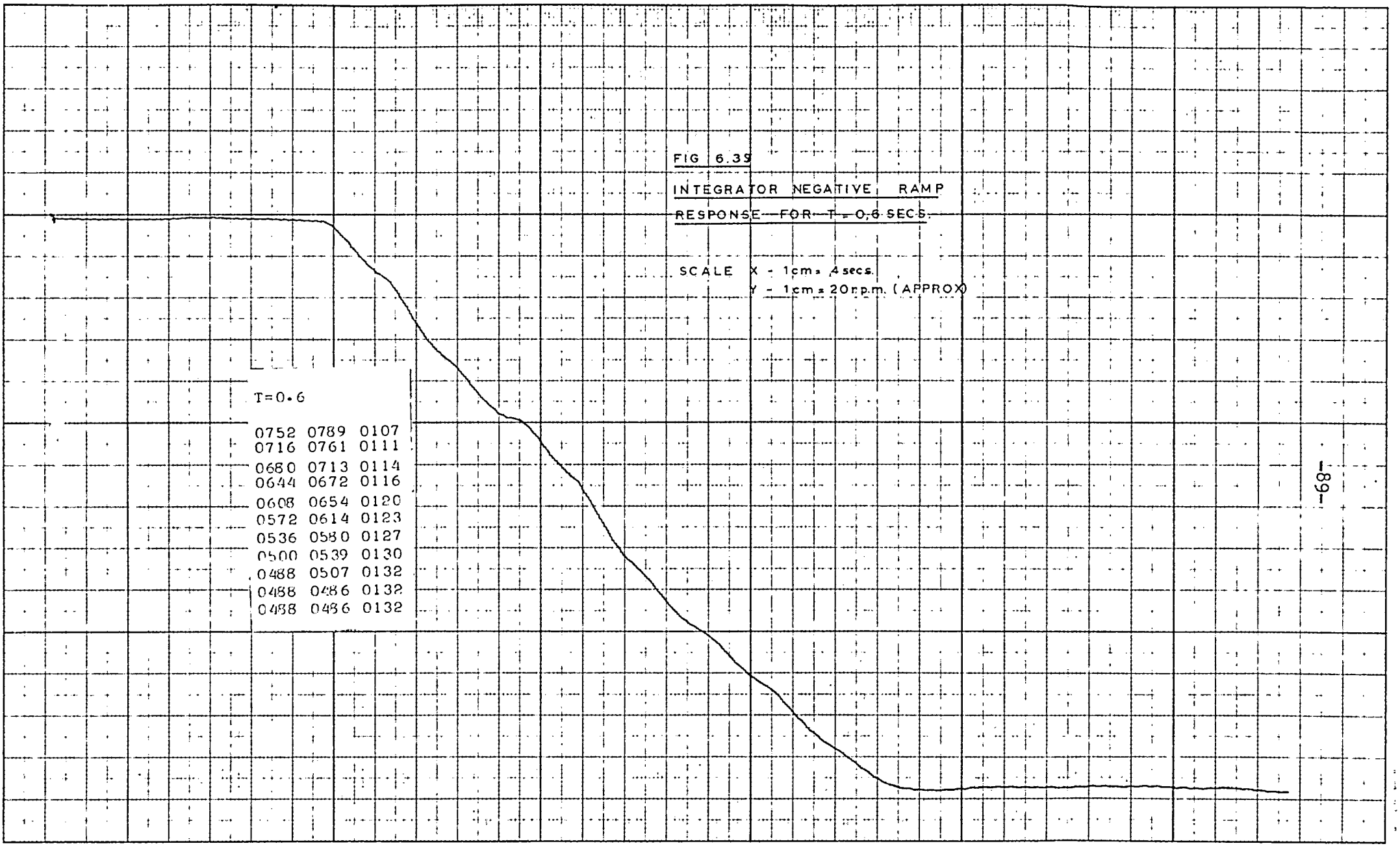

FIG 6.39

INTEGRATOR NEGATIVE RAMP RESPONSE FOR T = 0,6 SECS.

SCALE X - 1cm = 4 secs.
Y - 1cm = 20 r.p.m. (APPROX)

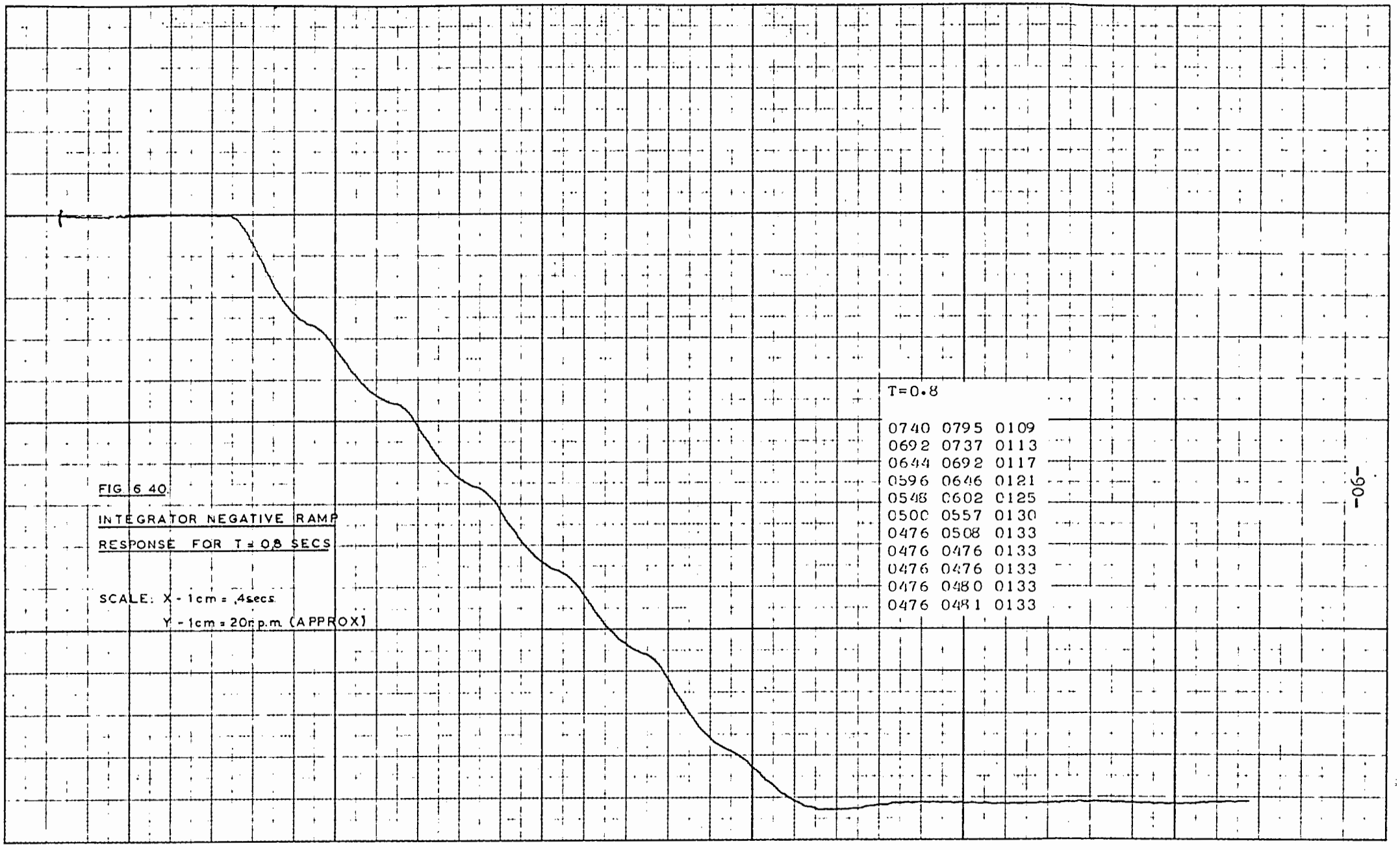

FIG 6 40

INTEGRATOR NEGATIVE RAMP RESPONSE FOR T = 0.8 SECS

SCALE: X - 1cm = .4secs

Y - 1cm = 20r.p.m. (APPROX)

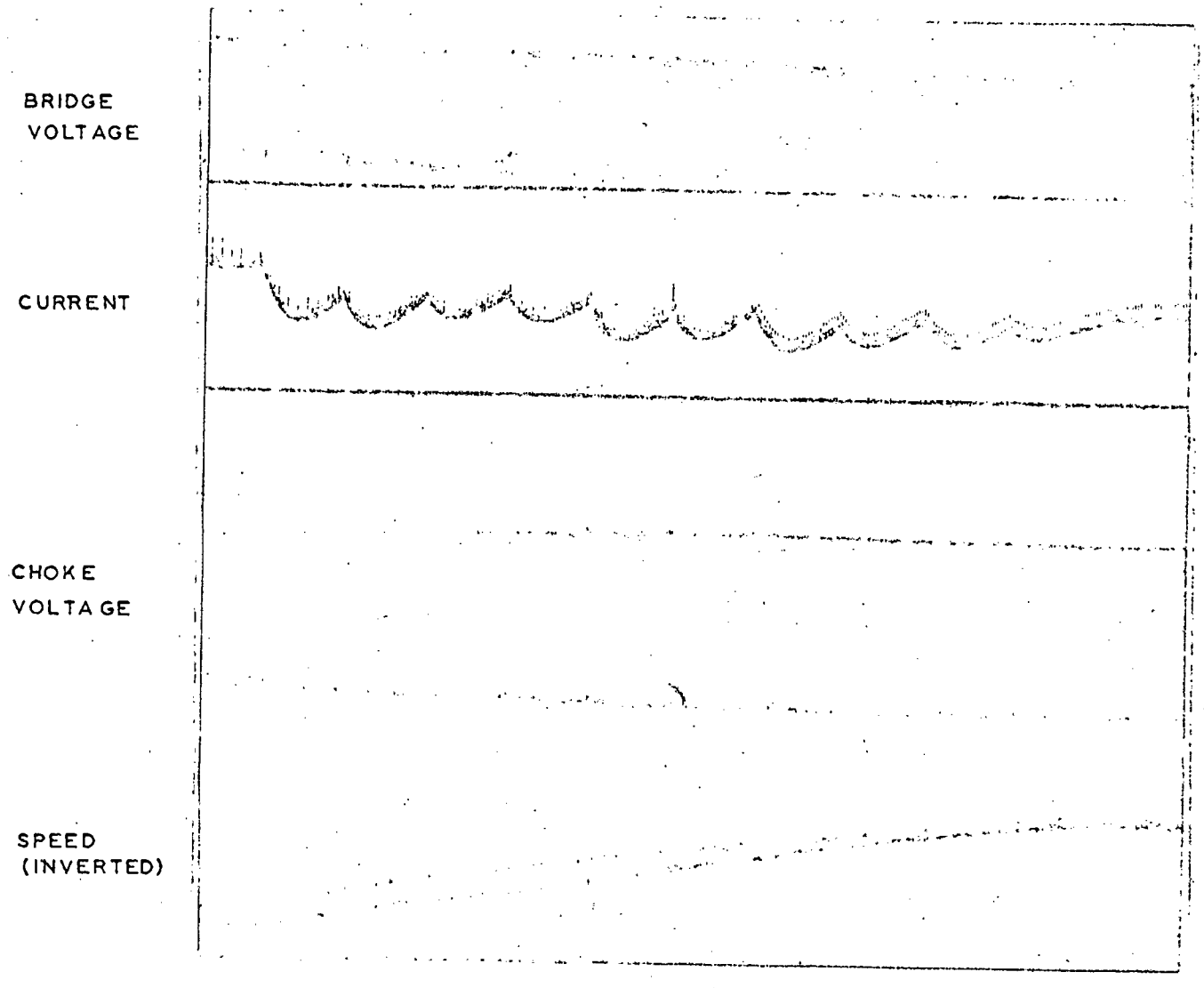

FIG. 6.41.

WAVEFORMS FOR NEGATIVE RAMP OF 60 R.P.M PER SEC AT T = 0,6 SECS.

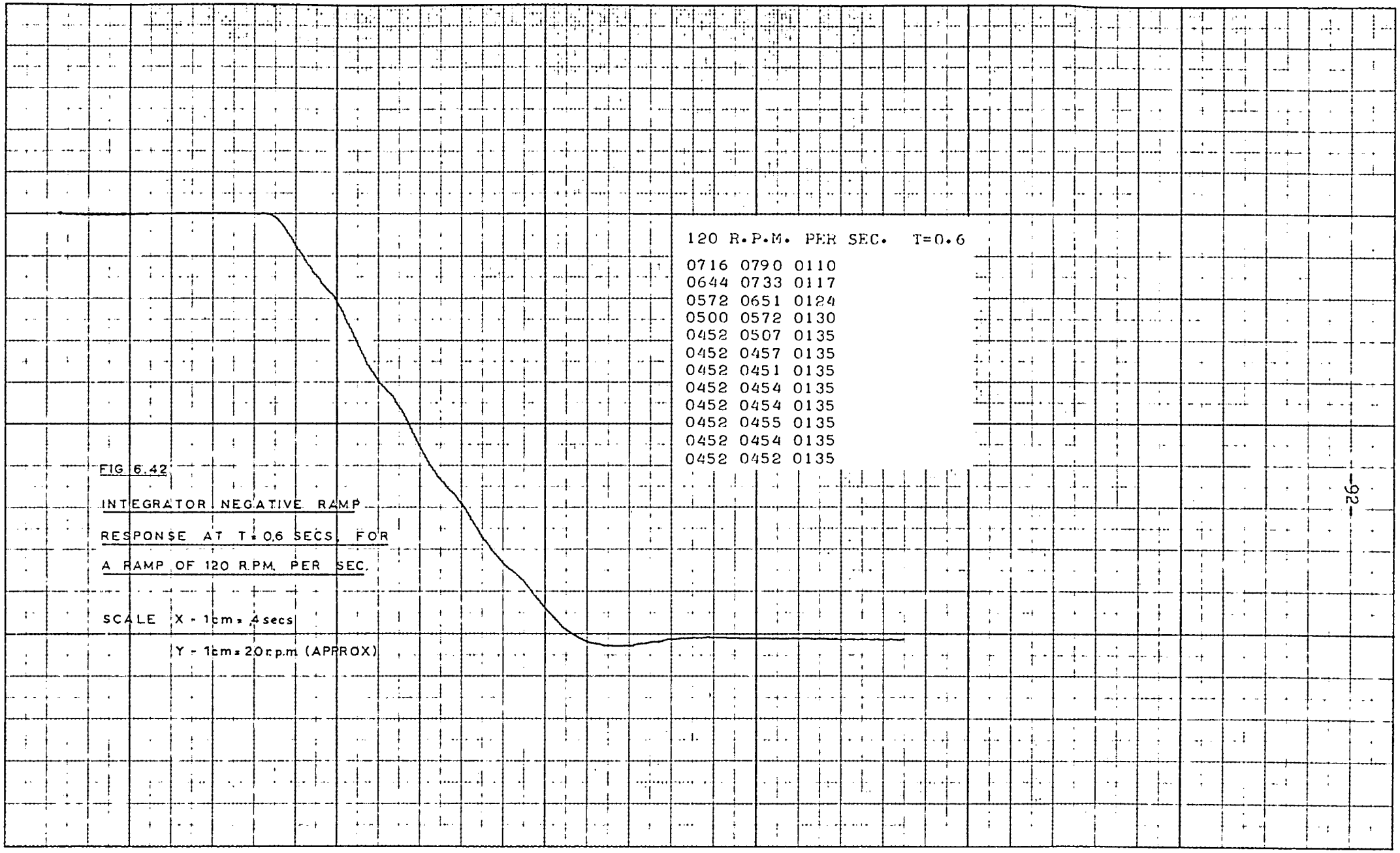

FIG 6.42

INTEGRATOR NEGATIVE RAMP RESPONSE AT T = 0.6 SECS. FOR A RAMP OF 120 R.P.M. PER SEC.

SCALE X - 1cm = .4secs

Y - 1cm = 20r.p.m (APPROX)

FIG. 6.43.

WAVEFORMS FOR NEGATIVE RAMP OF 120 R.P.M. PER SEC. WITH T = 0,6 SECS.

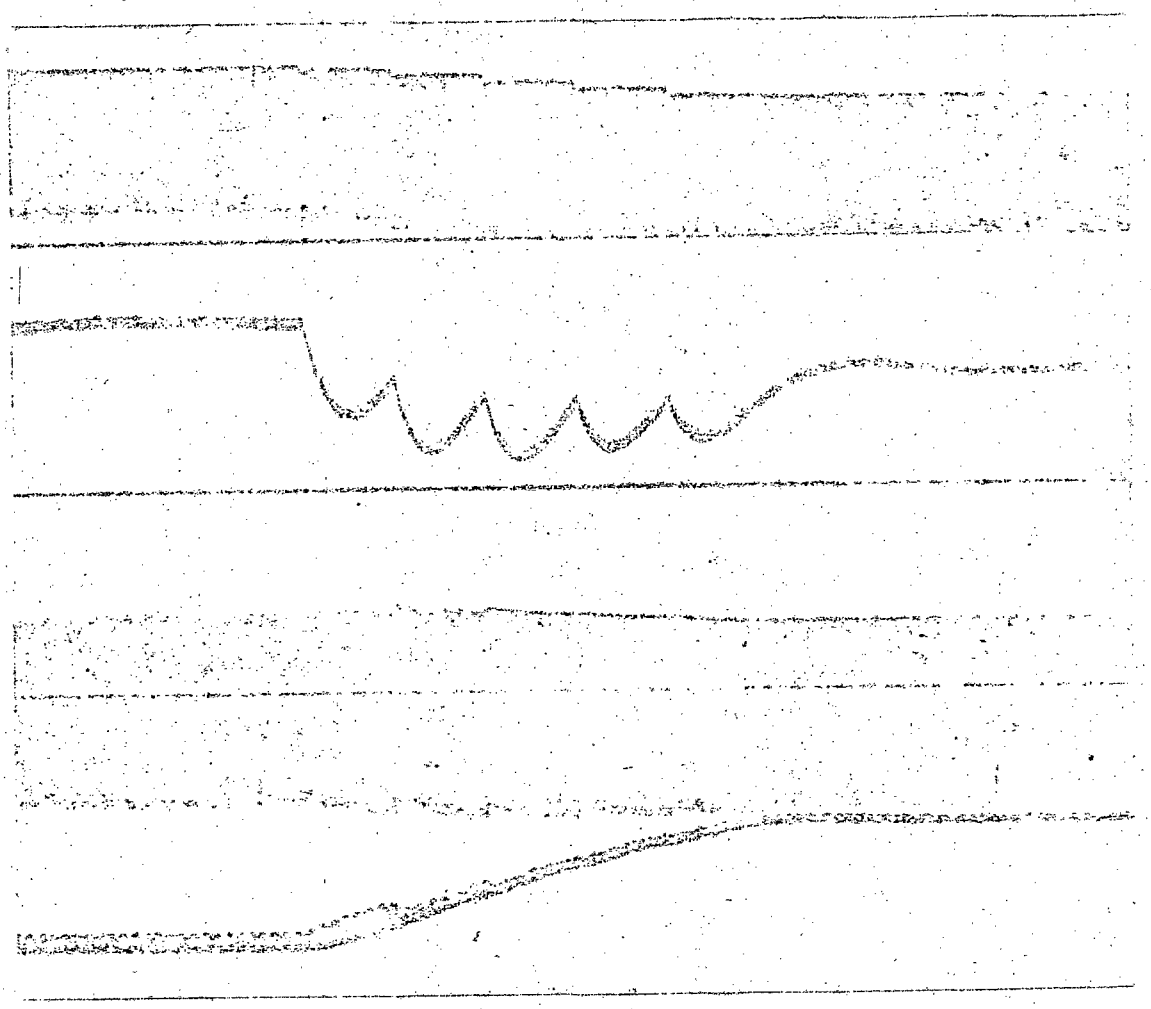

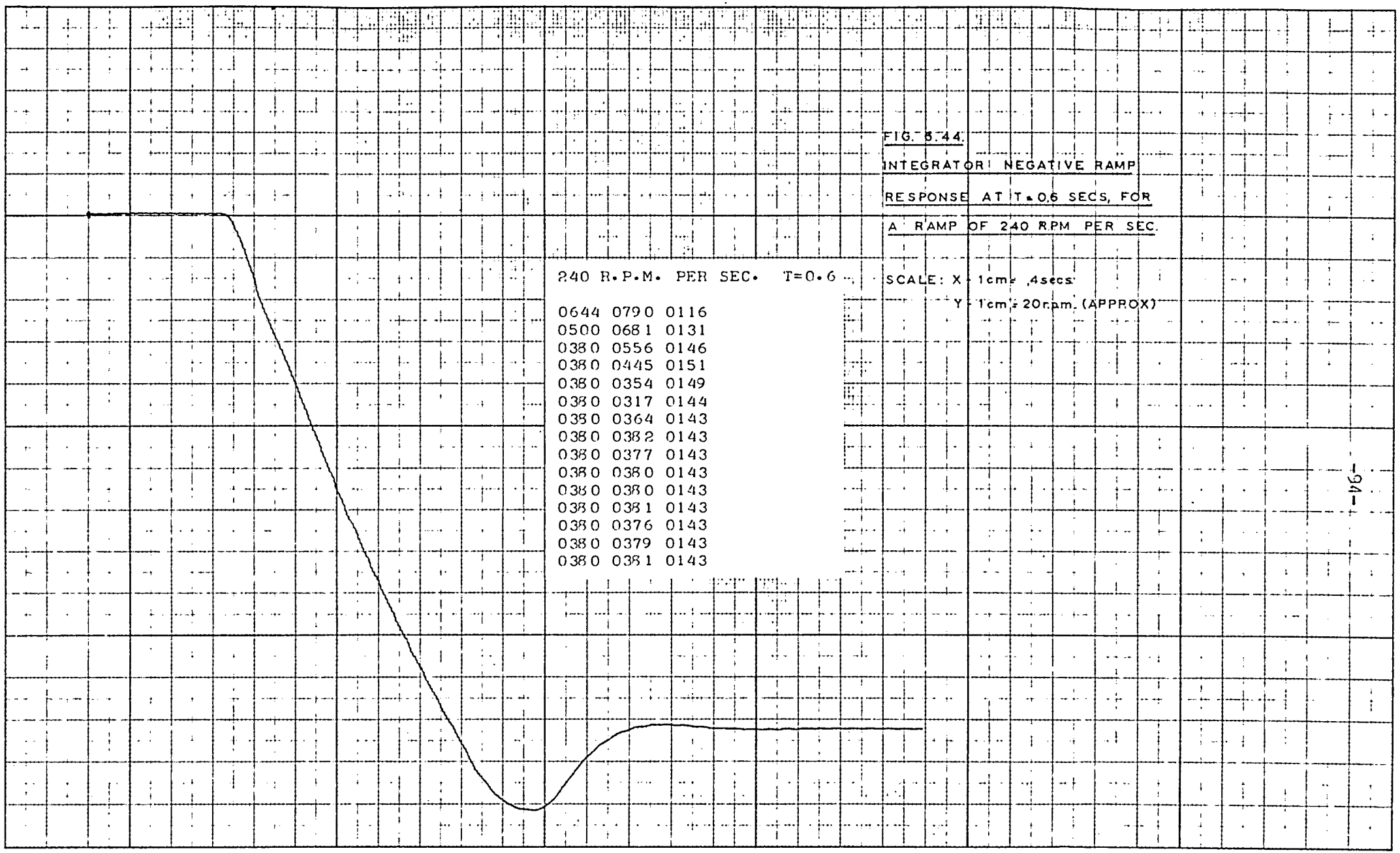

FIG. 5.44

INTEGRATOR NEGATIVE RAMP RESPONSE AT T = 0.6 SECS, FOR A RAMP OF 240 RPM PER SEC.

SCALE: X - 1cm = .4secs

Y - 1cm = 20r.p.m. (APPROX)

FIG. 6.45.

WAVEFORMS FOR NEGATIVE RAMP OF 240 RPM. PER SEC. AT T = 0,6 SECS.

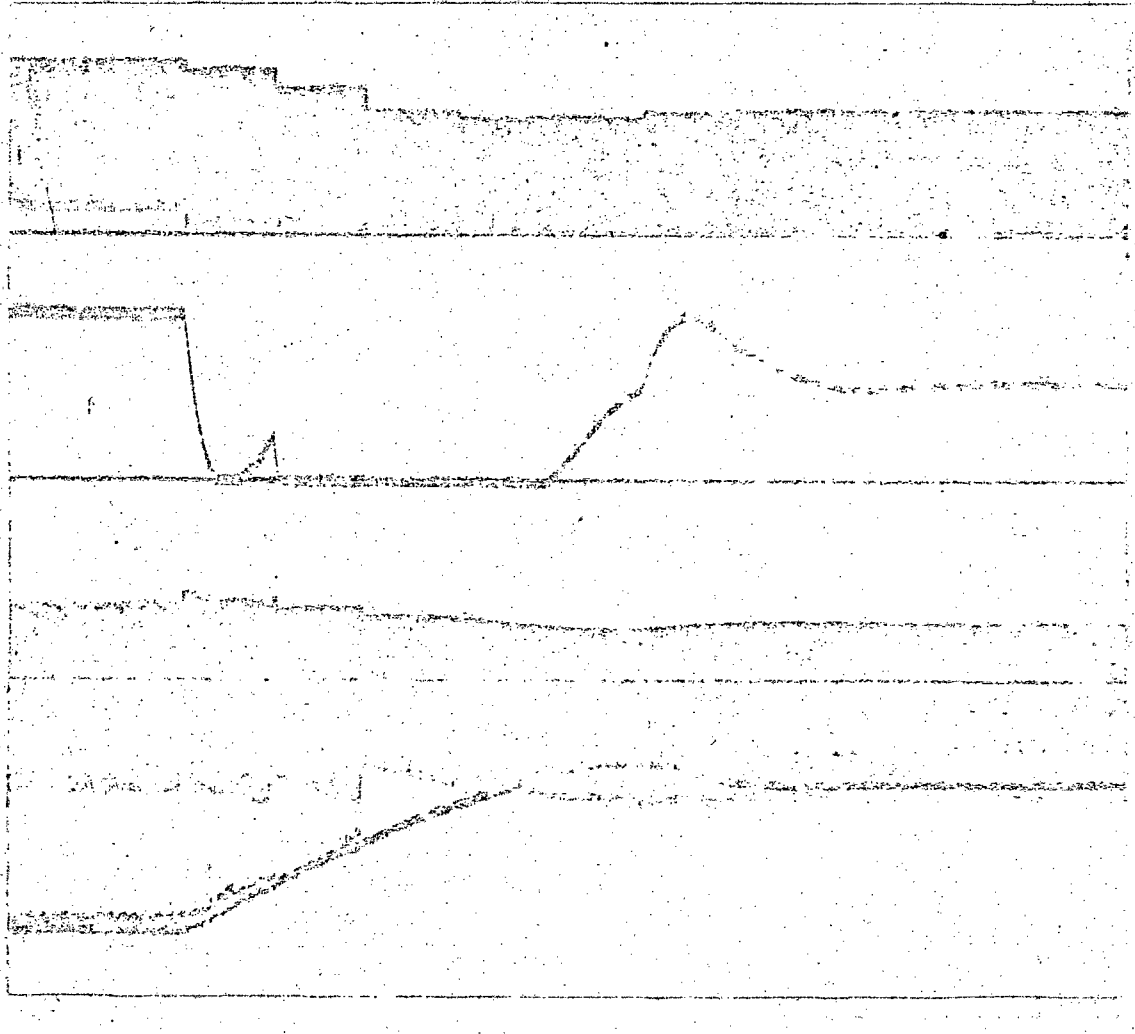

CHAPTER 7.

DIGITAL COMPENSATION.

7.1. THEORY OF DIGITAL COMPENSATION.

Bergen and Ragazzini [27] demonstrated in 1954 that the transfer function D(z) of a digital controller (such as a digital computer) could be expressed as a polynomial ratio in z^{-1}, if the output of the controller was a function of the previous input and output values. (See appendix 8).

The only restriction on this polynomial ratio would be imposed by the fact that no future samples could be considered in realizing the function D(z).

It was further shown in section 5.4 that the transfer function of the system under consideration (or in fact of any feedback system having a single feedback loop through a digital controller) is given by:

$$K(z) = \frac{C(z)}{R(z)} = \frac{D(z)G(z)}{1 + D(z)G(z)} \quad \ldots\ldots\ldots\ldots\ldots\ldots \quad (7.1)$$

This would seem to imply that a judicious choice of D(z) could lead to the implementation of any desired K(z), and with certain notable constraints [27,34], this is in fact so.

The implementation of a desired K(z) would be brought about by the cancellation of any unwanted poles or zeroes of G(z) by D(z). However, as Bertram [34] points out, this is not possible if such poles or zeroes lie outside the unit circle in the z plane, as under these circumstances any slight variation in parameters, leading to imperfect cancellation, would immediately result in instability. As shown in section 6.2, the poles and zero of the machine used for this thesis lie within the unit circle at all times, and therefore the above consideration is not significant.

Certain so-called "minimal prototype" response functions have been defined [27,29,34,35], which are designed to follow the specified input perfectly at each sampling instant after the

/..first..

first sampling period, eg. if a system is designed to have a minimal prototype step response, it will follow an applied step after one sampling instant, and its value, at subsequent sampling instants, will remain constant. However, it would be expected to follow a ramp input with a finite error . A system designed to have a minimal prototype ramp response, on the other hand, will follow a ramp perfectly after one sampling period (with the possibility of inter-sampling ripple), but would be expected to have a 100% overshoot if subjected to a step input [35]. The response has therefore to be "softened" by means of a so-called "staleness factor" [34], in order to decrease this overshoot. This, however, would mean that the ramp response would not settle down after one sampling period, but would take several sampling periods to do so.

The response of the given system when designed for the minimal prototype step response, and for the minimal prototype ramp response with staleness factors, was simulated and then determined in practice. An assessment was also made of the effect of changing the parameters by a small amount.

7.2. CALCULATION OF WEIGHTING FACTORS AND SIMULATION OF PERFORMANCE.

From equation (7.1), it can be shown that:

$$D(z) = \frac{1}{G(z)} \frac{K(z)}{1 - K(z)} \quad \ldots\ldots\ldots\ldots\ldots \quad (7.2)$$

Now, for a minimal prototype step response,

$$K(z) = z^{-1} \quad \ldots\ldots\ldots\ldots\ldots\ldots\ldots \quad (7.3)$$

Hence D(z) could be determined in terms of the system constants and values similarly obtained for the minimal prototype ramp response with a staleness factor, for which:

$$K(z) = \frac{(2 - c)z^{-1} - z^{-2}}{1 - cz^{-1}} \quad \ldots\ldots\ldots\ldots\ldots \quad (7.4)$$

where c is the staleness factor.

The derivation of D(z) in each of these cases is shown in appendix 9.

The use of $K(z) = z^{-1}$ for the minimal prototype step response resulted in a polynomial ratio for D(z) with three terms in the numerator and denominator, i.e. this would use only the previous two input and output values in the calculation of the firing angle setting, as opposed to the algorithm for the ramp response, where four term polynomials were used, implying the use of the previous three input and output values.

Multiplying z^{-1} by a factor $(z^{-1} - a)/(z^{-1} - a)$ had the effect of increasing the complexity of D(z) to a four term polynomial ratio without, however affecting the actual step response in any way. Tables 7.1 and 7.2 show the weighting factors for the three and four term ratios respectively.

The four term ratio was used in all actual implementation programs, with the idea that the use of additional data would have a filtering effect in the prescence of noise. As shown in appendix 10 however, this made no difference to the predicted behaviour of the system under normal conditions.

In calculating the weighting factors to be used, a degree of rounding off was necessary. This was because the control program did not make use of floating point arithmetic, as such routines would, it was felt, use too much computer time, and so all calculations were done using integer variables. In order to preserve accuracy, whenever fractional amounts would normally be expected (as, for example with the weighting factors, which varied in magnitude from ,001 to 1,5); the numbers were multiplied by 1 000, the calculations performed and the final answer divided by 1 000 again, being rounded off according to the remainder.

The weighting factors were therefore rounded off to the third

/..decimal..

decimal place. Tables 7.1 and 7.2 show the weighting factors determined, using a BASIC program on the Varian computer, for the minimal prototype step response, at various sampling rates. The first three (or four) factors are those which were applied to the present and previous two (or three) input values, while the following two (or three) factors are those applied to the previous two (or three) output values (the formula used is shown in appendix 9). The factors were rounded off in the simulation and implementation programs.

Once D(z) had been determined, it was only necessary to multiply the polynomials to find C(z) for a step input, and hence to find the time sequence by a power series expansion similar to that done in section 6.3.

The modified z-transform method was once again used to determine the full system response at various sampling rates. Appendix 10 shows the mathematical derivations and process used.

The minimal prototype step response simulations are shown in figures 7.1 to 7.12, along with the actual curves obtained. It is seen that it was to be expected that a small amount of intersampling ripple would be present, but that this would be considerably less than that experienced using integral control. The anticipated overshoot was also smaller.

It should be noted that the time scale used for these curves was not the same as that used for most of the curves in chapter 6, but that the vertical scale is the same.

The step response for a system designed for the minimal prototype ramp response was simulated for staleness factors of 0,5 and 0,85, and these results are shown in figures 7.13 to 7.24 along with the actual curves. It can be seen that one would expect both high overshoot and a long settling time from such systems.

TABLE 7.1.

T= .3

.219798 -.133546 5.61324E-02
-.37446 -.625543

T= .4

.149204 -3.96405E-02 2.41749E-02
-.473161 -.526838

T= .5

.116036 -2.06093E-03 1.19282E-02
-.562605 -.437394

T= .599999

9.84262E-02 1.39373E-02 6.41929E-03
-.643905 -.356094

T= .699999

8.86148E-02 2.00437E-02 3.66672E-03
-.717629 -.28237

T= .799999

8.32372E-02 2.10978E-02 2.18517E-03
-.783903 -.216096

T= .899999

8.06014E-02 1.94411E-02 1.34247E-03
-.842529 -.15747

T= .999999

7.97418E-02 1.63693E-02 8.42649E-04
-.893118 -.106881

TABLE 7.2.

T= .3

.219798 -.243446 .122905 -2.80662E-02
-.874471 -.438323 .312771

T= .4

.149204 -.114242 4.39951E-02 -1.20874E-02
-.973161 -.290257 .263419

T= .5

.116036 -6.00793E-02 1.29587E-02 -5.96411E-03
-1.0626 -.156091 .218697

T= .599999

9.84262E-02 -3.52757E-02 -5.49403E-04 -3.20964E-03
-1.1439 -3.41412E-02 .178047

T= .699999

8.86148E-02 -2.42636E-02 -6.35515E-03 -1.83336E-03
-1.21762 7.64438E-02 .141185

T= .799999

8.32372E-02 -2.05207E-02 -8.36376E-03 -1.09258E-03
-1.2839 .175854 .108048

T= .899999

8.06014E-02 -2.08595E-02 -8.37811E-03 -6.71238E-04
-1.34252 .263793 7.87353E-02

T= .999999

7.97418E-02 -2.35015E-02 -7.34201E-03 -4.21324E-04
-1.39311 .339678 5.34405E-02

The reason for the high overshoot experienced with the minimal prototype ramp system is that any error signal detected is assumed to be the start of a ramp, and the system tries to anticipate this ramp. This fact was borne out when a ramp input was applied to the system.

As the staleness factor was increased, it was seen that the anticipated overshoot would decrease. However, the trade-off here was in terms of settling time which would in all probability be so great as to be unacceptable (see for example fig. 7.23, which shows the simulation, with a staleness factor of 0,85, at a sampling rate of 1 sec.). The possibility should also be borne in mind that any tacho ripple might accentuate the error due to the long settling time, and make the system tend towards instability.

7.3. IMPLEMENTATION OF THE COMPENSATION PROGRAM - STEP RESPONSE.

The compensation program was similar to that used for integral control, except that the calculation routine became more complex, and facility had to be made for the storage of weighting factors, as well as of past input and output values (see appendix 11).

The weighting factors for the type of system to be implemented were fed into a specified area in the memory of the computer. Typing in of the sampling time for an actual run caused the relevant factors to be used for the program under execution. As mentioned previously, the weighting factors were stored as integers, and constituted the calculated values multiplied by 1 000, rounded off, and converted to octal numbers.

As before, steps were applied between 500 and 800 r.p.m., but only on load tests were taken in this instance, as the main purpose of these tests was to study the dynamic behaviour of the system, rather than the idiosyncrasies of the particular

/..configuration..

configuration used, as previously studied.

A deadband of 12 r.p.m. was again used.

Figures 7.1 to 7.12, along with the predicted curves, show the responses obtained. As before, the actual overshoot was generally smaller than predicted, but the times taken to reach the maximum overshoot and to settle were virtually identical to those predicted.

It is interesting to note that in most cases, the undershoot was greater than expected, and that as a result, the initial overshoot was not very much above the final value (see for example fig. 7.6, at a sampling rate of 0,6 secs.) This may have been due to small inaccuracies in the mathematical model used to derive the weighting factors, aided by the quantising errors caused by rounding off these factors.

The resonse for the ramp design system to a step input was, as anticipated, far from satisfactory, but did correlate fairly well with the predicted results. In particular, phenomena such as oscillation above the final value, and the gradual decay to the set point did make themselves evident, although any ripple on the tachometer must inevitably have led to more instability than might have been expected.

The curves are shown in figures 7.13 to 7.24, along with the predicted curves.

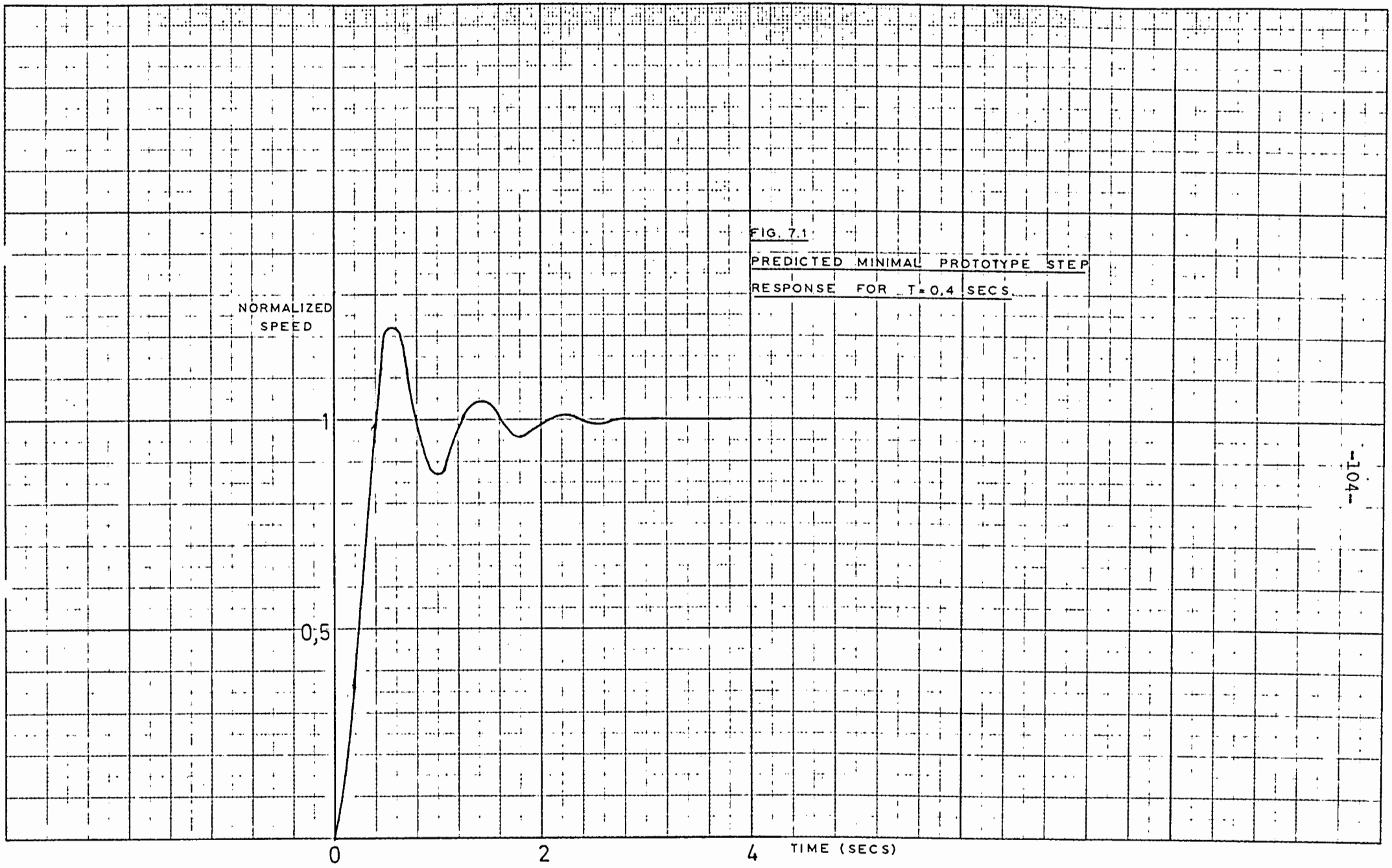

FIG. 7.1
PREDICTED MINIMAL PROTOTYPE STEP RESPONSE FOR T = 0,4 SECS.

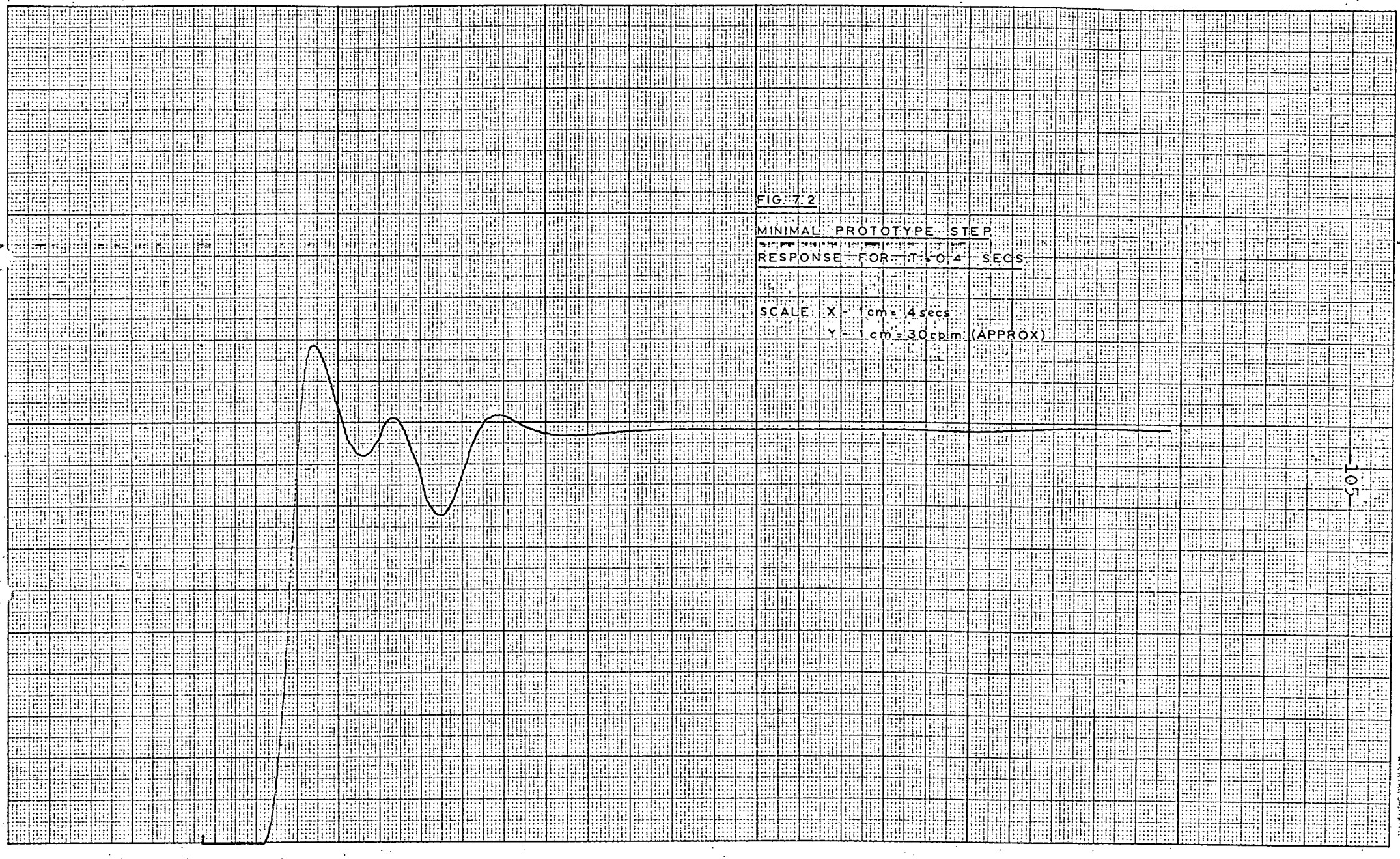

FIG. 7.2

MINIMAL PROTOTYPE STEP RESPONSE FOR T = 0.4 SECS

SCALE X - 1 cm = .4 secs

Y - 1 cm = 30 rpm (APPROX)

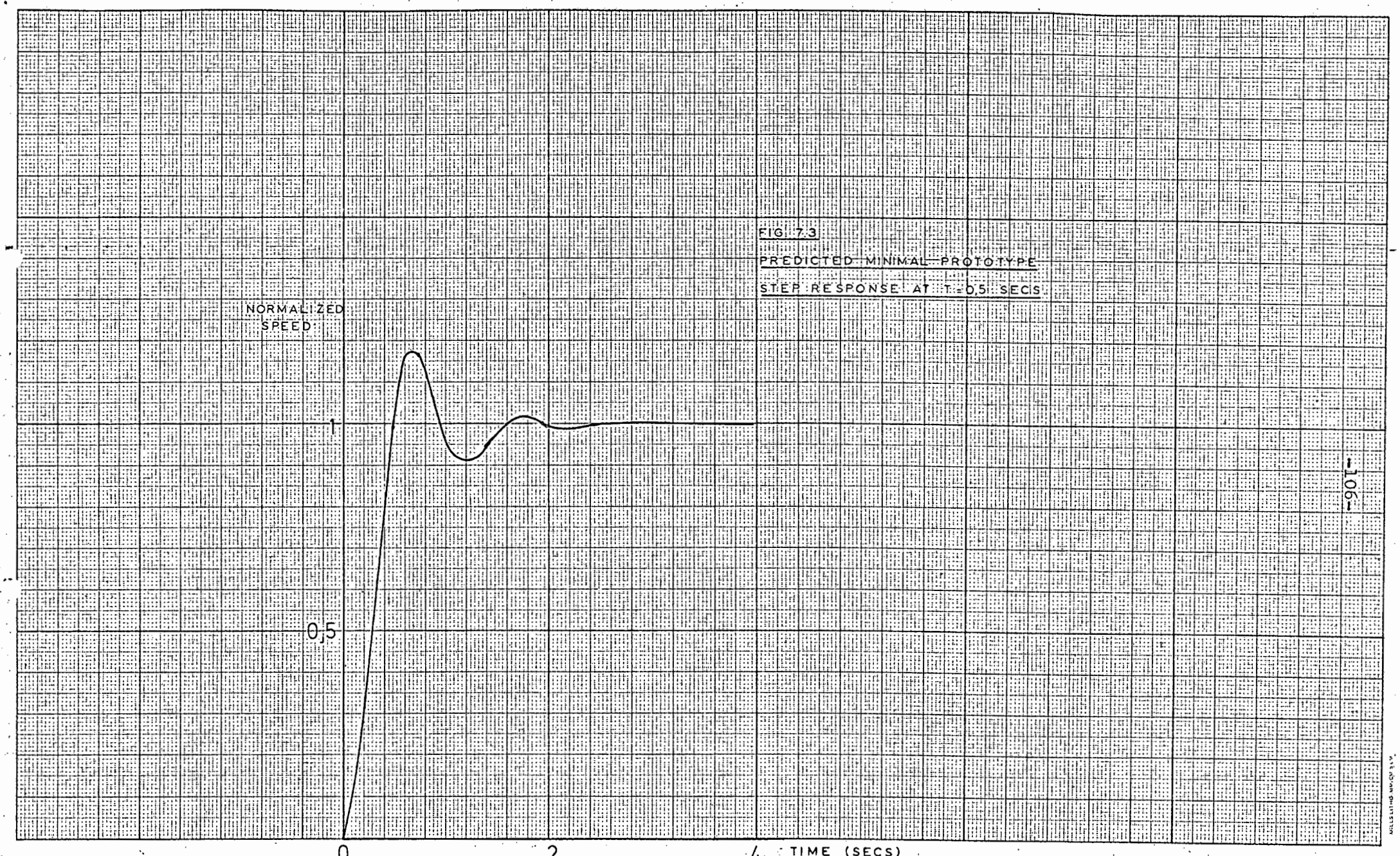

FIG. 7.3
PREDICTED MINIMAL PROTOTYPE STEP RESPONSE AT T = 0,5 SECS

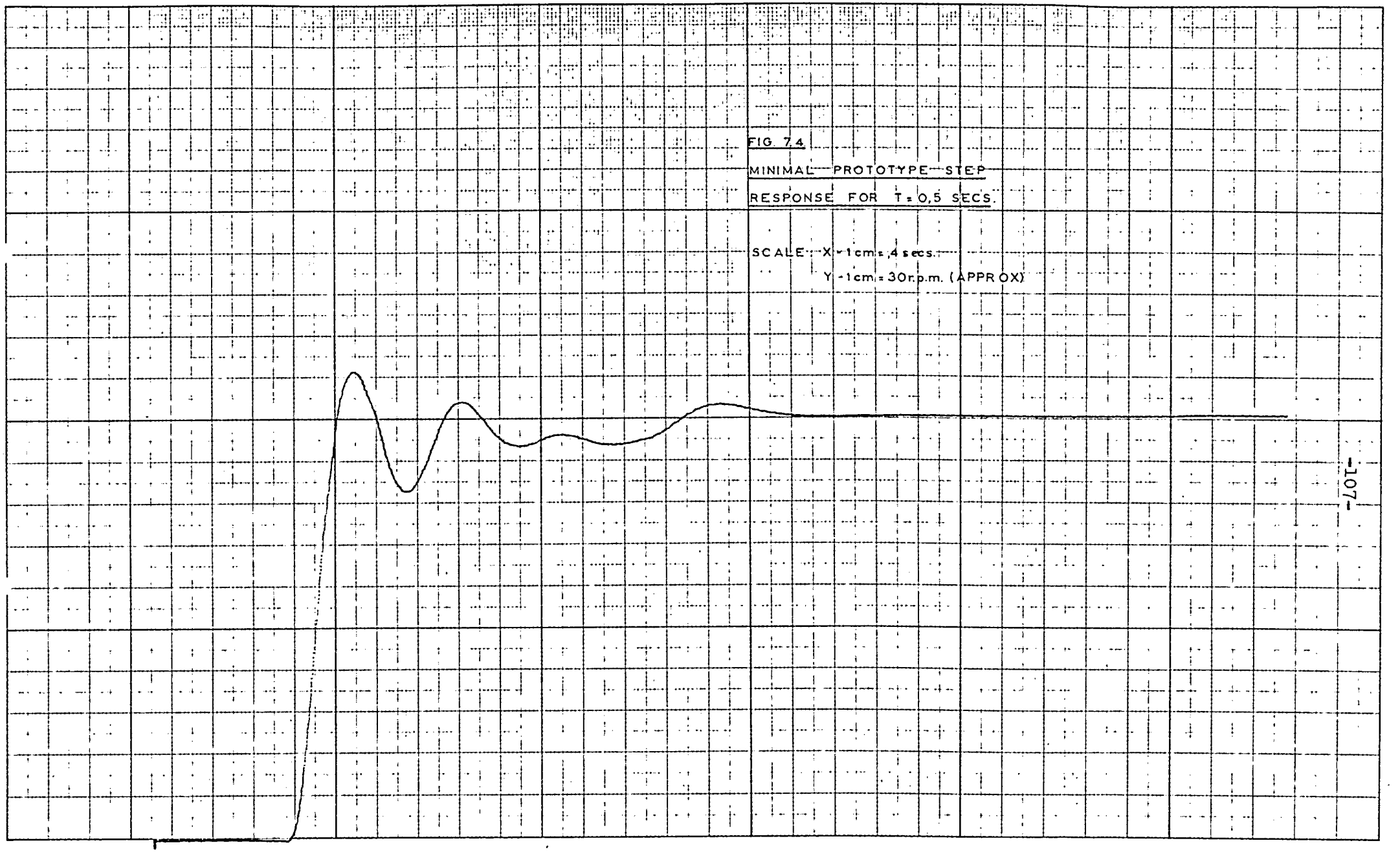

FIG 7.4

MINIMAL PROTOTYPE STEP RESPONSE FOR T = 0,5 SECS.

SCALE: X - 1cm = 4 secs.
Y - 1cm = 30r.p.m. (APPROX)

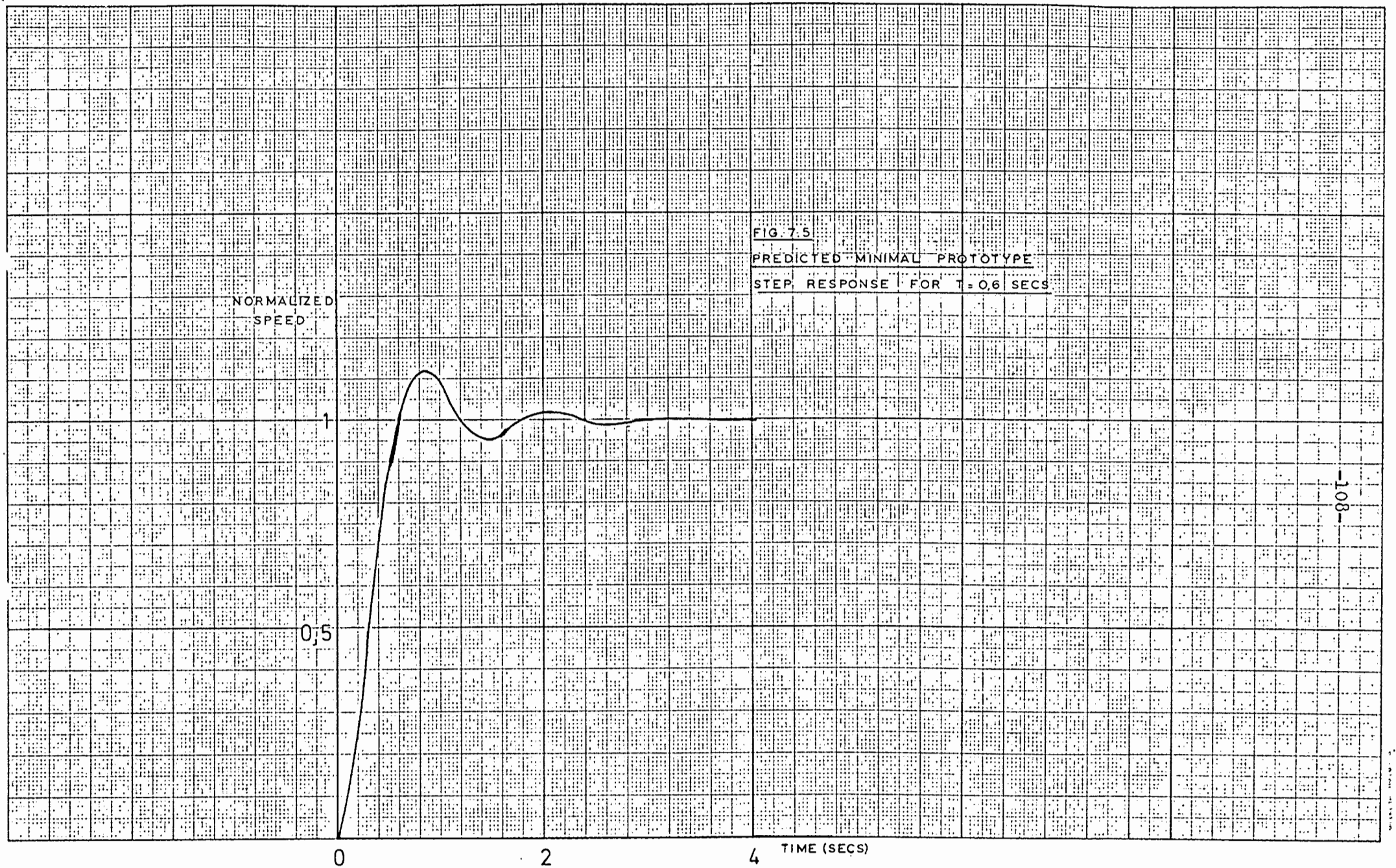

FIG. 7.5
PREDICTED MINIMAL PROTOTYPE STEP RESPONSE FOR T = 0,6 SECS

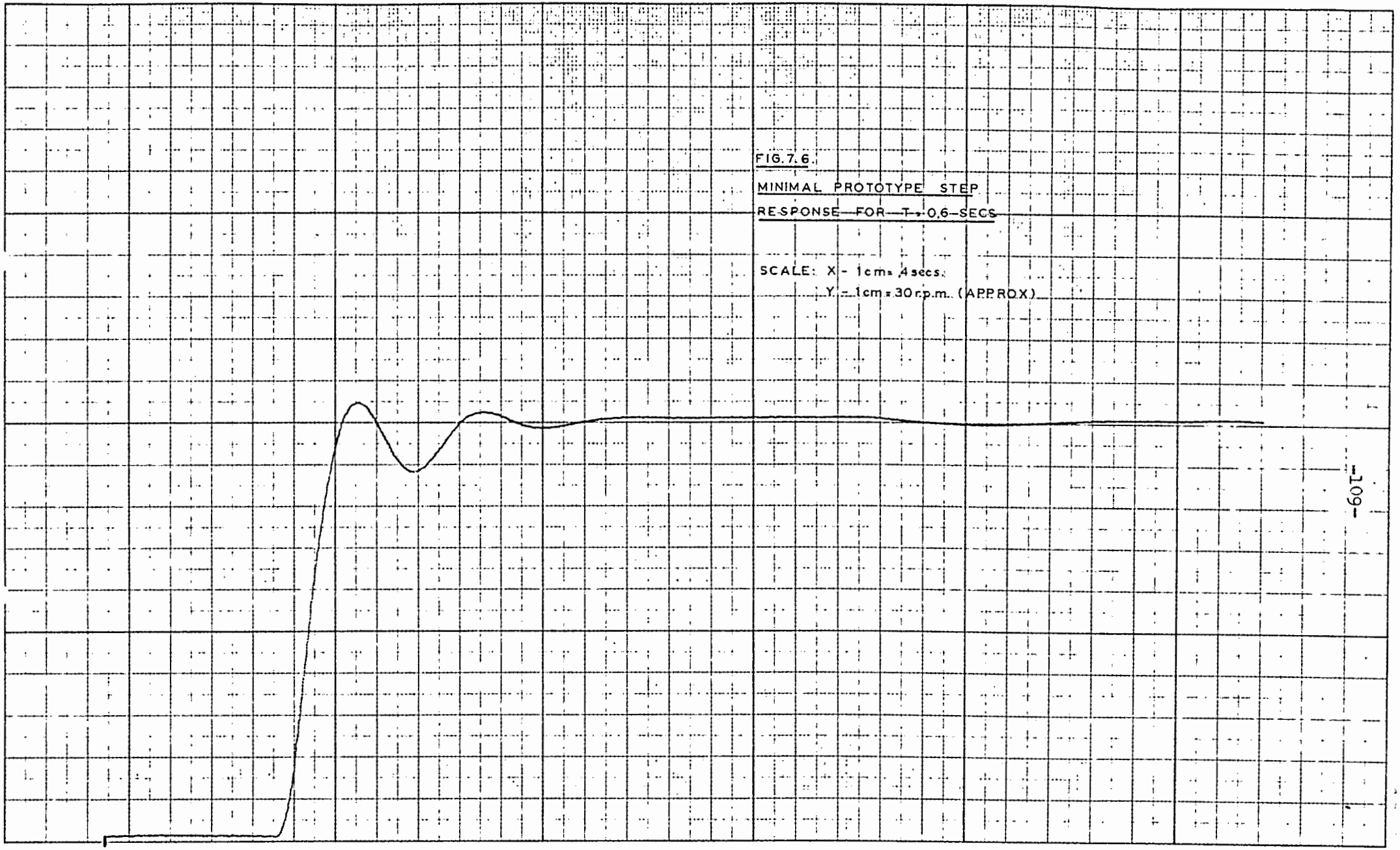

FIG. 7.6.

MINIMAL PROTOTYPE STEP RESPONSE FOR T = 0,6 SECS

SCALE: X - 1cm = 4 secs.
Y - 1cm = 30 r.p.m. (APPROX)

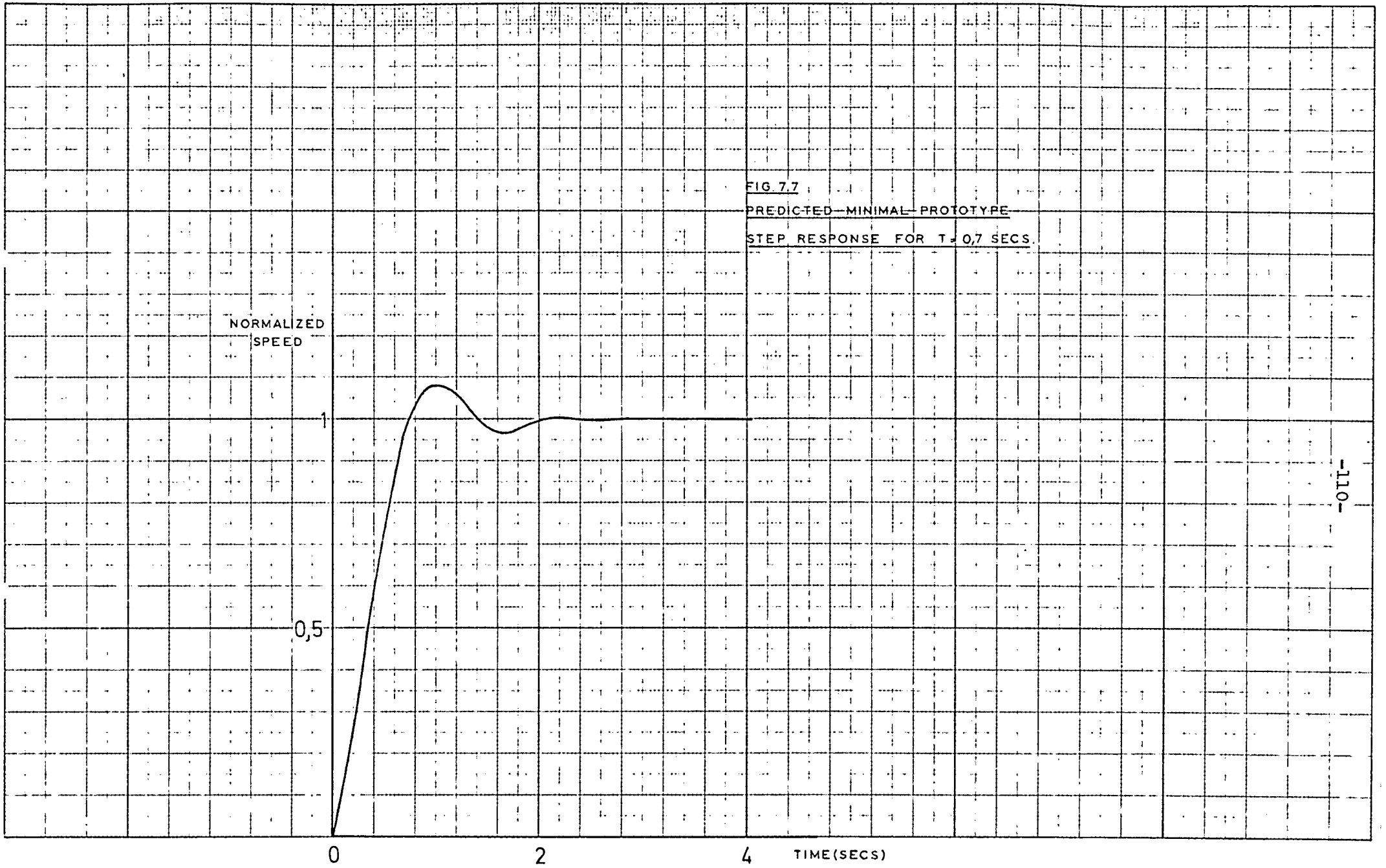

FIG. 7.7
PREDICTED MINIMAL PROTOTYPE STEP RESPONSE FOR T = 0,7 SECS.

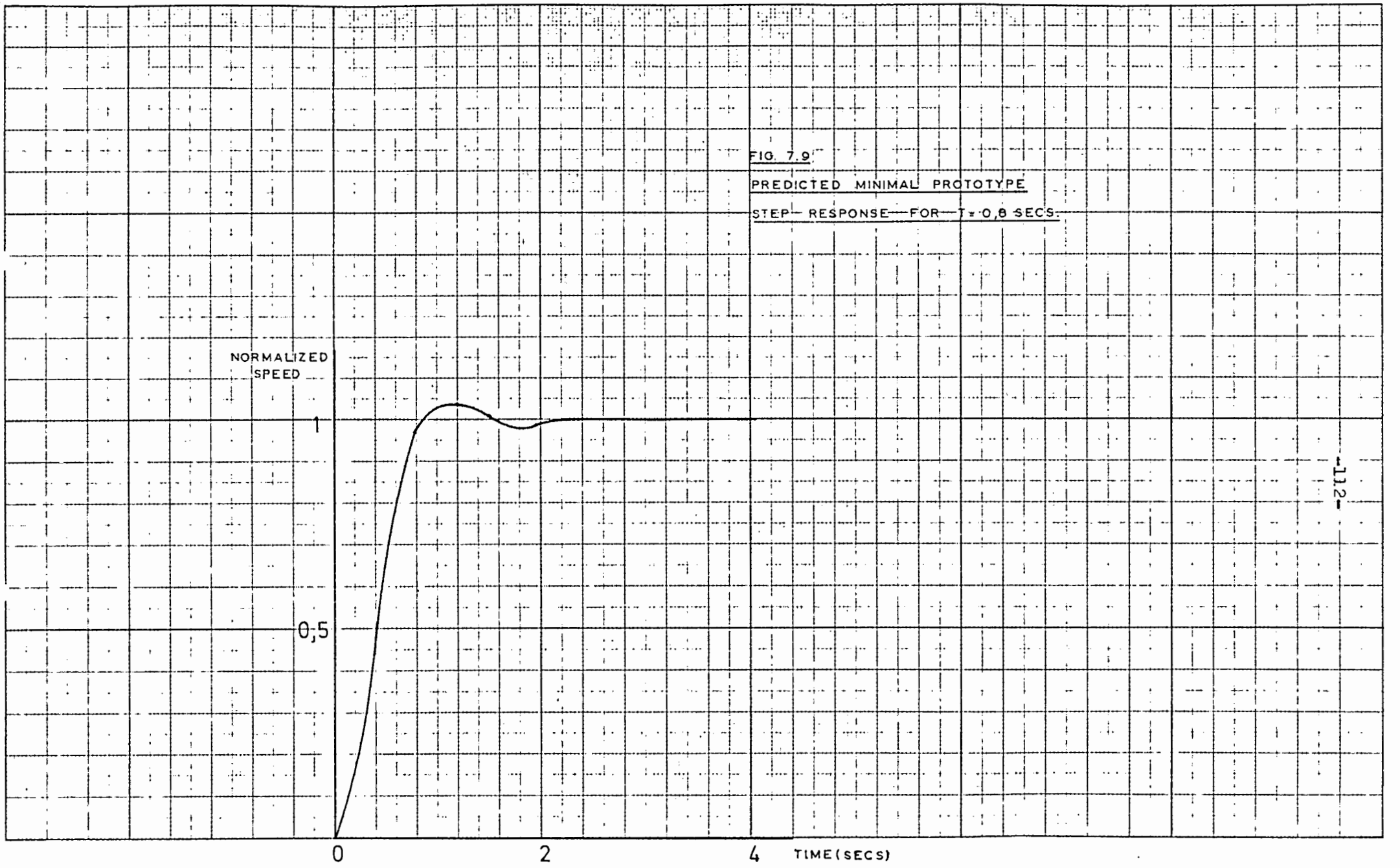

FIG. 7.9
PREDICTED MINIMAL PROTOTYPE
STEP RESPONSE FOR T = 0,8 SECS.

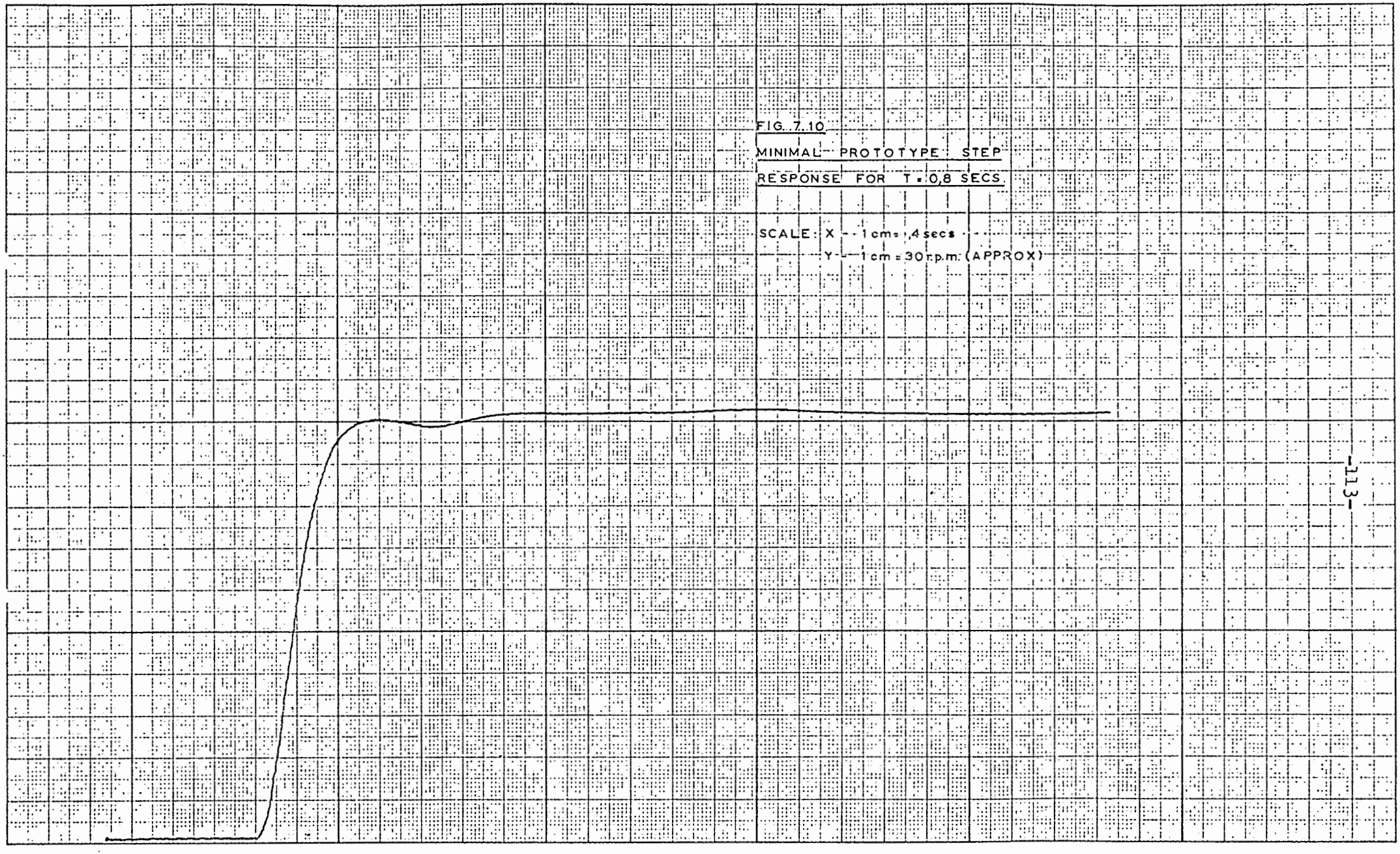

FIG. 7.10

MINIMAL PROTOTYPE STEP RESPONSE FOR T = 0,8 SECS.

SCALE: X - 1 cm = ,4 secs

Y - 1 cm = 30 r.p.m. (APPROX)

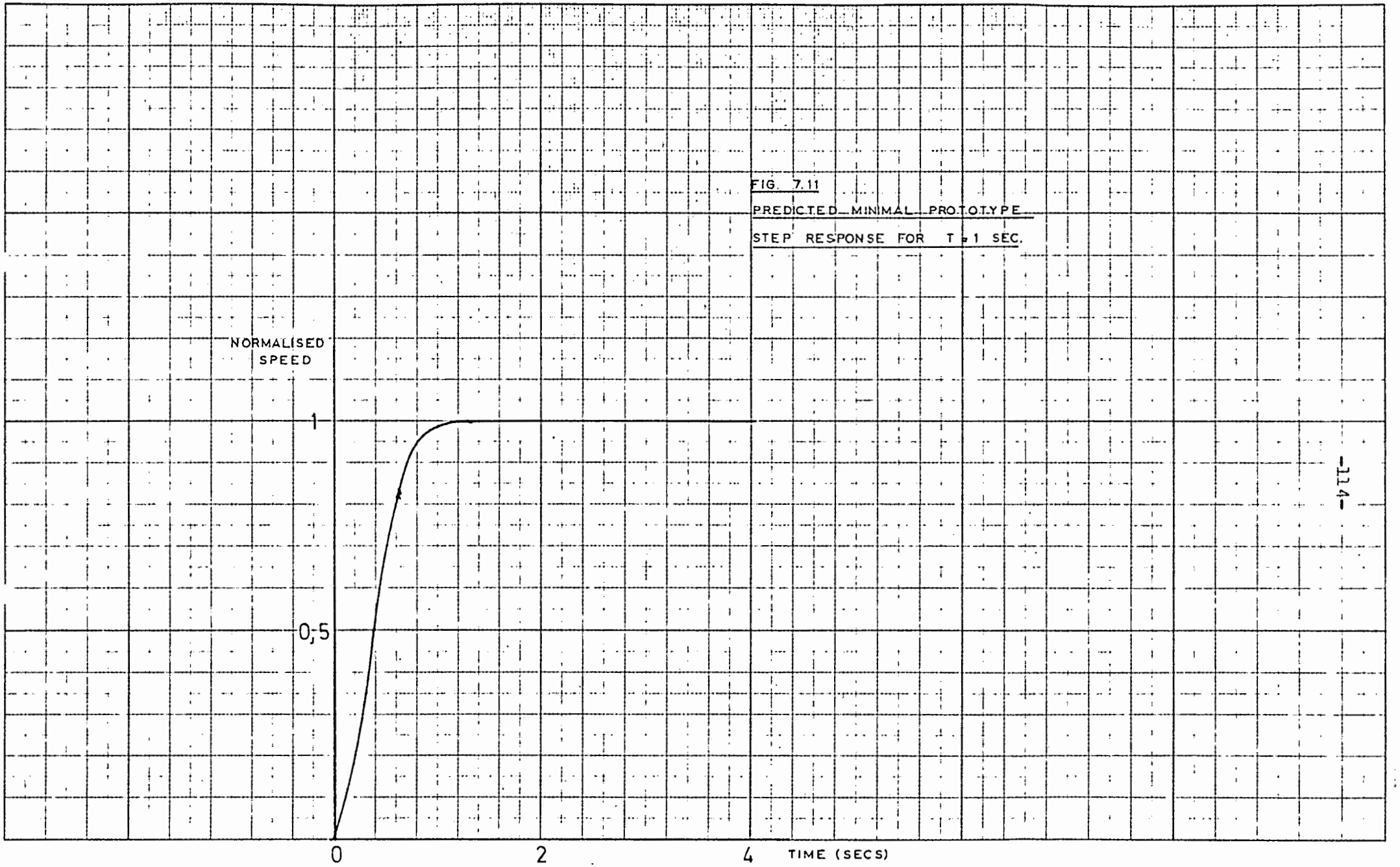

FIG. 7.11
PREDICTED MINIMAL PROTOTYPE STEP RESPONSE FOR T = 1 SEC.

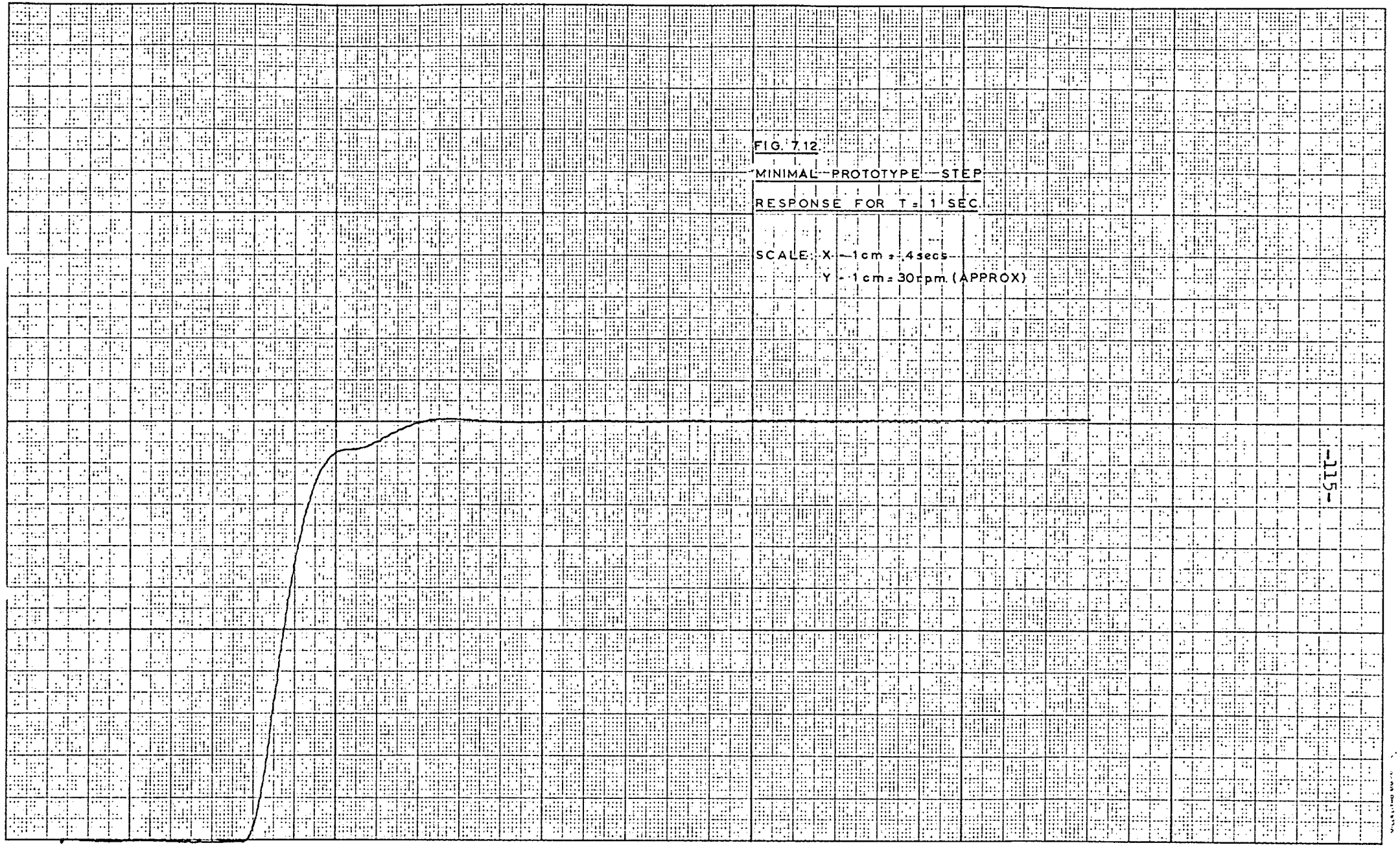

FIG. 7.12

MINIMAL PROTOTYPE STEP RESPONSE FOR T = 1 SEC.

SCALE: X — 1 cm = .4 secs

Y - 1 cm = 30 r.p.m. (APPROX)

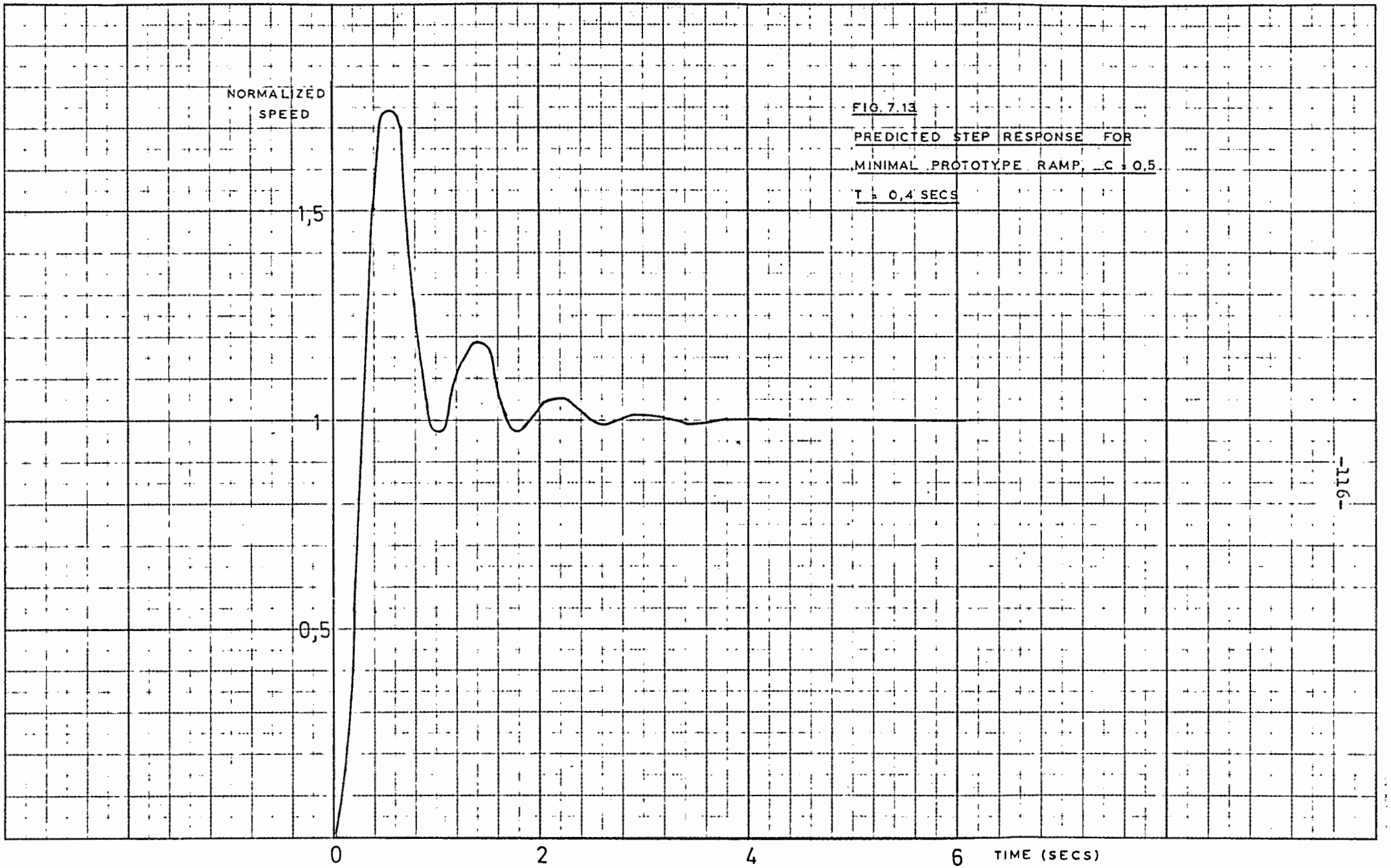

FIG. 7.13

PREDICTED STEP RESPONSE FOR MINIMAL PROTOTYPE RAMP, C = 0,5

T = 0,4 SECS

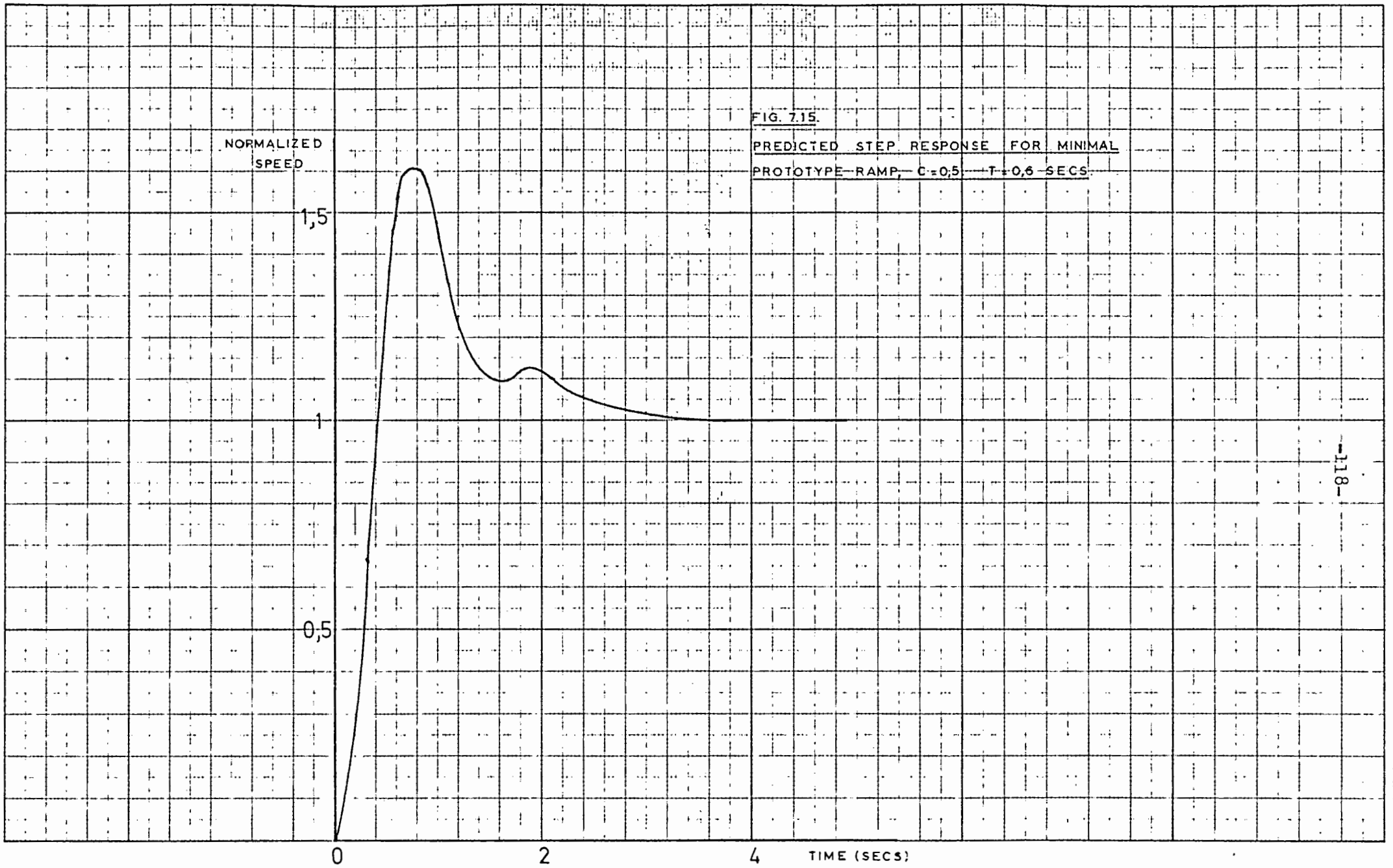

FIG. 7.15.

PREDICTED STEP RESPONSE FOR MINIMAL PROTOTYPE RAMP, C = 0,5 T = 0,6 SECS

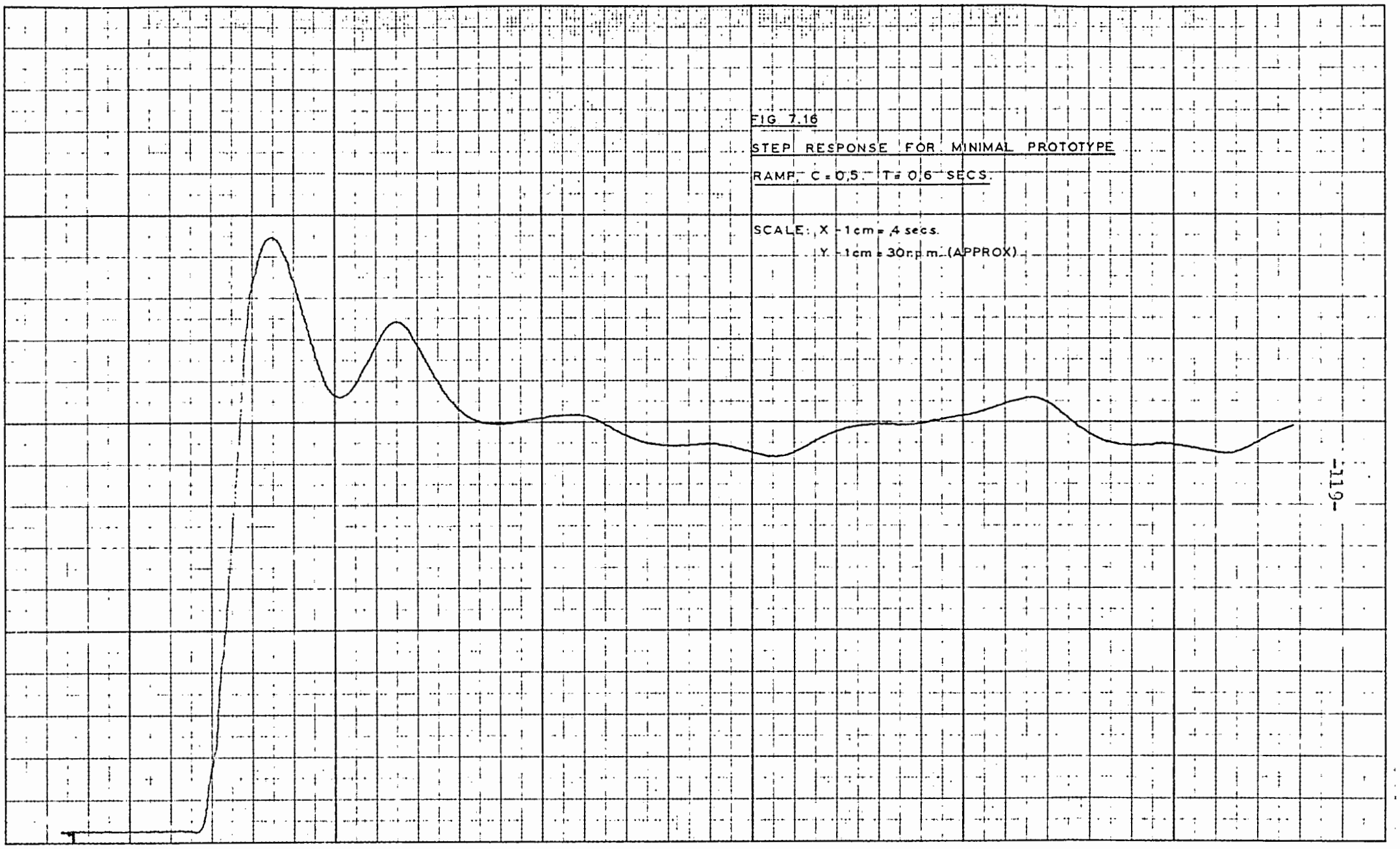

FIG 7.16

STEP RESPONSE FOR MINIMAL PROTOTYPE

RAMP, C = 0,5 T = 0,6 SECS.

SCALE: X - 1 cm = ,4 secs.

Y - 1 cm = 30 r.p.m. (APPROX)

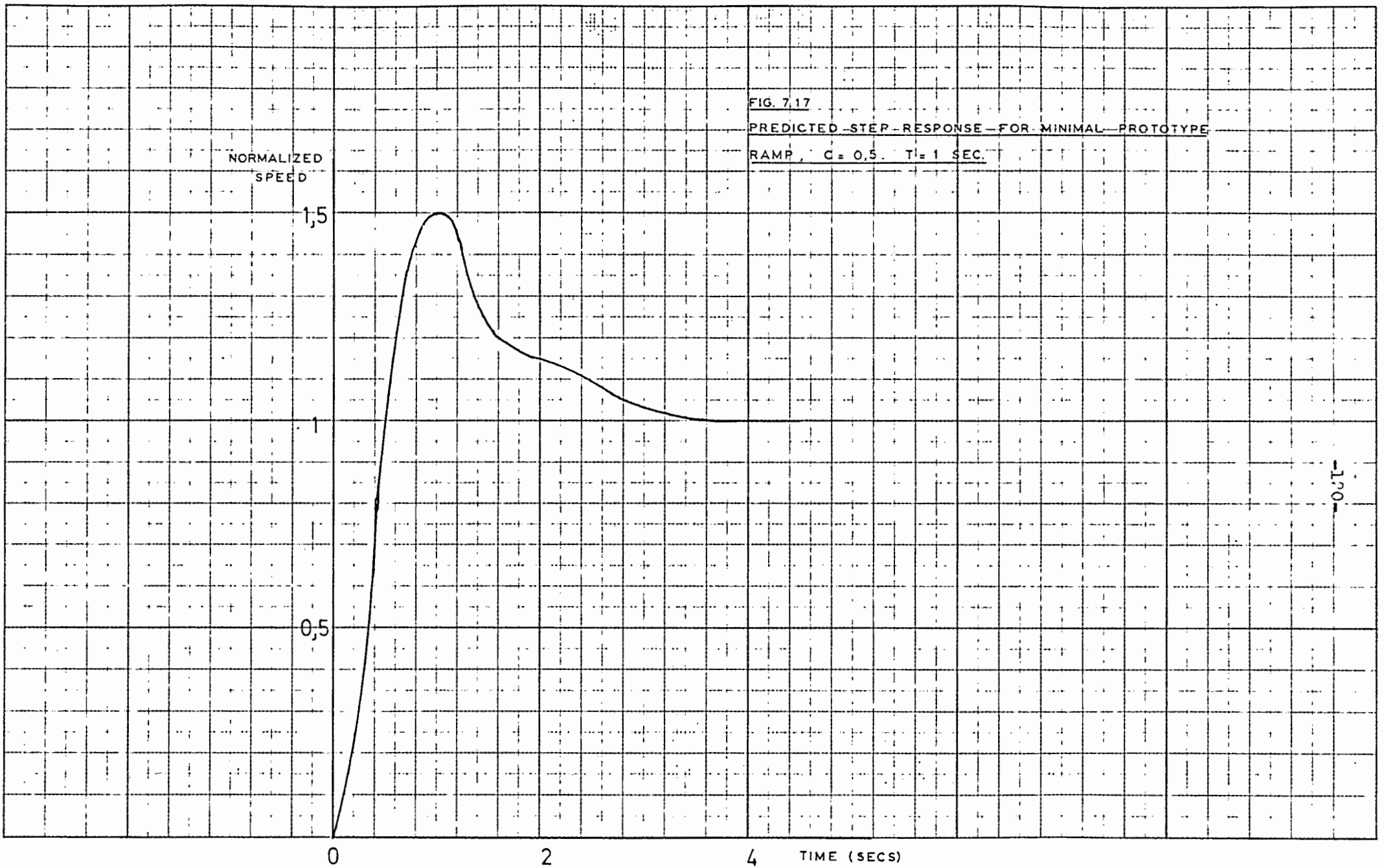

FIG. 7.17

PREDICTED STEP-RESPONSE FOR MINIMAL PROTOTYPE

RAMP, C = 0,5. T = 1 SEC.

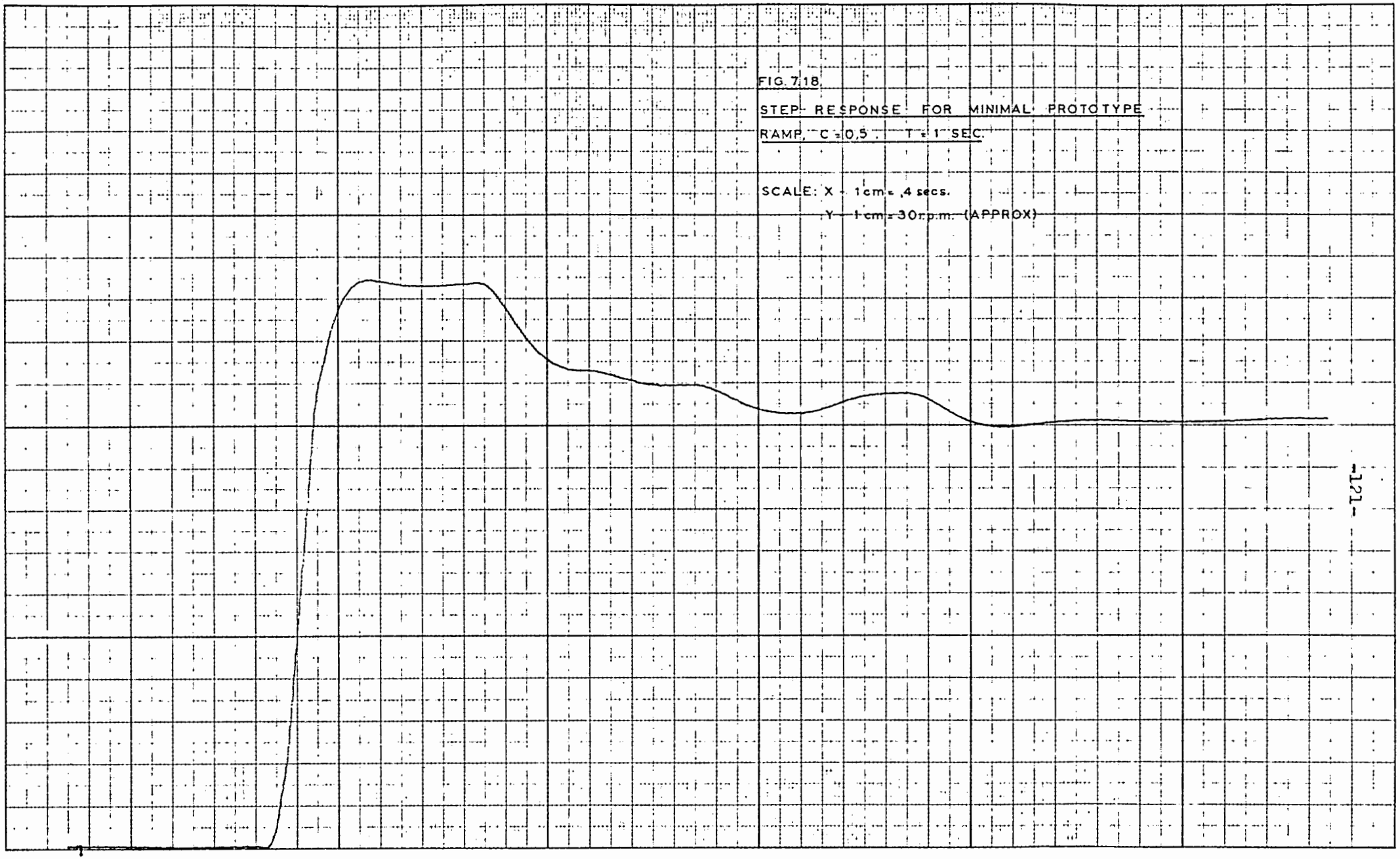

FIG. 7.18

STEP RESPONSE FOR MINIMAL PROTOTYPE

RAMP, C = 0,5 T = 1 SEC.

SCALE: X - 1cm = ,4 secs.

Y - 1cm = 30r.p.m. (APPROX)

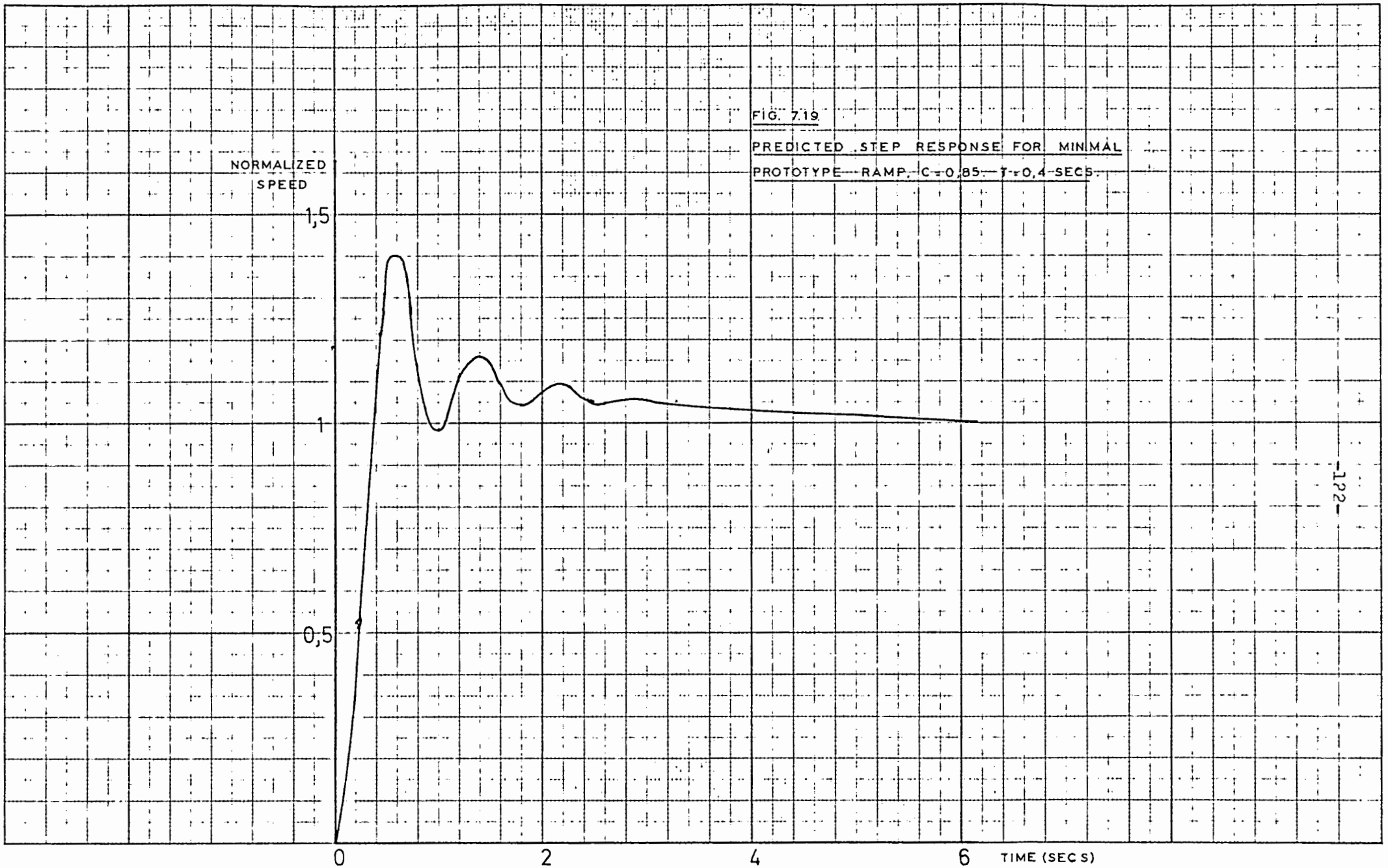

FIG. 7.19

PREDICTED STEP RESPONSE FOR MINIMAL PROTOTYPE - RAMP, C = 0,85 - T = 0,4 SECS.

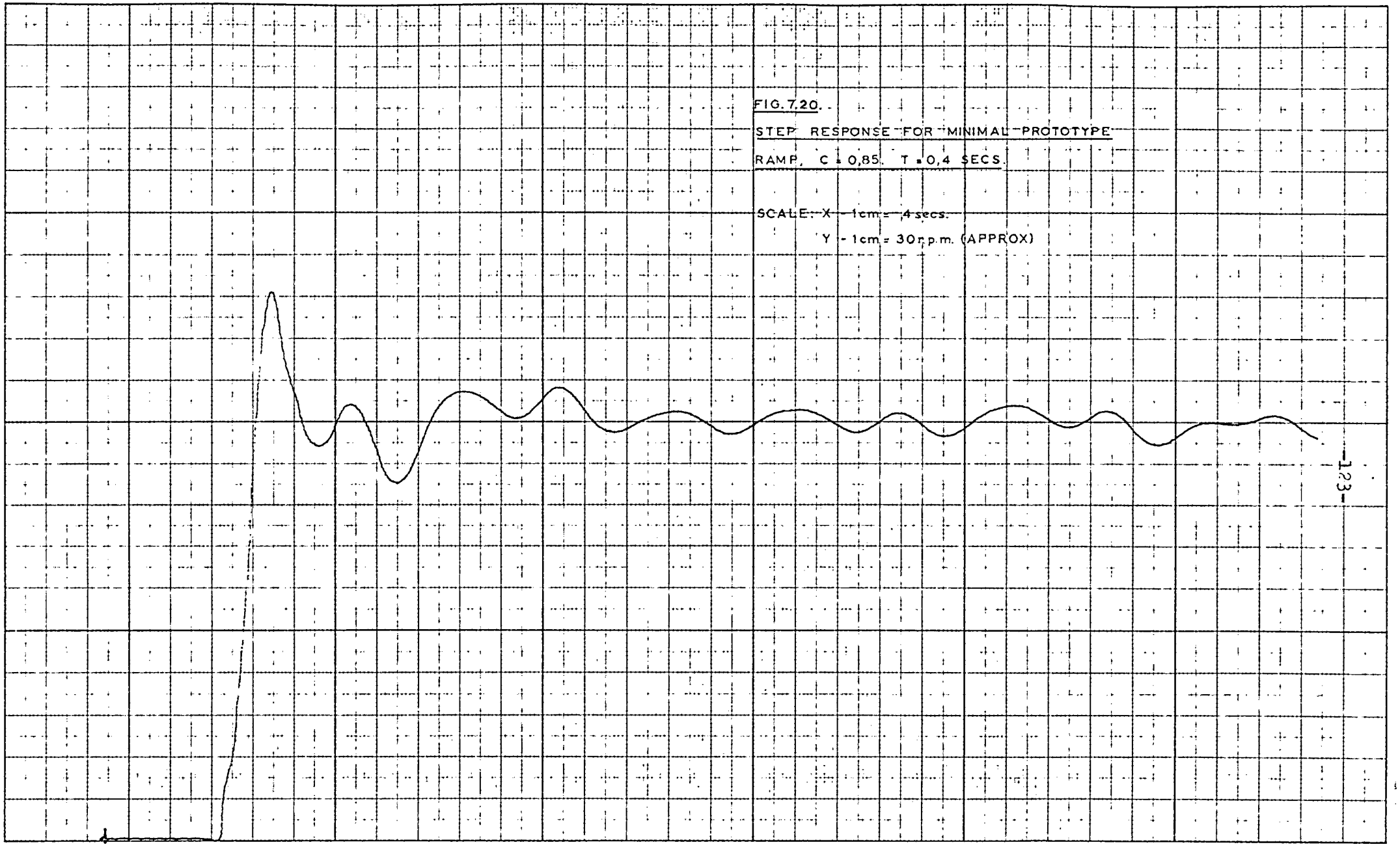

FIG. 7.20.
STEP RESPONSE FOR MINIMAL PROTOTYPE
RAMP, C = 0,85. T = 0,4 SECS.

SCALE: X - 1cm = ,4 secs.
Y - 1cm = 30 r.p.m. (APPROX)

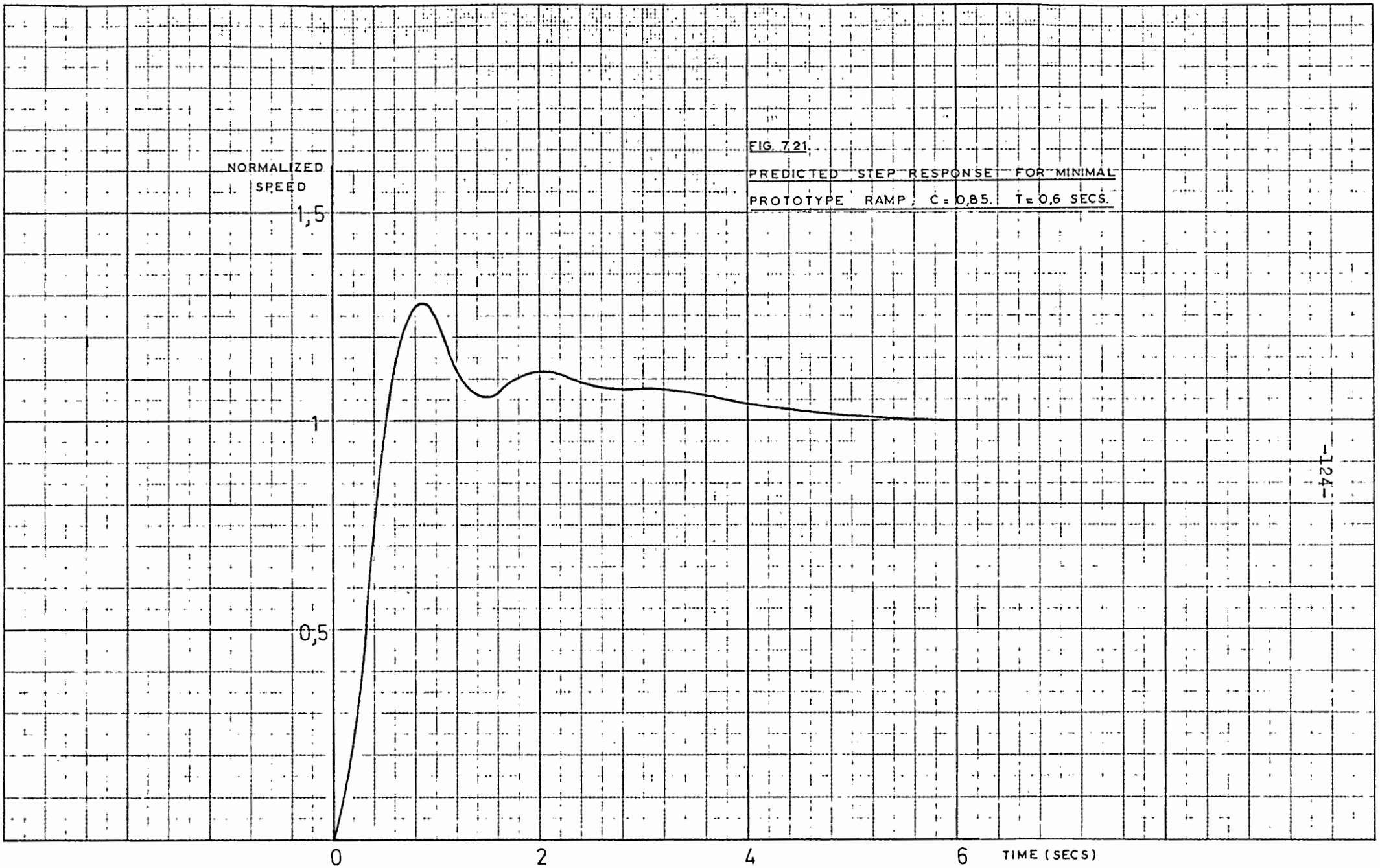

FIG. 7.21.
PREDICTED STEP RESPONSE FOR MINIMAL PROTOTYPE RAMP, C = 0,85. T = 0,6 SECS.

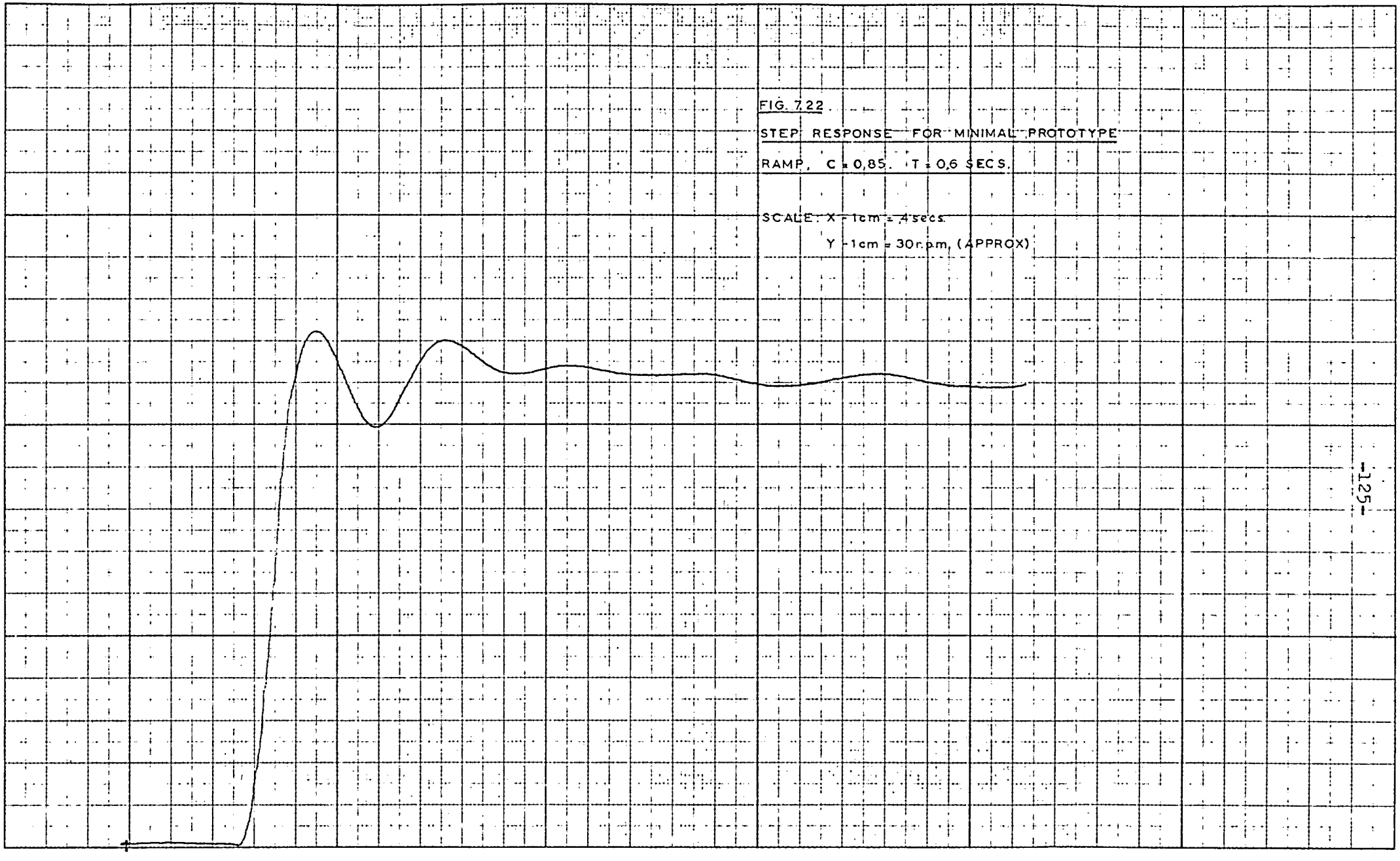

FIG. 7.22

STEP RESPONSE FOR MINIMAL PROTOTYPE

RAMP, C = 0,85. T = 0,6 SECS.

SCALE. X - 1cm = 4 secs.

Y - 1cm = 30 r.p.m. (APPROX)

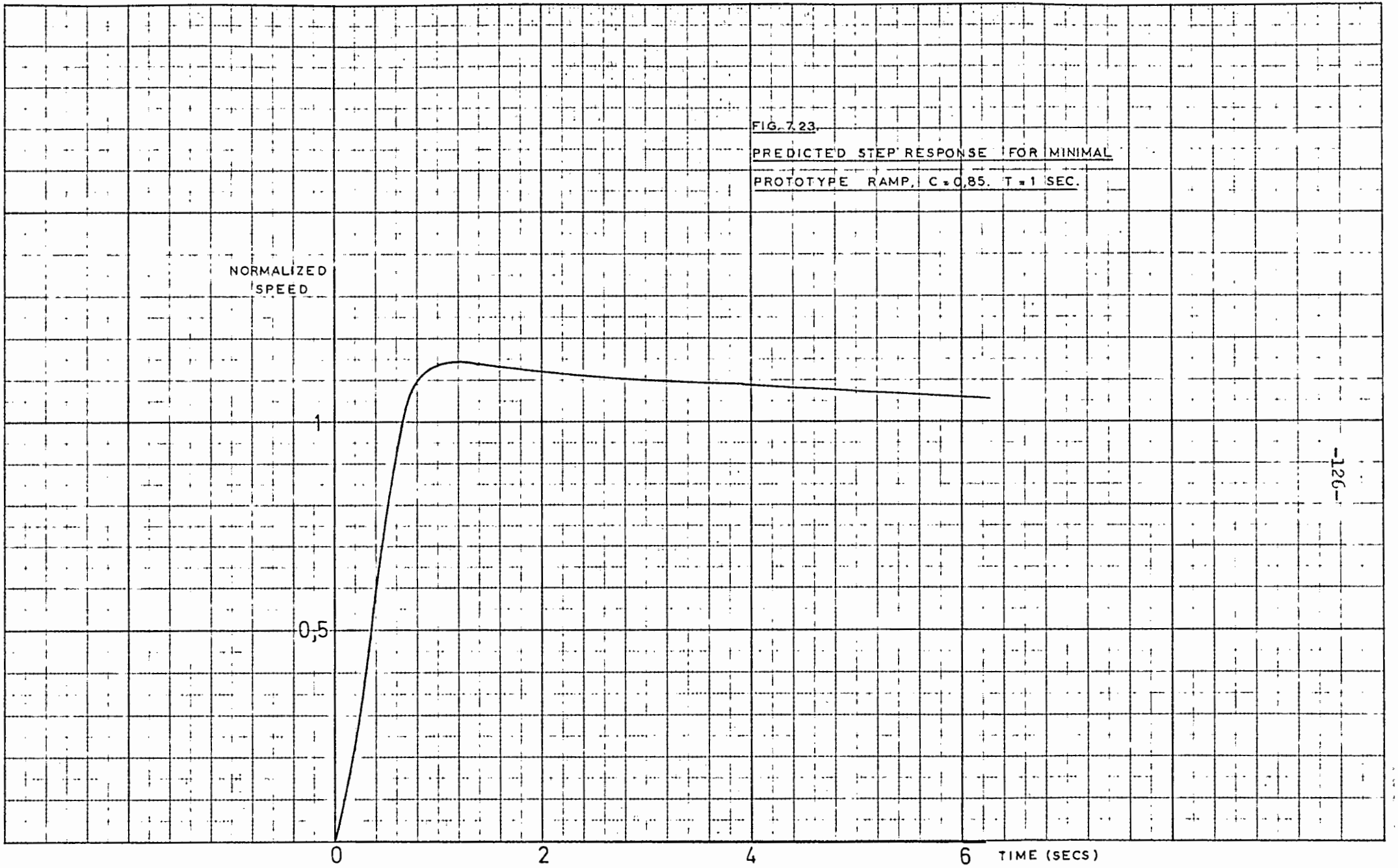

FIG. 7.23.

PREDICTED STEP RESPONSE FOR MINIMAL PROTOTYPE RAMP, C = 0,85, T = 1 SEC.

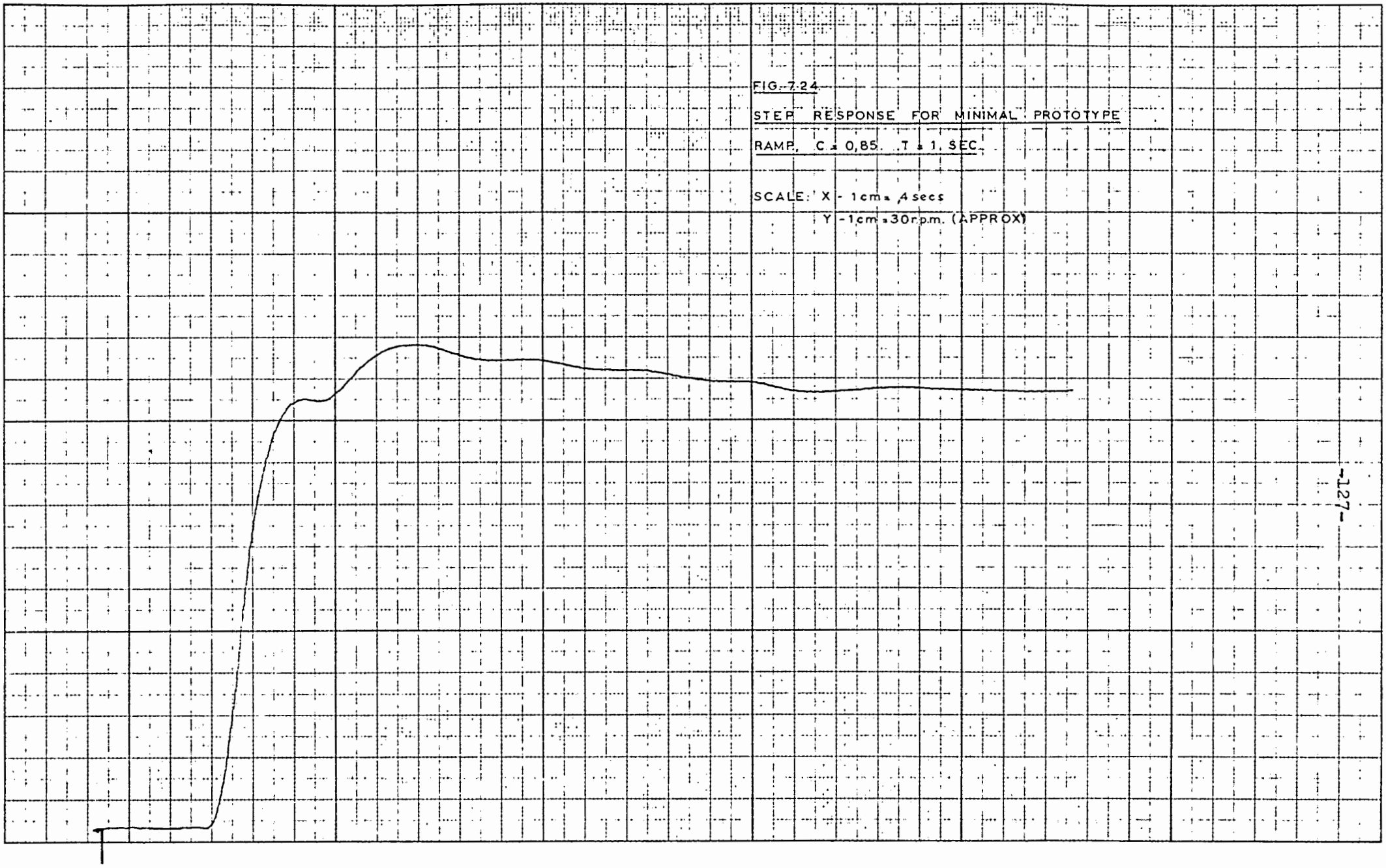
FIG. 7.24
STEP RESPONSE FOR MINIMAL PROTOTYPE
RAMP, C = 0,85 T = 1, SEC.
SCALE: X - 1cm = ,4 secs
Y - 1cm = 30 r.p.m. (APPROX)

One of the reasons behind the use of the ramp response design was the fact that it has been pointed out [30] that a disturbance to the system, other than at the input, when such a system is designed for the minimal prototype step response, might lead to a change in the output which could not be compensated for, i.e. the system might lose its integrating effect. However, the only disturbance which could be applied to the system under consideration is the application or removal of a load, which did not affect the minimal prototype step system, as is shown in fig. 7.25. This gives the speed curves for the removal and application of a load, of the same magnitude as that used in chapter 6, at a speed of 800 r.p.m. and a sampling rate of 0,6 secs. It is of interest to note that the deadband effect does not show as markedly here as was the case in figs 6.32 to 6.34, due possibly to the effect of filtering brought about by the use of past input and output values.

7.4. RAMP RESPONSE.

The ramp input response of the various compensated systems was tested, for a ramp of 300 r.p.m. at a rate of change of 50 r.p.m. per second, in both directions.

The results are shown in figs 7.26 to 7.37. Figures 7.26 to 7.29 show the upward ramp responses at 0,4, 0,6 and 0,8 secs sampling rates respectively, and a downward ramp at 0,6 sec sampling rate, for a staleness factor of 0,5. As the accompanying printouts show, the behaviour of the ramp was anticipated, generally by the fourth or fifth sample (so that a faster sampling rate would be of advantage here), but that the accuracy of the system when settling down to its new value was doubtful.

This behaviour was seen to improve for a greater staleness factor, as figures 7.30 to 7.33 show. These curves are for the same conditions as the previous four, with c = 0,85. The system was seen to take far more samples to actually "catch up" with the reference, although this was of advantage when settling to a required set value.

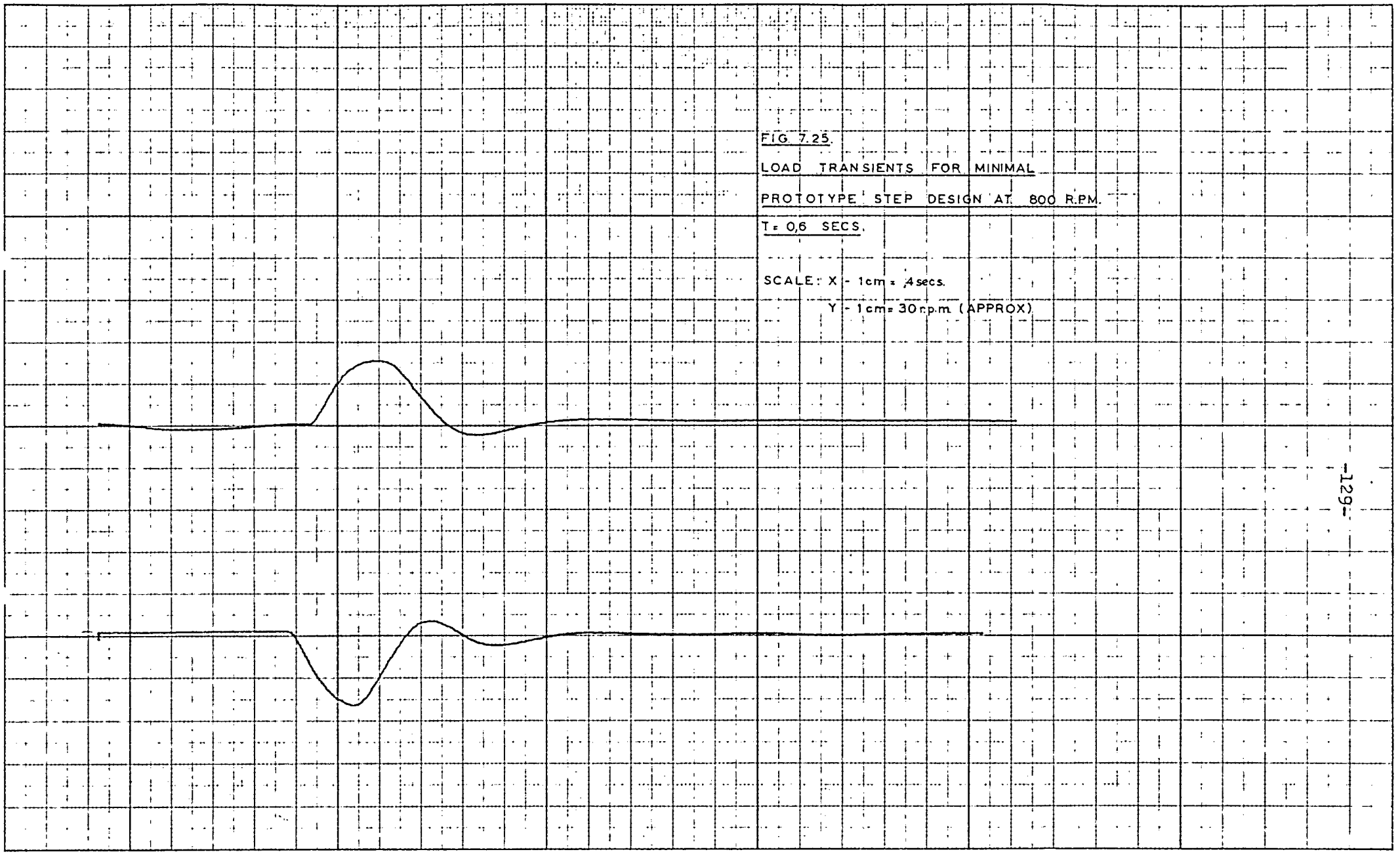

FIG 7.25.
LOAD TRANSIENTS FOR MINIMAL PROTOTYPE STEP DESIGN AT 800 R.P.M.
T = 0,6 SECS.

SCALE: X - 1cm = ,4secs.
Y - 1cm = 30r.p.m. (APPROX)

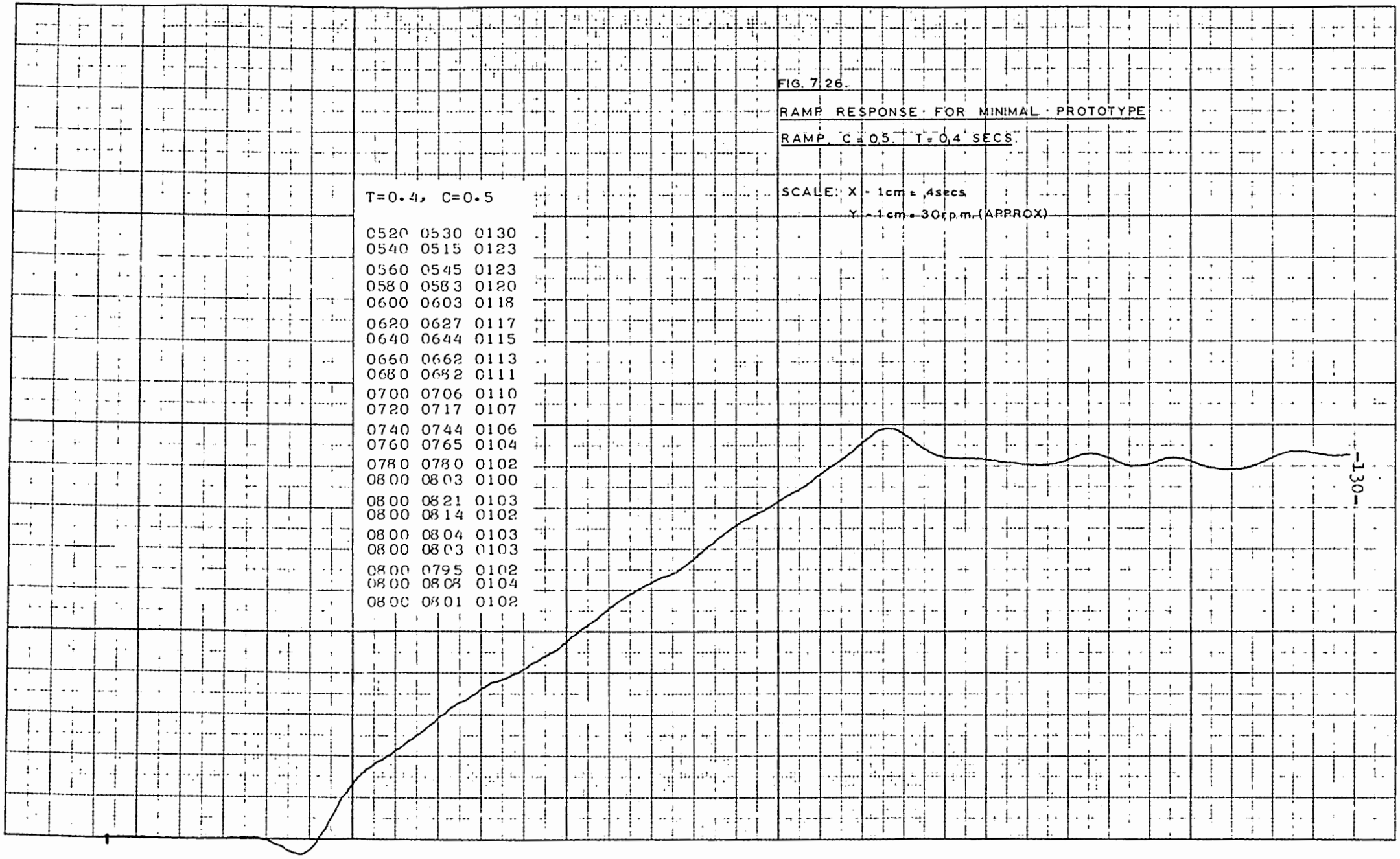

FIG. 7.26.

RAMP RESPONSE FOR MINIMAL PROTOTYPE

RAMP, C = 0.5 T = 0.4 SECS.

SCALE: X - 1cm = .4secs.

Y - 1cm = 30r.p.m. (APPROX)

T=0.6, C=0.5

0530	0535	0129
0560	0526	0124
0590	0571	0121
0620	0610	0117
0650	0653	0114
0680	0689	0112
0710	0710	0109
0740	0735	0106
0770	0775	0104
0800	0799	0101
0800	0822	0102
0800	0816	0102
0800	0819	0104
0800	0799	0104
0800	0796	0104
0800	0791	0103
0800	0805	0104
0800	0798	0104
0800	0793	0103
0800	0805	0104
0800	0797	0104
0800	0797	0104
0800	0798	0104

FIG. 7.27

RAMP RESPONSE - FOR MINIMAL - PROTOTYPE

RAMP, C = 0,5. T = 0,6 SECS

SCALE: X - 1cm = ,4 secs.

Y - 1cm = 30 r.p.m. (APPROX)

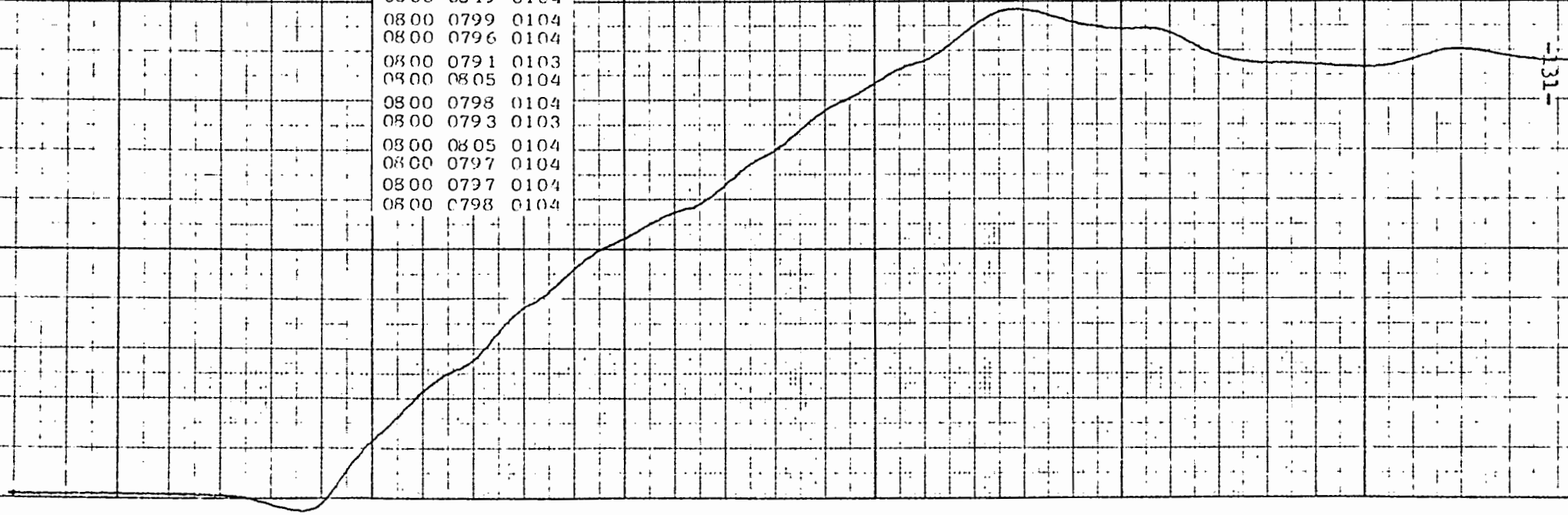

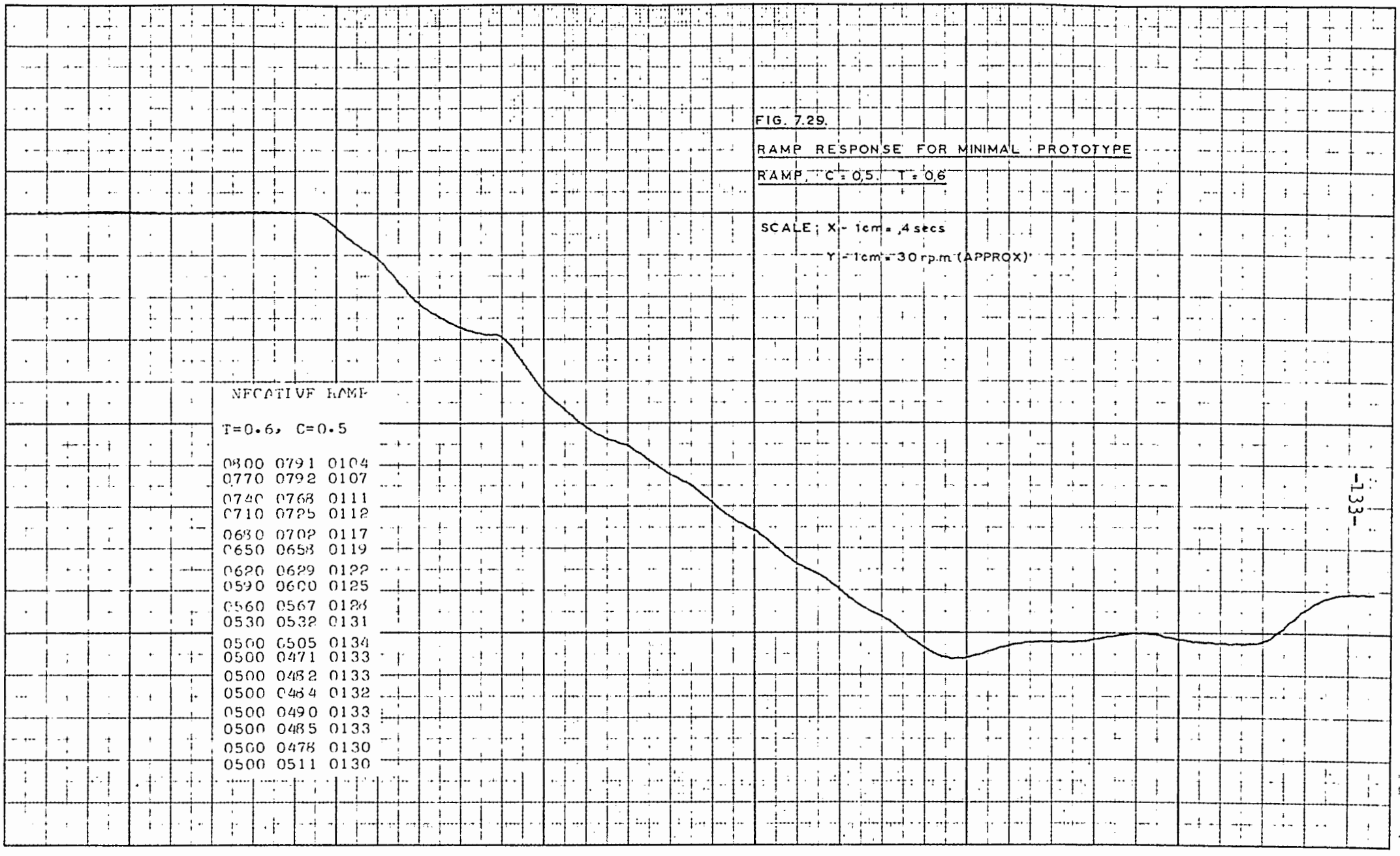

FIG. 7.29.

RAMP RESPONSE FOR MINIMAL PROTOTYPE

RAMP, C = 0,5. T = 0,6

SCALE; X - 1cm = ,4 secs

Y - 1cm = 30 r.p.m (APPROX)

T=0.4, C=0.85

0520 0515 0127
0540 0525 0125
0560 0540 0123
0580 0564 0121
0600 0581 0118
0620 0609 0117
0640 0630 0114
0660 0653 0113
0680 0678 0112
0700 0688 0109
0720 0710 0108
0740 0723 0105
0760 0754 0104
0780 0769 0101
0800 0792 0100
0800 0808 0100
0800 0817 0101
0800 0810 0101
0800 0797 0101
0800 0803 0101
0800 0803 0101
0800 0803 0101
0800 0804 0102
0800 0793 0100

FIG 7.30

RAMP RESPONSE FOR MINIMAL PROTOTYPE

RAMP, C = 0,85. T = 0,4 SECS.

SCALE: X - 1cm = 4secs.

Y - 1cm = 30 r.p.m. (APPROX)

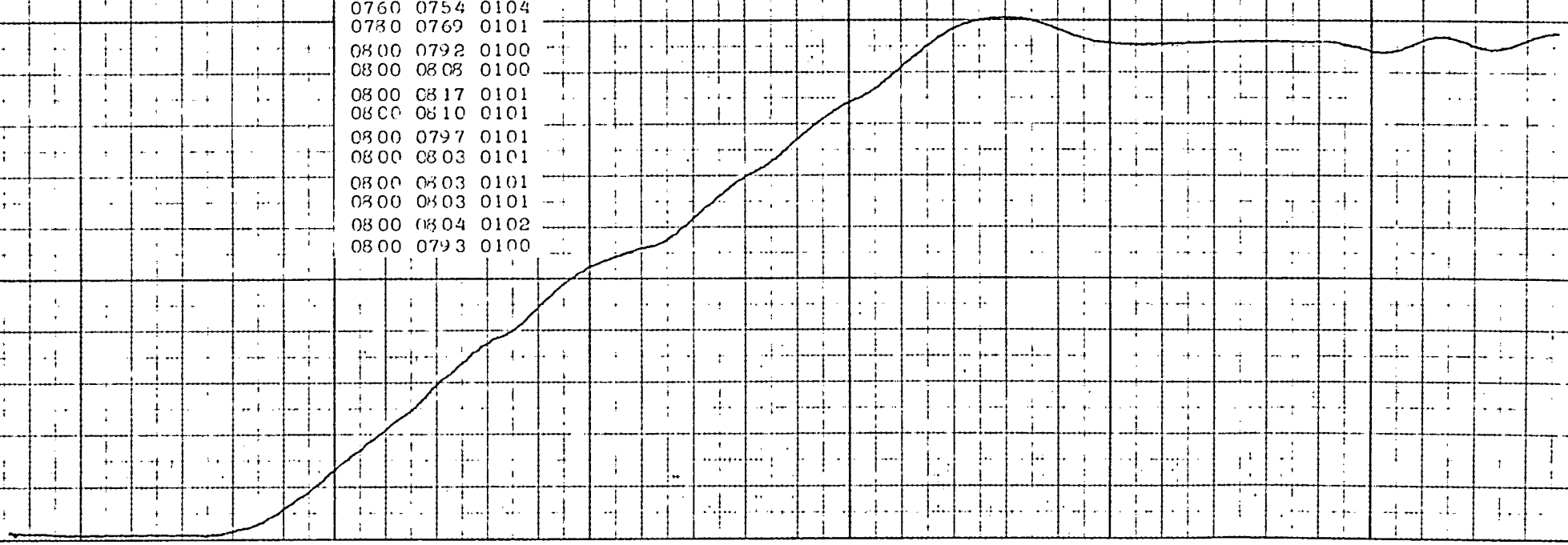

FIG. 7.31.

RAMP - RESPONSE - FOR MINIMAL - PROTOTYPE

RAMP, C = 0,85 T = 0,6 SECS.

SCALE: X - 1 cm = 4 secs.

Y - 1 cm = 30 r.p.m. (APPROX)

T=0.6, C=0.85

0530	0534	0128
0560	0528	0124
0590	0572	0122
0620	0599	0119
0650	0628	0116
0680	0659	0113
0710	0701	0111
0740	0721	0108
0770	0751	0105
0800	0786	0102
0800	0819	0103
0800	0810	0102
0800	0803	0102
0800	0809	0102
0800	0810	0102
0800	0809	0102
0800	0809	0102

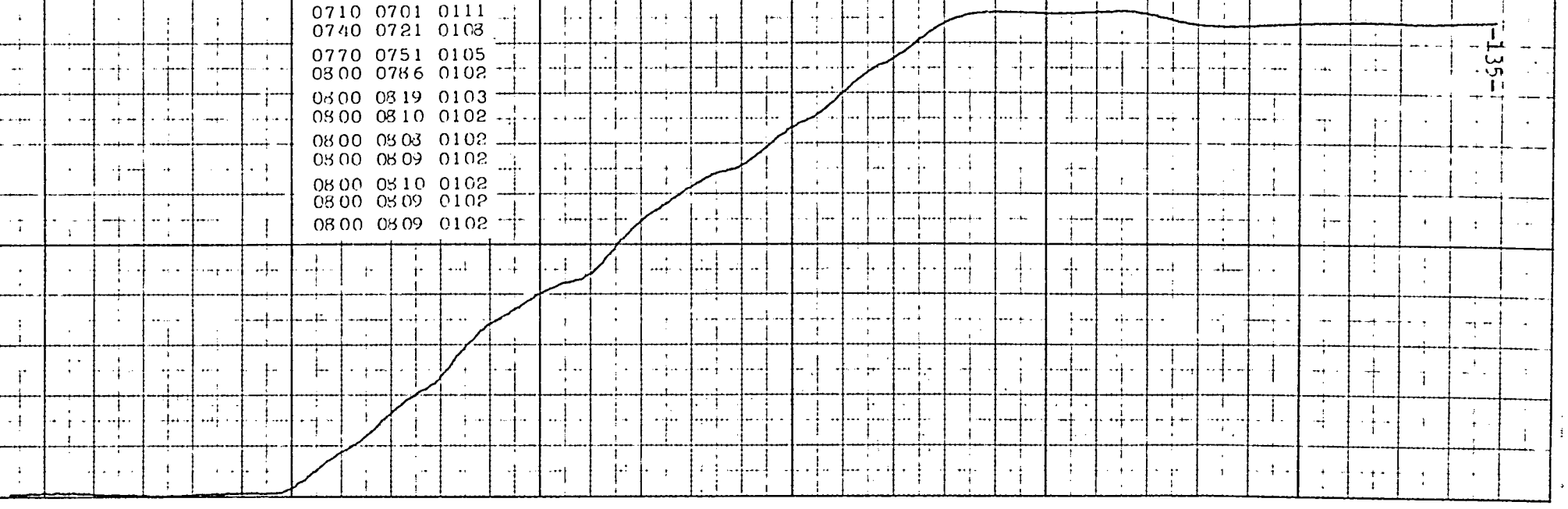

FIG. 7.32

RAMP-- RESPONSE-- FOR MINIMAL--PROTOTYPE

RAMP, C = 0,85. T = 0,8 SECS.

SCALE: X - 1cm = 4secs

Y - 1cm = 30 r.p.m. (APPROX)

T=0.8, C=0.85

0540	0534	0127
0580	0542	0123
0620	0587	0119
0660	0633	0115
0700	0674	0111
0740	0724	0108
0780	0755	0104
0800	0802	0102
0800	0821	0102
0800	0822	0102
0800	0812	0101
0800	0833	0102
0800	0812	0102
0800	0821	0103
0800	0809	0103
0800	0804	0103
0800	0807	0103
0800	0803	0103
0800	0806	0103

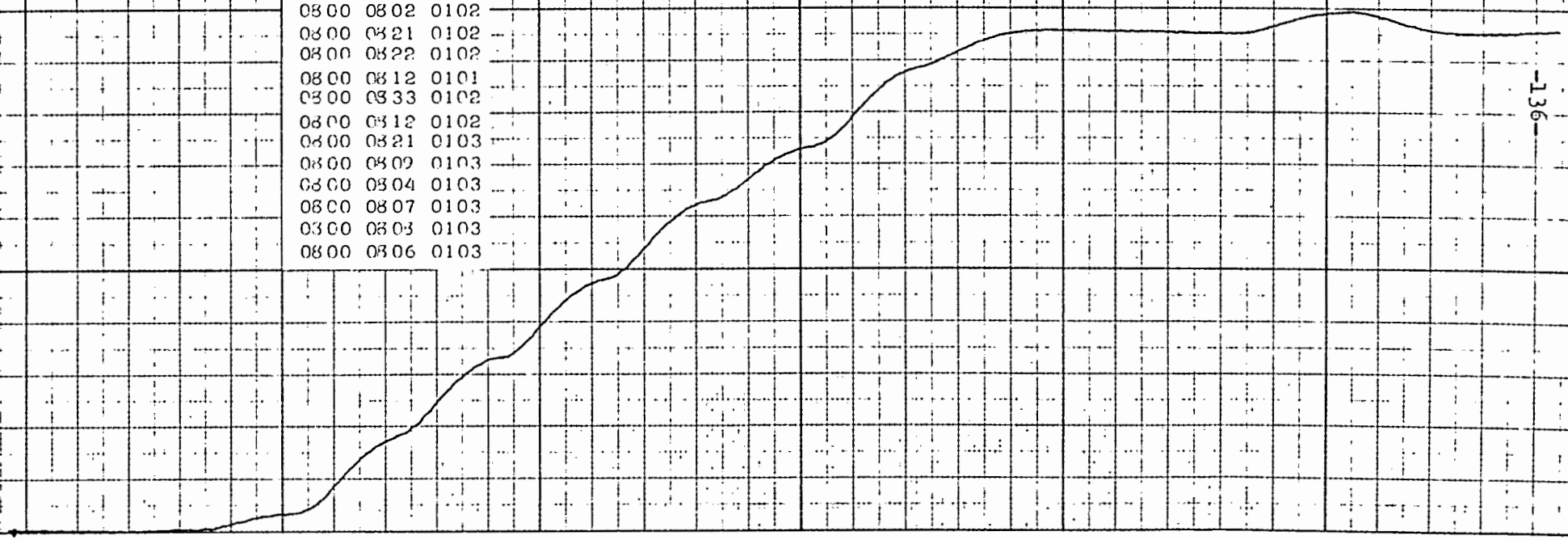

Particularly good responses were obtained using the minimal prototype step system, with the only disadvantage being that the actual speed was always one sampling instant behind the reference. However, this fact correlated particularly well at all times, and led to excellent smoothing off, with a little oscillation at the highest sampling rate used.

The responses, for the same conditions as previously, are shown in figures 7.34 to 7.37.

7.5. EFFECT OF VARIATION OF PARAMETERS.

Zinober [33], in a survey of various methods of optimization, pointed out that the z-transform minimal prototype compensation system was rather susceptible to small changes in parameters causing a previously stable system to become unstable or inaccurate. He did not, however, specify how his simulation varied either the parameters or the weighting factors.

For the purposes of this thesis it was decided to keep the weighting factors constant, but to vary the poles and zero of the machine-bridge system by varying the sampling time. The factors for a sampling period of 0,6 seconds were used, and the sampling time varied, in practice and simulation, between 0,5 and 0,7 seconds.

Fig. 7.38 shows how the step response would be expected to vary as the sampling time was altered from 0,5 to 0,7 secs. Here it may be seen that at faster sampling rates, the system would be expected to remain stable, but at slower sampling rates, oscillation would be expected.

The no load behaviour at a sampling rate of 0,5 secs confirmed the expected behaviour; a greater overshoot was obtained, and the system remained stable (fig. 7.39). However, application of a load tended to decrease the overshoot, and produced probably the best response obtained (fig. 7.40). Fig. 7.41 shows the response at a rate of 0,7 secs. The oscillation expected is apparent.

FIG. 7.34.

RAMP RESPONSE FOR MINIMAL PROTOTYPE STEP. T = 0,4 SECS.

SCALE: X - 1cm = .4 secs.
Y - 1cm = 30 c.p.m. (APPROX)

T=0.4, MIN. PROT. STEP

0520	0530	0129
0540	0526	0126
0560	0539	0125
0580	0558	0123
0600	0577	0121
0620	0593	0118
0640	0621	0117
0660	0645	0115
0680	0666	0114
0700	0681	0112
0720	0698	0110
0740	0713	0107
0760	0741	0106
0780	0764	0104
0800	0778	0102
0800	0805	0104
0800	0807	0103
0800	0801	0103
0800	0801	0103
0800	0798	0103
0800	0806	0104
0800	0797	0103

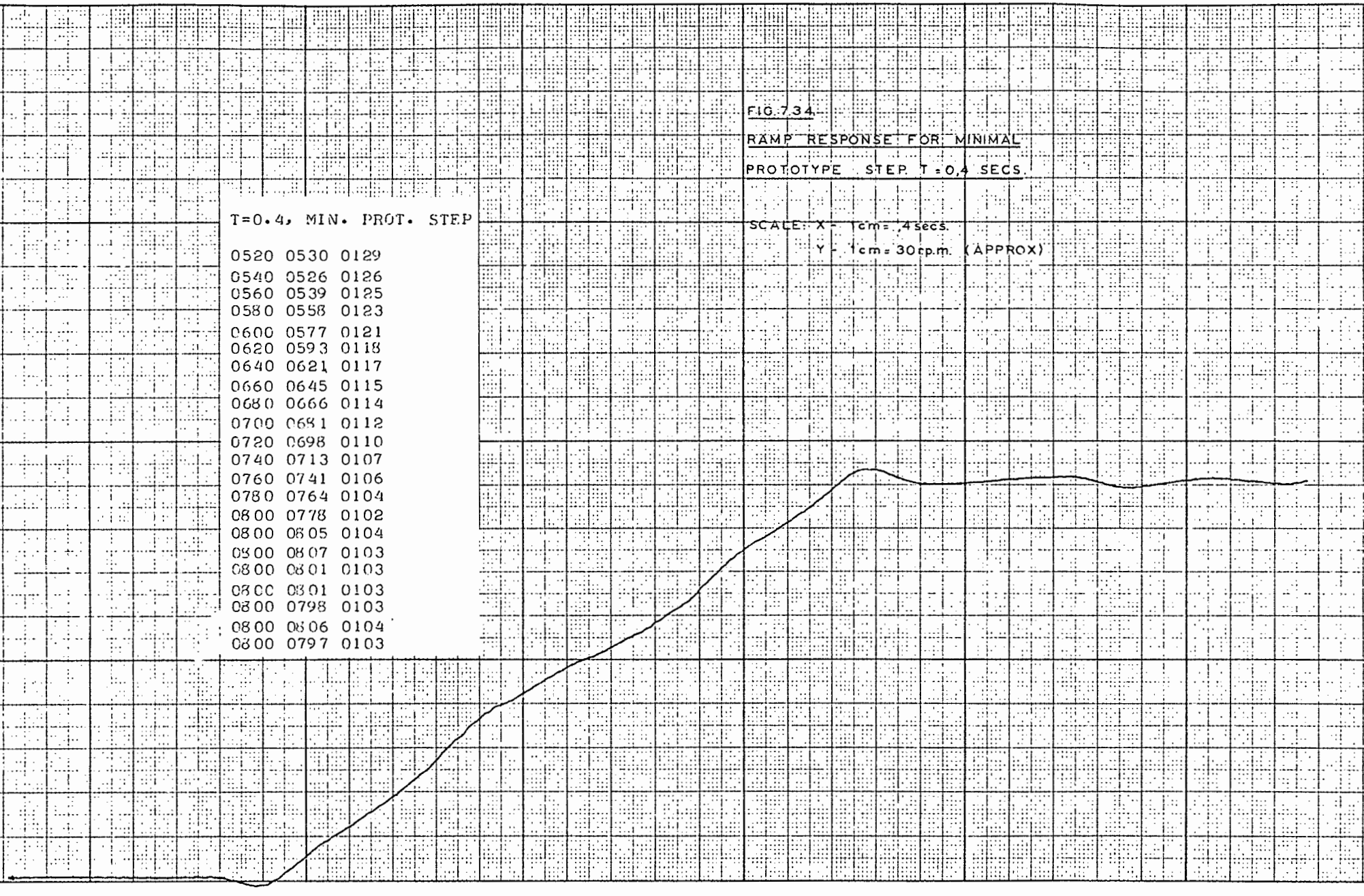

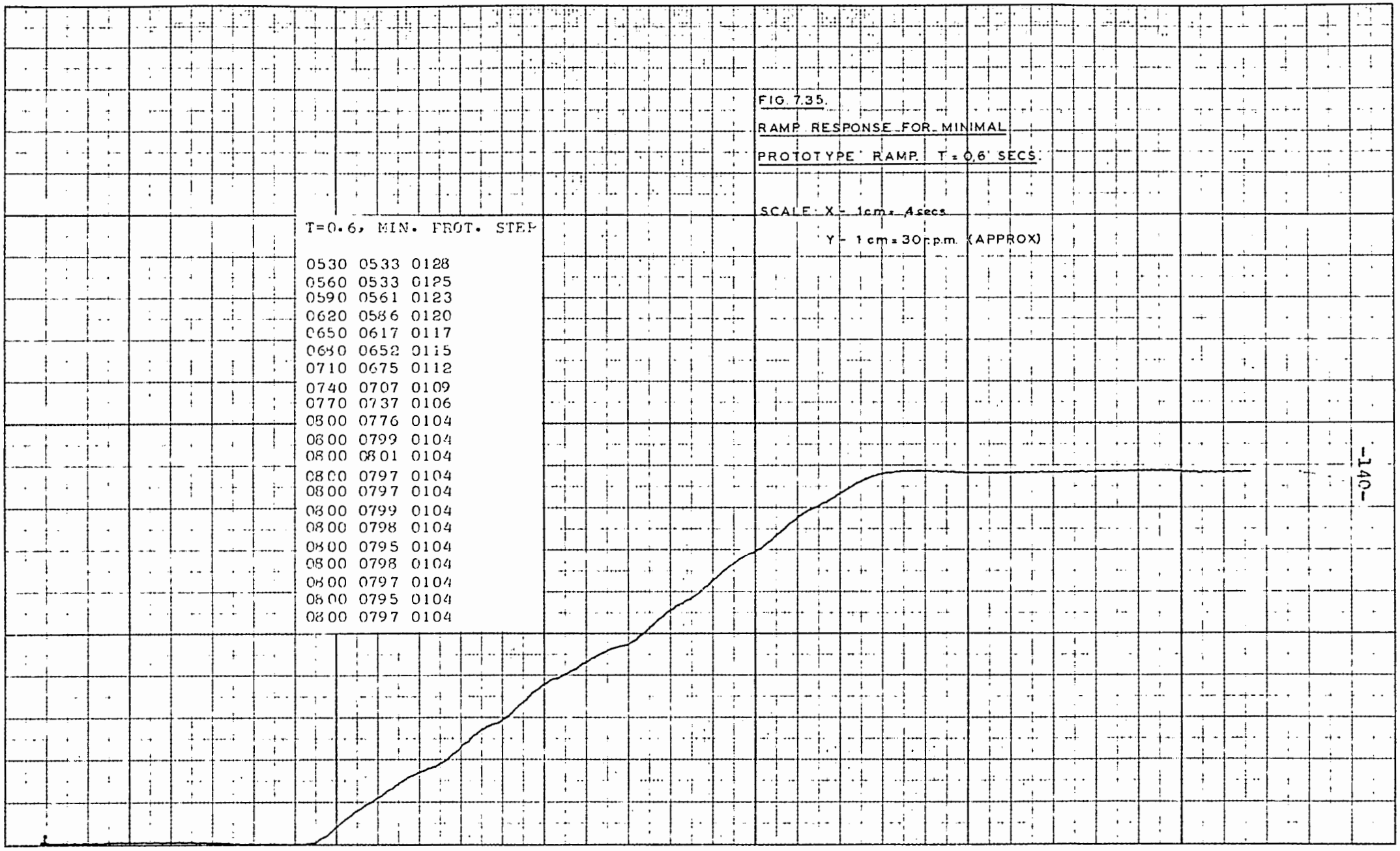

FIG. 7.35.

RAMP RESPONSE FOR MINIMAL PROTOTYPE RAMP. T = 0.6 SECS.

SCALE: X - 1cm = 4secs

Y - 1 cm = 30 r.p.m. (APPROX)

FIG. 7.36

RAMP RESPONSE FOR MINIMAL PROTOTYPE STEP T = 0,8 SECS.

SCALE: X - 1cm = 4 secs.

Y - 1cm = 30 r.p.m. (APPROX)

T=0.8, MIN. PROT. STEP

0540 0533 0127
0580 0550 0124
0620 0583 0121
0660 0614 0117
0700 0663 0114
0740 0690 0110
0780 0740 0107
0800 0774 0105
0800 0790 0104
0800 0805 0104
0800 0805 0104
0800 0797 0104
0800 0802 0104
0800 0806 0104
0800 0799 0104

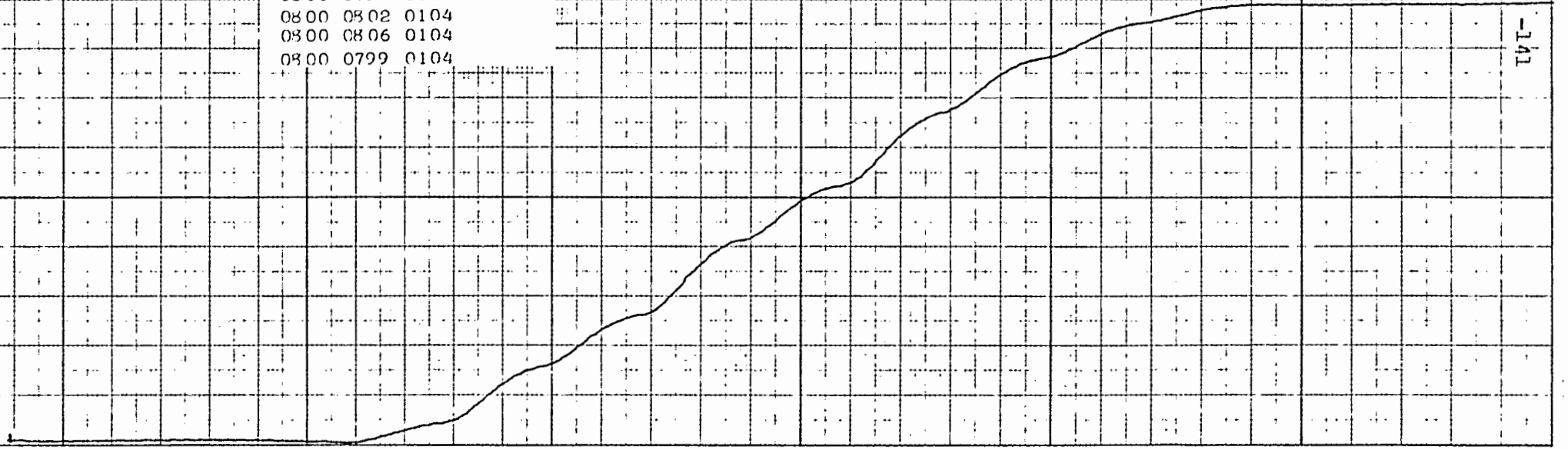

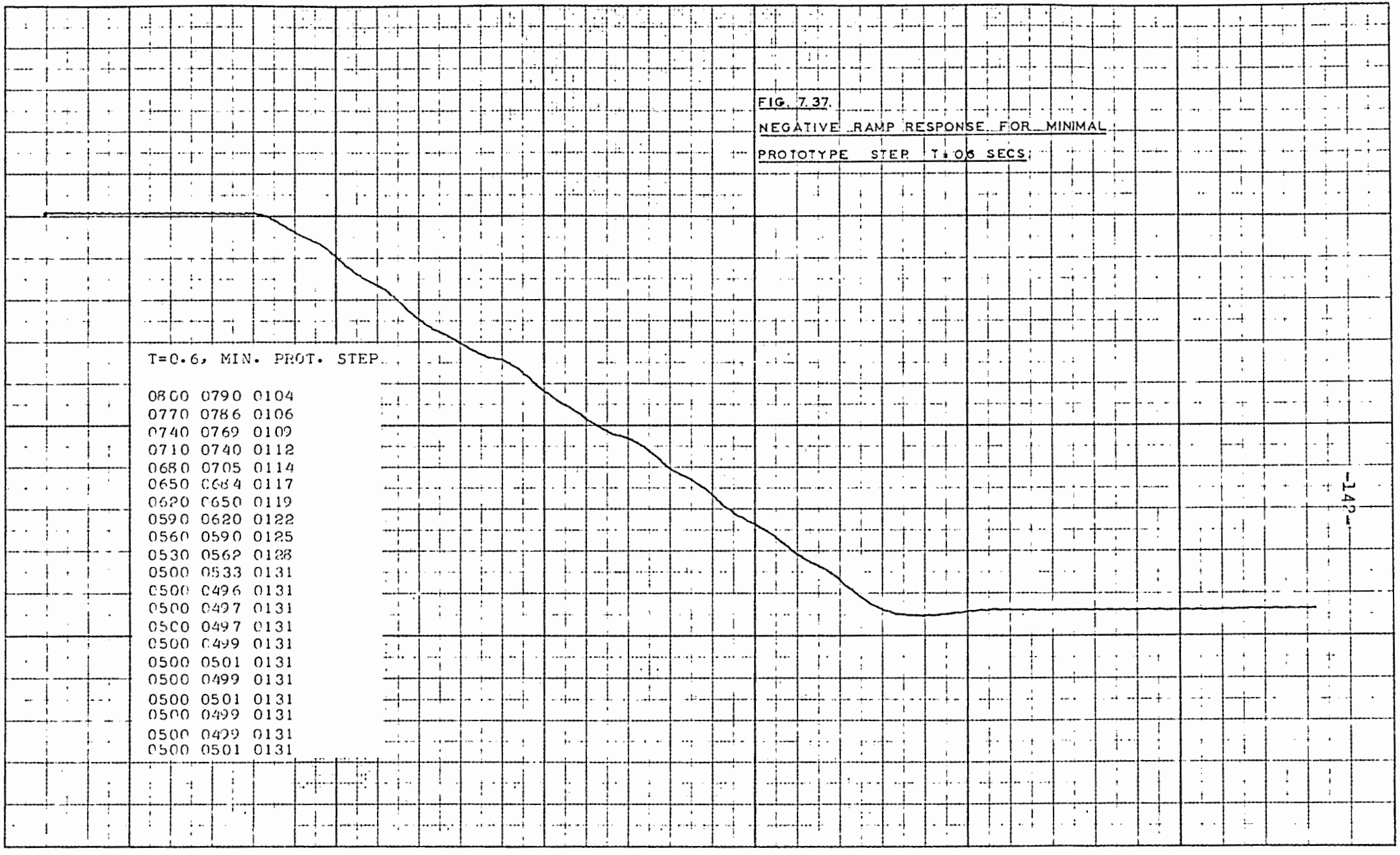

FIG. 7.37.
NEGATIVE RAMP RESPONSE FOR MINIMAL PROTOTYPE STEP T=0.6 SECS.

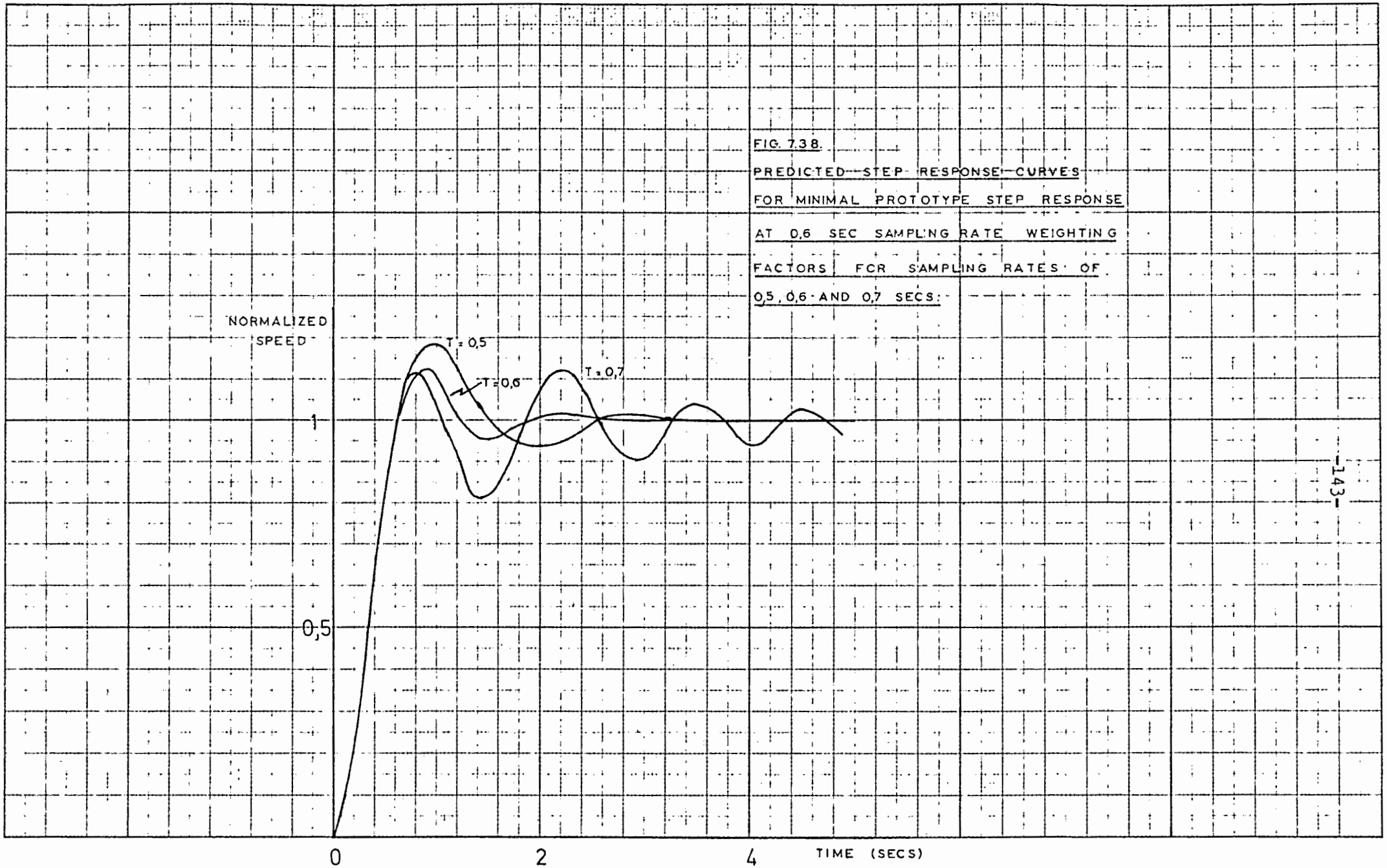

FIG. 7.3.8.
PREDICTED STEP RESPONSE CURVES FOR MINIMAL PROTOTYPE STEP RESPONSE AT 0,6 SEC SAMPLING RATE WEIGHTING FACTORS FOR SAMPLING RATES OF 0,5, 0,6 AND 0,7 SECS.

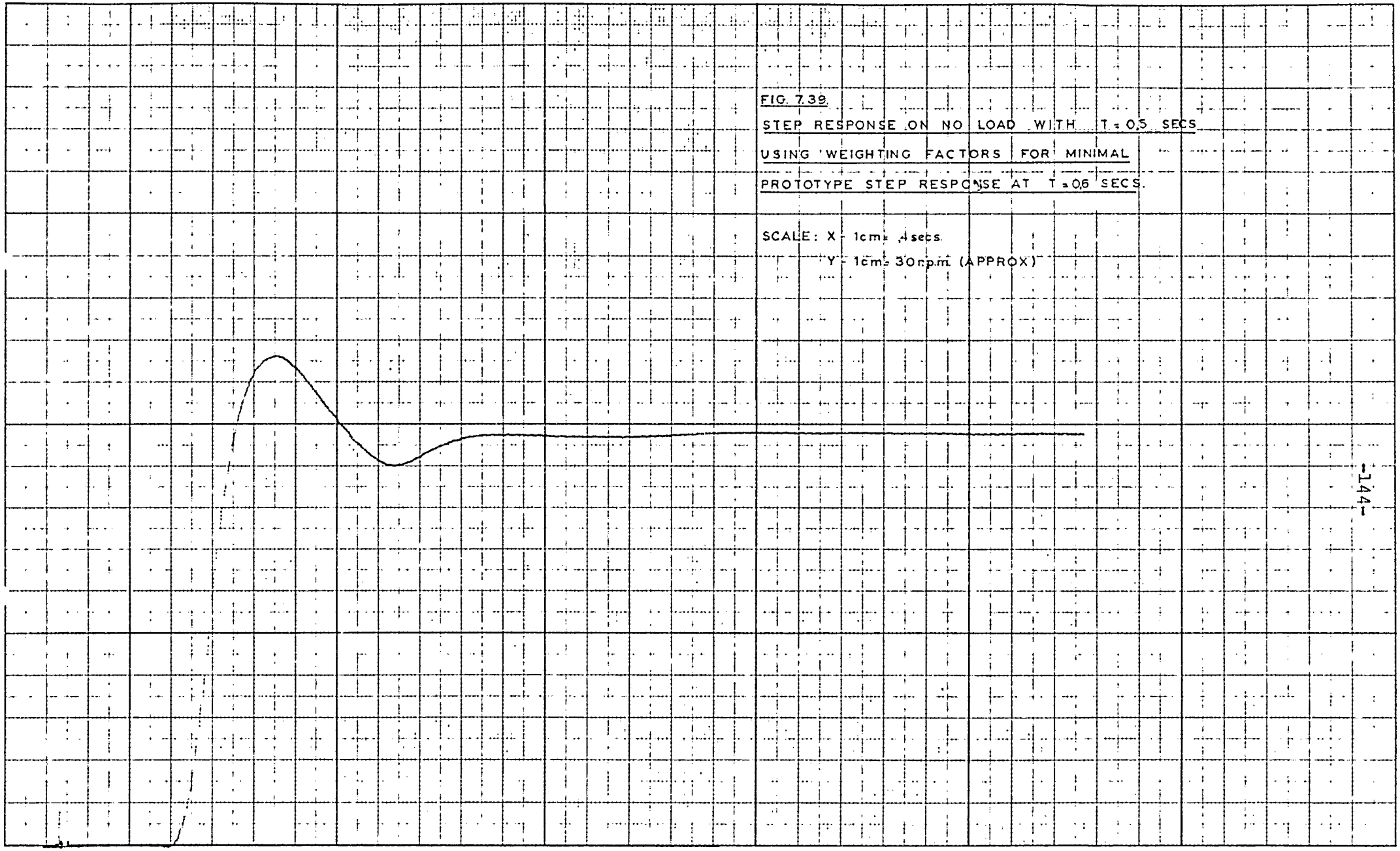

FIG. 7.39.
STEP RESPONSE ON NO LOAD WITH T = 0.5 SECS.
USING 'WEIGHTING FACTORS FOR MINIMAL
PROTOTYPE STEP RESPONSE AT T = 0.6 SECS.

SCALE: X - 1cm = 1 secs.
Y - 1cm = 30 r.p.m. (APPROX)

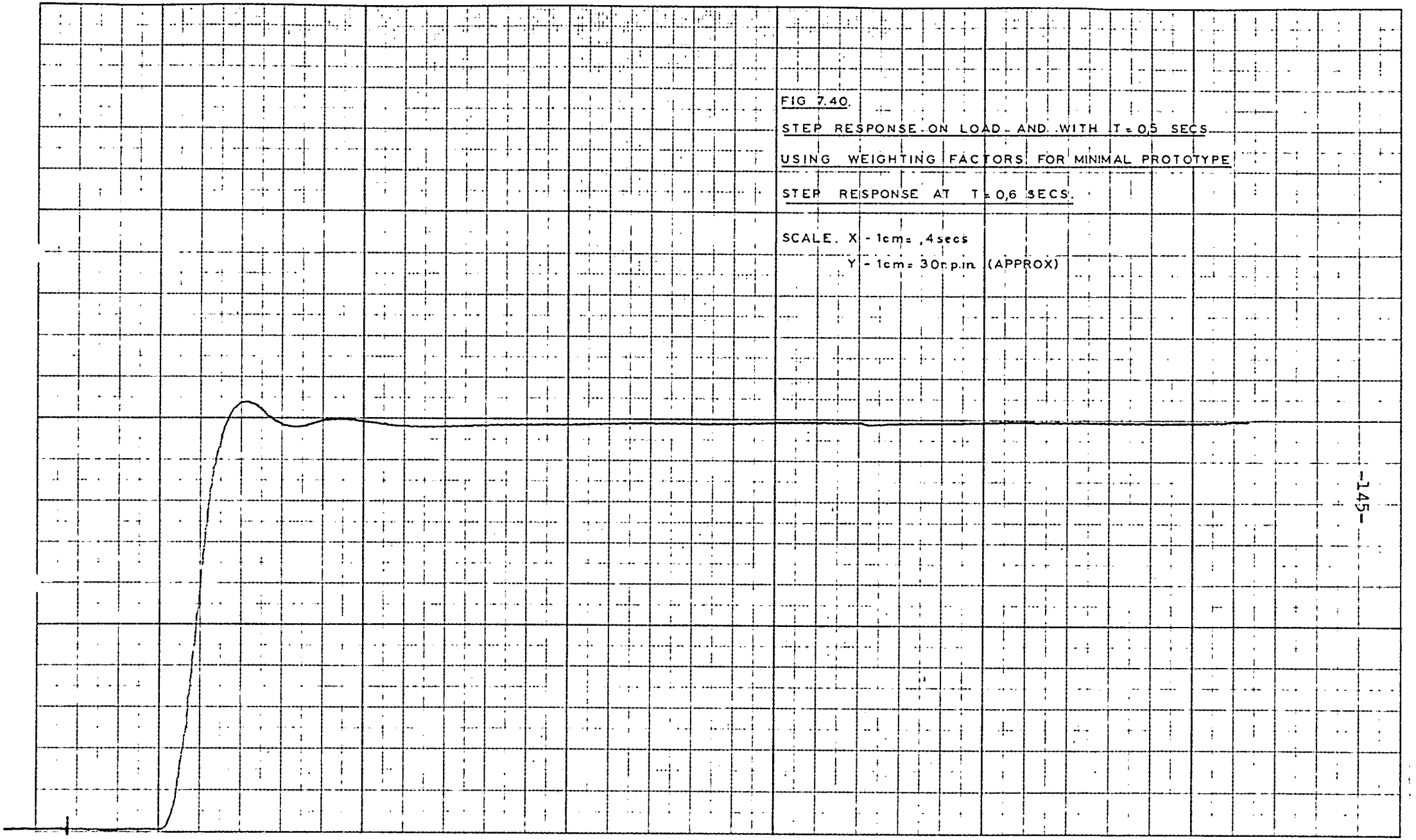

FIG 7.40.

STEP RESPONSE ON LOAD AND WITH T = 0,5 SECS

USING WEIGHTING FACTORS FOR MINIMAL PROTOTYPE

STEP RESPONSE AT T = 0,6 SECS.

SCALE. X - 1cm = ,4 secs

Y - 1cm = 30 r.p.m. (APPROX)

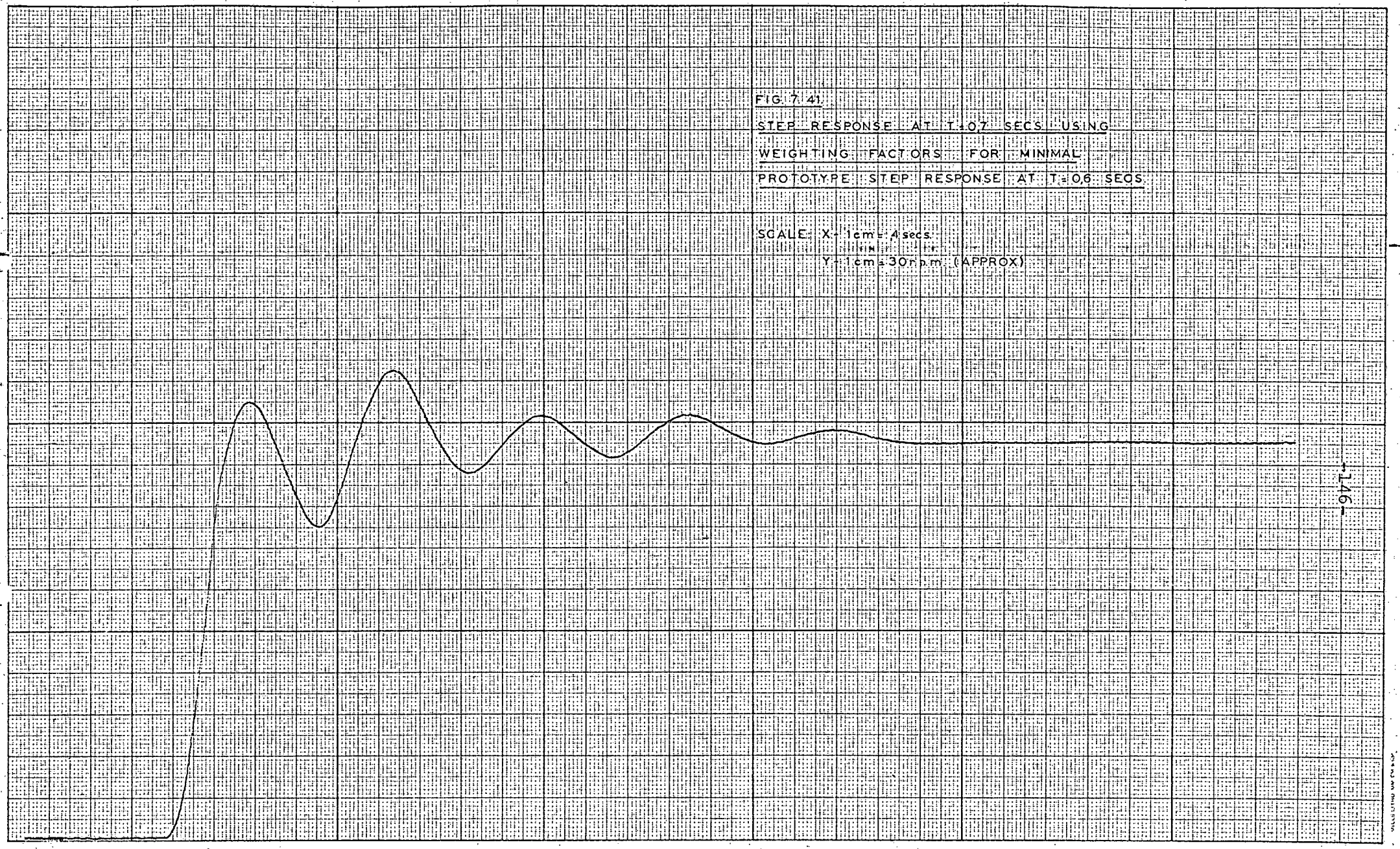

FIG. 7.41.

STEP RESPONSE AT T=0,7 SECS USING WEIGHTING FACTORS FOR MINIMAL PROTOTYPE STEP RESPONSE AT T=0,6 SECS.

SCALE: X - 1cm = 4 secs.
Y - 1cm = 30 r.p.m. (APPROX)

Hence it may be seen that incorrect weighting factors, provided the set of factors are not varied within themselves, will not necessarily tend to make the system unstable; in fact it was found that an even more satisfactory system could be produced if the rate was increased and a load applied.

7.6. COMMENT.

A very satisfactory correlation could be made between the theory of sampled-data systems and the actual practical system used for this thesis. It was found that the design for the minimal prototype step response produced the most satisfactory performance, both for step and ramp inputs, as this design led to the system following the input after one sampling period. An increase in sampling rate, with a load applied, was found to be in order or even beneficial.

The negative step response and negative ramp at higher rates of change displayed the same anomalies experienced using the integral control system, and for this reason are not shown. It could thus be concluded that as long as the current was able to flow, the system would behave dynamically as expected. If full control in both directions of speed change is desired, it is seen to be necessary to ensure that this condition always holds.

CHAPTER 8.

MULTI-MACHINE CONTROL.

8.1. INTRODUCTION.

The programs used for this thesis were not in general at all efficient as far as the time utilization of the computer was concerned. The actual execution time was of the order of 1 or 2 milliseconds (except when the punch was being used on line, when punching out of the values read and settings made used several tens of milliseconds), and most of the time was spent in a loop waiting for the next interrupt signal to occur.

From a practical point of view, if such a system as that set out in this thesis is to be used industrially, this is not an unsatisfactory situation. The spare time would however have to be utilized, either to perform similar control functions or to carry out arithmetic or mathematical calculations.

An attempt was made to perform similar control functions on two machines, at first running entirely independent of one another, and then to introduce a degree of interaction between them. This was made possible by the availability of the interface built by Mr. F. Weehuizen for his thesis [7], which served as a forerunner for the work done for this thesis. Although this interface, having been developed from one using the computer to perform the countdown routines etc, did not have separate counters for each phase or work in exactly the same way as did the one outlined in chapter 2, it utilised the same data lines, and only required additional strobe and enable lines. Weehuizen's system performed speed sampling, and the sampling of a reference voltage corresponding to the reference speed, by means of a multiplexed 12 bit analogue to digital converter.

8.2. GENERATION OF INTERRUPT SIGNALS.

The most important aspect to be taken into account when implementing the dual machine control system was the question of applying the interrupt signals at the correct rate and on the correct lines, without any two interrupt signals occurring simultaneously (if this did in fact occur, the program would act on the interrupt with the highest priority, and one sample for the second system would be lost). The program developed by Weehuizen was based on an analogue simulation and necessitated a sampling rate at least four times as great as that used for this thesis.

Figure 8.1 shows the simple divde by 8 counter used, which was fed by a square wave input and produced short negative going pulses from either of two monostable multivibrators whenever an interrupt was required.

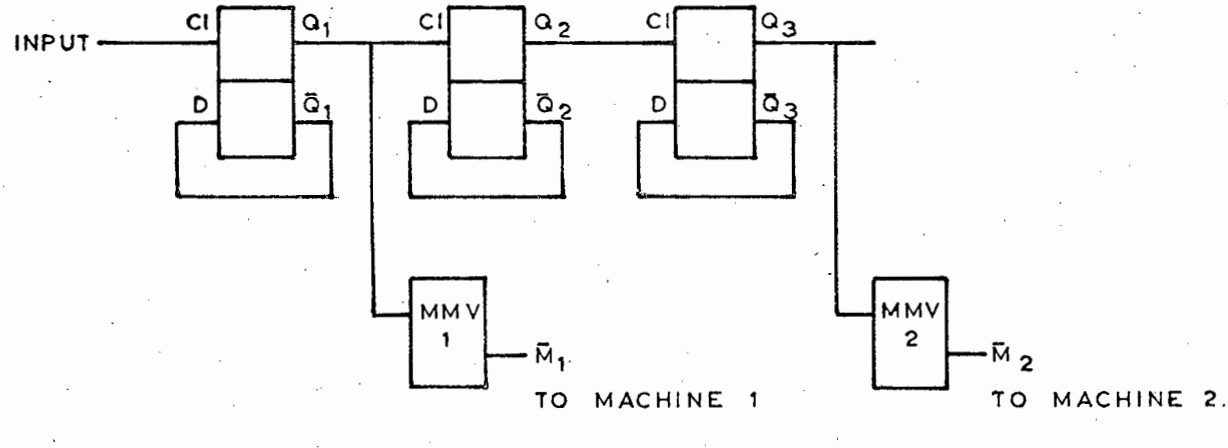

FIG. 8.1.

CIRCUIT FOR GENERATION OF TWO NON-COINCIDENT INTERRUPT SIGNALS, 1 AT FOUR TIMES THE RATE OF 2.

The waveforms of the interrupt generator are shown in fig. 8.2. It should be remembered that the D flip-flop triggers on a positive edge (see appendix 1), and as the M.M.V.'s are triggered by a negative edge, the use of Q_1 and Q_3 as the interrupt generating connections ensured that the two interrupt signals would never coincide.

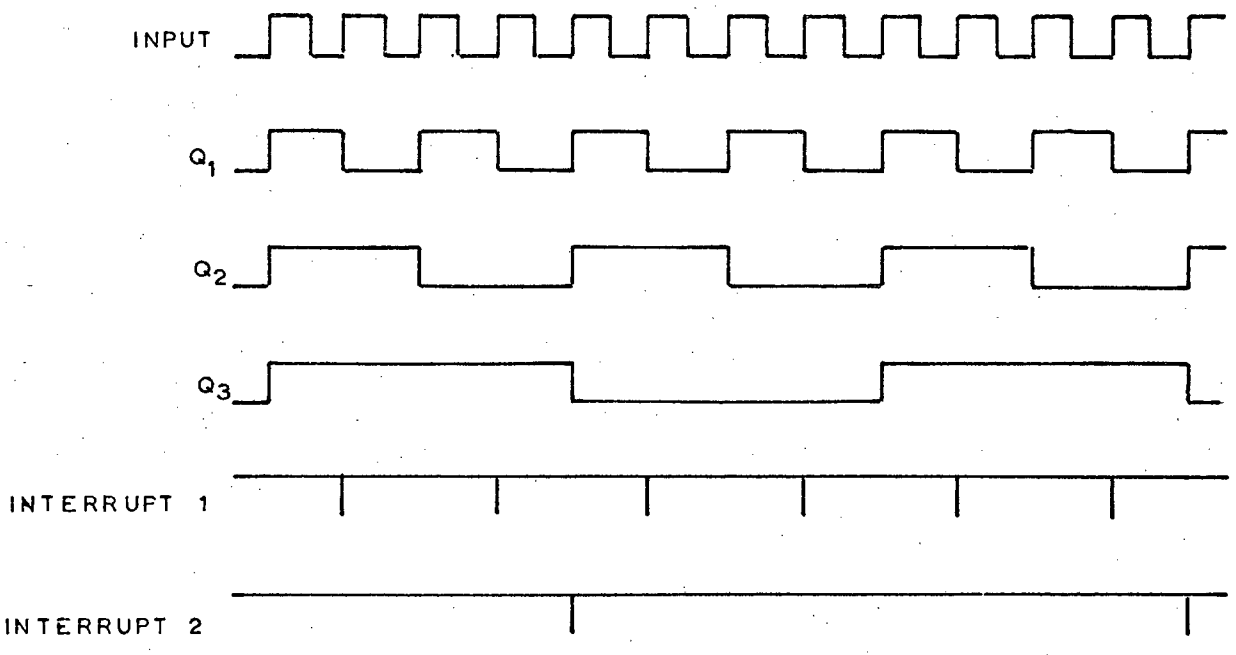

FIG. 8.2.
INTERRUPT GENERATING MODULE WAVEFORMS.

8.3. IMPLEMENTATION OF DUAL MACHINE CONTROL.

The two machines were each controlled by a different program, stored in a different part of the computer memory, and accessed by the appropriate interrupt signal. The reference speed for both machines was initially taken as that represented by the voltage read by the analogue to digital converter. Subsequently, the slower sampling machine (machine 2) used as its reference the actual speed of machine 1, using the program for the minimal prototype step response with a sampling rate of 0,5 secs.

A step input was applied to machine 1 via the voltage reference, and fig. 8.3 shows the response of the two machines. Machine 2 can be clearly seen to be following machine 1 after an interval corresponding to one sampling instant.

It was found that the most serious problem encountered was that of noise on the analogue speed signal, particularly as this signal had to be fed over several metres from the machine to the computer. The noise was reduced through the use of twin-cored screened cable with a filter immediately preceding the input to the computer. It is felt that the use of a digital tachometer would greatly reduce the noise problems. In addition, it was necessary to calibrate both the reference and speed feedback signals, so that the voltages read by the computer could be interpreted as the actual speed. This calibration was automatic in the case of the digital tachometer, and probably more accurate, if one was considering more than relative speed differences.

Further testing of the dual machine system was curtailed by the failure of the multiplexer of the analogue to digital converter. However, the tests performed did show the feasibility of such control, and stilled any fears that mains interference might prove a serious problem. It is clear from chapter 7 that the minimal prototype step response design used would follow any input signal, whether derived as a refence or from another machine (as far as the computer was concerned all this affected would be the location in which the reference speed was stored), with a one sampling period delay, and would therefore be the most generally useful form of program to use.

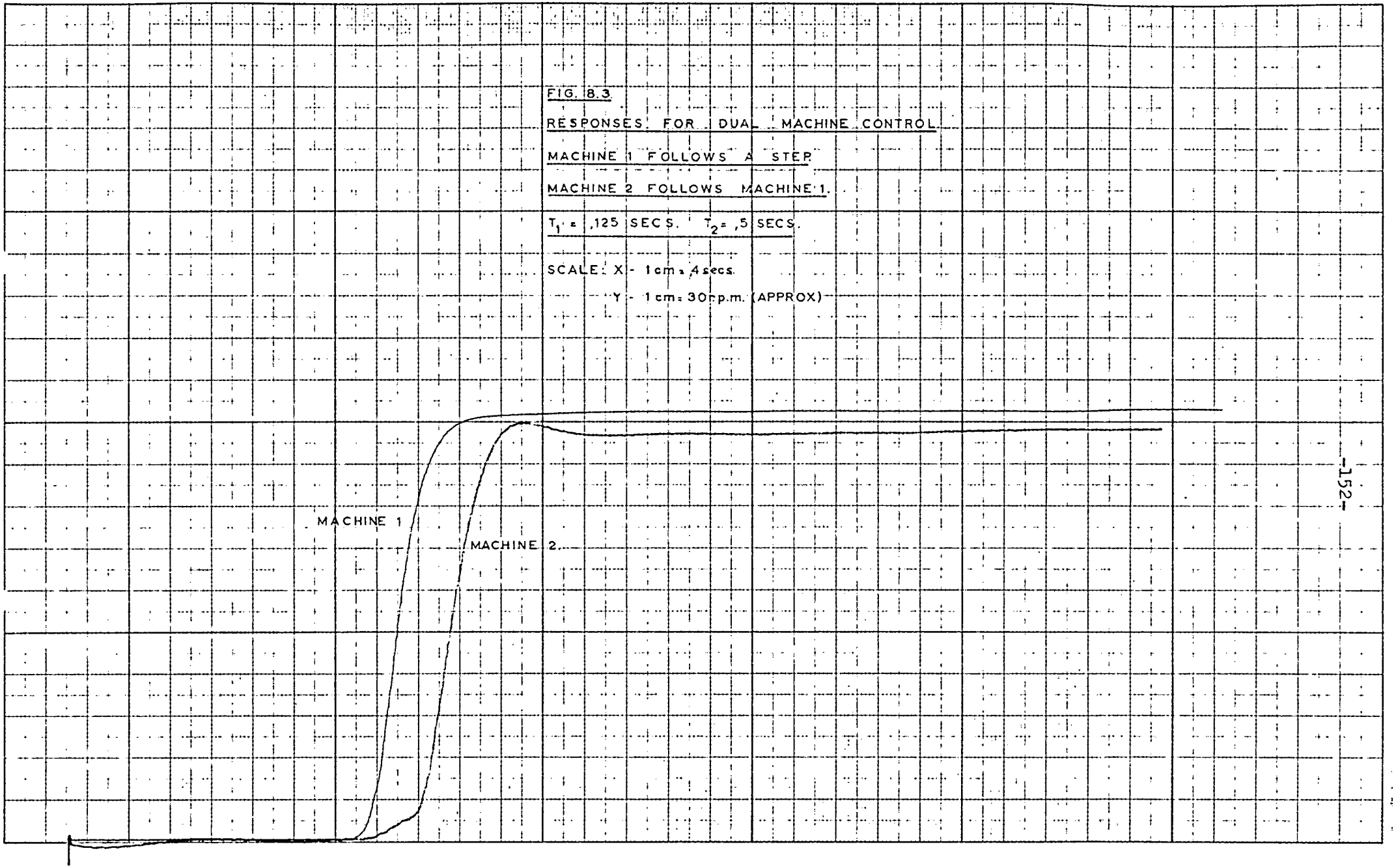
FIG. 8.3
RESPONSES FOR DUAL MACHINE CONTROL
MACHINE 1 FOLLOWS A STEP
MACHINE 2 FOLLOWS MACHINE 1.
T_1 = ,125 SECS. T_2 = ,5 SECS.
SCALE: X - 1 cm = 4 secs.
Y - 1 cm = 30 r.p.m. (APPROX)
MACHINE 1
MACHINE 2.

CHAPTER 9.

CONCLUSIONS.

The interface used to control the thyristor firing angles was found to be effective over the full control range. The one possible weakness in the designed interface is that a remote possibility does exist that the latches constituting the local memory may be reset at the same instant that a counter is reset, leading to a spurious count taking place. This probability is low, particularly in view of the relatively low sampling rates used, but could be allowed for by additional gating if the problem did in fact manifest itself. Finer control could be obtained merely by increasing the number of bits used in the count; this might them decrease the number of lines available for other applications, although as was seen in chapter 8, each additional machine to be controlled would only need two additional lines, since the data lines could be used in common.

The digital tachometer revealed more serious imperfections. The most important defect was the manifestation of "tacho ripple", a phenomenon necessitating the use of a deadband when implementing a control program. It was seen that this deadband did not affect the accuracy as much as expected when large disturbances were applied, the machine generally settling down to within 1 or 2 r.p.m. of the desired speed. However, small disturbances such as load transients gave more cause for concern, as no action would be taken if the speed was altered by some external means, but still remained within the limits of the deadband. However, as was seen when using both analogue and digital feedback in the dual machine tests described in chapter 8, the use of the digital tachometer reduced the problems of noise considerably, and the ripple problems were certainly no more serious than those experienced using a conventional D.C. tachogenerator. Use of the digital tachometer also eliminated calibration problems.

A more sophisticated digital tachometer would thus appear to be necessary for extremely fine control, allied possibly with more bits in the firing angle settings. This might also be able to widen the range of speeds able to be measured with the required accuracy.

One possible method of improving on the problem of ripple would be to count over a full revolution of the disc. In order to obviate the sampling delay inherent in such a scheme, more than one phototransistor - light combination would be needed, spaced around the disc. Each would accumulate a count over a full revolution, these counts being multiplexed so that the computer could be updated at least as frequently as was the case with the existing design.

The use of a three phase fully controlled bridge immediately imposed restrictions on the controllability of the machine used, owing to the inability of the system to allow regeneration. As the system stands, this difficulty may be decreased by running on load, thus ensuring that the machine is drawing current from the supply for most of the time, but complete control would require a switching arrangement to allow the machine to generate current should this be necessary.

One of the most important conclusions established by this thesis was the effectiveness of the z-transform method, both for the analysis of system performance (chapter 6), and as a design tool in the synthesis of compensated control algorithms (chapter 7). The method is admittedly tedious, but once the basic arithmetic and algebraic manipulation has been performed, weighting factors can be calculated fairly easily, after the parameters of the machine under consideration have been measured.

Admittedly, compensation of the system used was facilitated by the fact that the system itself was inherently stable, if oscillatory, and no open loop poles lay outside the unit circle in the z plane (fig. 6.1). The compensation of a

/..control..

control system having unstable open loop poles could be carried out in a manner similar to that shown in chapter 7, but under those circumstances the minimal prototype response functions could not be used in the simple forms shown.

It was concluded that, for the particular system used, the minimal prototype step response function could be implemented, and gave a satisfactory performance at sampling rates between 0,5 and 1 second for step and ramp inputs, and under load transient conditions. In general, use of such an algorithm would result in the output following any input, with a time lag of one sampling period.

It is possible, and indeed likely, that the design procedure outlined in this thesis will not yield the optimum performance under all conditions, although the minimal prototype step response has been seen to have wide applicability. Use of the quadratic performance index [33] or some form of adaptive control might be able to improve further on the performance of the machine.

No allowance for current limitation or control was provided, except for the rather primitive step size restriction imposed during the integral control steps. Such additional compensation would not be without its attendant problems, one of the most pressing being the method of measuring current digitally. However, the mathematical model developed should be able to predict the current drawn, and compensation in this manner might well be feasible.

This thesis is considered to have a number of practical implications. As shown in chapter 8, the control of one machine could easily be extended to several machines, this number being dependent on the number of input and output lines available, and on the sampling rated used. From a time sharing point of view, the program used in the dual machine tests could have been used to control five machines, if all were sampled once every 0,5 seconds. The use of the direct

/..memory..

memory access facility, allied with the use of the control lines for gating purposes, could probably extend the possible number of machines to be controlled considerably. Addition of a Buffer Interlace Controller for the computer could result in data being logged and displayed without wasteful use of computer time for this. If similar algorithms were used for all control loops, economical programming could ensure that lack of memory space would not be a problem.

No doubt control of interlinked machines would introduce complexities, as would any type of multi-loop control. However, such problems could be analysed using conventional control theory, with the aid of the z-transform method. Under such circumstances, the way is opened for the use of one computer to control a large number of interrelated machines, with all the advantages outlined in chapter 1.

Clearly, the economic implications of such a move would have to be carefully considered, and one would have to balance the saving in analogue controllers by the costs of the computer and interface equipment. The reliability of the computer becomes a vital factor when one considers industrial applications, and backup equipment would probably be necessary under most conditions.

This thesis has shown the practicability of a direct digital control system, giving control in this case of the speed of a machine to within 1% or better, and able to be fully analysed. Extension to multi-machine and multi-parameter applications is a logical and feasible step.

REFERENCES.

1. GOODGER, C.J. : 'Computers in Control', I.E.E. Students' Quarterly Journal, Dec. 1971, pp 319 - 321.

2. GIUSTI, A.L., OTTO, R.E. and WILLIAMS, T.J. : 'Direct Digital Computer Control', Control Eng. June 1962, pp 104 - 108.

3. KLOCH, H.F. and SCHOEFFLER, J.D.: 'Direct Digital Control at the Threshold', Electronics, March 23, 1964, pp 49 - 55.

4. FALLSIDE, F. and JACKSON, R.D.: 'Direct Digital Control of Thyristor Amplifiers', Proc. I.E.E. Vol. 6 no. 5, May 1969, pp 873 - 878.

5. WESTINGHOUSE : 'Silicon Controlled Rectifier Designers' Handbook', 1970.

6. RODD, M.G. : 'Direct Digital Control of Thyristor Networks', M.Sc. thesis, University of Cape Town, 1970.

7. WEEHUIZEN, H.F.: 'Direct Digital Control of a D.C. Machine', M.Sc. thesis, University of Cape Town, 1972.

8. KEMP, P.: 'A.C. Electrical Engineering' Macmillan , 1966.

9. NATIONAL SEMICONDUCTOR CORPORATION: 'Digital Integrated Circuits', 1971.

10. MILLMAN, J. and TAUB, H.: 'Pulse, Digital and Switching Waveforms', McGraw-Hill, 1965.

11. TEXAS INSTRUMENT CORP.: 'Integrated Circuit Data Book', July 1971.

12. SINHA, N.K., SZABADOS, B. and DI CENZO, C.D.: 'New High-Precision Digital Tachometer', Electronics Letters, Vol. 7 no.8, 22nd April 1971.

13. HOFFMAN DE VISME, G.: 'Digital Processing Unit for Evaluating Angular Acceleration', Electronic Eng. April 1968, pp 183 - 188.

14. DUNWORTH, A.: 'Digital Instrumentation for Angular Velocity and Acceleration', IEEE Trans. on Instrum. and Meas., Vol. IM-18 no.2, June 1969, pp 132 - 138.

15. BLISS, J.: 'Theory and Characteristics of Phototransistors', Motorola Applications Note AN-440.

16. VARIAN DATA MACHINES: 'Varian 620/i Computer Manual', 1968.

17. PHILIPS: 'Data Handbook on Semiconductors and Integrated Circuits', Part 1, Sept. 1969.

18. MULLARD: 'Techniques of Thyristor Power Control', Mullard Corp, 1970.

19. KORVINK, G.J.: 'A Design Procedure for Thyratron-Controlled Servo-Systems', Trans. SAIEE, Vol.58 part 5, May 1967, pp 93 - 99.

20. BINGLEY, P.: 'Characteristics and Control of Rectifier-Motor Variable Speed Drives', Proc. IEE, Vol.99 part II, 1952, p 189.

21. LINVILL, W.K.: 'Sampled-Data Control Systems Studied through Comparison of Sampling with Amplitude Modulation', Trans. AIEE, Vol. 70, 1951, pp 1779 - 1786.

22. LINVILL, W.K. and SALZER, J.M.: 'Analysis of Control Systems Involving Digital Computers', Proc. IRE, Vol. 41, July 1953, pp 901 - 906.

23. SALZER, J.M.: 'Frequency Analysis of Digital Computers Operating in Real Time', Proc. IRE, Vol. 42 no.2, Feb. 1954, pp 457 - 466.

24. RAGAZZINI, J.R. and ZADEH, L.A.: 'The Analysis of Sampled-Data Systems', Trans. AIEE, Vol. 71, part II, Nov. 1952, pp 225 - 234.

25. BARKER, R.H.: 'The Pulse Transfer Function and its Application to Sampling Servo Systems', Proc. IEE, Vol. 99, part IV, Dec. 1952, pp 302 - 316.

26. JURY, E.I.: 'Analysis and Synthesis of Sampled-Data Control Systems', Trans. AIEE, Vol 43 part I, Sept. 1954, pp 332 - 346.

27. BERGEN, A.R. and RAGAZZINI, J.R.: 'Sampled-Data Processing Techniques for Feedback Control Systems', Trans. AIEE, Vol. 73, part II, Nov. 1954, pp 236 - 246.

28. KUO, B.C.: 'Automatic Control Systems', Prentice-Hall, 1967.

28. RAGAZZINI, J.R. and FRANKLIN, G.F.: 'Sampled-Data Control Systems', McGraw-Hill, 1958.

30. TOU, J.T., 'Digital and Sampled-Data Control Systems', McGraw-Hill, 1959.

31. JOHNSON,G.W., LINDORFF, D.P. and NORDLING, C.G.A.: 'Extension of Continuous-Data System Design Techniques to Sampled-Data Control Systems', Trans. AIEE, Vol.74 part II, Sept. 1955, pp 252 - 263.

32. JURY, E.I.: 'Synthesis and Critical Sudy of Sampled-Data Control Systems', Trans. AIEE, Vol. 75 part II, July 1956, pp 141 - 151.

33. ZINOBER, A.: 'Linear Discrete-Time Control Using the Quadratic Performance Index', M.Sc. thesis, University of Cape Town, 1970.

34. BERTRAM, J.E.: 'Factors in the Design of Digital Controllers for Sampled-Data Control Systems', Trans. AIEE, Vol. 75 part II, July 1956, pp 151 - 159.

35. RAGAZZINI, J.R.: 'Digital Computers in Feedback Systems', 1957 IRE Convention Record, part IV, pp 33 - 42.

36. WILLIAMS, R.H.A.: 'Performance of a Laboratory S.C.R. Speed Control System', B.Sc. thesis, University of Cape Town, 1971.

APPENDIX 1.

DISCUSSION OF TTL LOGICAL COMPONENTS USED.

The logic components used for the interfaces described in chapters 2 and 3 were all of the TTL type and consisted of the following:

(i) D type flip-flops.
(ii) NAND gates.
(iii) Inverters.
(iv) Latches.
(v) Monostable multivibrators.

FLIP-FLOPS.

The D type flip-flop has one data input and a clock input. The logical level of the data input is transferred to the Q output when the clock input is raised to a logical 1, i.e. this type of flip-flop is triggered by a positive edge. In addition, this type of flip-flop has both preset and clear terminals available. A logical 0 on the clear input sets the Q output to a logical 0, while a logical 0 on the preset input sets the Q output to a logical 1.

GATES.

Various configurations of NAND gates, with from two to eight inputs, were used. All displayed the normal NAND gate behaviour, i.e. when all the inputs are in a logical 1 state the output goes to a logical 0 state. When a large number of components were to be driven by one gate, a buffer gate having a fan-out of 30, instead of the normal fan-out of 10, was used.

INVERTERS.

These merely served to invert the signal applied to them. A NAND gate could also be used as an inverter, if all the inputs except the one being used were tied to the supply rail.

LATCHES.

The operation of these components is fully described in section 2.4.

MONOSTABLE MULTIVIBRATORS.

These, as used, were triggered by negative edges, on application of which a pulse, of duration controlled by an external resistance and capacitor, was generated.[11].

APPENDIX 2.

CONVERSION OF TACHOMETER COUNT TO R.P.M.

It was shown in chapter 3 that the tachometer count was accumulated in 1/5 of a revolution. Each pulse counted corresponds to 10 μsecs.

Thus in one revolution, 5 times the number of pulses counted would be accumulated, being equivalent to $5N \times 10^{-5}$ secs, if N = the original count.

This is equal to a time of $\frac{5N \times 10^{-5}}{60}$ minutes to go through one revolution.

$$\text{i.e. the speed } s = \frac{60}{5N} \times 10^5 \text{ r.p.m.} \quad \ldots\ldots\ldots\ldots (A2.1)$$

$$\text{i.e. } s = \frac{12}{N} \times 10^5 \text{ r.p.m.} \quad \ldots\ldots\ldots\ldots (A2.2)$$

Thus in order for the speed in r.p.m. to be obtained, 12×10^5 was divided by the accumulated count.

In practice, 12×10^5 was converted to an octal number, and stored in the computer as such. Division was carried out using integers only, and the result was rounded off according to the remainder. Using such a system, the accuracy expected can be no more than 0,3% at low speeds, which is still better than the accuracy of the tachometer. Improved accuracy could, and probably would need to, be accompanied by greater precision in the division program. This could either be accomplished through multiplying the factor 12×10^5 by 100 or 10 before division took place, or by the use of floating point arithmetic, a step which would not be recommended, in view of the computer time which this would consume.

APPENDIX 3.

DERIVATION OF MACHINE AND BRIDGE TRANSFER FUNCTIONS.

The block diagram for a separately excited D.C. machine is shown in fig. A3.1 (19).

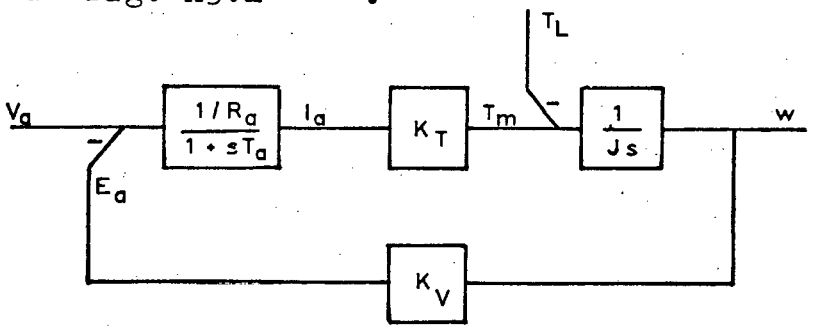

FIG. A3.1.

BLOCK DIAGRAM OF SEPARATELY EXCITED MOTOR

From this diagram, the machine transfer function may be obtained as:

$$\frac{w}{V_a} = \frac{K_T/JL_a}{s^2 + s(R_a/L_a) + K_V K_T/JL_a} \quad \text{.....(A3.1)}$$

Fig. A3.2 shows the V – I curve obtained using a low voltage supply across the choke and machine in series, giving a combined resistance of R_a of 0,9 ohms. The inductance of the choke, 0,2 H, was assumed to be large in comparison with that of the armature, which was therefore neglected.

The characteristic roots of a second order system can be written in general form as: (21)

$$s^2 + 2\zeta w_n s + w_n^2 \quad \text{.....(A3.2)}$$

whence, for an underdamped response, such as that shown in fig. 6.3 for this machine,

$$\text{Maximum \% overshoot} = 100 \exp(-\zeta\pi/(1-\zeta^2)^{\frac{1}{2}})$$

$$\text{Instant of maximum overshoot} = \pi/w_n(1-\zeta^2)^{\frac{1}{2}}$$

$$\text{Natural frequency } w_o = w_n(1-\zeta^2)^{\frac{1}{2}} \quad \text{.(A3.3)}$$

From fig. 6.3, it may be seen that the maximum overshoot obtained for this machine was 9,25%, and that this occurred after 1,08 seconds.

Hence, $\zeta = 0,62$

$w_n = 3,72$

and hence, $\frac{R}{L} = 4,6$ and $w_o = 3,19$ rads per second.

i.e. R = 0,92 ohms if L = 0,2 H, which corresponds closely with the measured values.

In an undergraduate thesis, Williams [36] found the inertia of the machine in question to be 0,64 Kg. m^2.

Using the values thus far obtained, and remembering that in the m.k.s. system $K_V = K_T$, values of K_V and K_T of 1,31 volts per radian per second and newton metres per amp respectively are obtained, leading to a final block diagram as shown in fig 4.1b.

Fig. A3.3 shows the bridge transfer function, of output voltage vs. firing angle, which was measured by setting up the firing angle by hand, while running the machine on no load, and measuring the bridge output D.C. voltage. From this curve it may be concluded that over a large part of the control range this transfer function may be assumed to be linear, with a value of -3,5 volts per degree. It should be noted that the firing angle plotted in this graph corresponds to the shifted waveform (see section 2.2), so that the zero origin actually corresponds to 30° displacement of the mains wave.

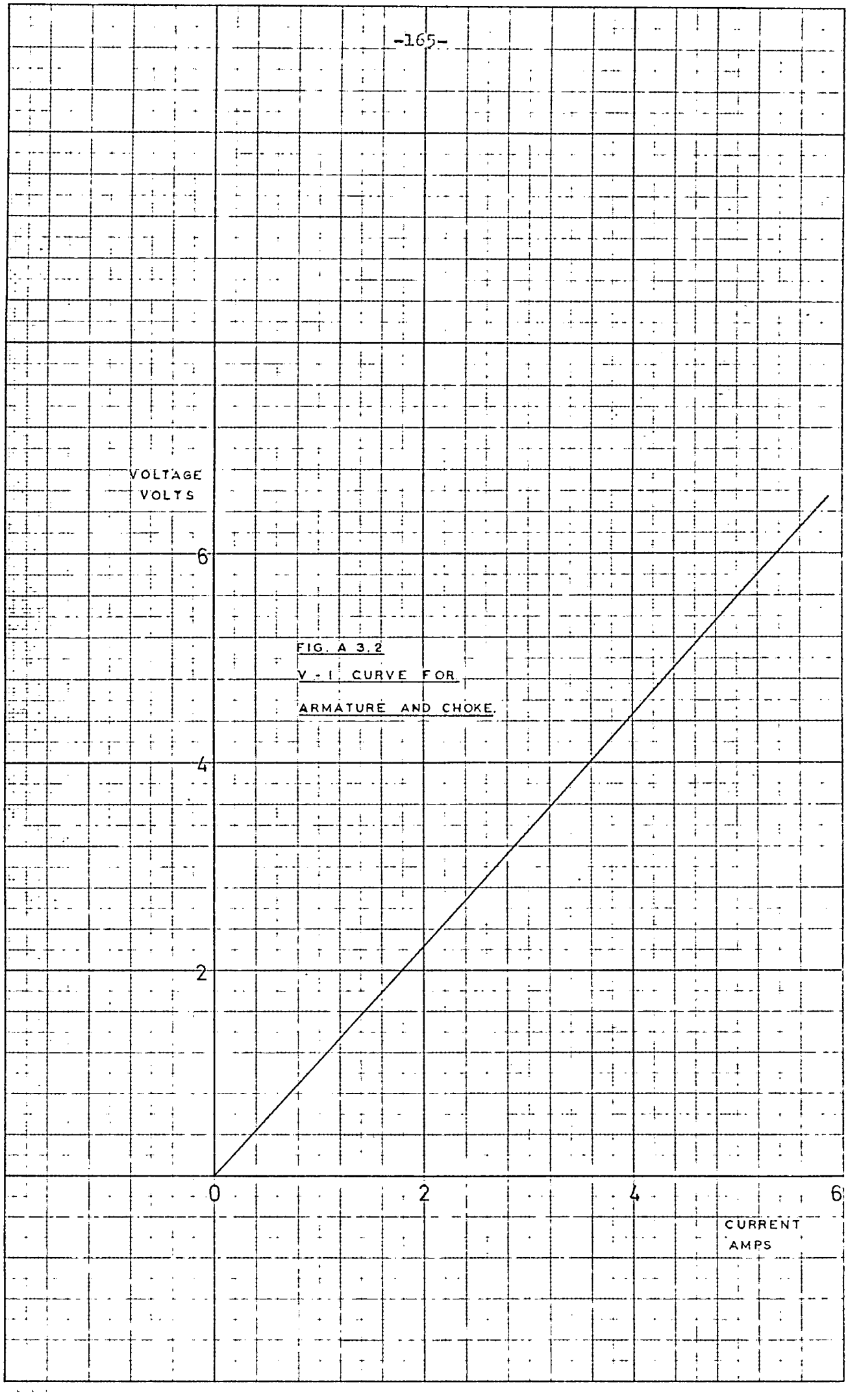

FIG. A 3.2
V - I CURVE FOR
ARMATURE AND CHOKE.

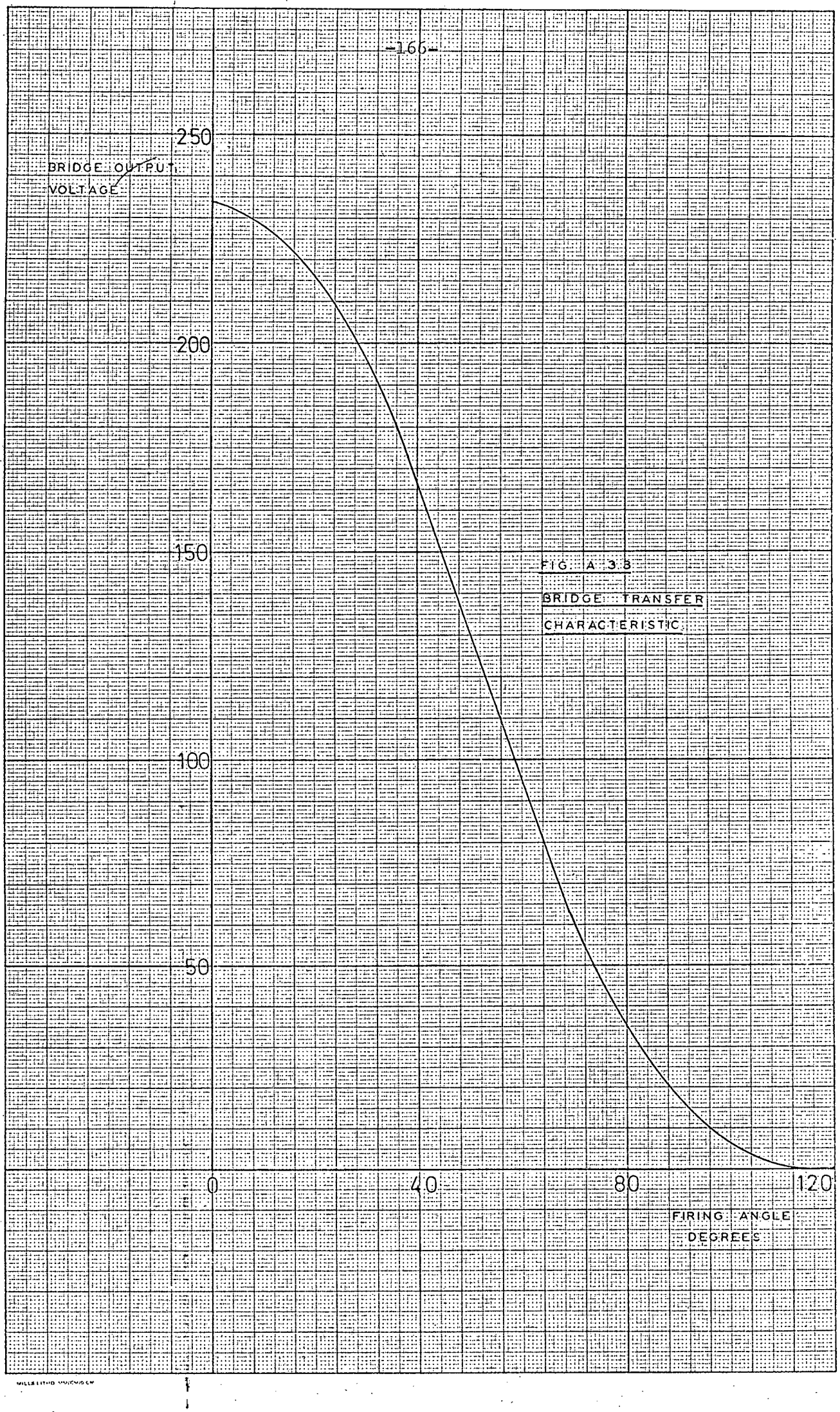

FIG. A 3.8

BRIDGE TRANSFER CHARACTERISTIC.

APPENDIX 4.

DERIVATION OF Z-TRANSFORM AND MODIFIED Z-TRANSFORM OF MACHINE TRANSFER FUNCTION.

The transfer function of the machine and bridge combination has been shown to be (equn. 6.3):

$$G(s) = \frac{K_T/JL}{s^2 + s\,R/L + K_V K_T/JL} \cdot \frac{K'(1 - e^{-Ts})}{s} \quad \ldots(A4.1)$$

$$= \frac{K'K_T}{JL}\left\{\frac{1}{s}\,\frac{1}{(s+a)^2 + b^2} - \frac{e^{-Ts}}{s}\,\frac{1}{(s+a)^2 + b^2}\right\} \quad \ldots(A4.2)$$

where $a = R/2L$

$$b = \left\{\frac{K_V K_T}{JL} - \frac{R^2}{4L^2}\right\}^{\frac{1}{2}}$$

The expression $\frac{1}{s}\,\frac{1}{(s+a)^2 + b^2}$ can be expanded into partial fractions as:

$$\frac{1}{a^2 + b^2}\left\{\frac{1}{s} - \frac{s+a}{(s+a)^2 + b^2} - \frac{a}{b}\,\frac{b}{(s+a)^2 + b^2}\right\} \quad \ldots(A4.3)$$

Hence G(s) can be written as a sum of fractions, each of which has a z-transform.

Doing so yields the following expression for G(s):

$$G(s) = \frac{K'K_T}{JL} \frac{1}{a^2 + b^2} \left\{ \frac{1}{s} - \frac{s + a}{(s + a)^2 + b^2} - \right.$$

$$\frac{a}{b} \frac{b}{(s + a)^2 + b^2} - \frac{e^{-Ts}}{s} + \frac{e^{-Ts}(s + a)}{(s + a)^2 + b^2} +$$

$$\left. \frac{a}{b} \frac{e^{-Ts}b}{(s + a)^2 + b^2} \right\} \qquad \text{(A4.4)}$$

Taking the z-transform of each of the terms of this form of G(s) yields the z-transform G(z), which after simplification becomes:

$$G(z) = \frac{K_1}{a^2 + b^2} \left\{ \frac{z(1 - e^{-aT}(\cos bT + a/b \sin bT))}{z^2 - 2ze^{-aT} + e^{-2aT}} - \right.$$

$$\left. \frac{e^{-aT}(\cos bT - a/b \sin bT - e^{-aT})}{z^2 - 2ze^{-aT} + e^{-2aT}} \right\} \text{.....(A4.5)}$$

$$\text{where } K_1 = \frac{K'K_T}{JL}$$

In a similar manner, the modified z-transform of G(s) may be obtained by taking the modified z-transform of each term in equation A4.4 and simplifying.

$$G(z,m) = \frac{K_1}{a^2 + b^2} \left\{ \frac{z^2(1 - e^{-amT}\cos bmT - a/b\ e^{-amT}\sin bmT)}{z^3 - 2z^2e^{-aT}\cos bT + ze^{-2aT}} + \right.$$

$$\frac{z(e^{-a(m+1)T}\cos (1-m)bT - 2e^{-aT}\cos bT +}{D}$$

$$\frac{e^{-amT}\cos bmT - a/b\ e^{-a(m+1)T}\sin (1-m)bT +}{D}$$

$$\frac{a/b\ e^{-amT}\sin bmT) + (e^{-2aT} - e^{-a(m+1)T}\cos (1-m)bT}{D}$$

$$\left. \frac{+ a/b\ e^{-a(m+1)T}\sin (1-m)bT)}{D} \right\} \quad \text{.....(A4.6)}$$

where $D = z^3 - 2z^2e^{-aT}\cos bT + ze^{-2aT}$

APPENDIX 5.

OPEN LOOP RESPONSE - THE POWER SERIES EXPANSION.

In order to predict the open loop response of the system, the transfer function G(z) was multiplied by the z-transform of the unit step function, and the resulting function expanded as a power series in z^{-1}.

The z-transform of the unit step function is given by

$$R(z) = \frac{z}{z - 1} \quad \ldots\ldots\ldots\ldots\ldots\ldots\ldots \quad (A5.1)$$

The output function of z, as shown in section 5.2, is given by

$$C(z) = R(z)G(z) \quad \ldots\ldots\ldots\ldots\ldots\ldots \quad (A5.2)$$

which, if multiplied out, becomes:

$$C(z) = \frac{z}{z - 1} \frac{a_o z + a_1}{z^2 + p_1 z + p_2} \quad \ldots\ldots\ldots \quad (A5.3)$$

where the values of a_o, a_1, p_1 and p_2 are as shown in appendix 4.

This can be written as:

$$C(z) = \frac{a_o z^{-1} + a_1 z^{-2}}{1 + b_1 z^{-1} + b_2 z^{-2} + b_3 z^{-3}} \quad \ldots \quad (A5.4)$$

By a series of long divisions, this expression can be expanded to a power series in z^{-1}.

The process is as follows:

$$C(z) = a_o z^{-1} + \frac{(a_1 - a_o b_1) z^{-2} - a_o b_2 z^{-3} - a_o b_3 z^{-4}}{1 + b_1 z^{-1} + b_2 z^{-2} + b_3 z^{-3}}$$

$$\ldots\ldots \quad (A5.5)$$

Equation A5.5 can be written as:

$$C(z) = a_o z^{-1} + \frac{a_o' z^{-1} + a_1' z^{-2} + a_2' z^{-3}}{1 + b_1 z^{-1} + b_2 z^{-2} + b_3 z^{-3}} \quad ..(A5.6)$$

which can in turn be divided.

Thus the sequence a_o, a_o', a_o'',etc represents the output at each sampling instant.

In order to obtain the open loop predicted response as shown in fig. 6.2, the expression C(z) was normalized.

APPENDIX 6.

SIMULATION OF CLOSED LOOP SYSTEM FOR INTEGRATOR.

Figure A6.1 shows the closed loop system.

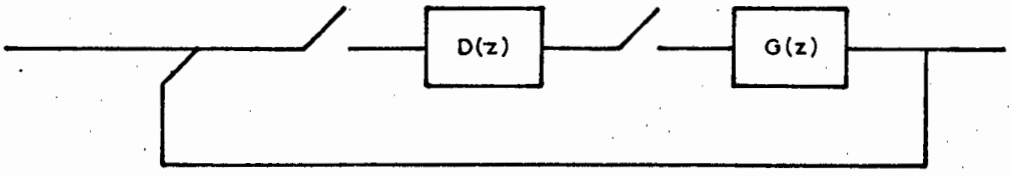

FIG.A6.1 BLOCK DIAGRAM OF CLOSED LOOP SYSTEM.

The closed loop transfer function is [28]:

$$C(z) = \frac{G(z,m)D(z)}{1 + G(z)D(z)} \; R(z) \quad \text{.....(A6.1)}$$

Appendix 4 showed the derivation of G(z,m) and G(z) as polynomial ratios in z. It should be remembered that the denominator of G(z,m) is equal to z times the denominator of G(z).

For an integrator, $D(z) = \frac{z}{z - 1}$

The unit step input $R(z) = \frac{z}{z - 1}$

Thus C(z) can be obtained by a process of multiplication of polynomials, giving a polynomial ratio in z^{-1} as follows:

$$C(z) = \frac{a_1 z^{-1} + a_2 z^{-2} + a_3 z^{-3}}{1 + b_1 z^{-1} + b_2 z^{-2} + b_3 z^{-3} + b_4 z^{-4}}$$

.....(A6.2)

Where: $a_1 = G(1 - e^{-amT}(\cos bmT + a/b \sin bmT))$

$a_2 = G(e^{-a(m + 1)T}(\cos (1 - m)bT - a/b \sin (1 - m)bT)$

$+ e^{-amT}(\cos bmT + a/b \sin bmT) - 2e^{-aT}\cos bT)$

$$a_3 = G(e^{-2aT} - e^{-a(m+1)T}(\cos(1-m)bT - a/b \sin(1-m)bT))$$

$$b_1 = G(1 - e^{-aT}(\cos bT + a/b \sin bT)) - 2(e^{-aT}\cos bT + 1)$$

$$b_2 = G(e^{-aT}(2a/b \sin bT + e^{-aT}) - 1) + e^{-2aT} + 4e^{-aT}\cos bT + 1$$

$$b_3 = Ge^{-aT}(\cos bT - a/b \sin bT - e^{-aT}) - 2e^{-aT}(e^{-aT} + \cos bT)$$

$$b_4 = e^{-2aT}$$

and:

$$a = R/2L$$

$$b = \left\{ \frac{K_V K_T}{JL} - \frac{R^2}{4L^2} \right\}^{\frac{1}{2}}$$

$$G = \frac{K_1 K_2}{a^2 + b^2}$$

$$K_1 = \frac{K_T K'}{JL}$$

$$K_2 = \frac{1}{K} \frac{3600}{256\pi}$$

(K is the integrator gain factor, $3600/256\pi$ is the conversion factor)

The power series expansion was carried out in a manner similar to that shown in appendix 5.

Thus the FORTRAN program did the following:

(i) T was varied from 0,3 to 1,0 seconds.

(ii) For each value of T, K was varied from 8 to 24 in steps of 4.

(iii) For each value of K, m was varied from 0 to 1 in steps of 0,1 and the power series expansion performed, for each value of m, up to 20 terms.

Table A6.1 shows a typical result.

TABLE A6.1.

TYPICAL INTEGRAL CONTROL SIMULATION PRINTOUT.

T= .50

K= 8

.02427	.08957	.18541	.30244	.43251	.56871	.70532	.83778	.96261	1.07725
1.17816	1.26308	1.33248	1.38725	1.42856	1.45781	1.47649	1.48614	1.48827	1.48436
1.46400	1.42030	1.35946	1.28695	1.20752	1.12519	1.04324	.96428	.89029	.82268
.76667	.72574	.69814	.68207	.67572	.67731	.68517	.69778	.71375	.73187
.75762	.79464	.83942	.88891	.94054	.99217	1.04212	1.08909	1.13214	1.17067
1.20018	1.21772	1.22513	1.22424	1.21676	1.20429	1.18824	1.16987	1.15025	1.13029
1.10753	1.08038	1.05060	1.01971	.98896	.95931	.93152	.90611	.88344	.86369
.85023	.84528	.84726	.85471	.86627	.88073	.89701	.91422	.93160	.94855
.96585	.98402	1.00228	1.02003	1.03677	1.05217	1.06600	1.07812	1.08849	1.09711
1.10171	1.10077	1.09545	1.08681	1.07581	1.06329	1.04998	1.03646	1.02323	1.01066
.99876	.98756	.97727	.96805	.95998	.95310	.94738	.94278	.93923	.93661
.93638	.93947	.94511	.95259	.96130	.97070	.98034	.98986	.99897	1.00745
1.01497	1.02132	1.02653	1.03065	1.03377	1.03600	1.03744	1.03821	1.03841	1.03816
1.03663	1.03327	1.02857	1.02295	1.01678	1.01038	1.00400	.99785	.99208	.98681
.98242	.97918	.97696	.97562	.97504	.97507	.97558	.97648	.97763	.97897
.98091	.98374	.98719	.99102	.99503	.99904	1.00294	1.00660	1.00997	1.01298
1.01530	1.01671	1.01733	1.01732	1.01679	1.01588	1.01468	1.01331	1.01183	1.01032
1.00858	1.00649	1.00418	1.00178	.99938	.99706	.99488	.99288	.99110	.98954
.98847	.98806	.98818	.98872	.98959	.99068	.99192	.99323	.99455	.99585
.99718	.99859	1.00001	1.00140	1.00271	1.00393	1.00502	1.00598	1.00681	1.00750

APPENDIX 7.

FLOW CHART OF INTEGRAL CONTROL PROGRAM.

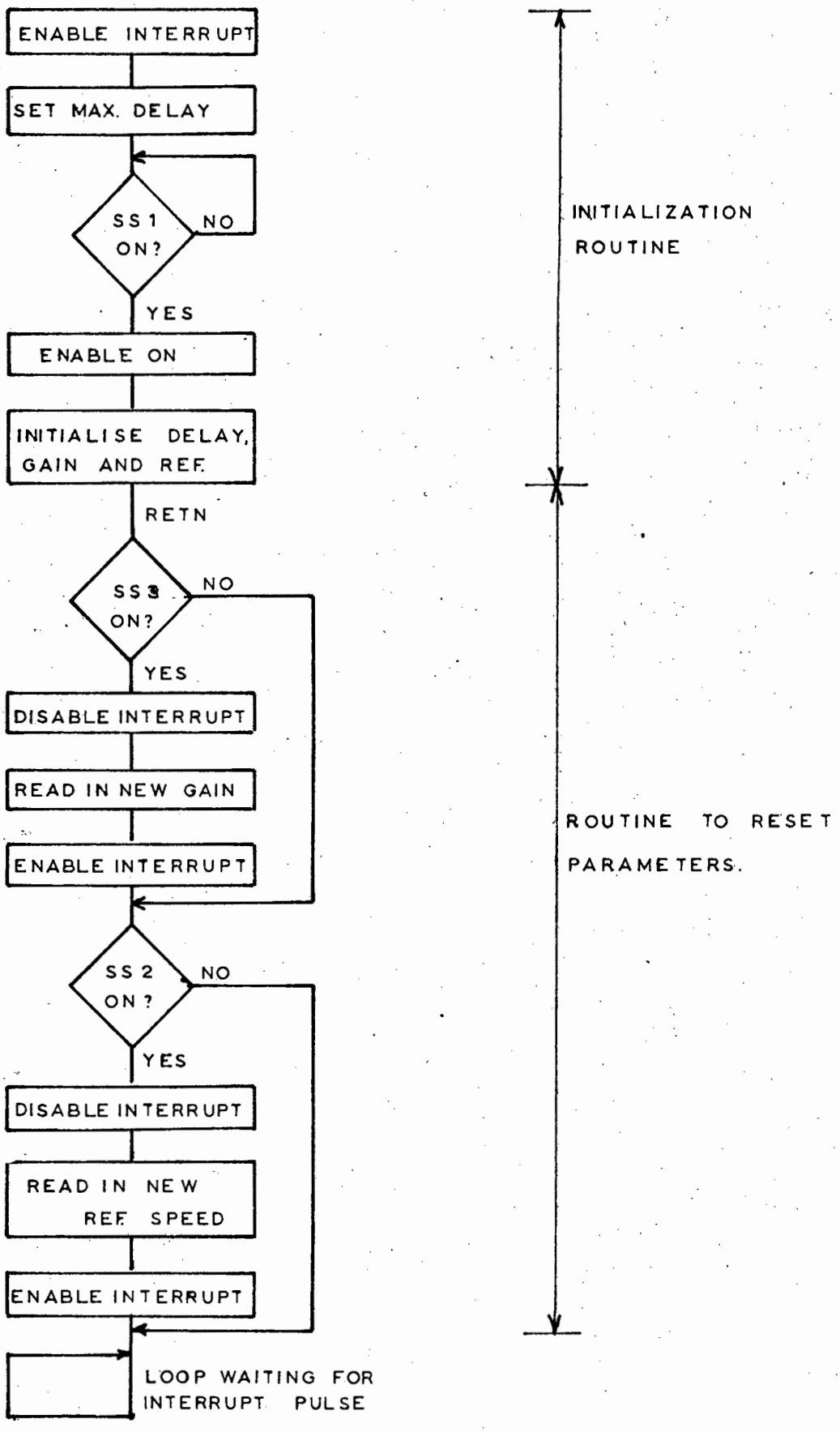

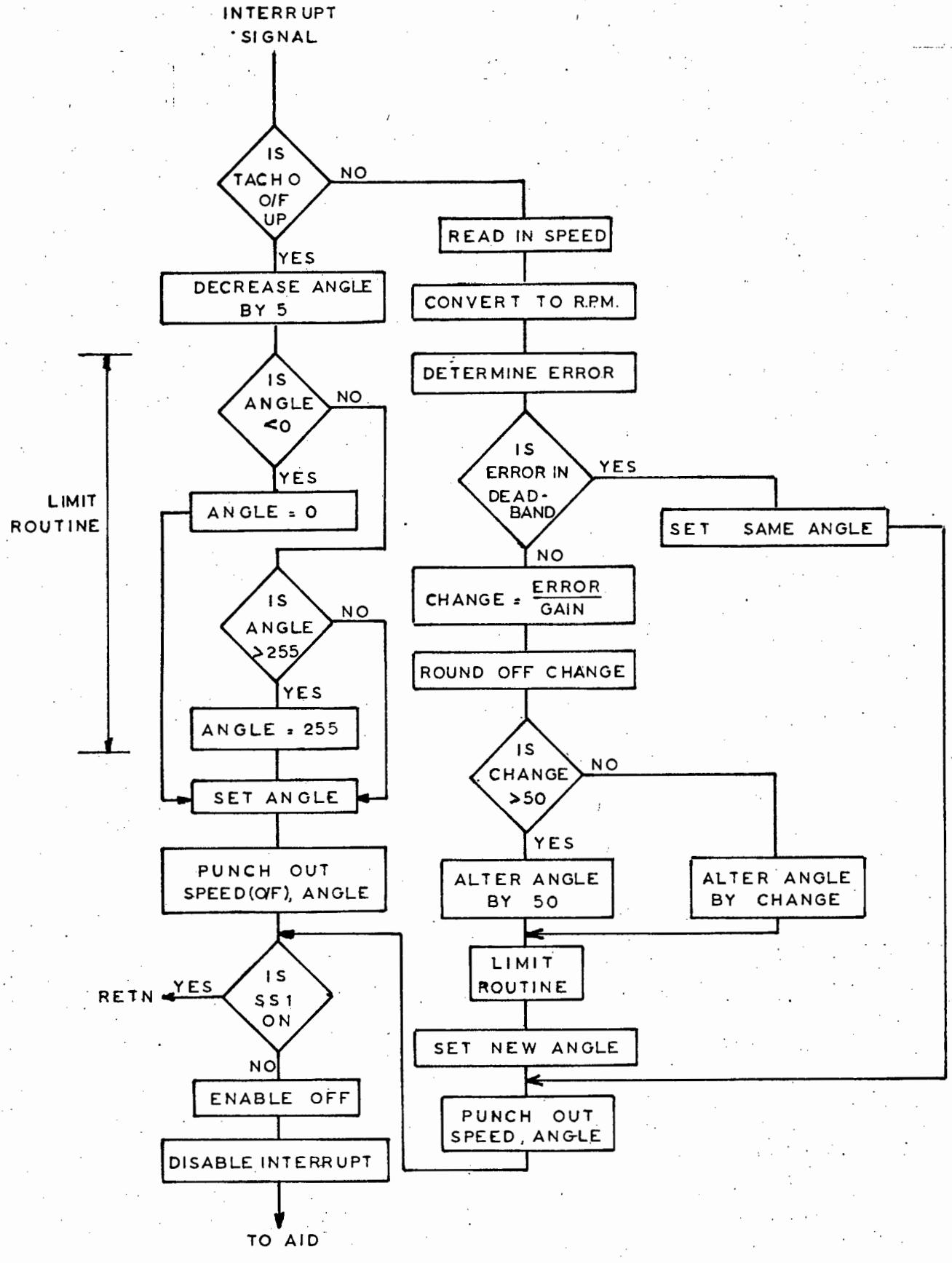
INTERRUPT SIGNAL
IS TACH O/F UP
NO
YES
READ IN SPEED
DECREASE ANGLE BY 5
CONVERT TO R.P.M.
DETERMINE ERROR
IS ANGLE <0
NO
YES
ANGLE = 0
IS ERROR IN DEAD-BAND
YES
SET SAME ANGLE
NO
LIMIT ROUTINE
IS ANGLE >255
NO
YES
ANGLE = 255
CHANGE = ERROR / GAIN
ROUND OFF CHANGE
IS CHANGE >50
NO
YES
SET ANGLE
ALTER ANGLE BY 50
ALTER ANGLE BY CHANGE
PUNCH OUT SPEED(O/F), ANGLE
LIMIT ROUTINE
IS SS1 ON
YES
RETN
NO
SET NEW ANGLE
ENABLE OFF
PUNCH OUT SPEED, ANGLE
DISABLE INTERRUPT
TO AID

APPENDIX 8.

DERIVATION OF COMPUTER PROGRAM TRANSFER FUNCTION.

The input to the computer is assumed to be a train of pulses at the sampling instants, given by i_j, i_{j-1}, i_{j-2}, etc, and the computer then produces a train of output pulses given by o_j, o_{j-1}, o_{j-2}, etc.

In order to obtain the present output sample o_j, the computer is able to make use of the previous input and output values, and the present input value [23, 30].

Thus:
$$o_j = a_o i_j + a_1 i_{j-1} + a_2 i_{j-2} + \ldots\ldots - b_1 o_{j-1} - b_2 o_{j-2} - \ldots\ldots \quad \ldots(A8.1)$$

$$= \sum_{k=0}^{m} a_k i_{j-k} - \sum_{k=1}^{m} b_k o_{j-k} \quad \ldots\ldots\ldots(A8.2)$$

if a finite number, m, of past samples is used.

Replacing each sample by an impulse of corresponding strength,

$$o^*(t) = \sum_{k=0}^{m} a_k i^*(t - kT) - \sum_{k=1}^{m} b_k o^*(t - kT) \quad \ldots.(A8.3)$$

Or, in Laplace transform form:

$$O^*(s) = \sum_{k=0}^{m} a_k e^{-kT} I^*(s) - \sum_{k=1}^{m} b_k e^{-kT} O^*(s) \quad \ldots\ldots(A8.4)$$

i.e.
$$\frac{O^*(s)}{I^*(s)} = \frac{a_o + a_1 e^{-Ts} + a_2 e^{-2Ts} + \ldots + a_m e^{-mTs}}{1 + b_1 e^{-Ts} + b_2 e^{-2Ts} + \ldots + b_m e^{-mTs}} \quad \ldots. (A8.5)$$

Equation (A8.5) may be written using z-transforms as:

$$\frac{O(z)}{I(z)} = \frac{a_o + a_1 z^{-1} + a_2 z^{-2} + \ldots + a_m z^{-m}}{1 + b_1 z^{-1} + b_2 z^{-2} + \ldots + b_m z^{-m}} \quad \ldots\ldots(A8.5)$$

Thus the program need merely be made up of a sequence of weighted past input and output values, and present input values, and may be represented as a rational polynomial in z^{-1}.

It is of interest to note that the integrator transfer function may be derived in this manner.

For any sample,

$$o(t) = o(t - 1) + 1/K\ i(t) \quad \ldots\ldots\ldots\ldots(A8.6)$$

Taking z-transforms,

$$O(z) = O(z)z^{-1} + 1/K\ I(z) \quad \ldots\ldots\ldots\ldots(A8.7)$$

i.e.
$$\frac{O(z)}{I(z)} = \frac{1/K}{1 - z^{-1}} \quad \ldots\ldots\ldots\ldots\ldots\ldots (A8.8)$$

which was the expression used.

APPENDIX 9.

DERIVATION OF COMPENSATION PROGRAM WEIGHTING FACTORS.

A9.1. MINIMAL PROTOTYPE STEP RESPONSE.

For the minimal prototype step response,

$$K(z) = z^{-1} \qquad \text{.....(A9.1)}$$

and, from equation 7.2, the computer transfer function D(z) is given by:

$$D(z) = \frac{1}{G(z)} \frac{K(z)}{1 - K(z)} \qquad \text{..... (A9.2)}$$

Thus, for this value of K(z), D(z) will be given by:

$$D(z) = \frac{z^2 + d_1 z + d_2}{c_1 z + c_2} \frac{z^{-1}}{1 - z^{-1}} \qquad \text{..... (A9.3)}$$

which, on expansion and simplification, yields a polynomial ratio in z^{-1}, of the form

$$D(z) = \frac{a_o + a_1 z^{-1} + a_2 z^{-2}}{1 + b_1 z^{-1} + b_2 z^{-2}} \qquad \text{.....(A9.4)}$$

with

$$a_o = \frac{1}{c_1} \qquad a_1 = \frac{d_1}{c_1} \qquad a_2 = \frac{d_2}{c_1}$$

$$b_1 = \frac{c_2 - c_1}{c_1} \qquad b_2 = -\frac{c_2}{c_1}$$

.....(A9.5)

In order to make D(z) a four term ratio, for reasons discussed in section 7.2, K(z) may be written as:

$$K(z) = z^{-1} \frac{2z^{-1} - 1}{2z^{-1} - 1} \qquad \text{..... (A9.6)}$$

Substituting (A9.6) in (A9.2) gives the following:

$$D(z) = \frac{a_o + a_1 z^{-1} + a_2 z^{-2} + a_3 z^{-3}}{1 + b_1 z^{-1} + b_2 z^{-2} + b_3 z^{-3}} \quad \ldots(A9.7)$$

with:

$$a_o = \frac{1}{c_1}$$

$$a_1 = \frac{2d_1 - 1}{2c_1} \qquad b_1 = \frac{2c_2 - 3c_1}{2c_1}$$

$$a_2 = \frac{2d_2 - d_1}{2c_1} \qquad b_2 = \frac{c_1 - 3c_2}{2c_1}$$

$$a_3 = -\frac{d_2}{2c_1} \qquad b_3 = \frac{c_2}{2c_1}$$

... (A9.8)

A9.2. MINIMAL PROTOTYPE RAMP RESPONSE WITH STALENESS FACTOR.

Here, from equation 7.3,

$$K(z) = \frac{(2 - c)z^{-1} - z^{-2}}{1 - cz^{-1}} \quad \ldots\ldots\ldots\ldots\ldots (A9.9)$$

Substituting this into equation A9.2 will give A9.7, with:

$$a_o = \frac{2 - c}{c_1}$$

$$a_1 = \frac{d_1(2 - c) - 1}{c_1} \qquad b_1 = \frac{c_2 - 2c_1}{c_1}$$

$$a_2 = \frac{d_2(2 - c) - d_1}{c_1} \qquad b_2 = \frac{c_1 - 2c_2}{c_1}$$

$$a_3 = -\frac{d_2}{c_1} \qquad b_3 = \frac{c_2}{c_1}$$

.....(A9.10)

APPENDIX 10.

SIMULATION OF CLOSED LOOP RESPONSE FOR COMPENSATION PROGRAM.

The derivation is exactly the same as for the integral control program, except that in this case, D(z) is given by a three or four term polynomial ratio. The calculation of the coefficients of these polynomials was shown in appendix 9.

Multiplication of the polynomials, in accordance with equation A6.1, ultimately yields the following type of result:

$$C(z) = \frac{c_o + c_1 z^{-1} + c_2 z^{-2} + c_3 z^{-3} + c_4 z^{-4} + c_5 z^{-5}}{1 + d_1 z^{-1} + d_2 z^{-2} + d_3 z^{-3} + d_4 z^{-4} + d_5 z^{-5} + d_6 z^{-6}}$$

..... (A10.1)

where the constants are functions of the factors in the polynomials D(z), G(z,m) and G(z).

The process of power series expansion, for different values of m, gave the output as a function of time.

The FORTRAN program therefore:

(i) Calculated the constants of G(z) and G(z,m).

(ii) Calculated D(z), and rounded off the coefficients.

(iii) Calculated C(z), by a process of division and addition of polynomials.

(iv) Calculated c(t) by a series of power series expansions for varying values of m.

A listing of this program is shown, for the minimal prototype step response, using the four term polynomial ratio of D(z).

Table A10.1 shows a typical output result for this program, while table A10.2 shows the same result using the three term ratio. The small differences may be attributed to the rounding off of the coefficients of D(z).

```
      DIMENSION T(8),Q1(8),Q2(8),R1(8),R2(8),A0(8),A1(8),A3(8),B1(8),
     CB2(8),B3(8),M0(8),M1(8),M2(8),M3(8),N1(8),N2(8),N3(8)
     C,E1(8),E2(8),E3(8),E4(8),E5(8),E6(8),D1(10),D2(10),D3(10),D4(10),
     CD5(10),P1(10),P2(10),P3(10),A2(8),F1(20,10),F2(20,10),F3(20,10),
     CF4(20,10),F5(20,10),F6(20,10),B6(10)
      REAL L,J1,KV,K,N(10)
5     READ(8,100)R,L,J1,C
      KV=SQRT(2.94*J1)
      K=((3.5*KV)/(J1*L))*(3600./(256.*(22./7.)))
      A=R/(2.*L)
      B=.5*SQRT(((4.*(KV**2.))/(J1*L))-(R**2.)/(L**2.))
      DO 2 I=1,8
      T(I)=(0.1*I)*0.2
      Q1(I)=(K/((A**2.)+(B**2.)))*(1.-EXP(-A*T(I))*(COS(B*T(I))+(A/B)
     C*SIN(B*T(I))))

      Q2(I)=(K/((A**2.)+(B**2.)))*(EXP(-A*T(I))*(COS(B*T(I))-(A/B)*
     CSIN(B*T(I))-EXP(-A*T(I))))
      Q2(I)=-Q2(I)
      R1(I)=-2.*EXP(-A*T(I))*COS(B*T(I))
      R2(I)=EXP(-2.*A*T(I))
      A0(I)=(2.+C)/Q1(I)
      A0(I)=1./Q1(I)
      A1(I)=(2.*R1(I)-1.)/(2.*Q1(I))
      A2(I)=(2.*R2(I)-R1(I))/(2.*Q1(I))
      A3(I)=-R2(I)/(2.*Q1(I))
      B1(I)=(2.*Q2(I)-3.*Q1(I))/(2.*Q1(I))
      B2(I)=(Q1(I)-3.*Q2(I))/(2.*Q1(I))
      B3(I)=Q2(I)/(2.*Q1(I))
      M0(I)=A0(I)*1000.
      M1(I)=A1(I)*1000.
      M2(I)=A2(I)*1000.
      M3(I)=A3(I)*1000.
      N1(I)=B1(I)*1000.
      N2(I)=B2(I)*1000.
      N3(I)=B3(I)*1000.
      A0(I)=M0(I)/1000.
      A1(I)=M1(I)/1000.
       A2(I)=M2(I)/1000.
      A3(I)=M3(I)/1000.
      B1(I)=N1(I)/1000.
      B2(I)=N2(I)/1000.
      B3(I)=N3(I)/1000.
      E1(I)=B1(I)+R1(I)+A0(I)*Q1(I)-1.
      E2(I)=B1(I)*R1(I)+B2(I)*R2(I)+A0(I)*Q2(I)+A1(I)*Q1(I)-B1(I)-R1(I)
     C-A0(I)*Q1(I)
      E3(I)=B1(I)*R2(I)+B2(I)*R1(I)+B3(I)+A1(I)*Q2(I)+A2(I)*Q1(I)
     C-B1(I)*R1(I)-R2(I)-R2(I)-A0(I)*Q2(I)-A1(I)*Q1(I)
      E4(I)=B2(I)*R2(I)+B3(I)*R1(I)+A2(I)*Q2(I)+A3(I)*Q1(I)-B1(I)*R2(I)
     C-B2(I)*R1(I)-B3(I)-A1(I)*Q2(I)-A2(I)*Q1(I)
      E5(I)=B3(I)*R2(I)+A3(I)*Q2(I)-B2(I)*R2(I)-B3(I)*R1(I)-A2(I)*Q2(I)
     C-A3(I)*Q1(I)
```

```
      E6(I)=-B3(I)*R2(I)-A3(I)*G2(I)
      DO 4 M=1,10
      N(M)=M/10.
      P1(M)=(K/((A**2.)+(B**2.)))*(1.-EXP(-A*N(M)*T(I))*(COS(B*N(M)*
     CT(I))+(A/B)*SIN(B*N(M)*T(I))))
      P2(M)=(K/((A**2.)+(B**2.)))*(EXP(-A*T(I)*(N(M)+1.))*COS(B*T(I)*
     C(1.-N(M)))-2.*EXP(-A*T(I))*COS(B*T(I))+EXP(-A*T(I)*N(M))*COS(B*T(I
     C)*N(M))-(A/B)*EXP(-A*T(I)*(N(M)+1.))*SIN(B*T(I)*(1.-N(M)))+(A/B)*
     CEXP(-A*T(I)*N(M))*SIN(B*T(I)*N(M)))
      P3(M)=(K/((A**2.)+(B**2.)))*(EXP(-2.*A*T(I))-EXP(-A*T(I)*(N(M)+1.
     C))*COS(B*T(I)*(1.-N(M)))+(A/B)*EXP(-A*T(I)*(1.+N(M)))*SIN(B*T(I)
     C*(1.-N(M))))
      D1(M)=A0(I)*P1(M)
      D2(M)=A0(I)*P2(M)+A1(I)*P1(M)
      D3(M)=A0(I)*P3(M)+A1(I)*P2(M)+A2(I)*P1(M)
      D4(M)=A1(I)*P3(M)+A2(I)*P2(M)+A3(I)*P1(M)
      D5(M)=A2(I)*P3(M)+A3(I)*P2(M)
      D6(M)=A3(I)*P3(M)
 4    CONTINUE
      DO 5 M=1,10
      F1(1,M)=D1(M)

      F2(1,M)=D2(M)
      F3(1,M)=D3(M)
      F4(1,M)=D4(M)
      F5(1,M)=D5(M)
      F6(1,M)=D6(M)
      DO 5 J=2,20
      F1(J,M)=F2(J-1,M)-F1(J-1,M)*E1(I)
      F2(J,M)=F3(J-1,M)-F1(J-1,M)*E2(I)
      F3(J,M)=F4(J-1,M)-F1(J-1,M)*E3(I)
      F4(J,M)=F5(J-1,M)-F1(J-1,M)*E4(I)
      F5(J,M)=F6(J-1,M)-F1(J-1,M)*E5(I)
      F6(J,M)=-F1(J-1,M)*E6(I)
 5    CONTINUE
      WRITE(5,101)T(I)
      WRITE(5,102)A0(I),A1(I),A2(I),A3(I)
      WRITE(5,103)B1(I),B2(I),B3(I)
      WRITE(5,105)D1(10),D2(10),D3(10),D4(10),D5(10)
      WRITE(5,106)E1(I),E2(I),E3(I),E4(I),E5(I),E6(I)
      WRITE(5,104)((F1(J,M),M=1,10),J=1,20)
 2    CONTINUE
      WRITE(5,110)
100   FORMAT(4F4.2)
101   FORMAT('1',' T=',F4.2,/)
102   FORMAT(5X,4F9.5,/)
103   FORMAT(5X,3F9.5,//)
104   FORMAT(5X,10F8.5)
105   FORMAT(5X,5F9.5,/)
106   FORMAT(5X,6F9.5,//)
110   FORMAT('1')
      END
```

TABLE A10.1

PRINTOUT FOR MINIMAL PROTOTYPE STEP RESPONSE, T = 0,5 SECS, USING 4 TERM D(z)

COEFFICIENTS SHOWN ARE FOR D(z) AND C(z) WITH $m=1$

T= .50

.11600 -.06000 .01200 -.00500

-1.06200 -.15600 .21800

.99969 -.07982 -.12275 .00214 -.01885

-1.08008 -.03407 .10300 -.00662 .02133 -.00356

.02252 .08312 .17206 .28966 .43137 .52776 .65453 .77746 .89330 .99969
1.08482 1.14074 1.17156 1.18136 1.17412 1.15353 1.12298 1.08550 1.04374 .99992
.96251 .93755 .92332 .91811 .92025 .92818 .94045 .95579 .97356 .99131
1.00714 1.01811 1.02486 1.02801 1.02821 1.02604 1.02206 1.01676 1.01060 1.00393
.99819 .99436 .99220 .99143 .99179 .99304 .99496 .99736 1.00014 1.00288
1.00524 1.00669 1.00736 1.00738 1.00690 1.00612 1.00487 1.00352 1.00217 1.00058
.99932 .99848 .99810 .99782 .99789 .99816 .99856 .99908 .99965 1.00026
1.00078 1.00112 1.00131 1.00136 1.00131 1.00118 1.00099 1.00075 1.00049 1.00022
.99999 .99983 .99973 .99969 .99970 .99973 .99980 .99989 .99999 1.00009
1.00018 1.00024 1.00026 1.00027 1.00025 1.00022 1.00019 1.00014 1.00009 1.00004
.99999 .99996 .99994 .99994 .99994 .99995 .99996 .99998 1.00000 1.00002
1.00004 1.00005 1.00005 1.00005 1.00005 1.00005 1.00004 1.00003 1.00002 1.00001
1.00000 .99999 .99999 .99999 .99999 .99999 .99999 1.00000 1.00000 1.00000
1.00001 1.00001 1.00001 1.00001 1.00001 1.00001 1.00001 1.00001 1.00000 1.00000
1.00000 1.00000 1.00000 1.00000 1.00000 1.00000 1.00000 1.00000 1.00000 1.00000
1.00000 1.00000 1.00000 1.00000 1.00000 1.00000 1.00000 1.00000 1.00000 1.00000
1.00000 1.00000 1.00000 1.00000 1.00000 1.00000 1.00000 1.00000 1.00000 1.00000
1.00000 1.00000 1.00000 1.00000 1.00000 1.00000 1.00000 1.00000 1.00000 1.00000
1.00000 1.00000 1.00000 1.00000 1.00000 1.00000 1.00000 1.00000 1.00000 1.00000

TABLE A10.2.

PRINTOUT FOR MINIMAL PROTOTYPE STEP RESPONSE, T=0,5 SECS, USING 3 TERM D(z)

T= .50

.11600 -.00200 .01100 .00000

-.56200 -.43700 .00000

.99969 .42002 .08726 .04146 .00000

-.58008 -.32411 -.05855 -.04071 .00346 .00000

.02252	.08312	.17206	.28066	.40137	.52776	.65453	.77746	.89330	.99969
1.08482	1.14074	1.17156	1.18136	1.17412	1.15353	1.12298	1.08550	1.04374	.99992
.96253	.93755	.92332	.91811	.92025	.92818	.94045	.95579	.97306	.99131
1.00703	1.01771	1.02403	1.02666	1.02628	1.02350	1.01891	1.01302	1.00630	.99913
.99301	.98905	.98692	.98632	.98696	.98857	.99090	.99373	.99685	1.00012
1.00286	1.00463	1.00556	1.00578	1.00544	1.00467	1.00357	1.00224	1.00079	.99927
.99799	.99714	.99667	.99652	.99662	.99693	.99738	.99794	.99856	.99921
.99977	1.00014	1.00035	1.00042	1.00039	1.00027	1.00008	.99985	.99958	.99931
.99907	.99892	.99883	.99881	.99883	.99888	.99897	.99907	.99919	.99931
.99941	.99948	.99951	.99952	.99951	.99949	.99945	.99940	.99935	.99930
.99925	.99922	.99921	.99920	.99920	.99922	.99923	.99925	.99928	.99930
.99932	.99933	.99934	.99934	.99934	.99934	.99933	.99932	.99931	.99930
.99929	.99929	.99928	.99928	.99928	.99926	.99929	.99929	.99930	.99930
.99930	.99931	.99931	.99931	.99931	.99931	.99931	.99930	.99930	.99930
.99930	.99930	.99930	.99930	.99930	.99930	.99930	.99930	.99930	.99930
.99930	.99930	.99930	.99930	.99930	.99930	.99930	.99930	.99930	.99930
.99930	.99930	.99930	.99930	.99930	.99930	.99930	.99930	.99930	.99930
.99930	.99930	.99930	.99930	.99930	.99930	.99930	.99930	.99930	.99930
.99930	.99930	.99930	.99930	.99930	.99930	.99930	.99930	.99930	.99930

APPENDIX 11.

FLOW CHART OF DIGITAL COMPENSATION PROGRAM.

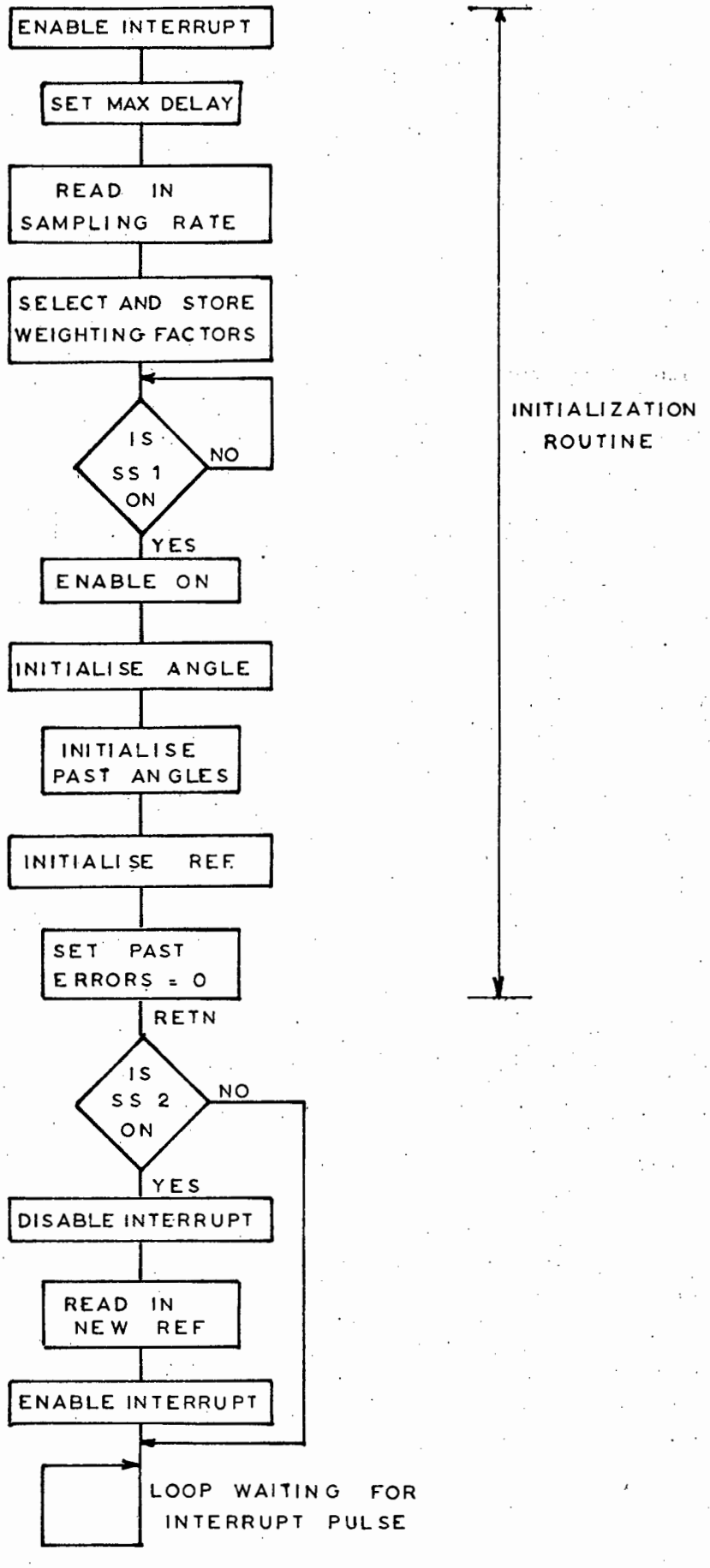

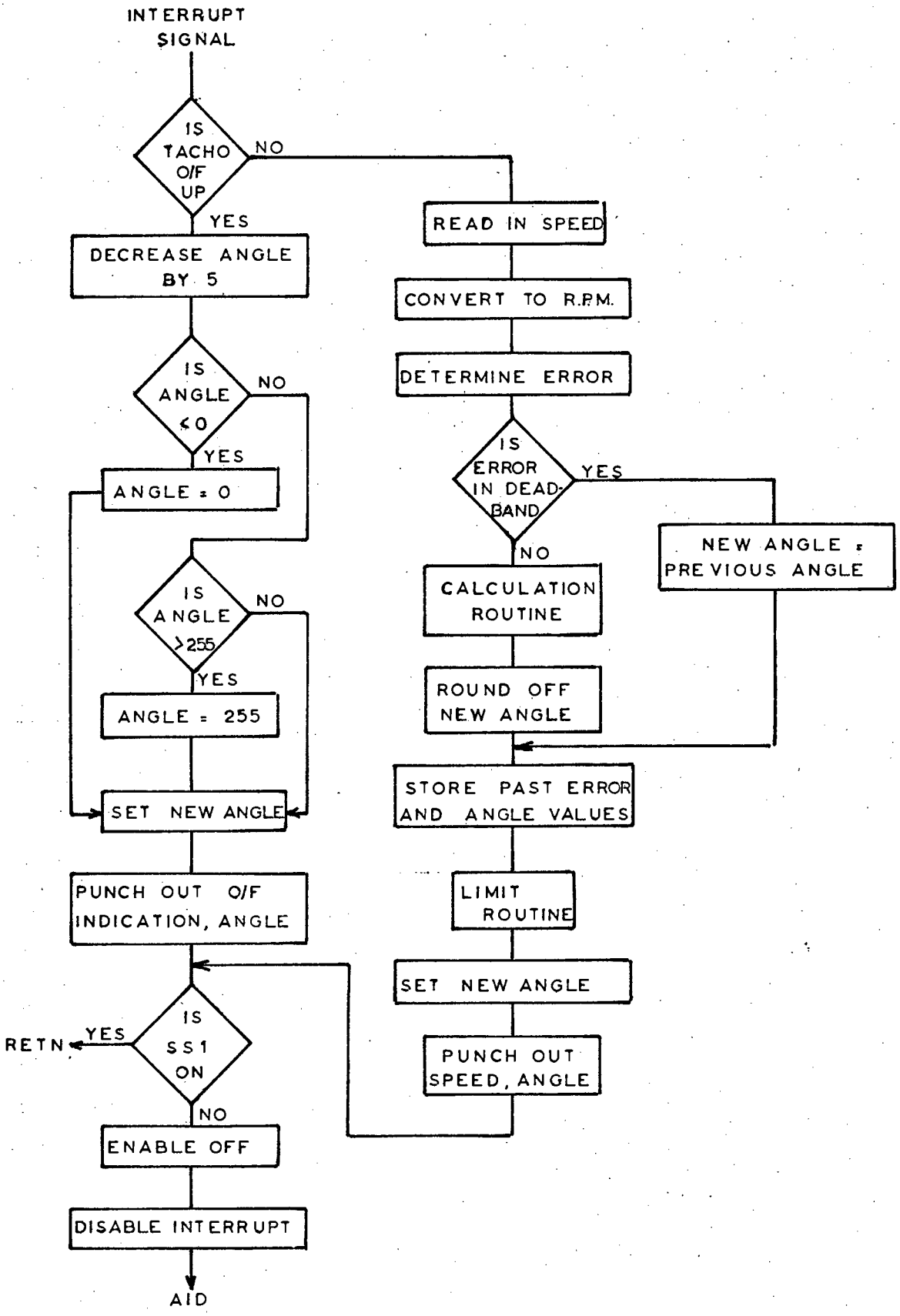
INTERRUPT SIGNAL
IS TACHO O/F UP
NO
YES
DECREASE ANGLE BY 5
IS ANGLE < 0
NO
YES
ANGLE = 0
IS ANGLE > 255
NO
YES
ANGLE = 255
SET NEW ANGLE
PUNCH OUT O/F INDICATION, ANGLE
IS SS1 ON
YES
RETN
NO
ENABLE OFF
DISABLE INTERRUPT
AID
READ IN SPEED
CONVERT TO R.P.M.
DETERMINE ERROR
IS ERROR IN DEAD-BAND
YES
NO
NEW ANGLE = PREVIOUS ANGLE
CALCULATION ROUTINE
ROUND OFF NEW ANGLE
STORE PAST ERROR AND ANGLE VALUES
LIMIT ROUTINE
SET NEW ANGLE
PUNCH OUT SPEED, ANGLE